

# TRENDS IN BACK-CALCULATED STIFFNESS OF IN-SITU RECYCLED AND STABILISED ROAD PAVEMENT MATERIALS

by  
Alan Gerald Lynch

*Thesis presented in fulfilment of the requirements for the degree of  
Master of Engineering (Research) in the Faculty of Engineering at  
Stellenbosch University*



Supervisor: Professor K.J. Jenkins PhD

December 2013







## SUMMARY

Two common methods of road pavement, granular material stabilisation used in road construction throughout South Africa today include Cold in Place Recycling (CIPR) and stabilisation with cement or bitumen and an active filler to create Bitumen Stabilised Materials (BSM).

As part of the updating of the South African Pavement Design Method (SAPDM) an experimental section, investigating the structural capacity of cement and lime stabilised and BSM pavement layers, was constructed and will be monitored over a two year period. As part of this study Falling Weight Deflectometer (FWD) measurements were taken on the various experimental stabilised pavement layers constructed. The FWD deflection data, measured at various time intervals over a 360 day period, forms the basis of the study presented here.

The objective of this thesis was to identify typical back-calculated layer stiffnesses and their variability over time for the various in-situ recycled and stabilised base layers constructed within the experimental section. Stabiliser type, content and layer thicknesses were varied across experimental sub-sections.

Trends in back-calculated stiffness of cement stabilised base layers consistently showed significant reductions in layer stiffness subsequent to construction traffic loading. Subsequent to the initial reduction in stiffness little change in stiffness was noted under normal traffic loads.

Observations on the trends in back-calculated stabilised layer stiffness per material type over time indicated that seasonal moisture and temperature fluctuations have an effect on the stiffness of the pavement structure as a whole. BSM materials showed significant variability over time in-line with seasonal variability in the supporting subgrade stiffness in the southbound lane. BSM materials with 1% cement added in the northbound lane show initial stiffness reductions due to direct rainfall application however a significant increase in layer stiffness occurs up to 360 days after construction. BSMs with 2% cement in the northbound lane show significant increases in layer stiffness over the 360 day observation period. No significant difference in stiffness trend was observed between BSM emulsion a BSM foam materials. The BSM emulsion with 0.9% residual bitumen and 1% cement was observed to show rapid reduction in stiffness upon opening to traffic and reverting to stiffness values similar to an unbound material of approximately 350 MPa.

Cement and lime stabilised materials showed typical post 28 –day average stiffnesses per sub-section ranging between 600 MPa and 1800 MPa. BSM foam with 1% cement added were observed to have average stiffnesses per sub-section in the range of 400MPa to 2200 MPa and BSM emulsion with 1% cement with stiffnesses between 400 MPa to 1700 MPa over the 360 day period. BSMs with 2%

cement added showed stiffness ranges between 900 MPa to 4300 MPa for BSM foam and 900 MPa to 3900 MPa for BSM emulsions over the 360 day period.

The spatial variability of back-calculated stiffness per sub-section of a particular stabilisation design was significant and was observed, through the Co-efficient of Variation (COV), to increase over time. The effect of the observed variability when incorporated into a pavement design scenario, requiring a design reliability of 90%, showed 50% of the pavement structure would be overdesigned by a factor of 4.

With respect to the current philosophies on the development of stiffness over time of cement and lime stabilised and BSM pavement layers some useful observations were made. Cement stabilised materials correlate well with stiffness development theories predicted by previous studies. Theories relating to the stiffness development of BSMs however did not predict the levels of variability in base layer stiffness observed on the experimental section.

The continued observation of the experimental section for another year will give greater insight to the stiffness trends of the stabilised materials discussed above.

## ACKNOWLEDGEMENTS

I express my gratitude to the following people who provided assistance in numerous ways during the creation of the study presented here:

- Professor Kim Jenkins – Stellenbosch University
- Professor Martin van de Ven – TU Delft
- Dr. Hechter Theyse – Pavement Modeling Corporation
- Mr. Philip Joubert – Royal HaskoningDHV
- Mr. Duncan Mason – Royal HaskoningDHV
- Mr. Ben Botes – Resident Engineer
- Mr. Edson Khathutshelo – Site Laboratory Manager MATROLAB
- Mr. Louw Kannemeyer – Road Network Manager South African National Roads Agency Ltd. (SANRAL)

## TABLE OF CONTENTS

CHAPTER 1	INTRODUCTION .....	1
1.1	Stabilised Pavement Materials in South Africa .....	1
1.2	Structural Role of Pavement Layers within a Pavement Structure .....	1
1.3	South African Pavement Design Method (SAPDM) and the R35 Experimental Section.....	3
1.4	Objectives .....	3
1.4.1	Back-analysis of Falling Weight Deflectometer (FWD) data .....	3
1.4.2	Trends in stabilised base layer back-calculated stiffness over time .....	4
1.4.3	Spatial variability in back-calculated base layer stiffness.....	4
1.4.4	Correlation between back-calculated base layer stiffness and engineering test results .....	4
CHAPTER 2	BACKGROUND .....	5
2.1	Characteristics of Granular Material Stabilisers .....	5
2.1.1	Cement stabiliser.....	5
2.1.2	Bituminous stabiliser.....	5
2.2	Curing of Stabilised Granular Materials .....	8
2.2.1	Cement stabilisation.....	9
2.2.2	Bitumen stabilisation.....	9
2.3	Defining pavement layer stiffness.....	10
2.4	Factors Influencing Stabilised Material Layer Stiffness .....	11
2.4.1	Compaction .....	11
2.4.2	Cement Content.....	11
2.4.3	Bitumen Content .....	11
2.4.4	Material grading .....	12
2.5	Theories on the stiffness and performance of stabilised pavement layers .....	12
2.5.1	Cement stabilised material .....	13
2.5.2	Bitumen stabilised material.....	13



2.6	Studies on the stiffness and performance of stabilised pavement layers .....	14
2.6.1	Engineering tests .....	15
2.6.2	Long term pavement performance (LTPP) .....	16
2.6.3	Heavy Vehicle Simulator (HVS) accelerated pavement testing .....	18
2.6.4	Summary .....	20
CHAPTER 3 RESEARCH METHODOLOGY .....		22
3.1	Experimental section field and laboratory data.....	23
3.1.1	Data collection .....	23
3.1.2	Data sorting and organisation .....	23
3.2	Experimental section data analysis .....	23
3.2.1	Deflection bowl parameters .....	23
3.2.2	Back-calculation.....	23
3.2.3	Visualisation of trends in stabilised base layer stiffness over time.....	24
3.2.4	Visualisation of spatial variability in stabilised base layer stiffness .....	24
3.2.5	Correlation between laboratory and field testing results.....	25
3.2.6	Conclusions and recommendations.....	25
CHAPTER 4 R35 EXPERIMENTAL SECTION LAYOUT, DESIGN & CONSTRUCTION.....		26
4.1	Geographical location and climate.....	26
4.2	Traffic Loading .....	28
4.3	Existing Pavement Structure .....	29
4.3.1	Layer thickness .....	29
4.3.2	Layer stiffness .....	30
4.4	Experimental Section Pavement Design .....	33
4.4.1	Structural Design.....	33
4.4.2	Stabilised material mix design .....	37
4.5	Experimental Section Construction .....	39

4.5.1	Base layer construction .....	39
4.5.2	Surface layer construction.....	42
4.5.3	Site laboratory quality control testing .....	43
CHAPTER 5 EXPERIMENTAL SECTION LABORATORY AND FIELD TESTING .....		46
5.1	Falling Weight Deflectometer (FWD) .....	46
5.2	Site Laboratory Testing.....	49
5.2.1	Unconfined Compressive Strength (UCS) .....	49
5.2.2	Indirect Tensile Strength (ITS) .....	49
5.2.3	Granular Material Grading.....	49
5.2.4	Degree of Compaction .....	50
CHAPTER 6 BACK-CALCULATION OF FWD MEASURED DEFLECTION BOWLS.....		51
6.1	Back-calculation software – backGAMES .....	51
6.2	Back-calculation procedure.....	52
6.2.1	Inputs.....	52
6.2.2	Outputs .....	53
6.3	Pavement structure model.....	53
6.3.1	Pavement surfacing layers .....	54
6.3.2	Base and sub-base layers.....	55
6.3.3	Semi-infinite subgrade .....	55
6.4	Back-analysis quality control.....	56
6.4.1	Combined sub-layer forming semi-infinite subgrade.....	56
6.4.2	Temperature correction .....	58
6.4.3	Correlation between stabilised base layer stiffness and deflection bowl parameters.....	65
6.4.4	Back-calculated stiffness and surface modulus correlation .....	68
6.4.5	FWD rubber buffer temperature and stiffness .....	70

CHAPTER 7	TRENDS IN STABILISED BASE LAYER STIFFNESS OVER TIME.....	71
7.1	Representation of stabilised base layer stiffness trend over time.....	71
7.1.1	Quantification of change in stiffness.....	71
7.1.2	Visualisation .....	72
7.2	Observed trends in base layer stiffness over time .....	75
7.2.1	Cement stabilised layers – 2% cement, 1% lime .....	75
7.2.2	BSM Emulsion - 0.9% residual bitumen, 1% cement.....	76
7.2.3	BSM Emulsion - 2.4% residual bitumen, 1% cement.....	76
7.2.4	BSM Emulsion - 2.4% residual bitumen, 2% cement.....	77
7.2.5	BSM Foam – 2.4% residual bitumen, 1% cement .....	78
7.2.6	BSM Foam – 2.4% residual bitumen, 2% cement .....	78
7.3	Identification of factors influencing observed trends.....	79
7.3.1	Pavement layer seasonal moisture content and temperature fluctuation.....	79
7.3.2	Rainfall.....	83
7.3.3	Construction Activity .....	84
7.3.4	Traffic .....	85
7.4	Observed and theorised stabilised material stiffness trends.....	87
7.5	Magnitudes of base layer stiffness observed.....	90
7.6	Conclusion .....	91
7.6.1	Trends in stabilised material stiffness over time and related influencing factors .....	91
7.6.2	Correlation of observed and theorised stabilised layer stiffness trends .....	93
7.6.3	Stiffness magnitudes per material type .....	93
CHAPTER 8	PRELIMINARY MODELS OF STABILISED MATERIAL CURING AND LAYER STIFFNESS VARIABILITY .....	95
8.1	Curing stiffness model .....	96
8.1.1	Model formulation .....	96

8.1.2	Factors influencing curing .....	98
8.1.3	Plot of $k_1$ versus $k_2$ .....	105
8.2	Seasonal variability in stabilised base layer stiffness .....	106
8.3	Conclusions.....	108
<b>CHAPTER 9 SPATIAL VARIABILITY OF STABILISED BASE LAYER STIFFNESS .....</b>		<b>110</b>
9.1	Stabilised base layer stiffness distribution per sub-section.....	110
9.2	Visualisation of stabilised base layer stiffness spatial variability .....	112
9.2.1	3-D plotting.....	112
9.2.2	2-D plotting.....	113
9.2.3	Spatial stiffness profile variability over time .....	114
9.3	Observed base layer stiffness spatial variability over time .....	116
9.4	Factors influencing base layers stiffness spatial variability .....	117
9.4.1	Support stiffness variability .....	117
9.4.2	Rainfall, prime application and traffic .....	118
9.5	Effects of base layer stiffness spatial variability on pavement design.....	119
9.5.1	Variability in pavement life of cement stabilised base layers .....	120
9.5.2	Variability in pavement life of CIPR BSM materials .....	121
9.6	Conclusions.....	123
<b>CHAPTER 10 CORRELATION BETWEEN BASE LAYER STIFFNESS AND ENGINEERING TEST RESULTS 124</b>		
10.1	Correlation of base layer stiffness with engineering tests.....	125
10.1.1	Indirect Tensile Strength (ITS) .....	125
10.1.2	Unconfined compressive Strength (UCS).....	128
10.2	Conclusions.....	130
<b>CHAPTER 11 CONCLUSIONS AND RECOMMENDATIONS .....</b>		<b>131</b>
11.1	Conclusions.....	131
11.1.1	Back-analysis of FWD data .....	131

11.1.2 Trends in back-calculated base layer stiffness per sub-section over time.....	132
11.1.2 Spatial variability in back-calculated base layer stiffness.....	134
11.1.3 Correlation between back-calculated base layer stiffness and engineering test results ..	134
11.2 Recommendations.....	134
11.2.1 Stabilised base layer moisture content and temperature measurement.....	134
11.2.2 Stabiliser content determination.....	135
11.2.3 Pavement layer thickness determination.....	135
BIBLIOGRAPHY.....	136

## LIST OF TABLES

Table 2.1: Types of bitumen emulsion (Ebels, 2008).....	7
Table 2.2: Selected road sections form Long and Jooste (2007).....	17
Table 2.3: HVS test site pavement structure at N2 Section near Kwelera, East London.....	19
Table 2.4: HVS test site pavement structure at N7 near Cape Town.....	20
Table 4.1: Characterisation of traffic on the R35 - P579 counting station.....	29
Table 4.2: Existing pavement layer thickness summary statistics.....	30
Table 4.3: Original pavement layer back-calculated stiffnesses – FWD on base (Theyse 2013).....	32
Table 4.4: Original pavement layer back-calculated stiffnesses – FWD on sub-base (Theyse 2013).....	32
Table 4.5: Existing pavement back-calculated stiffnesses –km 5.0 to km 10.0 northbound (Theyse 2013).....	33
Table 4.6: Existing pavement back-calculated stiffnesses –km 5.0 to km 10.0 southbound (Theyse 2013).....	33
Table 4.7: BSM materials modelled in structural analysis.....	35
Table 4.8: Crushing and stiffness reduction Monte Carlo simulation results (Theyse, 2013).....	36
Table 4.9: Permanent deformation Monte Carlo simulation (Theyse, 2013).....	36
Table 4.10: Pozzolanic Stabilisation Mix Design Results (Theyse, 2013).....	37
Table 4.11: Bitumen stabilisation selected mix design results (Theyse, 2013).....	38
Table 4.12: Base Layer Design Parameters - Southbound.....	39
Table 4.13: Base Layer Design Parameters - Northbound.....	39
Table 4.14: Quality control testing site laboratory average results - southbound.....	44
Table 4.15: Quality control testing site laboratory average results - northbound.....	44
Table 4.16: BSM classification - ITS and relative compaction requirements (Asphalt Academy, 2009).....	45
Table 5.1: Pavement condition and performance indicators.....	46
Table 5.2: FWD deflection bowl parameters.....	48
Table 6.1: Deflection bowls from BISAR modelling of pavement structures A and B.....	60
Table 6.2: Deflection bowls from BISAR modelling of pavement structures A* and B.....	61
Table 6.3: Deflection bowls from BISAR modelling of pavement structure A and A*.....	61
Table 6.4: Measured and automatic back-calculated deflection bowl comparison.....	62
Table 6.5: Degree of correlation.....	68
Table 6.6: Correlation of average back-calculated base layer stiffness and average RoC.....	68
Table 7.1: % Stiffness change - colour code.....	74
Table 7.2: Visualisation of % change in average base layer stiffness.....	74
Table 7.3: Symbology used in stiffness trend plots.....	75
Table 7.4: % Stiffness change - colour code.....	80
Table 7.5: Correlation of average stiffness trend with rainfall (mm) - Southbound.....	80
Table 7.6: Correlation of average stiffness trend with rainfall (mm) - Northbound.....	80
Table 7.7: D1800 <sup>-1</sup> deflection variation - model parameters.....	82

Table 7.8: Correlation of average stiffness trend with prime application - Southbound .....	85
Table 7.9: Correlation of average stiffness trend with prime application- Northbound .....	85
Table 7.10: Correlation of average stiffness trend with prime application - Southbound .....	86
Table 7.11: Correlation of average stiffness trend with prime application- Northbound .....	86
Table 7.12: Summary of factors influencing stabilised base layer stiffness .....	92
Table 8.1: Curing model parameters and 28 day model stiffness .....	97
Table 8.2: Sinusoidal stabilised base layer seasonal stiffness variation model parameters - southbound .....	107
Table 9.1: Degree of spatial trend correlation .....	115
Table 9.2: Degree of spatial trend correlation .....	119

## LIST OF FIGURES

Figure 2.1: Outline of Chapter 2.....	5
Figure 2.2: Bitumen and water phases within bitumen emulsion .....	6
Figure 2.3: Bitumen foaming nozzle (Romanoschi, 2003).....	8
Figure 2.4: Elastic and resilient modulus of a material.....	10
Figure 2.5: Long-term behaviour of cement stabilised material (Theyse et al, 1996) .....	13
Figure 2.6: Long-term behaviour of BSM Foam materials (Asphalt Academy, 2002) .....	14
Figure 2.7: Long-term behaviour of bitumen stabilised materials (Ebels, 2008).....	14
Figure 2.8: Effects of varying material type, bitumen and cement content on UCS (Long et al, 2004).....	15
Figure 2.9: Effects of varying material type, bitumen and cement content on ITS (Long et al, 2004).....	16
Figure 3.1: Outline of research methodology .....	22
Figure 4.1: Outline of Chapter 4.....	26
Figure 4.2: Location of R35 Experimental Section .....	27
Figure 4.3: Measured and historical average monthly maximum and minimum temperatures .....	28
Figure 4.4: Measured and historical average monthly rainfall .....	28
Figure 4.5: Test pit profiles - southbound.....	30
Figure 4.6: Test pit profiles - northbound.....	30
Figure 4.7: Broken-down cement stabilised granular material (Theyse 2013) .....	32
Figure 4.8: Experimental section pavement structure.....	34
Figure 4.9: Experimental Section traffic accommodation and construction sequence .....	40
Figure 4.10: Spreading of cement or lime before in-situ recycling. ....	41
Figure 4.11: Stabilised material grading and recommended grading zones .....	45
Figure 5.1: FWD Load Plate and Geophones .....	47
Figure 5.2: Representation of FWD geophone setup and pavement surface deflection bowl .....	48
Figure 5.3: FWD testing on the R35 Experimental Section .....	49
Figure 6.1: Outline of Chapter 6.....	51
Figure 6.2: Test-pit pavement structures - southbound.....	54
Figure 6.3: Test-pit pavement structures - northbound.....	54
Figure 6.4 Back-calculation pavement structure model.....	55
Figure 6.5: Subgrade model simplification - km 7.5 northbound (*Asphalt temperature = 39°C).....	56
Figure 6.6: Subgrade model simplification - km 6.5 northbound (*Cape seal and base layer combined).....	57
Figure 6.7: Asphalt stiffness back-calculation sensitivity – pavement structures.....	59
Figure 6.8: Deflection bowl variation due to asphalt layer stiffness variation.....	59
Figure 6.9: Pavement structures - automatic back-calculation error.....	62
Figure 6.10: Example load pulse from R35 FWD testing.....	64
Figure 6.11: Asphalt temperature – dynamic stiffness relationship at 5 Hz loading rate (CSIR) .....	65
Figure 6.12: Base layer stiffness and BLI trend comparison – 175mm BSM foam 2% cement SB .....	66
Figure 6.13: Base layer stiffness and RoC trend comparison – 175mm BSM foam 2% cement SB .....	66
Figure 6.14: Power function relationship between back-calculated stiffness and BLI .....	67
Figure 6.15: Average base layer stiffness to average RoC correlation - 175mm BSM foam 2% cement SB.....	67
Figure 7.1: Outline of topics covered in Chapter 7.....	71
Figure 7.2: Depiction of parameters used in determination of percentage drop in stiffness .....	72
Figure 7.3: Typical plot of back-calculated stiffness trend.....	73
Figure 7.4: 175 mm bitumen emulsion (2.4%b, 2%c) NB - Rainfall and average base stiffness plot.....	73
Figure 7.5: Cement stabilised base layer average layer stiffness plot.....	75
Figure 7.6: BSM Emulsion (0.9% residual bitumen and 1% cement) average layer stiffness plot .....	76

Figure 7.7: BSM Emulsion (2.4% residual bitumen and 1% cement) average layer stiffness plot .....	77
Figure 7.8: BSM Emulsion (2.4% residual bitumen and 2% cement) average layer stiffness plot .....	78
Figure 7.9: BSM Foam (2.4% residual bitumen and 1% cement) average layer stiffness plot.....	78
Figure 7.10: BSM Foam (2.4% residual bitumen and 2% cement) average layer stiffness plot.....	79
Figure 7.11: 175 mm BSM Emulsion (2.4% b, 1% c) base layer stiffness and 1800mm deflection - SB .....	81
Figure 7.12: Seasonal variability in subgrade stiffness correlating with seasonal rainfall pattern .....	82
Figure 7.13: Seasonal variability in air temperature correlating with D1800 model .....	82
Figure 7.14: 200 mm C3-1 (2% c, 1% l) base layer stiffness and 1800mm deflection - SB .....	83
Figure 7.15: Summary of average back-calculated base layer stiffnesses – northbound and southbound.....	91
Figure 8.1: Outline of Chapter 8.....	95
Figure 8.2: Curing stiffness model - 200mm C3-1 (2% c, 1% l) Southbound.....	96
Figure 8.3: Curing average stiffness model - 200 Foamed bitumen (2.4% b, 1% c) Southbound .....	97
Figure 8.4: 28 day modelled base layer stiffnesses.....	98
Figure 8.5: Curing model parameter $k_1$ versus curing period average daily temperature – southbound .....	99
Figure 8.6: Curing model parameter $k_1$ versus curing period average daily temperature – northbound .....	99
Figure 8.7: Curing model parameter $k_2$ versus curing period average daily temperature – southbound .....	100
Figure 8.8: Curing model parameter $k_2$ versus curing period average daily temperature - northbound.....	100
Figure 8.9: Rate of stiffness gain at a specific time versus moisture content - southbound and northbound .....	101
Figure 8.10: Curing model parameter $k_1$ versus bitumen content – southbound.....	101
Figure 8.11: Curing model parameter $k_1$ versus bitumen content – northbound .....	102
Figure 8.12: Curing model parameter $k_2$ versus bitumen content - southbound .....	102
Figure 8.13: Curing model parameter $k_2$ versus bitumen content – northbound .....	103
Figure 8.14: Curing model parameter $k_1$ versus cement content – southbound .....	104
Figure 8.15: Curing model parameter $k_1$ versus cement content – northbound .....	104
Figure 8.16: Curing model parameter $k_2$ versus cement content – southbound .....	105
Figure 8.17: Curing model parameter $k_2$ versus cement content – northbound .....	105
Figure 8.18: Curing model parameter plot - $k_1$ versus $k_2$ .....	106
Figure 8.19: 200mm C3-1 (2% c, 1% l) - Seasonal stiffness variation model.....	108
Figure 8.20: 175mm Foamed bitumen (2.4% b, 1% c) - Seasonal variation model .....	108
Figure 9.1: Outline of Chapter 9.....	110
Figure 9.2: Scatter plot – 200mm BSM Foam (2.4% b, 1% c) day 25 southbound.....	110
Figure 9.3: Cumulative sum plot 200mm BSM Foam (2.4% b, 1% c) day 25 southbound.....	111
Figure 9.4: 3-D spatial base layer stiffness profile - 200mm C3-1, 2% cement and 1% lime SB .....	112
Figure 9.5: Back-calculated stiffness colour range.....	113
Figure 9.6: Base layer spatial stiffness profile – 200 mm C3-1 2% cement, 1% lime.....	113
Figure 9.7: Scatter plot - 200 C3-1 day 7 and day 15 southbound.....	115
Figure 9.8: 200mm C3-1 day 7 versus day 15 southbound .....	115
Figure 9.9: Correlation of base layer stiffness trends – 200mm C3-2 Southbound .....	116
Figure 9.10: Back-calculated stiffness colour range.....	116
Figure 9.11: Spatial variability in layer stiffness - 175mm BSM Emulsion (2.4% b, 2% c) Northbound .....	117
Figure 9.12: Correlation between base and sub-base layer stiffness - 200mm BSM emulsion 2.4% b, 1% c.....	118
Figure 9.13: Correlation between base and subgrade layer stiffness - 200mm BSM emulsion 2.4% b, 1% c .....	118
Figure 9.14: Correlation between prime application and changes in spatial stiffness profile SB .....	119
Figure 9.21: Distribution of bearing capacities of 200 mm C3-1 Northbound .....	121
Figure 9.22: Depiction of Principal Stresses.....	122
Figure 9.23: SR analysis pavement structure and results.....	122
Figure 9.24: Variation in SR versus depth in pavement structure .....	123
Figure 10.1: Outline of Chapter 10.....	124
Figure 10.2: Correlation of cement stabilised material ITS and base layer stiffness - southbound .....	125
Figure 10.3: Correlation of BSM emulsion ITS and base layer stiffness – southbound .....	126
Figure 10.4: Correlation of BSM foam ITS and base layer stiffness – southbound .....	126
Figure 10.5: Correlation of BSM emulsion ITS and base layer stiffness – northbound .....	127
Figure 10.6: Correlation of BSM foam ITS and base layer stiffness – northbound.....	127
Figure 10.7: Correlation of cement stabilised material UCS and base layer stiffness – southbound.....	128
Figure 10.8: Correlation of cement stabilised material UCS and base layer stiffness – northbound.....	129
Figure 10.9: Correlation of UCS and base layer stiffness – bitumen emulsion stabilised materials NB .....	129
Figure 10.10: Correlation of UCS and base layer stiffness – foamed bitumen stabilised materials NB.....	130
Figure 11.1: Outline of Chapter 11 .....	131

## LIST OF ABBREVIATIONS AND SYMBOLS

### Abbreviations

3-D	Three dimensional
AASHTO	American Association of State Highway and Transportation Officials
BLI	Base Layer Index
BSM	Bitumen Stabilised Material
CIPR	Cold In-place Recycling
CoV	Co-efficient of Variation
CSIR	Council for Scientific and Industrial Research
D1800	Deflection measured at geophone 1800mm from FWD load plate
DCP	Dynamic Cone Penetrometer
DSR	Deviator Stress Ratio
FWD	Falling Weight Deflectometer
GPR	Ground Penetrating Radar
GPS	Global Positioning System
HMA	Hot Mix Asphalt
HVS	Heavy Vehicle Simulator
IT	Information Technology
ITS	Indirect Tensile Strength
LTPP	Long-term Pavement Performance
LFWD	Light Falling Weight Deflectometer
LLI	Lower Layer Index
MDD	Multi Depth Deflectometer
MESA	Million Equivalent Standard Axles
MLI	Middle Layer Index
MLLE	Multi Layer Linear Elastic
ms	Milliseconds
PTR	Pneumatic Tyred Roller
RoC	Radius of Curvature
SR	Deviator Stress Ratio
TG	Technical Guidance
TMH	Technical Methods for Highways
TRH	Technical Recommendations for Highways
UCS	Unconfined Compressive Strength
UTM	Universal Testing Machine
TDR	Time Domain Reflectometry
SAMDM	South African Mechanistic Design Method
SANRAL	South African National Roads Agency
SAPDM	South African Pavement Design Method

### Symbols

$\sigma_1$	Principal stress 1
$\sigma_{1f}$	Principal stress at failure = $((1 + \sin\phi)\sigma_{2,3} + 2c\cos\phi)/(1 - \sin\phi)$
$\sigma_2$	Principal confining stresses 2,
$\sigma_3$	Principal confining stresses 3
c	Cohesion
$\phi$	Angle of internal friction
$SM_0$	Surface modulus directly beneath the load plate
$\sigma_0$	Peak stress beneath the load plate



$\mu$	Poisson's ratio
$a$	Load plate radius
$d_0$	Deflection at load plate

## **CHAPTER 1 INTRODUCTION**

### **1.1 Stabilised Pavement Materials in South Africa**

Currently in South Africa two methods of pavement layer, granular material stabilisation are commonly utilised; bitumen stabilisation and cement stabilisation.

Bitumen stabilised road pavement materials comprise of the application of bitumen and an active filler, typically cement or lime, to an aggregate. This addition of stabiliser and filler to the granular, aggregate material creates a bond between the aggregate material particles, creating a new composite granular material with an increased ability to carry traffic load when shaped, compacted and cured.

The addition of cement to granular material also creates bonds between the particulates of a granular material. These bonds however are believed to be more rigid and extensive when compared with those created within BSMs. A material with an increased strength is produced which enhances the materials ability to carry traffic load.

In South Africa today both stabilisation methods are utilised extensively. Typically BSMs are placed as the base layer and cement stabilised materials constructed as the base or sub-base layer within a pavement structure. In the case of a sub-base, cement stabilised materials act as the anvil for the compaction of an overlying granular high quality crushed stone base.

Both stabilised materials can be constructed by in-situ recycling and stabilisation of existing pavement layers, using road recycling equipment. Virgin aggregate can also be used by importation of the material to the road site and mixed with stabilisers on-site.

### **1.2 Structural Role of Pavement Layers within a Pavement Structure**

The structural performance of a pavement layer, within a pavement structure, constructed through the shaping and compaction of a material can be considered from two points of view:

1. How does the layer spread the load applied to it from above to the next supporting layer?
2. How does the layer perform under the stresses and strains that exist within it due to this applied load?

The first point relates to the effective stiffness of the constructed layers within the pavement system. A constructed pavement structure, comprising of a certain layered system, will reach a balance under loading where a regime of stresses and strains will exist within each constituent layer dependent on the geometry and stiffness of each layer.

This stress and strain condition, within each layer, will be repetitively induced under traffic loading. The resultant stress and strain condition within each layer will then induce damage within the layer. The mode of the damage induced within a layer is dependent upon the properties of the layer material. Current theories relating to the modes of material damage for various material types are listed below:

- Bituminous / asphalt material – Fatigue cracking, permanent deformation
- Granular material – Shear deformation
- Cement stabilised material – Fatigue cracking, crushing at top of base layer
- Bituminous stabilised materials (BSM) – Shear deformation / fatigue cracking

Two theories relating to the mode of damage within BSMs are listed. Two theories are considered due to the fact that the mode of BSM deterioration is disputed between that of shear deformation, for granular type materials or fatigue cracking as theorised for cement stabilised and asphalt materials.

The damage that occurs within each layer due to repeated wheel load repetitions on the pavement structure can have a direct impact on the stiffness of each layer. For example, materials with a critical damage mode of fatigue cracking, such as cement stabilised and asphaltic materials, a change in stiffness due to the occurrence of fatigue cracks within the material is expected. This resultant change in stiffness of a single layer within the pavement system has an effect on the distribution of stresses and strains occurring within each pavement layer within the pavement system. This stress/strain distribution alteration then influences the damage occurring within a pavement layer under the adjusted stress/strain condition within the pavement structure. Therefore the modelling of pavement structure layer stiffnesses and the damage occurring within it is a dynamic process where the two material properties, stiffness and damage level, are inextricably linked.

Granular material pavement layers show further complexity through stress stiffening and stress softening behaviour. Pavement layers made from such materials show varying layer stiffness dependent upon the magnitude of the stress occurring within the material.

When additional external factors are considered, the determination and modelling of the evolution of pavement layer stiffness, stress/strain condition and subsequent damage becomes even more complex. Such factors include:

- Environment (Moisture, temperature)
- Traffic loading variability

It must also be understood that the above framework for the structural functioning of layers within a pavement structure has not been proven in reality, on an actual road, under normal traffic loads, to a

high degree of confidence. The models used in the determination of the stresses and strains within the pavement structure and the subsequent damage induced within each layer, incorporate many assumptions and show varying levels of correspondence with the behaviour observed in real in-service roads.

Many of the models produced and utilised today to predict the performance of pavement materials were developed from testing carried out on road construction materials within a laboratory and under accelerated testing conditions. The connection between laboratory, accelerated testing observations and the reality of an actual in-service pavement structure is an on-going research initiative.

### **1.3 South African Pavement Design Method (SAPDM) and the R35 Experimental Section**

The South African National Roads Agency (SANRAL) in 2007 initiated the upgrade of the South African Pavement Design Method (SAPDM). This is an extensive project which includes the creation of an Information Technology (IT) framework for the collection and analysis of pavement construction and condition data for the purposes of pavement design and network management. Behind this IT framework, an overhaul of the underlying pavement material models is being conducted based on the results from extensive laboratory and in-service pavement testing.

One of the projects, forming part of the upgrade of the SAPDM, includes the R35 Experimental Section constructed at Bethal, Mpumalanga, South Africa. The purpose of the experimental section is to observe and determine the mode of damage within various stabilised material types and the effects of this damage on the effective stiffness of the experimental section pavement structure layers over a two year period of traffic load application. Models describing the performance of the stabilised pavement layers will also be created and form part of the SAPDM. Of particular interest on this experimental section was the performance of BSMs, their mode of damage and subsequent failure as this topic is eagerly disputed within the South African pavement engineering community. Data collected from this experimental section project is utilised in the study presented here.

### **1.4 Objectives**

#### **1.4.1 Back-analysis of Falling Weight Deflectometer (FWD) data**

A large amount of FWD data was collected as part of the R35 experimental section research project. As this data forms the backbone of the study presented here, it was imperative to determine as accurately as possible, the effective stiffness of the Cold In-Place Recycled (CIPR) stabilised base layer, within the tested experimental section with the data available at the time of analysis.

#### 1.4.2 Trends in stabilised base layer back-calculated stiffness over time

Utilise the back-calculated stiffness values determined for the CIPR stabilised base layer to determine trends or variability of the average back-calculated stiffness of each stabilised material, constructed to a single design specification, with time.

Identify possible influencing factors on the stabilised base layer stiffness trends observed with explanations as to why these factors may be influential. Also identify where observed trends may have no explanation, based on the available data, and propose factors and testing which may identify reasons behind trends observed.

#### 1.4.3 Spatial variability in back-calculated base layer stiffness

Quantify and visualise the variability or distribution in back-calculated stiffness of a pavement material constructed by CIPR to a single design specification. This variability relates to the variation in back-calculated stiffness within a quantity of material which was constructed to a single design standard and is expected to have, within certain limits, certain stiffness characteristics.

#### 1.4.4 Correlation between back-calculated base layer stiffness and engineering test results

Current pavement structural design methods are bending evermore towards mechanistic-empirical procedures. One of the most fundamental inputs to such design methods is pavement layer stiffness. It therefore seems reasonable to expect that the laboratory and site quality control tests which determine the final pavement material mix-design and quality of the constructed materials to have some relationship with the structural properties utilised in the design of the pavement structure, such as pavement layer stiffness. An investigation into the possible correlation between laboratory test methods utilised in the mix design and construction quality control with back-calculated stiffness of constructed pavement layers is required.

## CHAPTER 2 BACKGROUND

Based on the objectives and focus areas set out in Chapter 1 research was carried out based on the following reading plan. The information collected from this background study was used to guide in the analysis of the data collected and assist with the synthesis and interpretation of the analysis results.

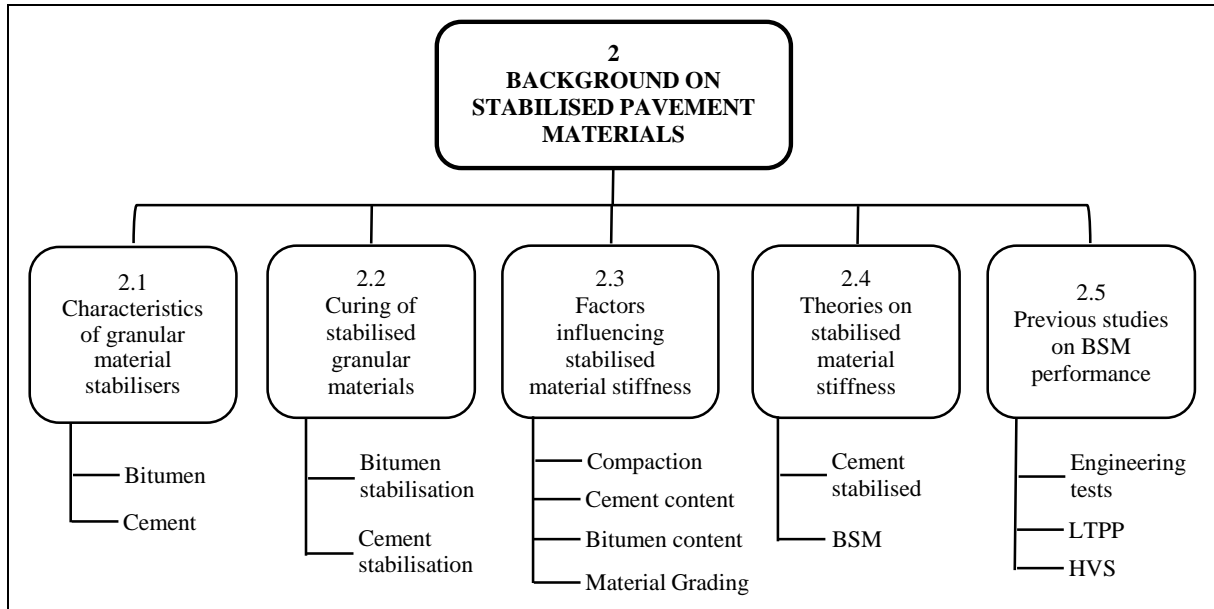


Figure 2.1: Outline of Chapter 2

### 2.1 Characteristics of Granular Material Stabilisers

#### 2.1.1 Cement stabiliser

Portland cement, which is often utilised to stabilise granular pavement materials, is created through the chemical combination of calcium carbonate, silica, alumina and iron ore within a kiln to produce clinker. The clinker is then ground to a fine powder with the addition of gypsum, to control the rate at which the cement will set when mixed with water. Supplementary materials, such as fly-ash, blast furnace slag and lime are often added to the Portland cement to alter the curing rate and long-term stiffness of the cementitious material produced.

#### 2.1.2 Bituminous stabiliser

##### 2.1.2.1 Bitumen emulsion

Bitumen emulsion comprises of fine droplets of bitumen dispersed within water along with the aid of emulsifying agents. For road stabilisation purposes the type of emulsion utilised is the oil in water emulsion type where bubbles of bitumen form the dispersed phase while water forms the continuous phase.

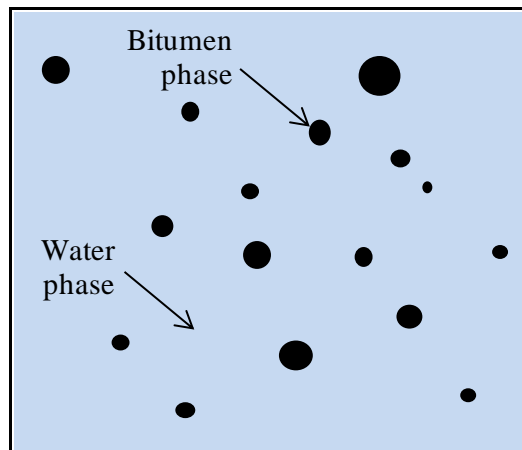


**Figure 2.2: Bitumen and water phases within bitumen emulsion**

With the creation of fine droplets of bitumen within the continuous water phase a significant interfacial area between the continuous water phase and the dispersed bitumen droplet phase is formed. The interfacial area is dependent upon the size of the dispersed bitumen droplets. To disperse the bitumen into droplets and hence create this large bitumen droplet surface area, a large amount of energy is required to form and maintain the droplet surface area and dispersion due to interfacial surface tension. Emulsifiers are added to the water, before the addition of bitumen, to reduce the energy required to disperse the bitumen within the continuous water phase and to maintain the bitumen droplets in a dispersed state.

Cationic and anionic emulsifiers are utilised to assist in the creation of bitumen emulsions. Emulsifiers have a molecular structure comprising of a hydrophilic head and hydrophobic tail. An emulsifier is termed cationic or anionic based on the charge of the emulsifier head. The hydrophobic part is also lipophilic, meaning that it is attracted to oil, in this case the bitumen droplets. The tail is adsorbed into the bitumen, dispersed phase with the hydrophilic head adsorbed into the continuous water phase.

As emulsifiers are insoluble in water, they need to be activated within the water phase before the introduction of bitumen. Anionic emulsifiers are neutralised with by the addition of basic compounds such as sodium hydroxide (NaOH), ammonium hydroxide (NH<sub>4</sub>OH) or potassium (kalium) hydroxide (KOH). Cationic emulsifiers are neutralised with acidic compounds such as hydrochloric acid (HCl), phosphoric acid (H<sub>3</sub>PO<sub>4</sub>) or sulphuric acid (H<sub>2</sub>SO<sub>4</sub>) emulsifiers.

The stability of the bitumen emulsion relates to the ability of the bitumen droplets to remain in a dispersed phase within the continuous water phase. The stability of the emulsion is dependent upon the quantity of emulsifier added to the water continuous phase. The stability of emulsions varies between rapid, medium and slow setting. The typical range of emulsion types are tabulated below.

**Table 2.1: Types of bitumen emulsion (Ebels, 2008)**

Head charge group	Grade	Type	Denotation
Anionic	Rapid setting	Spray	RS
	Medium setting	Pre-mix	MS
	Quick setting		QS
	Slow setting	Stable-mix	SS
Cationic	Rapid setting	Spray	CRS
	Medium setting	Pre-mix	CMS
	Quick setting		CQS
	Slow setting	Stable-mix	CSS

Bitumen emulsions are typically created by combining bitumen and the aqueous emulsifier solution within a colloidal mill. Mechanical energy is provided by means of an electrical motor which turns a rotor within a stator. A narrow gap exists between the wall of the stator and the rotor through which the bitumen and aqueous solution will flow and experience shearing forces. These shearing forces will break the bitumen up into droplets thus forming the dispersed bitumen phase within the water phase. The activated emulsifiers within the water will adsorb onto the surface of the bitumen, reducing interfacial tension between the bitumen and water phase reducing the shearing forces needed to disperse the bitumen.

#### 2.1.2.2 Foamed Bitumen

The current method of producing foamed bitumen involves the introduction of water, hot bitumen and air into an expansion chamber. The hot bitumen, at temperatures between 160 °C and 180 °C, enters the expansion chamber along with a fine mist of water, under a pressure of up to 5 bar, and air. Upon contact with the hot bitumen, the water vaporises and a volumetric expansion of the water occurs as it changes to a gaseous state. As this expansion occurs within the hot bitumen stream entering the chamber, foaming of the bitumen occurs and is subsequently discharged through the foaming nozzle. Figure 2.3 a diagrammatic representation of a foaming nozzle.



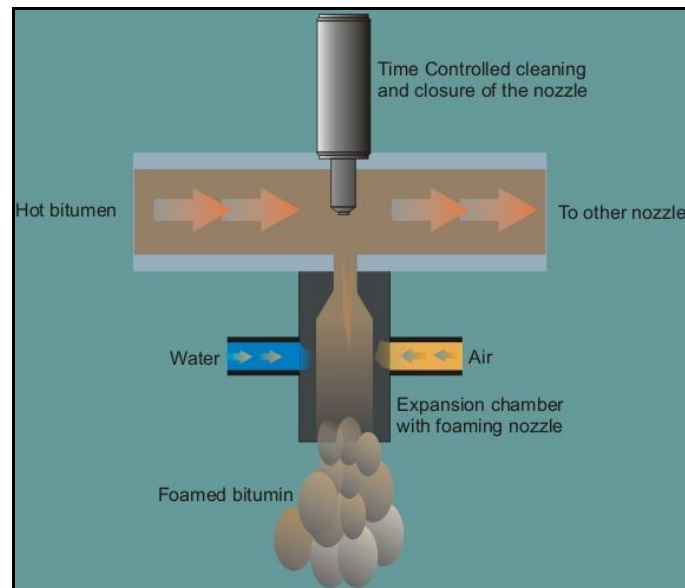


**Figure 2.3: Bitumen foaming nozzle (Romanoschi, 2003)**

The foaming of the bitumen is characterised by the expansion ratio and the half life time of the foamed bitumen. Expansion ratio is the ratio between the expanded foamed bitumen compared with the volume of the bitumen before foaming. The half life time relates to the time, in seconds, taken for the foamed bitumen to reduce from its maximum to half its maximum foamed bitumen volume (Jenkins, 2000).

### *2.1.2.3 Role of cement*

When stabilising granular material with bitumen, cement is often also added. The role of the cement filler and its effect on the performance of the BSM is disputed and two theories are proposed relating to continuous and non-continuously bound material models.

With respect to the continuously bound cement stabilised material theory the role of the active filler within purely cement stabilised materials is for the creation of cementitious bonds between the material granular particles thus improving the materials strength.

The role of the active filler within the granular type material theory of BSM performance varies between bitumen emulsion and foamed bitumen stabilisation. The cement filler in bitumen emulsion stabilised materials assists with the separation of the water phase within the emulsion to aid curing of the BSM. Within foamed bitumen stabilised materials the active filler is seen to aid in the transport of the bitumen droplets throughout the granular material (TG2, 2009).

## **2.2 Curing of Stabilised Granular Materials**

The mechanisms by which cement and bitumen stabilised materials gain strength over time are discussed.

### 2.2.1 Cement stabilisation

When water is added to Portland cement the calcium silicates within the cement hydrate to produce calcium hydroxide and calcium-silicate-hydrate (CSH). CSH gel is the fundamental bonding component responsible for the hardening and strength of cement stabilised granular materials. The process of cement hydration is termed curing. The strength of cement stabilised materials is dependent upon the water to cement ratio, extent of hydration and the environment, with respect to moisture and temperature, in which the curing process is taking place.

Factors influencing the rate of curing include chemical and environmental factors. The balance between dicalcium silicates  $(\text{CaO})_2\text{SiO}_2$  phase (slow curing) and tricalcium silicates  $(\text{CaO})_3\text{SiO}_2$  phase (rapid curing) will affect the rate and long term strength gain of the cement stabilised material. The interaction between sulphates and tricalcium aluminate  $(\text{CaO})_3\text{Al}_2\text{O}_3$  within the stabiliser, will also affect the early cementation strength. Secondary pozzolanic stabilisation occurs due to the production of hydrated lime which reacts with pozzolans within the granular material to produce a longer term stabilisation reaction. The secondary cementation process will continue over a long period once enough moisture is present within the stabilised material (Role of Portland Cement in Concrete, 2013).

The environmental influence on moisture content within the cement stabilised material will also affect the rate of curing. Increased levels of moisture will ensure that enough water is available for the hydration reaction of the cement and the maximisation of the granular material stabilisation. Temperature also affects the rate of stabilised material curing, with an increased rate of reaction observed with an increase in temperature (AusStab, 2012).

### 2.2.2 Bitumen stabilisation

The mechanism of curing inducing strength gain within BSMs, subsequent to their construction, is dependent upon the form of bitumen stabilisation utilised; foamed or emulsified bitumen.

The curing of bitumen emulsion stabilised material comprises of two phases; breaking and curing (TG2, 2009). The breaking of the bitumen emulsion involves the separation of bitumen particles, from within the emulsion water phase, to form bitumen films on aggregate particles. The curing of the stabilised material involves the removal of the remaining water phase resultant from bitumen particle flocculation. The coating of the aggregate particles within the granular material with bitumen, improves the cohesion of the granular material thus improving the materials ability to resist tensile and shearing forces. The reduction in volume of water within the material improves the friction between aggregate particles and releases further bitumen for aggregate coating and cohesion.

A curing phase is only present within the foamed bitumen stabilised material curing process. Water imparted to the hot bitumen, in order to expand and foam it, disperses the bitumen particles

throughout the granular material. The moisture utilised in the foaming process and present within the granular material, subsequent to mixing with the foamed bitumen, also acts an aid to the compaction of the stabilised granular material. Its removal from the stabilised granular material, subsequent to construction, occurs through evaporation. The reduction in moisture content reduces inter-particle lubrication, increasing friction, thus increasing material strength. The resultant dispersed bitumen throughout the granular material provides a bond between the granular material particles improving material cohesion and thus material strength.

### 2.3 Defining pavement layer stiffness

Pavement layer stiffness refers to the elastic modulus determined through the back-analysis of FWD deflection bowls measured on an actual pavement structure. The back-analysis method uses Multi Layer Linear Elastic (MLLE) theory to recreate the measured FWD deflection bowl within a pavement structure model representing the actual pavement structure. MLLE theory assumes that a pavement layer is homogenous, isotropic and performs linear elastically within the pavement structure model. As a result of this method the elastic moduli of each pavement layer within the pavement structure model can be estimated. The back-calculation of FWD deflection bowls is discussed in greater detail in Chapter 6.

The elastic modulus determined through this method is used to give an indication as to the resilient modulus of the pavement material present within a pavement layer. The difference between elastic and resilient modulus is illustrated in Figure 2.4. Typically the resilient modulus of a pavement material is determined in the laboratory through dynamic, repeat load triaxial testing.

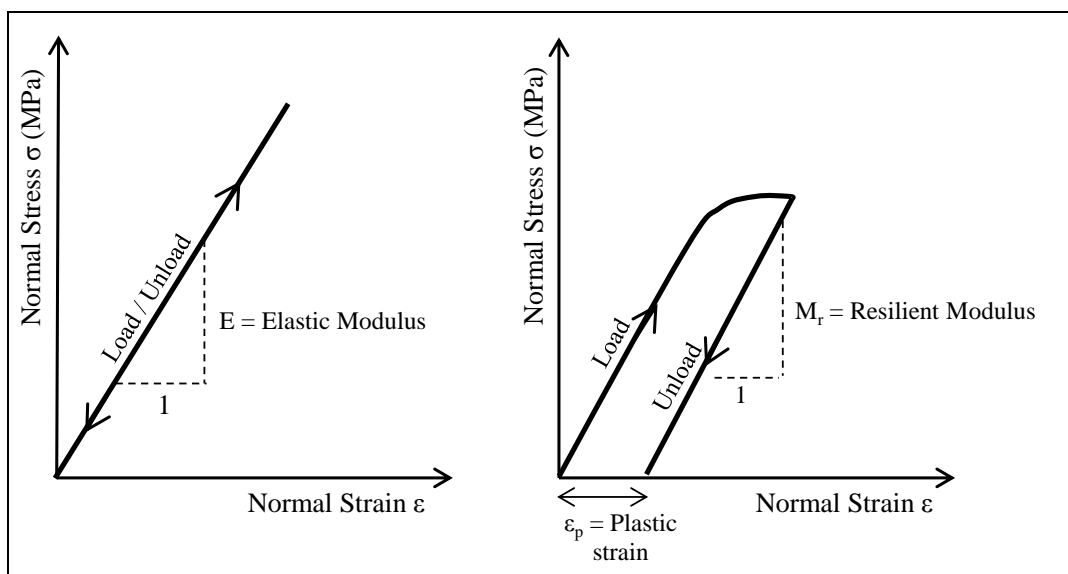


**Figure 2.4: Elastic and resilient modulus of a material**

The resilient modulus or back-calculated estimate of resilient modulus of a pavement layer material is used to determine the stress and strain occurring within a material under a wheel load through MLLE

theory. This pavement material response can then be input to empirical deterioration models to determine the extent of damage occurring within that material.

## **2.4 Factors Influencing Stabilised Material Layer Stiffness**

### **2.4.1 Compaction**

Compaction is the primary influencing factor on the strength and stiffness of an un-bound or bound granular material (van Niekerk, 2002). With increased compaction increased granular material shear resistance is provided. Compaction levels of 100% of the maximum dry density of the material compacted with modified AASHTO compaction energy is considered the standard for BSM 1 and BSM 2 materials (TG2, 2009).

### **2.4.2 Cement Content**

The recommended upper limit of cement content within BSMs is limited to 1% by mass, where the initial consumption of cement has already been satisfied (TG2, 2009). This quantity of cement or active filler is sufficient to provide for the effects described in section 2.1.2.3. Where cement contents in excess of 1% are introduced within BSMs, the character of the material begins to tend towards that of a cement stabilised, continuously bound material.

### **2.4.3 Bitumen Content**

Typical bitumen binder application rates utilised in South Africa range between 1% - 3% residual binder content. Imparting residual bitumen contents of less than 1.5% can be considered as material treatment rather than stabilisation aiding granular material compaction and improving the materials resistance to moisture ingress. With respect to constructability, minimum flow rates and pumping pressures of bitumen through the recycling machine are required for minimum levels of equipment performance. When pumping straight bitumen for the purposes of stabilisation with foamed bitumen, minimum bitumen contents of 1% are required to maintain the recycling machine at sufficient operational flowrates. When stabilising with bitumen emulsion lower residual bitumen contents are possible due to the water phase present within the emulsion. This allows for residual bitumen contents as low as 1% residual bitumen due to the presence of, typically 35% – 40%, water within the bitumen emulsion (Ebels, 2008).

Increasing the residual binder content within a BSM increases the material's cohesion, resistance to fatigue, durability and alignment with visco-elastic material characteristics. Increased residual bitumen contents however reduce the stabilised material's angle of internal friction.

#### 2.4.4 Material grading

Material grading is important for both the packing ability of the material under compaction and the interaction of the fine material with the bitumen stabiliser (TG2, 2009).

A material grading, tending towards that achieving the maximum packing density of the granular material, is suggested for BSM materials (TG2, 2009). In order to achieve maximum packing the grading, subsequent to in-situ recycling or in-plant processing, of the granular material should tend to follow the Nijboer grading curve. The Nijboer grading curve is described by the following relationship with  $n = 0.45$  for maximum granular material packing:

$$\% P = \left( \frac{d}{D} \right)^n \times 100 \quad \text{Equation 1}$$

% P = percentage material passing sieve size d

d = sieve size (mm) for which the percentage material passing the sieve is being determined

D = maximum sieve size (mm)

n = exponent of the power function (varies between 0.1 and 1)

This tight packing will allow for maximal interlock between the granular material particles but also provide greater contact points between the dispersed bitumen and the granular material particles (Jenkins, 2000).

The filler content, the granular material passing the 0.075mm sieve, should be in sufficient supply for BSMs. Stabilisation with bitumen emulsion allows for fines content of 2% minimum. As discussed previously in section 2.2.2, the residual bitumen in bitumen emulsion stabilised materials is understood to partially cover the larger particles thus providing cohesion. For foamed bitumen materials the fines content recommended increases to 5% as the fine material is utilised in the creation of a fines, bitumen and water mastic which is integral for binding the larger aggregate particles together.

### 2.5 Theories on the stiffness and performance of stabilised pavement layers

The main focus of the study presented here is to identify the stiffness development of stabilised materials, for both cement and bitumen stabilised materials, over a 360 day period in an accelerated testing experimental design setup. Current philosophies held with regard to the long term stiffness development of both cement and bitumen stabilised materials in South Africa are discussed below. The studies and experimental results which provide the foundation of these theories are then detailed.

### 2.5.1 Cement stabilised material

The trend in back-calculated stiffness of the cement stabilised layers is expected to follow the three phased stiffness-time profile proposed in the SAMDM (Theyse et al.,1996).

The current understanding of cement stabilised materials is that the initial rapid curing phase will climax and reach a peak stiffness value of between 3000 MPa to 4000 MPa at approximately 28 days after construction. Once traffic is applied, the first phase proposed by the SAMDM is that the cement stabilised layer will remain in an un-cracked condition for a short period of time. The second effective fatigue phase will initiate once cracks begin to form within the stabilised material. As the layer is now cracked the stiffness of the layer will reduce, the SAMDM proposes stiffnesses between 1500 MPa and 2000 MPa. This stiffness condition is expected to continue for the majority of the life of the stabilised layer. The final stage proposed is that of an equivalent granular phase. Within this period of the life of the stabilised layer it is believed that the cement stabilised material has cracked and broken down to such an extent that the pavement layer takes the form of a matrix interlocking blocks of stabilised material. The equivalent granular terminology may be misleading in this respect as the reversion of a cement stabilised material to a granular state has never been observed in reality. The effective stiffness provided by the stabilised layer in this condition is expected to be between 200 to 300 MPa. Figure 2.5 illustrates the expected long term stiffness behaviour of cement stabilised materials showing the three phases discussed.

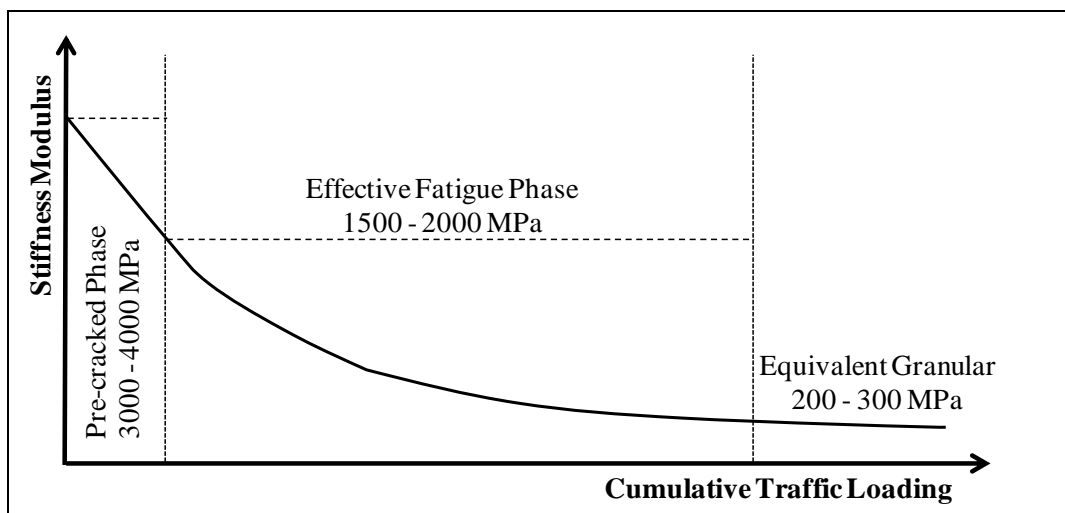


Figure 2.5: Long-term behaviour of cement stabilised material (Theyse et al, 1996)

### 2.5.2 Bitumen stabilised material

Two theories relating to the trend in stiffness of bitumen stabilised pavement layers, over its lifetime, are proposed within the South African pavement engineering community. Theory 1 predicts that the BSM behaves as a continuously bound, cement stabilised type material performing in a manner described in Figure 2.6 (Asphalt Academy, 2002).

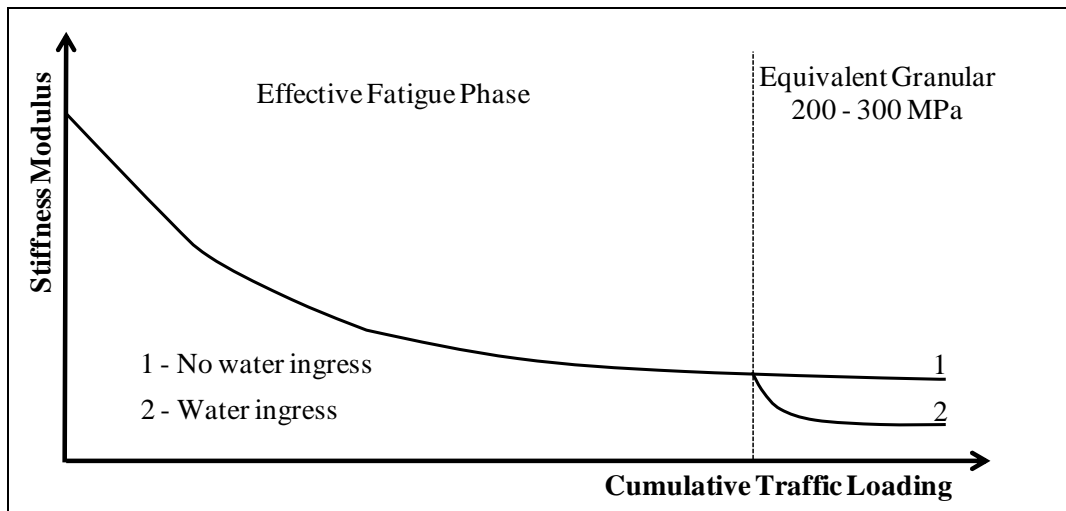


Figure 2.6: Long-term behaviour of BSM Foam materials (Asphalt Academy, 2002)

The opposing theory, Theory 2, predicts that BSMs perform as a non-continuously bound material, stress dependent material similar in character to granular material with additional cohesion provided by the bitumen. The curing period can continue for a significant period of time between 6 – 18 months (Ebels, 2008) after which stiffness reduction will occur with continued traffic loading. This stiffness development philosophy is depicted in Figure 2.7. The experimental and field studies utilised in developing the above philosophies are now discussed.

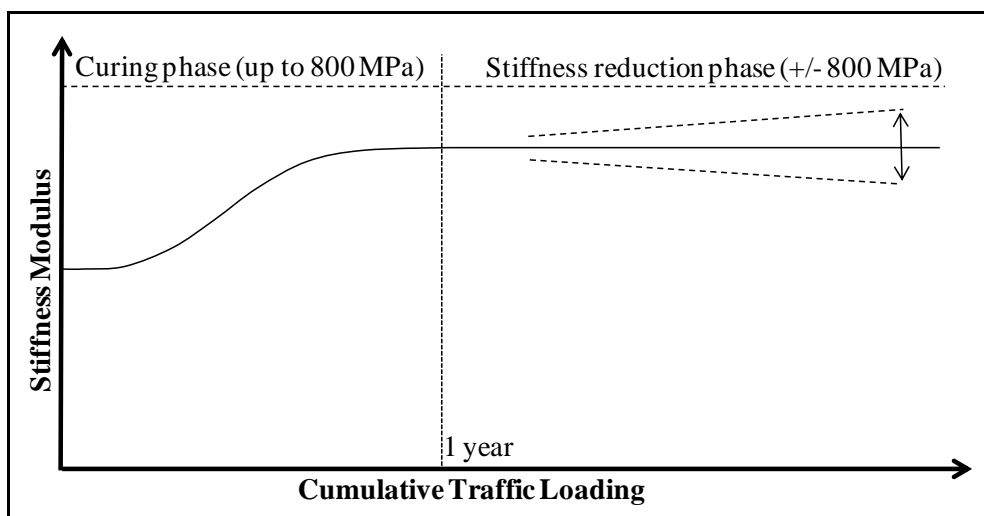


Figure 2.7: Long-term behaviour of bitumen stabilised materials (Ebels, 2008)

## 2.6 Studies on the stiffness and performance of stabilised pavement layers

The characterisation of cement stabilised materials and BSMs will be detailed by examining studies into the performance of these materials under various testing and monitoring procedures, these include engineering, laboratory, accelerated testing and observations from long term pavement performance (LTPP).

### 2.6.1 Engineering tests

Engineering tests include ITS (Indirect Tensile Strength) and UCS (Unconfined Compressive Strength) testing. Long et al (2004) detail the results from engineering tests carried out on samples of granular material, taken from the N7 HVS test site outside Cape Town, stabilised with various cement and bitumen contents. Foamed bitumen was applied to the granular material. The stabilised and tested granular materials were a crushed stone hornfels of G2 quality and a previously cement stabilised laterite gravel of G7 quality as classified by TRH 14 material classification (CSRA, 1985). Both materials satisfied the requirement of 5% fines content for foamed bitumen stabilisation. Results from UCS tests carried out on un-soaked specimens of both hornfels and laterite material samples indicated an increase in UCS values with the addition of cement alone. Where 1% cement is added along with 1% bitumen, the UCS of the laterite material reduced compared with material stabilised with 1% cement alone. Hornfels material, stabilised with 1% cement, did not show a reduction in UCS until 3% bitumen was added to the stabilised material. A similar trend was observed on the laterite material stabilised with 2% cement, as the bitumen content increased the UCS values decreased. The trend described above is shown in Figure 2.8

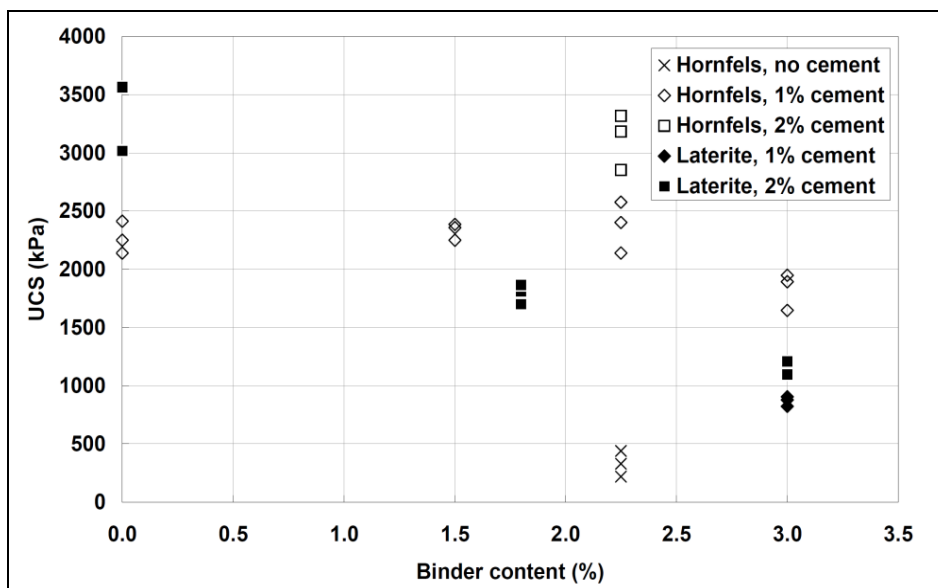


Figure 2.8: Effects of varying material type, bitumen and cement content on UCS (Long et al, 2004)

Results from ITS tests indicated that for laterite material with 1% cement content and increasing levels of bitumen content from 1.8% up to 4.2% the ITS values increased. Hornfels material showed a different trend with ITS values remaining constant for cement contents of 1% and bitumen contents up to 3%. The trends in ITS for both materials with varying stabiliser contents are described in Figure 2.9.



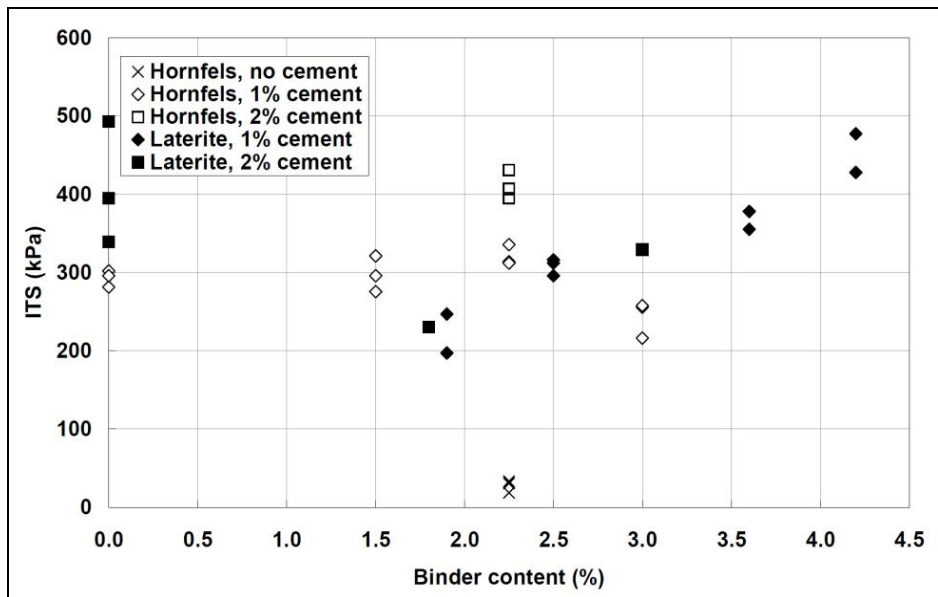


Figure 2.9: Effects of varying material type, bitumen and cement content on ITS (Long et al, 2004)

## 2.6.2 Long term pavement performance (LTPP)

### 2.6.2.1 Athens to Corinth Highway (Loizos & Papavasilou, 2007)

The 6-lane highway between Corinth and Athens was rehabilitated by CIPR with foamed bitumen at 2.3% residual bitumen and 1% cement. FWD measurements were taken along the highway over a four year period at intervals of 1 month, 6 months and each subsequent year since the BSM foam construction for a four year period. The results of the deflection measurements indicate that the deflection of the pavement structure decreased consistently over the four year period observed. An asymptotic curve describing the curing on subsequent performance of the BSM layer stiffness over time is proposed as the stiffness of the BSM foam layer increases due to curing and reaches a steady state stiffness under traffic loads.

### 2.6.2.2 Summary of LTPP Emulsion and Foamed Bitumen Treated Sections (Jooste & Long, 2007)

The most significant study currently available into the long term performance of BSMs, from actual in-service pavement performance data, was carried out by Jooste and Long (Jooste & Long, 2007). Their study consisted of the analysis of long term pavement performance data from 30 pavement structures, incorporating BSMs, throughout South Africa. The information collected included pavement construction, pavement performance indicators (DCP, deflections) and traffic accommodated. The analysis formed the basis for the Pavement Number method to determine the structural capacity of pavement structures. This method is incorporated within Technical Guidance 2 document (Asphalt Academy, 2009). Three sites investigated as part of the Jooste and Long study, which has similar construction aspects to the experimental section, forming the basis of this thesis, will be discussed. The sites selected and related details are tabulated below.

**Table 2.2: Selected road sections form Long and Jooste (2007)**

LTPP Section	Climate (Weinert)	Pavement Structure	Traffic (MESA)	Age (Years)
N1 Section 1 (Kraaifontein)	Moderate	80 mm Hot mix asphalt	12 - 16	21
		100 mm BSM Emulsion (1% residual bitumen)		
		100 mm C3		
		150 mm G5		
		G8 subgrade		
N1 Sections 13 (Springfontein to Trompsburg)	Dry	30 mm HMA + Seal	10 - 13	25
		150 mm BSM Emulsion (1% cement and 0.7% residual bitumen)		
		100 mm C3/C4		
		150 mm G6		
		Subgrade		
N3 section 4 (near Mooi River)	Wet	40 mm Hot mix asphalt	9 - 21	17
		200 mm BSM Emulsion (1.2% residual binder)		
		150 mm C3		
		Subgrade		

The construction of all of the above road sections consisted of the CIPR of an existing cement stabilised base layer with emulsion. The performance of the selected pavement sections with respect to deflection and DCP tests are discussed.

(a) *Deflection*

Observations from deflection data collected along the BSM pavements investigated showed relatively small increases in deflection subsequent to carrying significant traffic loads. The N1 Section 1 near Kraaifontein was reported as showing 95<sup>th</sup> percentile deflectograph readings of 365 and 499 microns in 1989 for the north and southbound lanes respectively, 5 years subsequent to construction. After 21 years of service pavement deflections of 413 and 320 microns were measured in the northbound lane by FWD.

Deflection measurements from the N1 Sections 13 taken in 1994 and 2006 show little change for deflection measurements taken in these years, with a maximum change in average deflection of 50 micron. An average deflection of 621 microns was determined in 1994 for both directions. In 2006 average deflection measurements of 613 and 659 microns were determined for the north and southbound lanes respectively.

The N3 Section 4 showed little decrease in deflection of the pavement structure over the service period between 1990 and 2004. In 1990 95<sup>th</sup> percentile deflection measurements were recorded at 238

micron by deflectograph on the southbound lane. FWD measurements from 2004 in the northbound report deflection measurements of below 200 micron. A direct comparison of northbound and southbound measurements is inaccurate. However due to the fact both lanes have the same pavement construction and subgrade and the northbound lane carries higher traffic loading than the south, the deflection measurement comparison is indicative.

(b) *Dynamic Cone Penetrometer (DCP)*

DCP measurements taken on the BSM emulsion pavement listed showed low penetration rates. For the DCP measurements taken on the N1 Section 1 pavement structure in 1989 penetration rates of 1mm/blow were observed. Penetration through the supporting cement stabilised sub-base layer was not possible due to its highly stabilised condition.

DCP tests taken on the N1 Section 13 showed that the BSM emulsion base was penetrated by the DCP.

DCP test taken in 1990 on the N3 Section 4 indicated low penetration rates in the BSM emulsion base layer while again no penetration was possible through the supporting cement stabilised sub-base layer.

Deflection measurements taken over the analysis period of the LTPP case studies discussed indicate that the stiffness of the pavement structures studied as a whole do not reduce significantly under traffic accommodated over the analysis period. Due to the fact that no significant pavement structure deflection reduction and thus pavement structure stiffness over the LTPP analysis period was observed it can be said that no stiffness reduction phase, as proposed within the three phase stabilised model described in section 2.5.1, occurred within the base layer or any other layer within the pavement structures studied.

The observations with respect to DCP deflection measurements indicate that the performance of the BSM emulsion base layers differ to that of purely cement stabilised materials. The low DCP penetration of the BSM emulsion layer early and later in the pavement service life indicates that it is in a less bound condition compared with purely cement stabilised materials through which the DCP could not penetrate in many cases.

### 2.6.3 Heavy Vehicle Simulator (HVS) accelerated pavement testing

Accelerated pavement testing with the Heavy Vehicle Simulator (HVS) induces accelerated deterioration of test pavement structures, on which the HVS unit is placed, through the repetitive loading of the test pavement by heavy wheel loads. The equivalency of the HVS heavy wheels loads to the axle loads typically experienced in the field is determined to allow for the comparison of HVS test results with real-life pavement structure and traffic loading situations. A number of HVS test sites, with emulsion or foamed stabilised pavement base layer materials, have been constructed

around South Africa. Two of these sites, one utilising foamed bitumen stabilisation and the other bitumen emulsion, will be discussed with respect to the development of stiffness within these layer of over time under HVS loading.

### 2.6.3.1 HVS site N2 Section near Kwelera, East London

Jordaan and Nienaber as modelled the structural behaviour of bitumen emulsion stabilised pavement layers from results of HVS testing carried out on the N2 Section near Kwelera, East London in 1987 (Jordaan, 2011). The pavement structure constructed comprised of that outlined in Table 2.3.

**Table 2.3: HVS test site pavement structure at N2 Section near Kwelera, East London**

Layer	Thickness (mm)	Materials
Surfacing	60	AG
Base	100	ETB (1% residual bitumen, 1% cement)
Sub-base	130	C4 (1.5% lime, 1.5% slagment)
Selected	100	G6 (Sandstone)
Subgrade	-	G8 (in-situ material containing clay)

Permanent deformation, the extent of cracking in the pavement and the deflections within each pavement layer, measured by the Multi-Depth Deflectometer (MDD), were recorded at various times during the repetition of various load levels. In order to account for the contribution of the reduction in stiffness of the asphalt layer to increased MDD measured deflections, incrementally reducing asphalt layer stiffnesses through the testing period were utilised in the back-calculation procedure. The maximum axle load applied was a 100 kN dual wheel load which was related to the effective standard 80kN axle utilising a load equivalency factor. The equivalency factor was determined in a similar manner to that established during the AASHTO road test as outlined below.

$$F = \left( \frac{P}{80} \right)^d \quad \text{Equation 2}$$

F = Load equivalency factor

P = Wheel load applied (kN)

d = Damage factor

The damage factor is determined by comparing the rate of deformation induced by the wheel load P with that of an 80kN standard axle. After the application of approximately 1.05 million equivalent standard axle load repetitions a significant reduction in stiffness of the bitumen emulsion stabilised layer was noted based on the back-calculation of MDD deflection measurements. This dramatic reduction in stiffness is purported to indicate a change in phase of the material from a bound material

to one cracked and broken up due to fatigue. No indication of the temperature of the pavement materials during the test period was given.

### 2.6.3.2 HVS site N7 near Cape Town

Theyse (2004) showed, from the analysis of MDD defections recorded on the N7 HVS site near Cape Town, an example of a foamed bitumen stabilised crushed stone base layer which exhibited a reduction in stiffness under traffic loading. The nominal test section pavement structure is depicted in Table 2.4.

**Table 2.4: HVS test site pavement structure at N7 near Cape Town**

Layer	Thickness (mm)	Materials
Surfacing	55	Novachip and HMA
Base	250	BSM foam (2.3% residual bitumen, 1% cement, crushed hornfels)
Sub-base	120	G3 (Hornfels)
Subgrade	-	G8 (Sand)

Asphalt temperatures measured during the testing period ranged between 12°C and 27°C. It was deemed unnecessary to correct observed deflections for temperature as no extreme temperature values were measured.

MDD deflections and their subsequent back-calculation showed an increase in stiffness of the BSM foam layer during the initial curing period however a significant drop off was observed once traffic was applied. The reduction in stiffness stabilised and a steady state was achieved after which no further stiffness reduction was observed even as increased wheel loads were applied. Theyse proposed that the reduction in stiffness was due to the breaking of the bituminous bonds between the particulates of the granular material, indicating a change in phase, and the reversion of the initially stabilised material to an equivalent granular state of constant stiffness. It was also shown that the stiffness of the combined support beneath the foamed bitumen treated base layer reduced significantly during the test period in-line with the base layer stiffness reduction.

The effective fatigue life, or time to change of phase, modelled for the foamed bitumen stabilised hornfels, under an 80kN wheel load, ranged between as  $2.2 \times 10^5$  and  $4.75 \times 10^5$  load repetitions and between  $5.42 \times 10^6$  and  $9.80 \times 10^6$  under a 40kN wheel load. The equivalency of the wheel loads applied was determined by Equation 2 as detailed in Section 2.6.3.1.

### 2.6.4 Summary

From engineering tests carried out on samples of bitumen stabilised materials as part of the N7 HVS investigation into the performance of foamed bitumen stabilised material it is clear that the cement and bitumen stabiliser contents have significantly different effects on the results of UCS and ITS tests. According to the study cited, increasing bitumen content reduced UCS and increased ITS of a

stabilised material at a constant cement content, while increasing cement content reduces ITS and increases UCS at a single bitumen content.

The results from HVS accelerated pavement deterioration testing on BSM materials indicate that these materials show stiffness reduction under traffic loading due to what is proposed as fatigue of the stabilised material and the breaking of bituminous, cohesive bonds within the stabilised layer.

In contrast to observations from HVS testing, studies by Jooste and Long (2007) on LTPP sections and Loizis and Papavasilou (2007) on the Athens to Corinth Highway on pavements in-service for a number of years, under normal traffic conditions, no stiffness reduction phase was observed. Deflection measurements, DCP penetration and visual assessments were utilised to substantiate this observation.

### CHAPTER 3 RESEARCH METHODOLOGY

In order to investigate and reduce the deficiency in knowledge regarding the performance and behaviour of stabilised pavement materials in the most efficient and productive manner the research methodology depicted in Figure 3.1 was implemented.

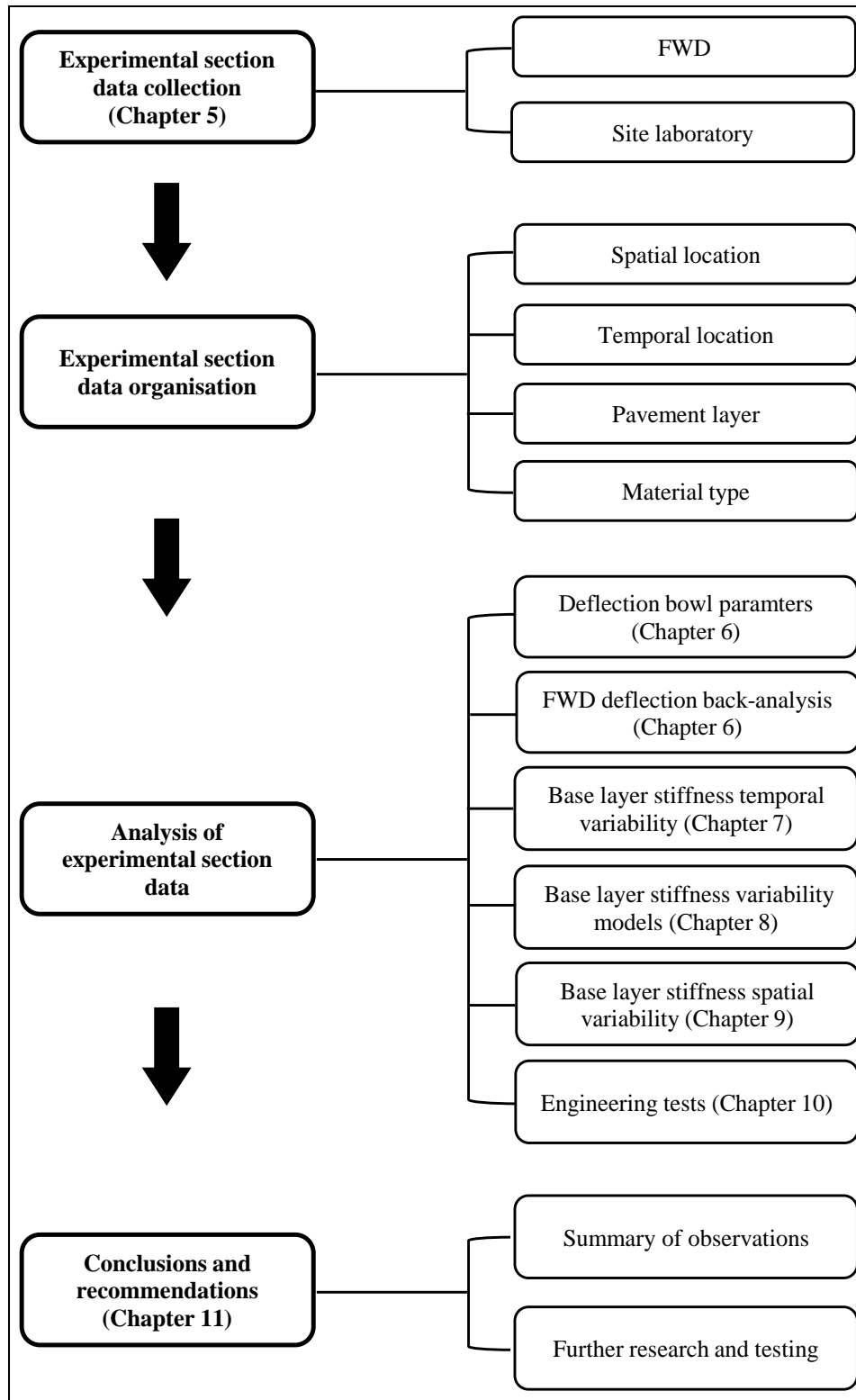


Figure 3.1: Outline of research methodology

### **3.1 Experimental section field and laboratory data**

#### **3.1.1 Data collection**

Data relating to the existing pavement condition before the construction of the experimental section were collected from the main rehabilitation project and experimental section design reports. Information describing the properties of the granular material from which the experimental pavement layers were constructed was determined from site laboratory testing which forms part of the construction quality control procedures on the constructed stabilised base layers. Pavement layer performance testing methods included the measurement of pavement structure deflection by FWD over a period of 1 year. This pavement testing apparatus is discussed in detail in Chapter 5.

#### **3.1.2 Data sorting and organisation**

Large volumes of data were collected from field and laboratory testing over the construction period and subsequent one and a half year performance monitoring period. The testing procedures to determine material and layer properties and performance over time are discussed in detail in Chapter 5.

Before any analysis was started the data set was sorted so that it was known to which experimental sub-section material type, pavement layer, spatial and temporal location each material property value measured was associated with. This sorting process allowed for the easy referencing of data as required by the proposed methods of analysis to follow.

### **3.2 Experimental section data analysis**

#### **3.2.1 Deflection bowl parameters**

A common method of analysis of FWD deflection bowls is the determination of deflection bowl parameters. These parameters are determined by isolating sections of the deflection bowl which represent the contribution of segments of the pavement depth to the deflection bowl measured. Radius of Curvature (RoC), base (BLI), middle (MLI) and lower (LLI) layer indices are determined

#### **3.2.2 Back-calculation**

The primary parameter under investigation in this study was the back-calculated stiffness of in-situ recycled and stabilised granular pavement materials. The back-calculated stiffness of a pavement layer was used to estimate the resilient modulus of the pavement layer material within a pavement structure. It is widely used for assessing the structural capacity of a pavement structure by determining the response (stress/strain) of the pavement structure under wheel loads and their input into empirical deterioration models.



Pavement layer stiffnesses were determined from the FWD deflection bowls measured at 5m intervals along each experimental sub-section and at various temporal intervals. The complete testing schedule is attached in Addendum A. Through the back-calculation of the measured deflection bowls a stiffness value for each layer within the pavement structure, at each location where FWD testing was carried out, was determined. Due to the complexities in existing and experimental pavement structures encountered assumptions relating the back-calculation procedure utilised were made and their effects on the analysis results investigated. The back-calculation process and the tools utilised in this analysis are discussed in detail in Chapter 6.

The back-calculated stiffness values were compared with pavement deflection parameters to investigate the correlation between the elaborately determined back-calculated layer stiffnesses and more fundamental pavement deflection parameters (RoC, BLI, MLI, LLI) which in essence are representing the same base layer property. While a trend between these parameters would be expected as the stiffness is back-calculated from the deflection data, this analysis does assist in ensuring that there are no large errors in stiffnesses determined from the back-calculation process.

### 3.2.3 Visualisation of trends in stabilised base layer stiffness over time

Subsequent to the back-calculation of pavement layer stiffness values, for the pavement structures, and their constituent layers, at each FWD tested location, the trends in average stiffness per experimental sub-section over time were determined. The analysis focuses on the average stiffness trends within the in-situ recycled and stabilised base layers. The development of the stabilised base layer stiffness within each experimental sub-section over the initial curing period and the subsequent period where the experimental section is opened to traffic and moving wheel loads are applied to the pavement structures is considered.

In addition to displaying the observed trends in the base layer stiffness values back-calculated, supplementary data collected from the site laboratory and the experimental construction record are utilised to intimate a possible reasoning behind the observed stiffness trends. This comparison was achieved by attempting to correlate the trends in stiffness with the trends observed in the supplementary data set which are expected to have some relationship to the stiffness of stabilised granular base layer material. This analysis is discussed in detail in Chapter 5.

### 3.2.4 Visualisation of spatial variability in stabilised base layer stiffness

An analysis of the distribution of FWD deflection data collected and the subsequently back-calculated pavement layer stiffnesses along the length of each experimental section was conducted and is presented in Chapter 8. The variability of the pavement deflection parameters and the back-calculated pavement layer stiffnesses per experimental sub-section are summarised along with a deeper investigation into possible reasoning behind the variability observed in the data collected along the

length of each experimental sub-section. Material properties such as moisture content and granular material grading, determined by the site laboratory, are utilised in the investigation into the causes of pavement deflection and layer stiffness variability. The effect of the observed variability on the results and recommendations formulated through typical pavement design methods utilised in South Africa today was also investigated.

### 3.2.5 Correlation between laboratory and field testing results

The ITS and UCS of laboratory prepared samples of the in-situ recycled and stabilised pavement material were determined at a number of locations along the experimental section. These laboratory determined strength parameters of the various stabilised materials were compared with the stabilised base layer stiffness values determined along the experimental section.

### 3.2.6 Conclusions and recommendations

A synthesis of the analysis results from the topics discussed above was developed which attempted to indicate whether the observations made had any significant influence on our understanding and modelling capabilities of cement stabilised and BSM pavement layers. By comparing the objectives outlined in Chapter 1 and the results of analyses carried out in the following chapters, an assessment of whether the set objectives had been fulfilled was made.

Based on the knowledge gained as a resulting of the study outlined above, recommendations on additional testing or information which it is proposed would enhance our understanding of the load spreading capability of cement and bitumen stabilised materials during curing and under traffic loading was made. This further testing or information required was identified based on gaps in the data set or unknown variables which were seen to be influential on the analysis results.

## CHAPTER 4 R35 EXPERIMENTAL SECTION LAYOUT, DESIGN & CONSTRUCTION

Figure 4.1 outlines the topics covered in this chapter. The aim of the material presented here is to provide the reader with background to the location and environmental condition in which the experimental section is situated. Information relating to the condition of the pavement structure present before the construction of the experimental section is also discussed.

The R35 experimental section design report (Theyse, 2013) is referred to in many instances throughout Chapter 4 in order to give background to the pavement design process and analyses which were carried out to determine the experimental pavement structures and stabilised material mix design.

Background to the methods utilised for both the construction of the in-situ recycled base layer and wearing course is provided.

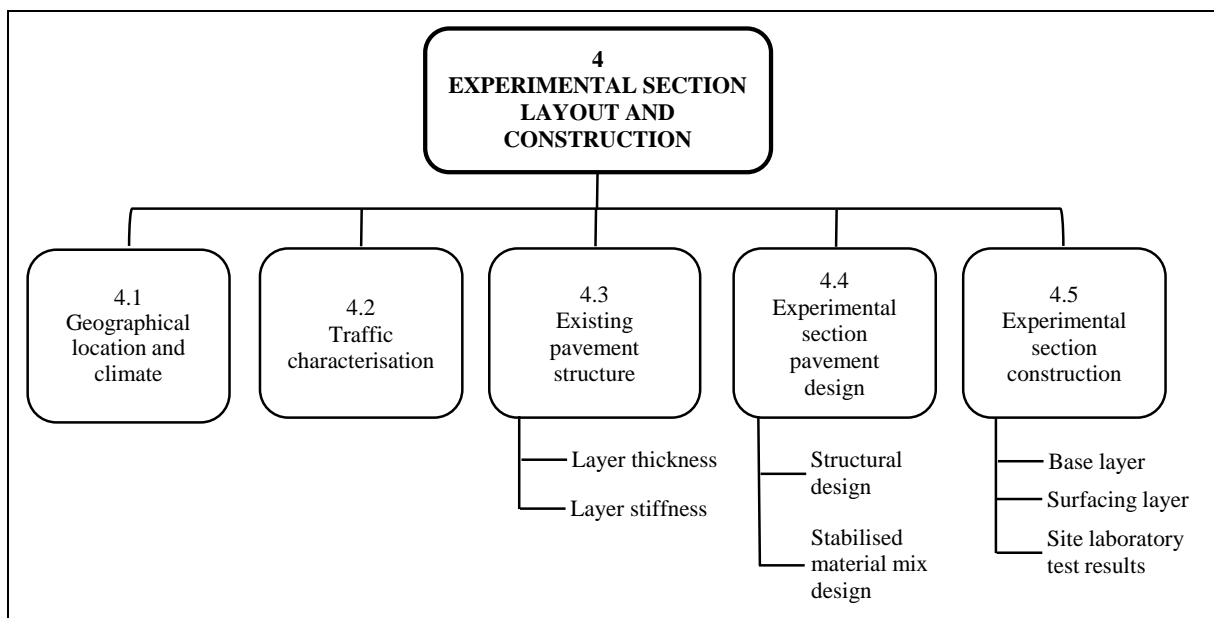


Figure 4.1: Outline of Chapter 4

### 4.1 Geographical location and climate

The section of road identified for the construction of the experimental section to be studied lies approximately 5km to the north of Bethal, Mpumalanga, South Africa. The experimental section was selected and isolated from a larger rehabilitation project encompassing 74.3 kms of the R35 from km 0.0 at the intersection of the R38 with the R35, north of Bethal, to km 74.3 at Middleburg. The larger and original rehabilitation project will be referred to as the main rehabilitation project within this study. The experimental section spans 5kms from chainage km 5.5 to km 10.0 along the R35. Both northbound and southbound carriageways were constructed to an experimental section pavement

design and will be monitored, through various testing procedures, over a period of two years. Its geographical location is depicted in Figure 4.1.



**Figure 4.2: Location of R35 Experimental Section**

The climate in this region is classified as ‘moderate’ as identified within TRH 4’s macroclimatic regional classification, adapted from Weinert (1980). The Weinert N-value for such a region lies between 2 and 5 which indicate that the weathering of rock materials will be due to mechanical mechanisms during drier months and chemical means during warmer, wetter months. According to the modified Thornwaite Moisture Index (Leyland & Paige-Green, 2010) the experimental section falls within a region with a modified Thornwaite Index of 0 – 20, classifying the locality as having a moist sub-humid climate.

Weather data obtained from the Bethal weather station, spanning a 26 year period from 1962 to 1998, is utilised to give insight into the historical rainfall and temperature statistics in the locality of the town of Bethal. In addition to the weather station historical data, rainfall and temperature data were collected at the construction site office located to the north of Bethal on a daily basis.

Measured and historical temperature data are depicted in Figure 4.3 below. Comparing historical and measured temperatures values it is apparent that the monthly average maximum temperatures over the majority of the year 2012 do not correspond with historical average monthly maximums therefore indicating that 2012 was an exceptionally warm year. Measured average monthly minimum temperatures are in-line with historical temperatures. Figure 4.4 depicting measured and historical average monthly rainfall values indicate that rainfall below historical levels have fallen over the late

2011 to early 2013 period however the rainfall pattern and month of occurrence follow the historical trend.

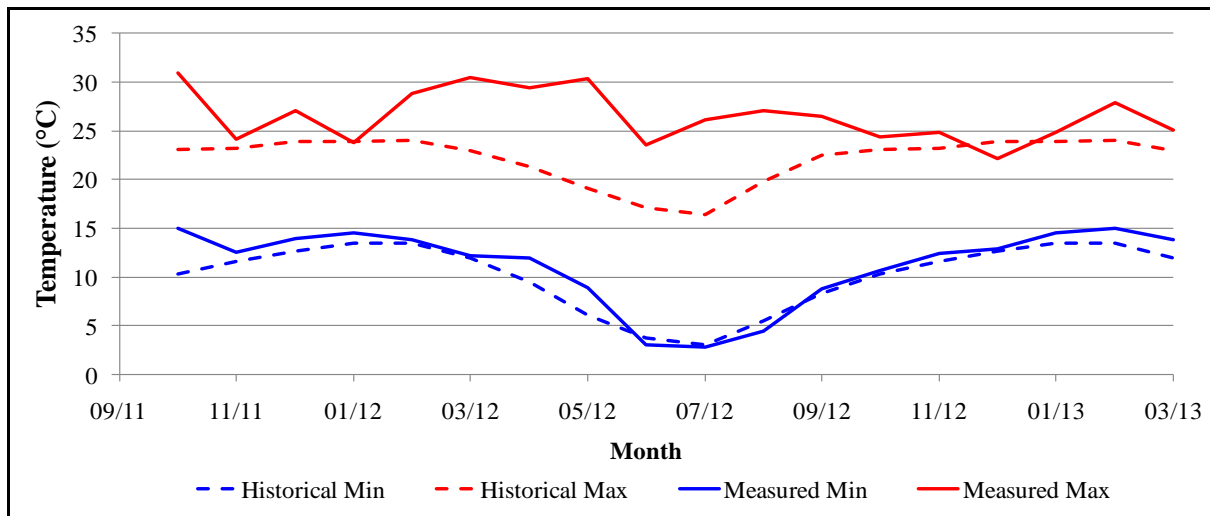


Figure 4.3: Measured and historical average monthly maximum and minimum temperatures

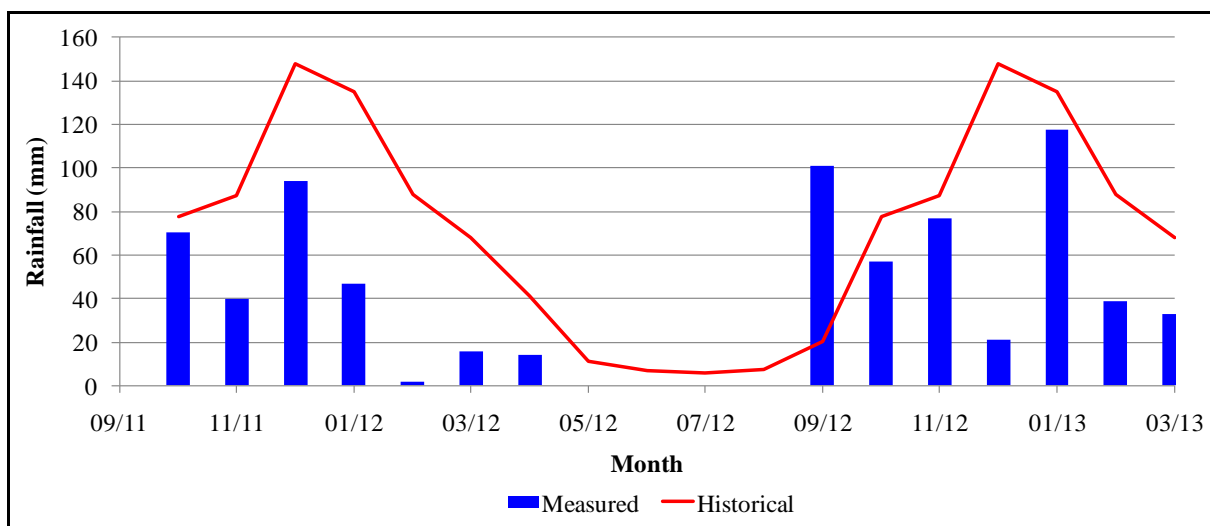


Figure 4.4: Measured and historical average monthly rainfall

## 4.2 Traffic Loading

Information from the R35 main rehabilitation project design report is utilised to characterise the traffic loading on the R35 experimental section. WIM (Weigh In Motion) stations were constructed on the experimental section however data from the WIM was not available at the time of compiling this thesis.

A traffic counting station (P579) to the north of Bethal, in 2010, recorded an average daily truck traffic volume of 610 and 700 vehicles per day in the northbound and southbound lanes respectively. Assumptions on heavy vehicle axle loads resulted in the use of the same E80 per heavy vehicle factor

in both the northbound and southbound lanes. Table 4.1 lists the traffic parameters and values used in determining the design traffic load.

**Table 4.1: Characterisation of traffic on the R35 - P579 counting station**

Lane	NB	SB
Average Daily Traffic (ADT)	1651	1769
Average Daily Truck Traffic (ADTT)	610	700
E80s / HV	1.9	1.9

The design traffic used in the pavement rehabilitation design for the main R35 project was based on the higher traffic volume counted in the southbound lane. For an 8 year design period and 4% truck traffic growth rate, a design traffic of 6.5 million E80s was determined. For the 2 year design period specified in the experimental section design a traffic load of 1.1 million E80s is predicted using the P579 counting station data and 4% traffic growth rate.

### 4.3 Existing Pavement Structure

Information relating to the existing pavement structure along the experimental section before the construction of the experimental pavement structures was sourced from the main rehabilitation project and the experimental section design documents.

#### 4.3.1 Layer thickness

Existing pavement structure materials information was taken from the design reports prepared for the main rehabilitation project by Stewart Scott International (now Royal HaskoningDHV) and Bigen Africa. Test pits excavated as part of the rehabilitation design were utilised in gaining insight into the material properties of the existing pavement structure. Observations from the test pit investigations concluded that the existing base layer was highly stabilised dolerite gravel, the sub-base a broken-down stabilised dolerite gravel and the subgrade a dolerite gravel. The original surfacing was a chip and spray seal. It is also apparent from the test pit information that the existing surfacing, base and sub-base layers were constructed upon a pre-existing pavement structure also comprising of a stabilised base and sub-base construction. The pavement structure layer thicknesses from the available information are depicted in Figure 4.5 and Figure 4.6.

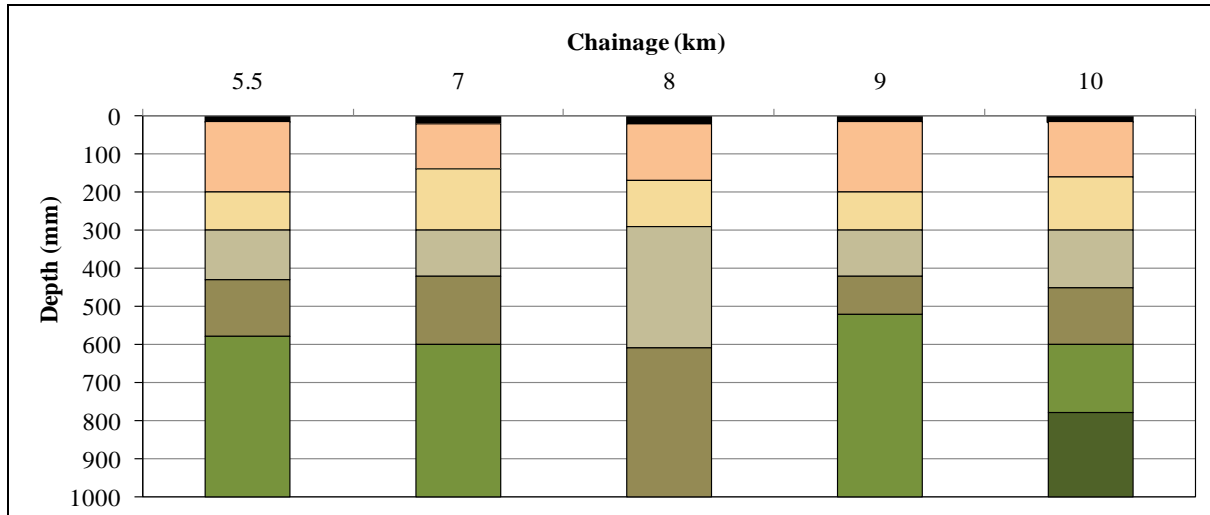


Figure 4.5: Test pit profiles - southbound

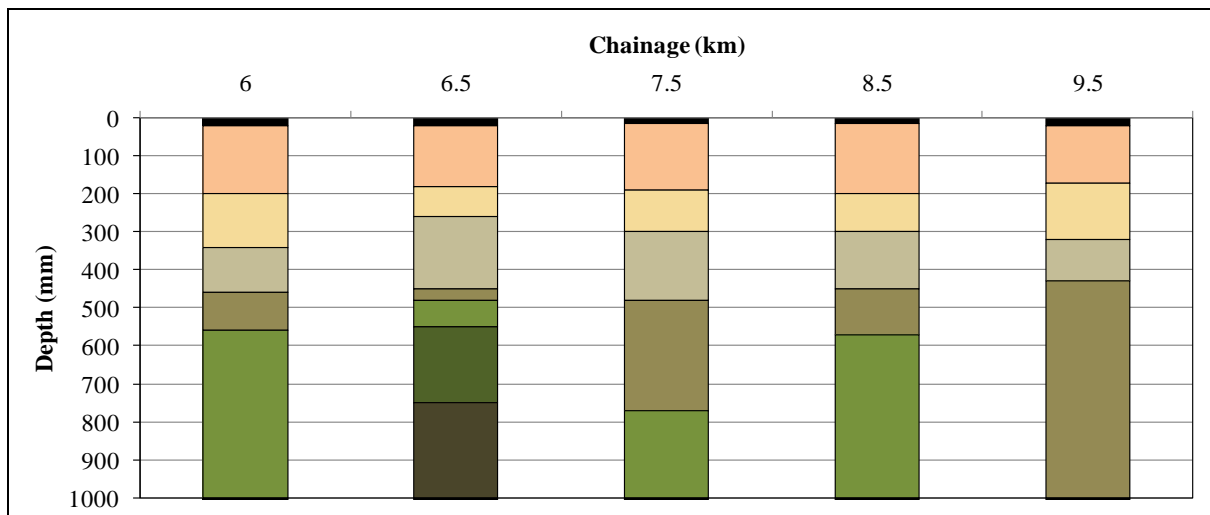


Figure 4.6: Test pit profiles - northbound

The average layer thickness determined from the test-pit data depicted in Figure 4.5 and Figure 4.6 are outlined in Table 4.2 for the top five layers recorded at each test-pit location.

Table 4.2: Existing pavement layer thickness summary statistics

Layer	Southbound		Northbound	
	Average (mm)	CoV (%) n = 5	Average (mm)	CoV (%) n = 5
1	17	16	18	15
2	157	18	170	9
3	124	21	116	25
4	168	51	150	24
5	194	58	222	98

#### 4.3.2 Layer stiffness

For the experimental section design, FWD testing and core samples were taken along the length of the proposed experimental section (Theyse, 2013). The milling out of some of the in-situ base material for

the purposes of stabilised material mix design took place at km 6.440 in the southbound lane. FWD tests were taken at the location of this bulk sampling on top of the original pavement surface and on-top of the pavement sub-base subsequent to milling out of the base. For the back-calculation of the pavement layer stiffnesses the base layer was split into two 110mm thick layers in order to investigate the stresses and strains occurring in the top and bottom half of the base layer (Theyse, 2013). According to Theyse (2013) the result of this analysis corresponded with the observations made during test pitting and sampling carried out for the main rehabilitation project, that the existing pavement structure comprises a well bound cement stabilised base and poorly bound, broken-down cement stabilised sub-base. The reference to a poorly bound sub-base describes a previously cement stabilised material now in a broken-down and interlocking matrix of stabilised granular material segments. Stabilised material, extracted through coring during the design phase, in a broken-down condition, is depicted in Figure 4.7.

The back-analysis of the FWD measurements taken on the original pavement structure indicates that the sub-base stiffness values are extremely low. Theyse (Theyse, 2013) relates this low stiffness in the lower base and sub-base to its cracked, deteriorated condition as depicted in Figure 4.7 and the stress/strain distribution created by the FWD load within the pavement structure. The hypothesis is that the broken-down cement stabilised material occurring within a zone experiencing tensile strains will provide little resistance hence contribute little to the stiffness of the pavement, see Table 4.3. This stress/strain dependency of the back-calculated stiffness of the broken-down cement stabilised material is according to Theyse (2013) corroborated by FWD tests carried out upon the existing sub-base after the milling and removal of the existing surfacing seal and base layer. The subbase layer stiffnesses back-calculated in this situation are much greater, see Table 4.4. Theyse (2013) relates this increased stiffness to the compressive stress/strain environment in which the sub-base layer is present, forcing the broken-down cement stabilised material blocks of the sub-base together.





Figure 4.7: Broken-down cement stabilised granular material (Theyse 2013)

Table 4.3: Original pavement layer back-calculated stiffnesses – FWD on base (Theyse 2013)

Layer	Layer Thickness (mm)	Back-calculated Stiffness (MPa)		
		Minimum	Average	Maximum
Surfacing and Upper Base	110	761	1276	2163
Lower base	110	32	78	172
Sub-base	110	18	31	49
Semi-infinite Subgrade	infinite	177	211	239

Table 4.4: Original pavement layer back-calculated stiffnesses – FWD on sub-base (Theyse 2013)

Layer	Back-calculated Stiffness (MPa)		
	Minimum	Average	Maximum
Sub-base	261	526	839
Upper subgrade	70	137	195
Lower subgrade	23	28	39
Semi-infinite subgrade	210	221	239

In addition to FWD testing along the 12 metre milled section at km 6.440 further testing at 5m intervals was carried out in both the north and southbound lanes for the structural design of the whole experimental section between km 5.0 and km 10.0. The results of the back-calculation of this deflection data are summarised in Table 4.5 and Table 4.6. The splitting of the existing base layer into two sub-layers was also conducted for the back-calculation of this FWD data.

**Table 4.5: Existing pavement back-calculated stiffnesses –km 5.0 to km 10.0 northbound (Theyse 2013)**

Layer	Layer Thickness (mm)	Back-calculated Stiffness (MPa)	
		Average	Standard Deviation
Surfacing and Upper Base	110	2214	1552
Lower base	110	132	132
Sub-base	110	89	72
Semi-infinite Subgrade	infinite	255	38

**Table 4.6: Existing pavement back-calculated stiffnesses –km 5.0 to km 10.0 southbound (Theyse 2013)**

Layer	Layer Thickness (mm)	Back-calculated Stiffness (MPa)	
		Average	Standard Deviation
Surfacing and Upper Base	110	1602	1019
Lower base	110	90	82
Sub-base	110	75	79
Semi-infinite Subgrade	infinite	234	36

#### 4.4 Experimental Section Pavement Design

The purpose of constructing and subsequent performance monitoring of the experimental sections was to understand and model the long-term performance of purely cement stabilised materials and bitumen stabilised materials (BSM). The material properties of the pavement structures which were eventually constructed as the experimental section were determined through structural design and stabilised material mix design processes. Both design processes were conducted by Theyse and are detailed in the R35 experimental section design document (Theyse, 2013). Summaries of both are presented here.

##### 4.4.1 Structural Design

The basic format of the pavement structure to be constructed within the experimental section is shown in Figure 4.8. A number of sub-sections with varying structure and material properties were to be constructed within the experimental section. The base layer properties which were varied in order to investigate the behaviour of stabilised pavement material performance are listed:

- Layer thickness
- BSM active filler / cement content
- Bitumen introductory form (Emulsion / Foam)
- Residual bitumen content

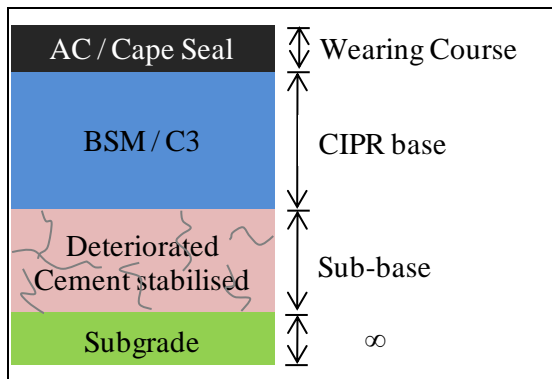


**Figure 4.8: Experimental section pavement structure**

The bituminous surfacing layer type is also varied in order to investigate the degree of crushing at the top of the stabilised layer at the high stress interface between the bituminous surfacing and base layer directly beneath the wheel load. This aspect is not considered in this study and is noted as surface layer type will affect the analysis of data collected from the experimental test section.

The aim of the experimental pavement structural design process was to specify pavement structures which would show measurable levels of distress under a traffic load of 2 million equivalent standard axles. This relates to approximately a two year period for traffic load levels and quantities estimates along the R35. This setup is expected to produce a form of accelerated pavement deterioration under normal traffic loading conditions.

For each stabilised material type a Monte Carlo Simulation of the structural capacity analysis of a selection of pavement types was carried out by Theyse (2013). This simulation takes input values, at random, from the user defined distribution to determine the stresses and strains occurring at pertinent locations within the pavement structure and their input into the appropriate material deterioration models. This simulation will produce a distribution of pavement bearing capacities based on the input variable distributions specified. From this pavement bearing capacity distribution the level of risk or the extent to which a certain mechanism of deterioration will occur after a specific cumulative traffic load, applied to the pavement, can be estimated.

The cement stabilised base layer parameters input to the structural analysis include:

- (i) Thickness: An average base layer thickness of 200mm, along with a typical standard deviation, was utilised in the analysis.
- (ii) Resilient Modulus: An average cement stabilised layer modulus dependent upon the cement content to be utilised was estimated along with a typical standard deviation.
- (iii) Poissons Ratio: Typical average and standard deviation values for cement stabilised material are used.

Deterioration models describing the development of three mechanisms of distress are used with inputs of stresses or strains from the structural analysis. The cement stabilised material properties considered in the refinement and application of the deterioration models are given in brackets:

- (i) Crush Initiation (Unconfined Compressive Stress (UCS))
- (ii) Stiffness Reduction (Strain-at-Break)
- (iii) Permanent Deformation (Cohesion, Angle of Internal Friction)

A similar approach as described above was utilised in the assessment of the structural capacity of the design pavement structures with a bitumen stabilised base layer. For the bitumen stabilised base layers two scenarios are considered for both foam and emulsion stabilised materials. EB 2 and FB2 are characterised as stiffer mixes with higher residual bitumen content and lower cement content when compared with the more flexible mixes EB4 and FB4.

**Table 4.7: BSM materials modelled in structural analysis**

<b>Identifier</b>	<b>Bitumen form</b>	<b>Residual bitumen (%)</b>	<b>Cement content (%)</b>
EB2	Emulsion	2	1.5
FB2	Foam	2	1.5
EB4	Emulsion	3	1
FB4	Foam	3	1

The same layer properties, as for the cement stabilised analysis, were utilised and varied within the Monte Carlo simulation of the structural analysis of the BSM layers:

- (i) Thickness: An average base layer thickness of 200mm, along with a typical standard deviation, was utilised throughout the analysis.
- (ii) Resilient Modulus: An average bitumen stabilised layer modulus dependent upon the cement and bitumen content to be utilised was estimated along with a typical standard deviation.
- (iii) Poisson's Ratio: Typical average and standard deviation values for cement stabilised material are used.

Two mechanisms of distress were considered for BSMs however:

- (i) Stiffness Reduction (Strain-at-Break)
- (ii) Permanent Deformation (Cohesion, Angle of Internal Friction)

The applicability of a fatigue or stiffness reduction distress mechanism is questioned by Jenkins et al (2007) who propose that a granular material type, stress dependent, permanent deformation deterioration model should be used.

The Monte Carlo simulation of the structural analysis carried out by Theyse (2013) determined the risk of the selected distresses relevant to BSMs occurring within the pavement structures modelled. The calculated risks for crushing on cement stabilised materials and stiffness reduction on all material types with an asphalt overlay are tabulated below.

**Table 4.8: Crushing and stiffness reduction Monte Carlo simulation results (Theyse, 2013)**

Surfacing	Material Type	Mix Description	Thickness (mm)	Distress Risk %	
				Crushing	Complete Stiffness Reduction
45mm Asphalt	Cemented	Stiff and Brittle	150	13%	73%
			175	14%	53%
			200	15%	23%
	Foam	FB2 - Less flexible mix higher shear strength	150	-	23%
			175	-	6%
			200	-	1%
		FB4 - Flexible mix with lower shear strength	150	-	20%
			175	-	5%
			200	-	1%
	Emulsion	EB2 - Less flexible mix higher shear strength	150	-	20%
			175	-	4%
			200	-	1%
		EB4 - Flexible mix with lower shear strength	150	-	32%
			175	-	9%
			200	-	2%

The expected level of permanent deformation or rutting induced within the pavement over the 2 year performance monitoring period for all material types with a base layer thickness of 200mm are shown in Table 4.9.

**Table 4.9: Permanent deformation Monte Carlo simulation (Theyse, 2013)**

Surfacing	Base Layer	Rut (mm)		
		Minimum	Average	Maximum
45mm Asphalt	C3	0.1	0.2	0.4
	FB 4	0	0.2	26
	FB 2	0	0.1	0.4
	EB 4	0.4	1.1	2.6
	EB 2	0.2	0.5	0.9
Cape Seal	C3	0.1	0.2	0.4
	FB 4	0	0.3	3.6
	FB 2	0	0.1	0.5
	EB 4	0.4	1.1	2.3
	EB 2	0.2	0.5	1

#### 4.4.2 Stabilised material mix design

The experimental mix design was carried out for the three forms of stabilisation to be utilised in the recycling of the base layer of the experimental section, namely cement stabilisation and bitumen stabilisation using either foamed or emulsified bitumen. The cement stabilisation mix design was carried out at the CSIR, Pretoria and bitumen stabilisation at the University of Stellenbosch. A bulk sample of material was sampled from the existing base layer at the experimental site location and utilised in the cement and bitumen stabilised material mix design. Greater detail of the mix design process can be found in the SANRAL SAPDM Contract Report (Theyse 2013).

##### 4.4.2.1 Cement stabilisation

The mix design for cement stabilised materials comprised of the determination of the optimum cement and lime content within a granular material sample to produce UCS and ITS values required to produce a material of C3 quality. UCS and ITS values were determined according to TMH 1 test methods A14 and A16T. Cement and lime contents were varied to produce a number of specimens whose UCS and ITS were determined. The results of the mix design are tabulated below.

**Table 4.10: Pozzolanic Stabilisation Mix Design Results (Theyse, 2013)**

Cement Content %	Lime Content %	UCS (kPa) – 7 days	ITS (kPa) – 7 days
1	0	936	16
		833	19
2	0	1786	84
		1733	76
3	0	2801	171
		3053	159
1	1	1818	155
		1780	151
2	1	2249	168
		2547	164
1	2	2122	44
		2012	43

Only one stabiliser content combination, tabulated above, fails the required UCS of 1500 kPa for a C3 material. None of the mixes reach the required ITS criteria of 250kPa for a C3 material, however this is perceived as being an unreasonable ITS value to achieve.

According to the experimental section design report Theyse specifies that the stabiliser contents selected for use in the experimental section cement stabilised layers were to be the 2% cement and 2% cement with 1% lime. However it was decided before the actual construction of the cement stabilised

sub-sections that the 2% cement and 1% lime contents would be utilised for all cement stabilised sub-sections.

#### 4.4.2.2 Bitumen stabilisation

The mix design for bitumen stabilised materials was carried out according to the requirements set out in Technical Guidance Document 2 – Bitumen stabilised Materials (Asphalt Academy, 2009). Accelerated curing of specimens as set out in TG2 was implemented for BSM mix design. Cement, lime and bitumen contents were all varied to determine the constituents required to create a BSM 1 standard mix based on UCS and ITS requirements only. The final mixes selected utilise a cement content of 1% by mass and a residual bitumen content of 2.4% by mass to create the flexible mix with lower shear resistance while a mix containing 2% by mass cement and 2.4 % residual bitumen is utilised to create a stiffer, higher shear strength mix. Their UCS and ITS results are shown in Table 4.11.

**Table 4.11: Bitumen stabilisation selected mix design results (Theyse, 2013)**

Cement Content %	Lime Content %	Bitumen Stabilisation		UCS (kPa)*	ITS (kPa)*	
		Type	Content %		Dry	Wet
1	0	Emulsion	2.4	1403	226	205
2	0		2.4	2133	414	405
1	0	Foam	2.4	2130	256	203
2	0		2.4	3130	330	284

\*Accelerated curing according to TG2

Combining the results of the structural design, in which the layer thickness and general material properties were investigated, along with the more material specific mix design, where the strength and flexibility of the materials with varying stabiliser contents were examined, the final base layer thicknesses and stabiliser contents were selected which were expected to provide the greatest insight into the performance of stabilised pavement materials. The experimental section was divided into 12 sub-sections each constructed with various combinations of layer thickness, stabiliser type and contents. 10 of the sub-sections are considered in the study presented here. Five sub-sections in the northbound and southbound directions were constructed as with an in-situ recycled C3 sub-base with an imported crushed stone G1 base. Data from these sub-sections were not considered in this study. Table 4.12 and Table 4.13 below outline the final in-situ recycled and stabilised base layer thicknesses and stabiliser contents. A graphical representation of the experimental section as a whole is depicted in Addendum B.

**Table 4.12: Base Layer Design Parameters - Southbound**

Section Identifier	Chainage (km)		Base Layer Thickness (mm)	% additive by mass		
	From	To		Bitumen	Cement	Lime
200 C3 1	6.50	6.85	200	-	2	1
200 C3 2	6.85	7.20	200	-	2	1
175 ETB 1	7.20	7.55	175	2.4	1	0
200 ETB 1	7.55	7.90	200	2.4	1	0
175 ETB 2	7.90	8.25	175	2.4	2	0
200 ETB 2	8.25	8.60	200	2.4	2	0
175 FTB 1	8.60	8.95	175	2.4	1	0
200 FTB 1	8.95	9.30	200	2.4	1	0
175 FTB 2	9.30	9.65	175	2.4	2	0
200 FTB 2	9.65	10.00	200	2.4	2	0

**Table 4.13: Base Layer Design Parameters - Northbound**

Section Identifier	Chainage (km)		Layer Thickness (mm)	% additive by mass		
	From	To		Bitumen	Cement	Lime
200 C3 1	6.50	6.85	200	-	2	1
200 ETB 3	6.85	7.20	200	0.9	1	0
175 ETB 1	7.20	7.55	175	2.4	1	0
200 ETB 1	7.55	7.90	200	2.4	1	0
175 ETB 2	7.90	8.25	175	2.4	2	0
200 ETB 2	8.25	8.60	200	2.4	2	0
175 FTB 1	8.60	8.95	175	2.4	1	0
200 FTB 1	8.95	9.30	200	2.4	1	0
175 FTB 2	9.30	9.65	175	2.4	2	0
200 FTB 2	9.65	10.00	200	2.4	2	0

## 4.5 Experimental Section Construction

The pavement structures to be constructed along the R35 experimental section are outlined in Addendum B. The method selected to construct the experimental pavement structures comprised of the in-situ recycling and stabilisation of the existing seal surfacing and cement stabilised base layer. The original sub-base and subgrade materials remain unaltered. Asphalt and cape seal surface layers were paved on top of the in-situ recycled and stabilised base layers.

### 4.5.1 Base layer construction

The R35 experimental section in-situ recycled and stabilised base layers were constructed in half widths beginning with the southbound lane. The experimental section base layers were constructed in the southbound direction of the R35 from km 5.0 to km 10.0 between the 11<sup>th</sup> of April 2012 and the 7<sup>th</sup> of May 2012. The experimental section base layers in the northbound lane of the R35 were



constructed between the 1<sup>st</sup> August 2012 and the 29<sup>th</sup> August 2012. A diagram of the road layout during construction and traffic accommodation utilised is depicted in Figure 4.9. Before in-situ recycling of the lane, the cement and lime, as specified per experimental sub-section design, is spread manually on the road surface using squeegees, see Figure 4.10. The required cement and lime contents required as per the experimental section plan, outlined in Table 4.12 and Table 4.13, were achieved by placing the required number of cement or lime packets at specified distances along the experimental sub-section to be constructed. As the mass of cement per packet is known and the mass of material to be recycled, as approximated by the recycling depth, sub-section length, width and expected material density, the cement and lime packet spacing along the road can be determined.

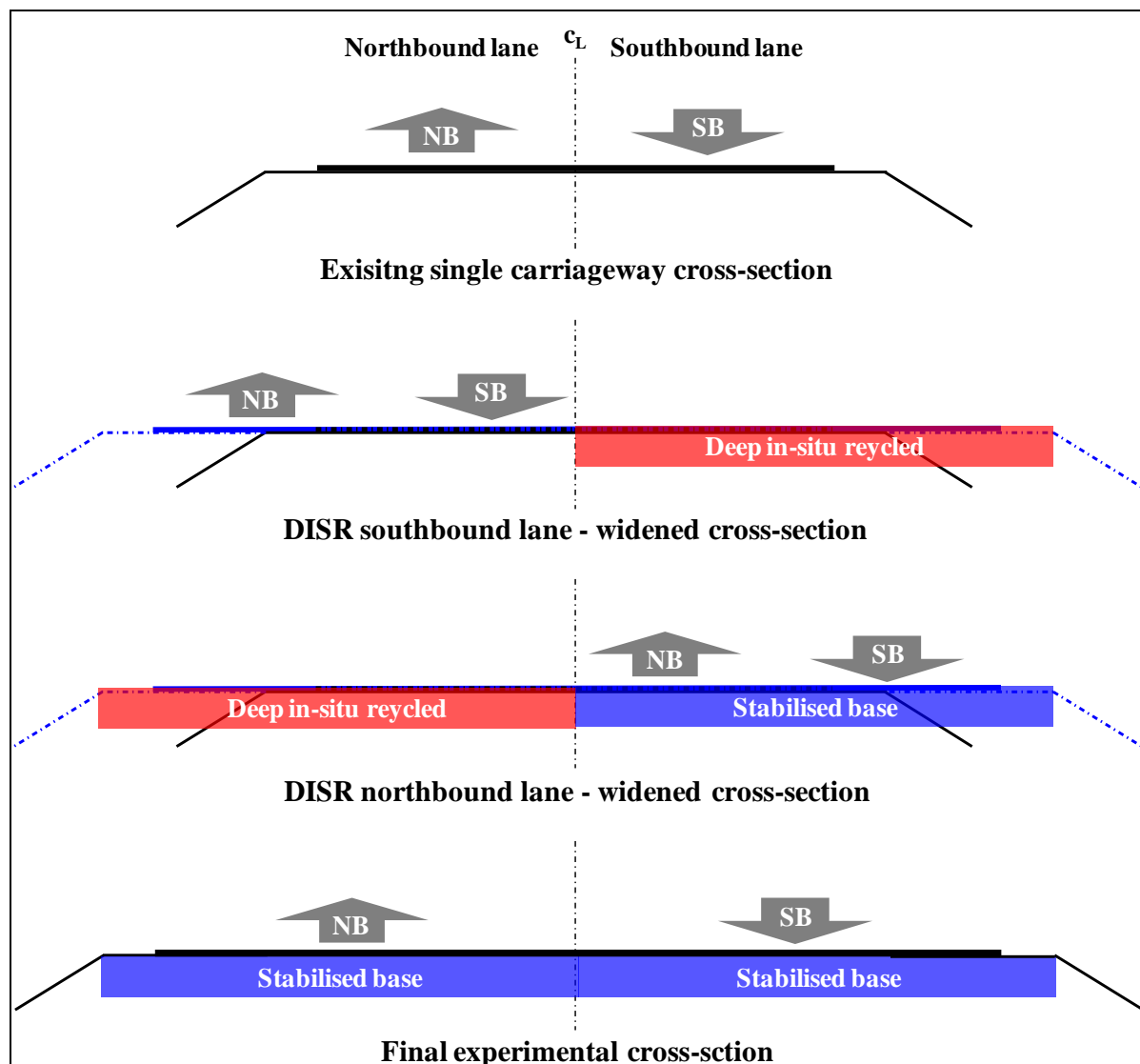


Figure 4.9: Experimental Section traffic accommodation and construction sequence

Once the required cement and lime is spread evenly the recycling train begins to in-situ recycle the specified sub-section. For the construction of the R35 experimental sections a Wirtgen WR2500s is utilised for the purpose of in-situ recycling. The remainder of the recycling train consists of a water

tanker and bitumen supply tanker, required only for the emulsion and foamed bitumen stabilised sections preceding the recycling machine. The recycling depth is specified as per the requirements of the base layer thickness as set out in experimental section base layer design described in Table 4.12 and Table 4.13. The bitumen content is determined by the input to the control system of the recycling machine. For bitumen stabilised base layers the emulsion is supplied from a tanker at the front of the recycling train and applied through jets within the recycling drum. For bitumen stabilised materials utilising foamed bitumen, a heated tanker containing 70/100 penetration bitumen supplies the bitumen to the recycling machine. The foaming of the bitumen occurs at a specialised jet head, on top of the recycling drum, which combines the heated bitumen and water at the recycling drum and applies the foamed bitumen to the material milled from the in-situ road base.



**Figure 4.10: Spreading of cement or lime before in-situ recycling.**

For the recycling and construction of the C3 base layers, with only cement and lime stabilisation added to the recycled base, a recycling machine which adds water alone to the recycled layer was utilised. A Caterpillar recycling machine was used to in-situ recycle and stabilise with cement and lime stabiliser.

The in-situ recycled cement stabilised and BSM layers were compacted by steel drum vibratory compaction rollers. The vibratory rollers utilised were equipped with intelligent compaction systems. Intelligent compaction is described as the compaction of road materials using modern vibratory rollers equipped with in-situ measurement system, feedback control, GPS based mapping and software that

automates documentation of the results, which are all integrated to allow automatic real-time monitoring and correction of the compaction process. Vibratory rollers with intelligent compaction systems inbuilt were utilised as part of a SANRAL study to determine the usefulness of data collected from the intelligent compaction systems, during construction, and linking the information collected to pavement failures or poor performance later in the pavements service life. Three different vibratory rollers, produced by three different manufacturers, were utilised in the compaction process subsequent to the in-situ recycling of the existing base layer. Different compaction regimes, utilising the three different intelligent compaction rollers, were implemented between the northbound and southbound lanes. The compaction process and intelligent compaction study is described in detail in the CSIR report (Leyland & Paige-Green, 2013). A brief summary of the compaction process is outlined here.

In the southbound direction the following compaction regime was followed:

- Intelligent compaction was applied to the in-situ recycled material for a number of passes by a single manufacturer's roller.
- Compaction was stopped for the intelligent compaction research study testing.
- Once testing was complete the compaction process, with the same roller, continued until sufficient density was achieved.
- At the point of adequate compaction the other two manufacturer's rollers carried out a single pass each for the comparison of data collected.
- A final pass by the initially selected roller was carried out.

In the northbound direction a different compaction process was implemented:

- A single intelligent compaction roller was applied to each experimental sub-section.
- Compaction of the in-situ recycled material within a specific sub-section was compacted, by a single, selected manufacturer's roller, until sufficient compaction was achieved.

The final cutting of the recycled layer to the required levels was then carried out. In general intelligent compaction was the only compaction device applied to the in-situ recycled base material. In some cases however, a pneumatic tyre roller (PTR) was utilised to finish the cut-to-level surface in order to provide a smooth finish for the construction of the bituminous wearing course.

#### 4.5.2 Surface layer construction

Two surfacing types were specified for construction on the R35 Experimental Section. A 40mm elastomeric modified (A-E2) asphalt layer and cape seal surfacing have been constructed on each experimental sub-section, each covering half of a sub-section as depicted in the experimental layout in Addendum B. The rationale behind the inclusion of varying surface types in the pavement design was to investigate the crushing induced at the top of the cement and lime stabilised base materials under wheel loads. These two surfacing types provide different levels of protection to the top of the

stabilised base material. The thinner, more flexible cape seal has a much reduced load spreading capability than that of the asphalt layer, thus greater stresses are induced at the top of the cement/lime stabilised material. The differing level of crushing induced at the top of the base layer is not the focus of this study and is described here to give the reasoning behind the varying bituminous surfacing.

The varying surface types constructed on the experimental section will affect this study when analysing the stiffnesses of the base layer from FWD data collected on the surfaced experimental section stabilised base layers. The varying layer stiffness, layer thicknesses and temperature dependent properties attributed to a cape seal or asphalt surfacing need to be considered when analysing FWD deflection measurements taken on top of the surfaced experimental pavement structure. FWD deflection bowls represent the deflection in the pavement structure as a whole, therefore as the focus of the study presented in this thesis is to observe the performance of the stabilised base layer materials during curing and under traffic loading, the contribution of the base layer to the measured deflection bowls needs to be determined. The complicating factor introduced by the cape seal and asphalt surfacing on the FWD analysis of the experimental pavement structures is described in detail in Chapter 6.

#### 4.5.3 Site laboratory quality control testing

A summary of the results from quality control testing carried out on each experimental sub-section is tabulated below. Samples of milled material were taken from behind the recycler during construction and a number of tests conducted. The quality control testing included the following:

- Indirect tensile strength (ITS) on 100mm diameter samples in both wet and dry condition
- ITS on 150mm diameter samples in dry condition
- Unconfined compressive strength (UCS) on 150mm diameter samples in a wet condition
- Determination of maximum dry density at the modified AASHTO compaction effort

Stabilised material specimens prepared for quality control UCS and ITS testing were allowed to cure for 28 days.

The degree of field compaction of the recycled base layers was determined using a Troxler nuclear density gauge. The Troxler readings were calibrated with the maximum dry densities determined in the lab to give a degree of compaction in comparison to the maximum dry density determined in the lab under the modified AASHTO compaction effort. Maximum dry densities were determined at locations in the proximity of each Troxler density test. This was done in order to improve the accuracy of the degree of compaction of the base layer determined at each Troxler density measurement location. Levels of compaction of the stabilised material are shown in Table 4.14 and Table 4.15.

**Table 4.14: Quality control testing site laboratory average results - southbound**

Sub-section	ITS 100mm (Wet)	ITS 100mm (Dry)	ITS 150mm (Dry)	UCS 150mm (Soaked)	% relative compaction Mod AASHTO	TG2 Classification
200 C3-1 (2% c, 1% l)	-	-	220.0	2.0	99.6	C3
200 C3-2 (2% c, 1% l)	-	-	198.0	1.3	99.6	C3
175 E (1% c, 2.4% b)	160.0	349.7	192.0	-	101.1	BSM 1
200 E (1% c, 2.4% b)	146.0	245.7	66.0	-	99.0	BSM 2
175 E (2% c, 2.4% b)	276.7	531.7	268.0	-	97.0	BSM 2
200 E (2% c, 2.4% b)	199.8	427.2	296.0	-	100.6	BSM 1
175 F (1% c, 2.4% b)	126.8	312.2	192.0	-	99.4	BSM 1
200 F (1% c, 2.4% b)	180.3	412.8	176.0	-	97.5	BSM 1
175 F (2% c, 2.4% b)	208.5	415.8	206.0	-	98.7	BSM 1
200 F (2% c, 2.4% b)	196.0	395.0	200.0	-	100.5	BSM 1

**Table 4.15: Quality control testing site laboratory average results - northbound**

Sub-section	ITS 100mm (Wet)	ITS 100mm (Dry)	ITS 150mm (Dry)	UCS 150mm (Soaked)	% relative compaction Mod AASHTO	
200 C3-1 (2% c, 1% l)	-	-	213.3	2.0	98.0	C3
200 E (1% c, 0.9% b)	90.6	168.8	82.0	-	101.0	BSM 2
175 E (1% c, 2.4% b)	87.0	199.8	150.0	-	98.5	BSM 2
200 E (1% c, 2.4% b)	163.3	289.8	172.5	-	99.3	BSM 2
175 E (2% c, 2.4% b)	131.0	296.0	170.0	-	101.1	BSM 2
200 E (2% c, 2.4% b)	137.0	324.3	263.3	-	101.6	BSM 1
175 F (1% c, 2.4% b)	67.8	167.5	170.0	-	97.9	BSM 2
200 F (1% c, 2.4% b)	160.0	255.7	146.7	-	100.0	BSM 2
175 F (2% c, 2.4% b)	184.5	360.8	255.0	-	102.2	BSM 1
200 F (2% c, 2.4% b)	204.0	385.8	252.5	-	98.6	BSM 1

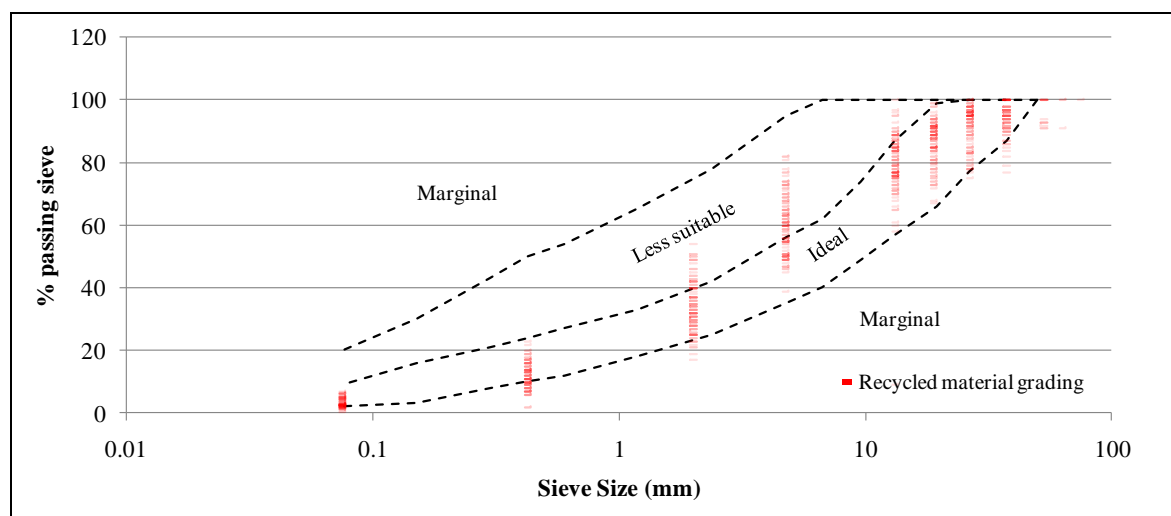
According to TG2 (Asphalt Academy, 2009), giving guidance on the design and construction of BSMs, many of the above materials will fit into a BSM 1 classification based on the testing depicted in Table 4.14 and Table 4.15. Some materials however fall within the BSM 2 category based on ITS and compaction results. The values defining the classification, with respect to ITS, of the in-situ recycled materials to a BSM material are tabulated below.

None of the BSM materials constructed fall within a BSM 1 classification when the full set of requirements outlined in TG2 are considered. This is due to the requirement that BSM 1 materials contain a minimum of 80% crushed stone within the mix.

**Table 4.16: BSM classification - ITS and relative compaction requirements (Asphalt Academy, 2009)**

Parameter	Limits	
	BSM 1	BSM 2
ITS <sub>dry/equil</sub> 100mm (kPa)	> 225	175 – 225
ITS <sub>wet</sub> 100mm (kPa)	> 100	75 - 100
ITS <sub>dry/equil</sub> 150mm (kPa)	> 175	135 – 175
Relative density (%)	> 98%	95% to 98%

Sieve analyses were also carried out on samples of stabilised material taken from behind the recycling machine during construction. Figure 4.11 below indicates the spread of gradings for all sieve analyses carried out.

**Figure 4.11: Stabilised material grading and recommended grading zones**

The boundaries shown in Figure 4.11 are specified in Technical Guidance document 2 (Asphalt Academy, 2009) as identifying materials which are ideal, less suitable and marginal for the purposes of in-situ recycling with foamed or bitumen emulsion. From the lab data depicted in Figure 4.11 the majority of the material recycled falls within the ideal and less suitable zone for bitumen stabilisation. Some deviations into the marginal grading zones can be seen at the percentage passing 0.425mm, 2mm, 26.5 and 37.5mm sieves.

**CHAPTER 5 EXPERIMENTAL SECTION LABORATORY AND FIELD TESTING**

The analyses implemented in this thesis make use of data from the testing and data collection procedures planned for the R35 experimental section. Testing carried out by the site laboratory as part of the quality control required during the construction of the experimental section is also utilised. A summary of the testing apparatus and data collected is outlined in Table 5.1.

**Table 5.1: Pavement condition and performance indicators**

Source	Data
Falling Weight Deflectometer (FWD)	Pavement surface deflections
	Pavement surface temperature
	Air temperature
Site laboratory	Indirect tensile strength (ITS)
	Unconfined compressive strength (UCS)
	Moisture contents
	Degree of compaction
	Air Temperature
	Rainfall

**5.1 Falling Weight Deflectometer (FWD)**

Data collected from FWD testing forms the basis of this study. Each experimental sub-section was tested at 5m spatial intervals with temporal intervals as outlined in Addendum A. The purpose of FWD testing is to imitate the dynamic loading of a moving wheel load travelling on a pavement structure. The FWD loads the pavement structure through a falling weight onto rubber buffers on top of a loading plate of specified dimensions, which sits directly on top of the pavement. FWD drops are performed three times at each location or station 5m metres apart. Figure 5.1 and Figure 5.3 depict the FWD utilised for tests carried out on the R35 Experimental Section.



**Figure 5.1: FWD Load Plate and Geophones**

The parameters measured during FWD testing are:

- Peak load and loading rate applied to the pavement beneath the plate
- Deflections measured at each geophone
- Air temperature
- Pavement surface temperature

The load applied to the pavement is measured as this parameter replicates the load applied to a pavement structure through a moving wheel load. The magnitude of the load applied is controlled by the mass of the falling weight and the height from which the weight is dropped onto the pavement. Typically the FWD replicates the application of a standard axle, moving wheel load to the pavement structure. The standard axle is an 80kN axle comprising of two dual wheels with each dual wheel applying a peak load of 40kN to the pavement structure. For the FWD utilised in this study the FWD drop height and mass were selected so as to recreate the standard half axle peak load application of 40kN. The pressure induced by the falling weight beneath the 300 mm diameter load plate is then calculated at 566 kPa. The actual peak stress varies slightly in reality as the peak load applied by the falling weight is not always exactly 40 kN due to variation in buffer properties and random variability. The rate of load application to the pavement structure is controlled by the rubber buffers which sit between the load plate and the falling weight. The load mass and the height from which it is dropped also affect the loading rate. The loading rate is also measured as this parameter has significant effects on the performance of bituminous materials. The loading frequency which occurred during FWD deflections was calculated at 5Hz. The determination of loading frequency is detailed in Section 6.4.2.

Geophones spaced at intervals along the pavement surface, as depicted in Figure 5.2 with length units in millimetres, measure the deflection of the pavement surface during the application of the falling weight onto the pavement surface. The measurement of this deflection bowl along with the knowledge



of the magnitude and geometry of the stress applied at the pavement surface allows the analysis and determination of the stiffnesses of the pavement layers which make up the whole structure through the method of back-calculation. The back-calculation process utilised will be discussed in Chapter 6. More fundamental deflection bowl parameters are also utilised to indicate the structural condition of the pavement tested. These parameters and their calculation are detailed in Table 5.2. Also shown are the approximate pavement structure elements whose structural condition these parameters describe.

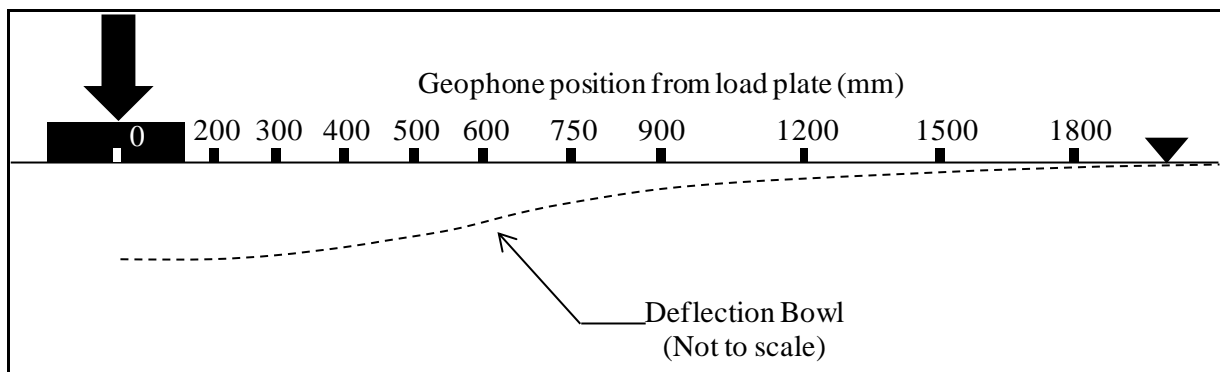


Figure 5.2: Representation of FWD geophone setup and pavement surface deflection bowl

Table 5.2: FWD deflection bowl parameters

Parameter	Formula	Pavement Layer
Maximum deflection	Deflection measured at point of loading	Whole pavement structure
Radius of Curvature (RoC)	$RoC = \frac{L^2}{2D_0 \left( 1 - \left( \frac{D_{200}}{D_0} \right) \right)}$ <p style="text-align: center;">L = 200 mm D<sub>x</sub> = Deflection at geophone x mm from load plate</p>	Surfacing layer and base
Base Layer Index (BLI)	BLI = D <sub>0</sub> - D <sub>300</sub>	Surfacing layer and base
Middle Layer Index (MLI)	MLI = D <sub>300</sub> - D <sub>600</sub>	Sub-base and upper selected
Lower Layer Index (LLI)	LLI = D <sub>600</sub> - D <sub>900</sub>	Lower selected and subgrade

The air and surface temperature are also measured for each station where an FWD drop sequence is carried out. These temperatures are used when the FWD test has been carried out on a bituminous surfacing such as a surfacing seal or asphalt layer. The visco-elastic properties and hence stiffness of a bituminous surfacing is greatly affected by its temperature and loading rate. Relationships exist which allow for the estimation of the stiffness of an asphalt mix at various temperatures and loading rates. Such relationships will be utilised in the stiffness determination of the pavement structures to be analysed in the study presented. This analysis is conducted in Chapter 6.



**Figure 5.3: FWD testing on the R35 Experimental Section**

## 5.2 Site Laboratory Testing

Additional data relating to the properties and performance of the stabilised pavement materials constructed on site were collected from the suite of testing normally carried out during a road construction project. A brief outline of each of the site laboratory tests whose results were used in the analysis presented in this study follows.

### 5.2.1 Unconfined Compressive Strength (UCS)

The UCS is the vertical compressive stress level which induces failure within a cylindrical specimen of a cohesive granular material. The specimen is prepared as a cylinder with a height of 127 mm and diameter of 152.4 mm. The complete procedure for the determination of the UCS of a material is described in TMH1: Test Method A14.

### 5.2.2 Indirect Tensile Strength (ITS)

The ITS is the stress level at which failure of a cylindrical sample occurs under a tensile stress induced within the sample by the direct application of compressive stresses on the cylindrical sample of material. The test method which describes the process of ITS determination is detailed in TMH 1: Test Method A16T.

### 5.2.3 Granular Material Grading

Material grading is determined by the test method TMH 1: Test Method A1. This involves the separation of the soil fines, material passing the 0.425 mm sieve, from the coarser granular material.

The soil fines are then utilised for the mechanical analysis and determination of the Atterberg limits. The separated coarse granular material is analysed further to determine the percentage mass of material retained on sieve sizes ranging from 63 mm to 2 mm.

#### 5.2.4 Degree of Compaction

The degree of compaction of the in-situ recycled, stabilised and subsequently compacted base layer material is determined utilising TMH 1: Test Method A7 – The determination of the maximum dry density and optimum moisture content of gravel, soil and sand, in conjunction with TMH 1: Test Method A10 (b) – Method for determining the in-place density and moisture content of soils and gravels by nuclear methods.

Method A7 determines the moisture content at which the material to be recycled will achieve its maximum density under the standard modified AASHTO compaction force. Following Method A10 (b) and specifically the flush backscatter method, the in-situ density of the constructed base layer is determined. The in-situ dry density determined through nuclear methods is then compared with the maximum dry density achieved as in Method A7, at the modified AASHTO compaction effort. The in-situ, as constructed level of compaction, is represented by the in-situ dry density as a percentage of maximum dry density achievable under the modified AASHTO compaction.

## CHAPTER 6 BACK-CALCULATION OF FWD MEASURED DEFLECTION BOWLS

Chapter 6 details the procedures followed in carrying out the back-analysis of FWD deflection bowls. As the back-calculation of pavement layer stiffnesses from FWD data provided the basis for characterising the performance of the stabilised base layers constructed along the experimental section, extensive analysis and data checking procedures were implemented. The extent of deflection data collected from FWD testing along each experimental sub-section at 5m intervals at various time intervals are detailed in Addendum A. The software package Back-GAMES was utilised for the back-calculation of the FWD data, determining layer stiffnesses of the pavement structures modelled.

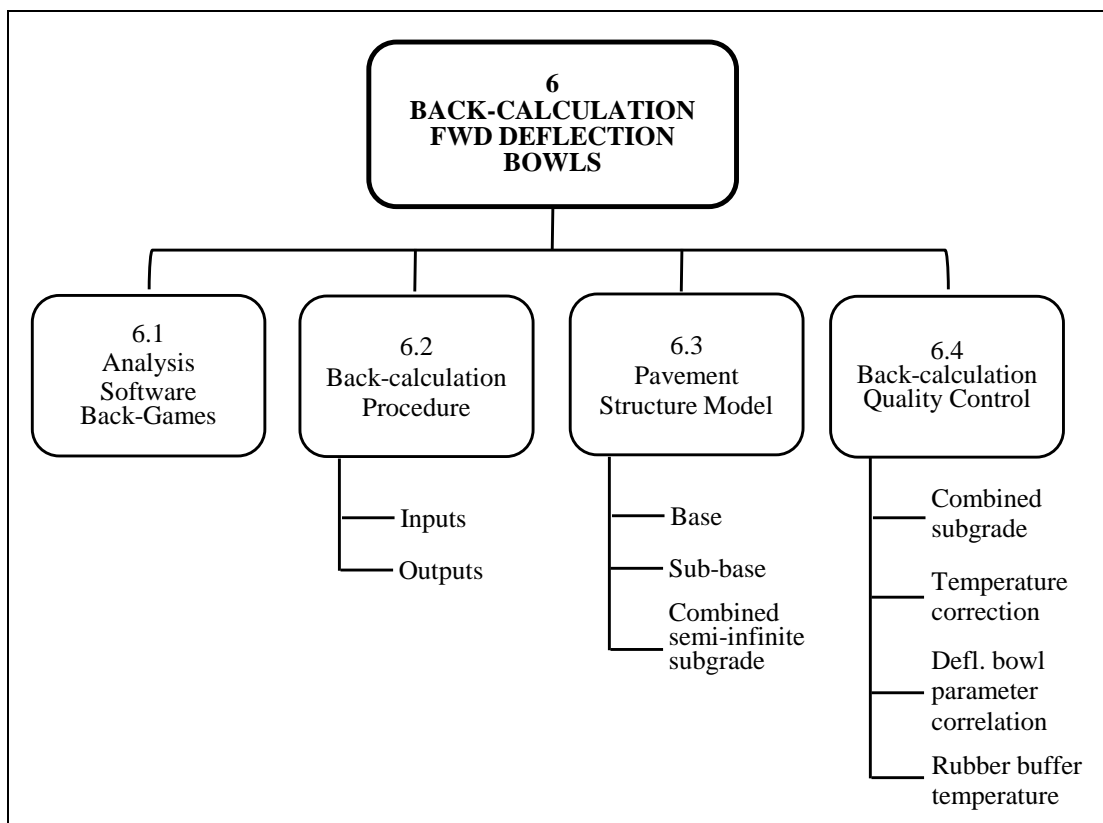


Figure 6.1: Outline of Chapter 6

### 6.1 Back-calculation software – backGAMES

Back-GAMES is an automatic, pavement surface deflection bowl, back-calculation software package. Back-calculation determines the effective pavement layer stiffnesses within a pavement model of an actual pavement structure in which pavement surface deflection bowls are induced and measured by an FWD. Back-GAMES was developed by James Maina of the Council for Scientific and Industrial Research (CSIR) and will be utilised within the new South African mechanistic-empirical pavement design system. It replaces the back-PADS system previously developed at the CSIR. Rather than using the ELSYM5 pavement structure modelling engine as with back-PADS, the General Analysis of Multi-layered Elastic Systems (GAMES) modelling engine (Maina & Matsui, 2004) is utilised.

Improvements provided by the GAMES pavement modelling engine are reported by Maina et al. (2008) as including:

- Improved definition of loading from one to three dimensions
- Possibility of modelling interlayer friction properties between layers
- Improved response modelling close to the pavement surface

## **6.2 Back-calculation procedure**

### **6.2.1 Inputs**

Inputs to the back-calculation software include the following:

- FWD deflection measurements
- FWD load
- Pavement model
- Seed layer stiffness values
- Poisson's ratio for pavement layer material

FWD deflection measurements are input to the back-calculation software as raw FWD files of .f25 file format.

The geometry and load applied by the FWD to the pavement is also part of the data input to the back-analysis software through the raw FWD data file.

A model describing the pavement structure as it occurs in reality is required to be input to the back-calculation software. The definition of the pavement model and its constituent layer thicknesses utilised in this thesis is based on test-pit data. The determination of the pavement model is described in Section 6.3.

Seed pavement model layer stiffness values, indicating the expected stiffness of the pavement layers, gives the back-calculation process a starting point to begin the comparison of modelled pavement deflection bowls with those measured in the field.

An estimate of the poisson's ratio of each pavement layer material is also input to the back-calculation software. Poisson's ratio is the ratio of the axial versus transverse strain of the pavement layer material.

### 6.2.2 Outputs

Multi Layer Linear Elastic (MLLE) theory is used to model the deflection of the pavement structure model under the FWD load. The pavement layer stiffnesses within the model are varied until an acceptably fit of modelled and FWD measured deflection bowls is achieved. The pavement layer stiffnesses within the pavement model providing an adequate fit between modelled and measured deflection bowls are then output as the resultant pavement layer stiffnesses.

Each of the three deflection bowls measured at an FWD station were analysed and a back-calculated stiffnesses for each layer within the pavement structure determined. The analysis carried out in this thesis utilises the third deflection bowl measured. Improved accuracy in deflection measurement is expected when using deflection data from the third drop due to the bedding in of the load plate and improved contact with the pavement after the first two drops.

### 6.3 Pavement structure model

The pavement structure models to be utilised in the back-analysis were determined from test-pit data collected during investigations relating to the rehabilitation design of the main R35 project and from the as-built data prepared by the resident engineer subsequent to the R35 experimental section construction. This information is detailed in Chapter 4.

The experimental section pavement design calls for the in-situ recycling of the existing pavement to varying depths with varying cement and bitumen stabiliser contents. The new base layers which were constructed by in-situ recycling were designed to be either 200mm or 175mm in depth. The experimental section layout is depicted in Addendum B. For the purposes of the back-calculation of FWD deflection data with the back-GAMES analysis package a pavement structure model for each experimental sub-section had to be selected.

In Chapter 4 the existing pavement structure, as determined from five test-pits dug in both the northbound and southbound lanes, was discussed. The existing pavement structure was indicated by available test-pit information and is described in Figure 6.2 and Figure 6.3. It was observed that a complex and variable pavement structure exists along the length of the experimental section. It was also observed however that the existing base and sub-base layers, which were constructed on a pre-existing pavement structure also comprising of stabilised layers, remain at a relatively constant depth of 300mm. In order to create a pavement structure model for the back-calculation process which was representative of the existing pavement structure yet remaining convenient and economical to the back-calculation process, some simplifications to the pavement structure model were made.

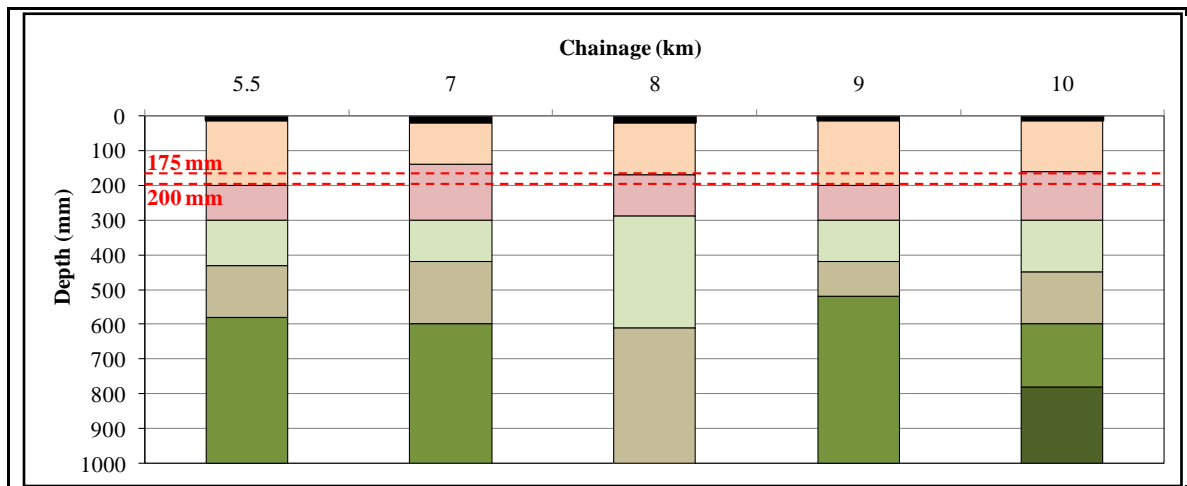


Figure 6.2: Test-pit pavement structures - southbound

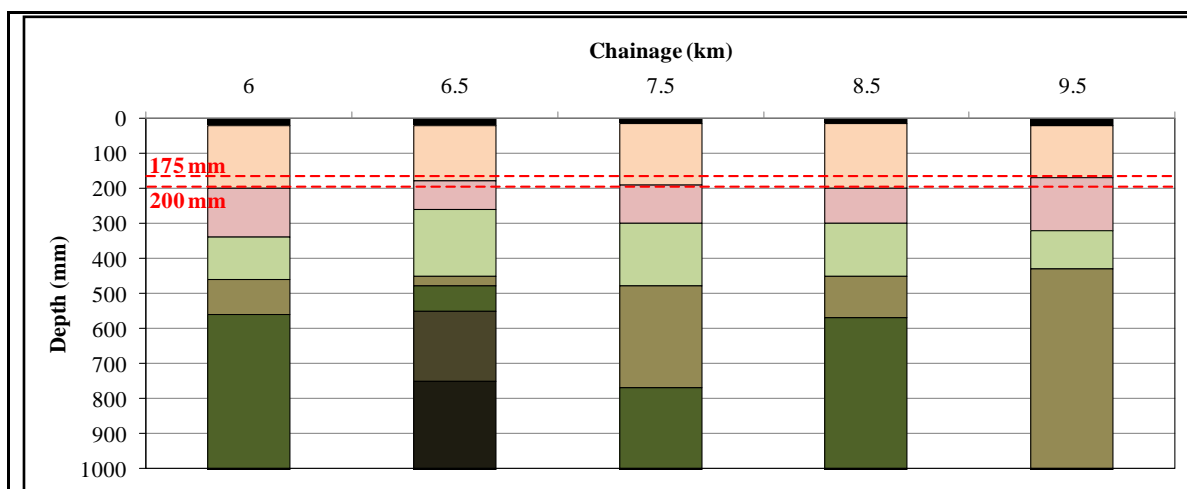


Figure 6.3: Test-pit pavement structures - northbound

### 6.3.1 Pavement surfacing layers

FWD deflection measurements taken before the 90 days since construction testing period were performed directly on top off the experimental section base layers without a bituminous surfacing as the cape seal and asphalt layers had not yet been constructed. Therefore the surfacing layers, as depicted in Figure 6.4, were not included within the pavement model utilised for the back-calculation analyses of FWD measurement taken during this period.

From the 90 day FWD testing period onwards, deflection data collected was back-analysed utilising pavement structures including the surfacing layer. As discussed in Chapter 4, the surfacing layers were varied within each sub-section, one half surfaced with a 45mm asphalt layer, the remainder with a cape seal. For the FWD measurements taken on a cape seal surfaced portion of an experimental sub-section the effect of the cape seal on the deflection bowl was deemed negligible and the thin surfacing, of nominal thickness 20mm, was combined with that of the underlying base layer within the pavement structure model. Where FWD measurements took place on asphalt, the 45mm thick

surface layer was included within the pavement model. The determination of the stiffness of this asphalt layer is discussed in Section 6.4.2.

### 6.3.2 Base and sub-base layers

When examining the existing base and sub-base layer thicknesses it was noted that for the experimental sub-sections where a 200 mm depth of recycling is required, the complete existing base layer is removed in both northbound and southbound lanes. For the experimental sub-sections where a depth of recycling of 175mm is specified, some thin, residual layers of the existing base would remain. This is depicted in Figure 6.2 and Figure 6.3 with the recycling depths demarcated by red broken lines. For the purposes of the back-calculation analyses to be carried out in this study it was assumed that subsequent to recycling to depths of 175mm and 200mm a residual existing sub-base of 125mm and 100mm thicknesses respectively remained.

### 6.3.3 Semi-infinite subgrade

As described in Chapter 4 and depicted in Figure 6.2 and Figure 6.3, test pits excavated along the length of the experimental section show that a pre-existing pavement structure is present beneath the existing base and sub-base layers. In order to ensure a reliable and economical back-calculation process it was decided to investigate the effects of combining the observed layered system beneath the existing base and sub-base to a single unified semi-infinite subgrade. The effects of this simplification are investigated in Section 6.4.

The resultant simplified pavement structure models used in the back-analysis of FWD deflection bowls are summarised in Figure 6.4.

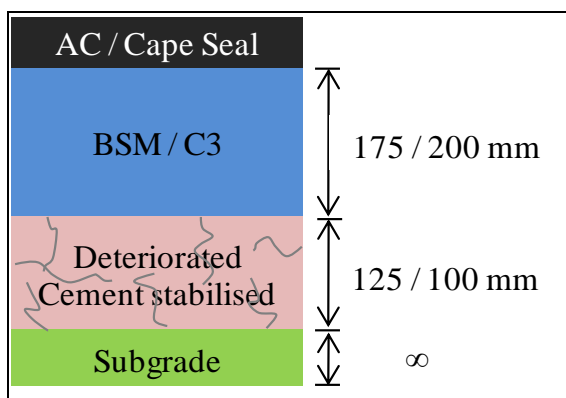


Figure 6.4 Back-calculation pavement structure model



## 6.4 Back-analysis quality control

In order to ensure the accurate representation of the stiffness of the in-situ recycled and stabilised base layers, adjustments to the back-calculation process and checks on the results of the back-analysis were conducted.

### 6.4.1 Combined sub-layer forming semi-infinite subgrade

As discussed previously in Section 6.3.3, the combining of the existing pavement structure sub-layering to a hypothetical semi-infinite subgrade, within the back-calculation model was seen necessary in order to allow for an economical back-calculation procedure. The effects of this simplification on the back-calculated stiffness of the in-situ recycled base and remaining sub-base was determined by carrying out the back-calculation of FWD deflections measured in the vicinity of test-pits from which the existing pavement structure was determined. A comparison of the back-calculated stiffnesses of the pavement layers within the simplified and actual pavement structure models indicated the effects of the subgrade simplification.

Figure 6.5 depicts the pavement structure at km 7.5 in the northbound lane of the experimental section after in-situ recycling the existing base with bitumen emulsion stabilisation to a depth of 175mm and the construction of a 45mm asphalt layer as surfacing. The layered system beneath the in-situ recycled base and remaining sub-base was identified from test-pits excavated at km 7.5 in the northbound lane. Also shown is the simplified pavement structure model that combines the lower layers of the pavement structure to create a unified subgrade. The back-calculated stiffnesses for both scenarios are shown. It can be seen that the change in stiffness of the base layer is minimal at 6% increase within the simplified model. The sub-base layer stiffness reduces by some 18% due to the simplification.

Pavement Structure	Thickness (mm)	Back-calculated stiffness (MPa)	Pavement Structure	Thickness (mm)	Back-calculated stiffness (MPa)	% change
Asphalt	45 mm	1326*	Asphalt	45 mm	1326*	-
BSM	175 mm	662	BSM	175 mm	703	6%
Broken-down cement stabilised	125 mm	396	Broken-down cement stabilised	125 mm	326	-18%
Dolerite gravel	180 mm	336	Subgrade	∞	290	-
Dolerite gravel (slight stab.)	290 mm	270				
Subgrade	∞	282				

Figure 6.5: Subgrade model simplification - km 7.5 northbound (\*Asphalt temperature = 39°C)

Figure 6.6 depicts the same investigation carried out at km 6.5 on the northbound lane of the experimental section comprising of a cement and lime stabilised base layer. This example, while dealing with the effects of combining the lower pavement layering system, also gives insight to the effects of the assumption that the existing sub-base is present to a depth of 300mm below the existing pavement surface along the entire experimental section.

Pavement Structure	Thickness (mm)	Back-calculated stiffness (MPa)	Pavement Structure	Thickness (mm)	Back-calculated stiffness (MPa)	% change
In-situ recycled C3	220 mm*	1984	In-situ recycled C3	220 mm*	2062	4%
Broken-down cement stabilised	60 mm	119	Broken-down cement stabilised	100 mm	91	-24%
Stabilised dolerite gravel	190 mm	315				
Stabilised Dolerite gravel	100 mm	347	Subgrade	∞	316	-
Highly stabilised dolerite gravel	200 mm	719				
Subgrade	∞	325				

**Figure 6.6: Subgrade model simplification - km 6.5 northbound (\*Cape seal and base layer combined)**

From the above analyses it is shown that the influence of combining the existing lower pavement layers to form a semi-infinite subgrade has induced an increase in back-calculated stiffness of the base layer. This stiffness increase however is minimal and the error is seen as acceptable and will not significantly affect the base layer stiffness trends observed.

The subgrade simplification effect on the existing sub-base is significant but as the focus of the study presented here is on the stiffness of the in-situ recycled and stabilised base layers the sub-base error was not seen as prohibitive for the analysis presented in this study. The significant errors observed in the sub-base layers and the merging of lower pavement layers to form the semi-infinite subgrade must be considered when interpreting these layer's back-calculated stiffness values.

The pavement model simplification presented above will allow for a more refined analysis of the large volume of FWD deflection data collected during this project. It also removes the requirement to consider the variation in layer thickness and composition of the lower, existing pavement layers.

Therefore for the purposes of the back-calculation and stiffness determinations required in this study the pavement structure model depicted in Figure 6.4 is used with confidence.

#### 6.4.2 Temperature correction

##### 6.4.2.1 *Effect of asphalt layer stiffness on modelled deflection bowl*

A 45mm layer of asphalt was constructed over half the length of each of the experimental subsections as depicted in Addendum B. It is well known that the determination of the stiffness of layers less than 75mm in depth through the method of back-calculating FWD measured deflection bowls is inaccurate and un-reliable (Oh et al, 2012). The reason for the inability of the back-calculation process to determine the stiffness of thin layers is due to the resolution of the measured deflection bowl along the surface of the pavement structure tested. For a surfacing layer of asphalt, 45mm thick, the portion of the deflection bowl which is influenced by the stiffness of the asphalt layer is measured by the geophones beneath the load plate and 200 mm from the centre of the load plate. In order to get an accurate picture of the attribution of the stiffness of the asphalt layer, isolated from the influence of the supporting upper layers, to the formation of a deflection bowl beneath the FWD load, a much greater number of geophones would be required to determine the shape of the deflection bowl between the geophones within the load plate and 200mm from the load plate. Currently this is not the case as there are only geophones within the load plate and 200mm from the load plate centre. An additional factor attributing to the difficulty in assessing the stiffness of a thin surfacing layer from FWD deflection bowl back-analysis is that the deflection bowl formed along the surface of the pavement is often distorted in the vicinity of the load plate due to edge effects of the load plate when applying a load to the pavement surface. The combination of these observations requires the utilisation of another method to determine the stiffness of the asphalt layer, outside of the back-calculation process. The inaccuracy in the automatic back-calculation of asphalt layer stiffness is illustrated by the following analysis.

If the stiffnesses of the asphalt surface layers were determined from the back-analysis of deflection bowls, a wide range of stiffness values could be attributed to the asphalt layer while still creating an adequate fit between the measured and modelled deflection bowls. In the highly likely case that an inaccurate stiffness is attributed to the asphalt layer through the back-calculation process, it is expected that the result of this inaccuracy will subsequently affect the determination of the stiffness of the supporting layers within the pavement structure.

To show the effect of the variation of the asphalt layer stiffness on the shape of the deflection bowl as modelled with MLLE theory, a comparison between two pavement structures with varying asphalt layer stiffnesses was investigated under the same loading conditions. The pavement structures utilised in the analyses are representative of those present within the experimental sections and are depicted in Figure 6.7.

	Thickness (mm)	Resilient Modulus (MPa)		
		A	A*	B
Asphalt	45 mm	2500	2500	10000
In-situ recycled C3 / BSM	175 mm	800	1000	800
Broken-down Cement Stabilised	125 mm	150	150	150
Subgrade	$\infty$	300	300	300

**Figure 6.7: Asphalt stiffness back-calculation sensitivity – pavement structures**

Both pavement structures A and B were modelled using BISAR, a pavement modelling software package produced by Shell which models a pavement structure with MLLE theory. When comparing the deflection bowls produced by pavement structures A and B within the MLLE model, see Figure 6.8, it is clear that there is a minor change in the shape of the deflection bowl. This change has been quantified by calculating the percentage difference between both modelled and measured deflections as shown in Table 6.1. It can be seen that very little difference is produced between both scenarios with asphalt stiffness differing by a factor of 4.

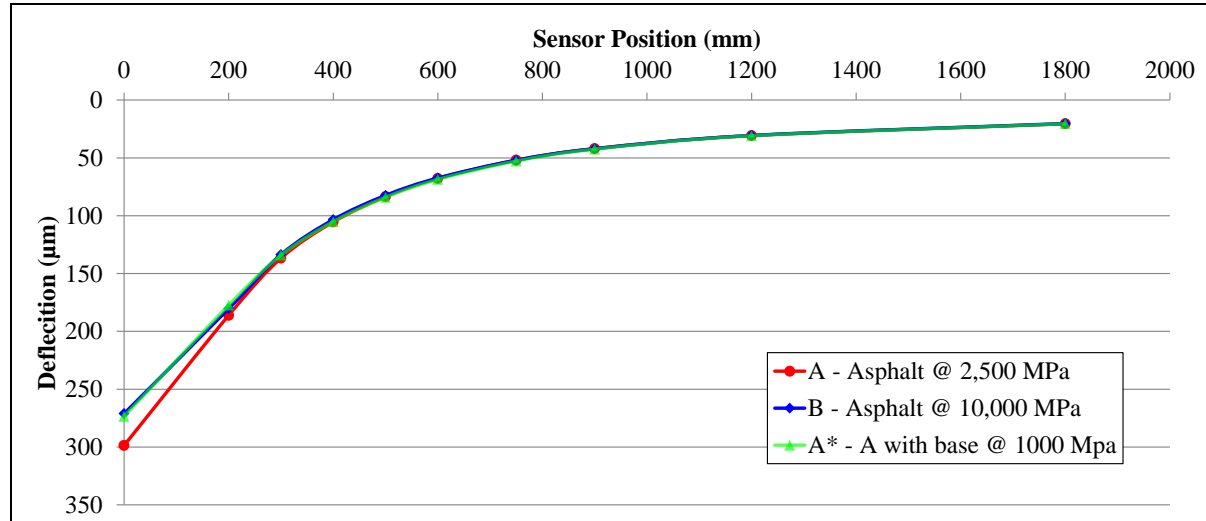


**Figure 6.8: Deflection bowl variation due to asphalt layer stiffness variation**

For both pavement structure scenarios A and B, one could be back-calculated and accepted to represent the other if typical automatic back-calculation, measured versus modelled, deflection bowl fitting error is utilised. That is if the deflection bowl modelled with pavement structure scenario A was in reality a better fit to an FWD measured deflection bowl than the deflection bowl modelled with pavement structure B, it is not always the case that the automatic back-calculation process will converge on the stiffness values representative of pavement structure A, even though the deflection

bowl is a better fit. This observation is due to the fact that in the process of fitting modelled deflection bowls to measured deflection bowls a perfect fit will never occur and allowances for error must be allowed in the process. Typically a precision error of +/- 5 micron is allowed thus any difference between deflections at the same location on measured and modelled deflection bowls less than 10 microns is ignored and the error taken as zero (Modelling and Analysis Systems CC, 2005). This allowance is made to take account of the level of measurement precision provided by the FWD geophone instrumentation. In addition to the error allowed for precision of the instrumentation, an error is allowed for the fact that the modelled deflection bowls will never be an exact fit to those measured thus a level of error between measured and modelled deflection bowls must be allowed. Typically an average error per sensor of 10 % is deemed acceptable (Modelling and Analysis Systems CC, 2005).

**Table 6.1: Deflection bowls from BISAR modelling of pavement structures A and B**

Pavement Structure	Load (kN)	Stress (kPa)	Deflection ( $\mu\text{m}$ )									
			0	200	300	400	500	600	750	900	1200	1800
A	40	570	298.6	186.1	136.7	105.4	83.4	67.7	52.0	42.0	30.7	20.5
B	40	570	271.1	180.3	133.6	103.4	82.4	67.4	52.0	42.1	30.6	20.3
Difference			27.7	6.9	0.9	2.4	1.1	0.3	0.1	0.1	0.1	0.2
% Difference			9%	4%	1%	2%	1%	0%	0%	0%	0%	1%
Precision + Error %			6%	0%	0%	0%	0%	0%	0%	0%	0%	0%

Taking the above precision and allowable average per sensor errors into account for the comparison of pavement structures A and B, it is clear the difference between the two deflection bowls is within the allowable error commonly utilised for back-calculation purposes. In this case the maximum error achieved at the geophone within the load plate was calculated at 9%. This error reduces to 6% when the precision of the measurement instrument is taken into account. The average percentage error per sensor at 2% is within allowable limits. While one could tighten the allowable average error at each sensor, it still remains that that shape of the deflection bowl in the vicinity of the load plate is measured at an inadequate resolution to model the asphalt layer accurately. The above analysis shows that with significant variation in the asphalt layer stiffness alone, a reasonable fit of measured and calculated deflection bowls can be achieved.

#### 6.4.2.2 Effect of asphalt layer stiffness inaccuracy on base layer stiffness back-calculation

While it has been shown that automatic back-calculation techniques will have difficulty in accurately determining the stiffness of thin asphalt layers, it must also be considered to what extent the inaccurate asphalt layer stiffness determination will have on the back-calculated stiffnesses of supporting pavement layers whose stiffness also influences the deflection bowl shape in the vicinity of the central load plate and the geophone 200mm from the load plate. During the automatic back-calculation the layer stiffness optimisation process may adjust the base layer stiffness in an effort to

reduce the error in deflection bowl fit which may actually be due to the asphalt layer stiffness. The effect of the automatic back-calculation of inaccurate asphalt layer stiffnesses on the back-calculated stiffnesses of the other pavement layers is now investigated.

By taking the pavement structure A and adjusting the stiffness of the base to produce A\*, as depicted in Figure 6.7, three very different pavement structures are now formed which produce similar deflection bowls when modelled, well within the allowable limits of error. Table 6.2 and Table 6.3 outline the deflection bowls modelled and the resultant errors between each which are well within allowed tolerances.

**Table 6.2: Deflection bowls from BISAR modelling of pavement structures A\* and B**

Pavement Structure	Load (kN)	Stress (kPa)	Deflection ( $\mu\text{m}$ )									
			0	200	300	400	500	600	750	900	1200	1800
A*	40	570	273.4	177.3	134.1	105.1	84.1	68.64	52.76	42.5	30.82	20.48
B	40	570	271.1	180.3	133.6	103.4	82.4	67.4	52	42.1	30.6	20.3
Difference			2.3	3.0	0.5	1.7	1.7	1.2	0.8	0.4	0.2	0.2
% Difference			1%	2%	0%	2%	2%	2%	1%	1%	1%	1%
Precision + Error %			0%	0%	0%	0%	0%	0%	0%	0%	0%	0%

**Table 6.3: Deflection bowls from BISAR modelling of pavement structure A and A\***

Pavement Structure	Load (kN)	Stress (kPa)	Deflection ( $\mu\text{m}$ )									
			0	200	300	400	500	600	750	900	1200	1800
A	40	570	298.6	186.1	136.7	105.4	83.4	67.7	52	42	30.7	20.5
A*	40	570	273.4	177.3	134.1	105.1	84.1	68.64	52.76	42.5	30.82	20.48
Difference			25.2	8.8	2.6	0.3	0.7	0.9	0.8	0.5	0.1	0.0
% Difference			8%	5%	2%	0%	1%	2%	2%	1%	0%	0%
Precision + Error %			5%	0%	0%	0%	0%	0%	0%	0%	0%	0%

The effect of differing asphalt layer stiffness on the base layers stiffness back-calculated is extended to an actual FWD deflection bowl measured on the R35 experimental section. For two pavement structure model scenarios where the asphalt layer stiffnesses are fixed to significantly different stiffness values, the selected deflection bowl is automatically back-analysed. Figure 6.9 describes the pavement structures modelled and the resultant back-calculated stiffnesses of all layers. Both scenarios of fixed asphalt stiffness within the automatic back-calculation process produce levels of deflection bowl comparison error well within the allowable limits. A significant variation in back-calculated stiffness of the upper three layers can be observed between both surfacing layer stiffness scenarios.

Material Type	Thickness (mm)	Back-calculated stiffnesses (MPa)		% Difference
		C	D	
Asphalt	45 mm	2500	10000	300%
In-situ recycled BSM emulsion	175 mm	662.7	463.1	-30%
Broken-down cement stabilised	125 mm	139.4	204.3	47%
Subgrade	$\infty$	293.57	281.5	-4%

**Figure 6.9: Pavement structures - automatic back-calculation error**

Table 6.4 below outlines the actual and modelled deflection bowls for pavement structure scenarios C and D outlined in Figure 6.9. It is clear that even though a modelled deflection bowl is fit to a measured deflection bowl within allowable error tolerances, a highly variable range of asphalt stiffnesses can be back-calculated. This effect will have significant effects on the back-calculated stiffnesses of the pavement layers beneath the surfacing.

**Table 6.4: Measured and automatic back-calculated deflection bowl comparison**

Pavement Structure	Stress (kPa)	Deflection ( $\mu\text{m}$ )										
		0	200	300	400	500	600	750	900	1200	1500	1800
Measured	570	328	191	143	113	85	67	53	42	30	25	21
C	570	326	197	141	107	85	69	53	43	32	25	21
% Error		1%	3%	1%	5%	0%	3%	0%	2%	7%	0%	0%
Precision + Error %		0%	0%	0%	0%	0%	0%	0%	0%	0%	0%	0%
D	570	324	203	141	105	83	68	53	44	33	26	22
% Error		1%	6%	1%	7%	2%	1%	0%	5%	10%	4%	5%
Precision + Error %		0%	1%	0%	0%	0%	0%	0%	0%	0%	0%	0%

As the determination of base layer stiffness is one of the major aims of this study it was required to reduce the error in the stiffness of the asphalt layer utilised within the back-calculation stiffness model and the subsequent error induced within the back-calculated base stiffness. To achieve this goal the stiffness of the asphalt layer was determined outside of the back-calculation process.

#### 6.4.2.3 Determination of accurate asphalt layer stiffness

Asphalt stiffness can vary based on a number of factors; these include mix type, temperature, and extent of cracking. In this study experimental data from the dynamic modulus testing of asphalt samples of varying mix types carried out by the CSIR was utilised (Anochie-Boateng et al, 2011). The experimental procedure involved the testing of different asphalt mix types prepared as 100mm x 150mm gyratory compacted cylindrical samples. The samples' dynamic moduli were determined

using a UTM-25 test setup with a sample from each mix type tested at different temperatures and loading rates. During testing samples were subjected to a haversine, uni-axial load pulse. From the CSIR study master curves for asphalt at a range of temperatures were developed which allowed for the determination of an asphalt dynamic modulus at a specific loading rate. Master curves relating to the asphalt mix, similar to that used for the asphalt surfacing of the R35 experimental sections, was used in this thesis to estimate the asphalt layer stiffness. These curves were used to estimate the asphalt layer stiffness in the field based on the air temperature, surface temperature and loading time recorded by the FWD during testing.

In order to determine the loading frequency applied to the asphalt pavement surfacing, load pulse duration data collected by the FWD was used. A loading frequency of 5 Hz was determined from Figure 6.10 describing the loading rate beneath the FWD load plate during actual FWD testing on the R35 experimental section. The load pulse duration was determined by taking twice the time gap between the occurrence of the maximum applied load and initiation of load application. In this example the loading time was calculated at 32.9 ms. The cyclic frequency was then determined by equation 3. Loulizi et al (2006) showed that the cyclic frequency gives an improved correlation between HMA resilient modulus and dynamic modulus hence its utilisation in the analysis presented here.

$$f = \frac{1}{2\pi t} \quad \text{Equation 3}$$

f = cyclic frequency (Hz)

t = loading time (ms)

The cyclic frequency was determined at 4.82 Hz for the load pulse depicted in Figure 6.10. For the purposes of the determination of the resilient modulus of asphalt from the CSIR determined dynamic moduli, to be incorporated within the back-calculation pavement model, a nominal loading frequency of 5 Hz was used throughout this analysis.



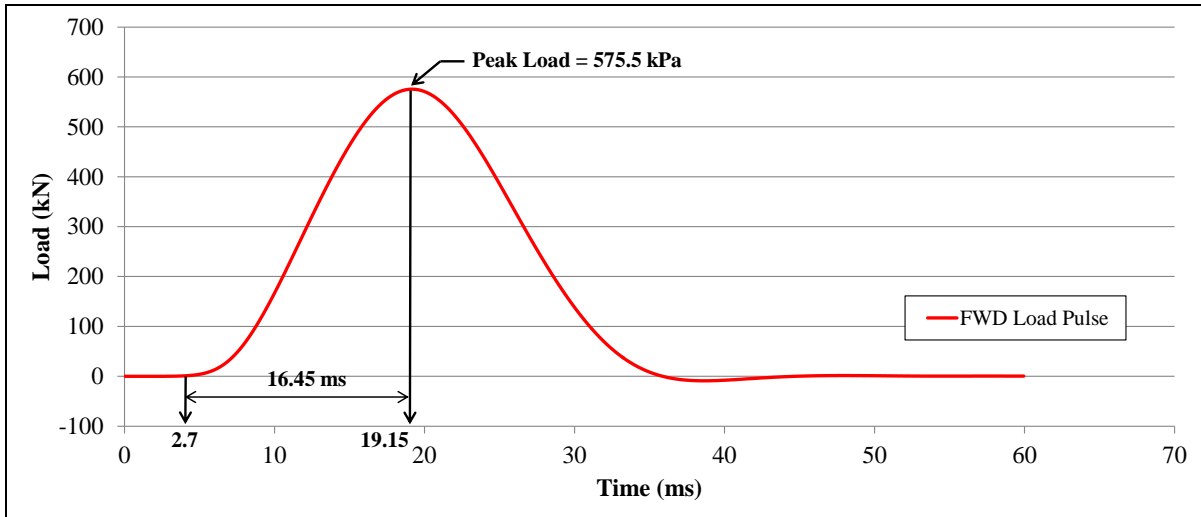


**Figure 6.10: Example load pulse from R35 FWD testing**

The asphalt temperature in the field was determined by using the air and surface temperatures measured by the FWD while testing. Due to the fact that the asphalt surface temperature may not be representative of the temperature throughout the depth of the asphalt at a particular location the BELLS 2 equation (Lukanen et al, 1998) was utilised to estimate the asphalt temperature within the layer. The BELLS 2 relationship is described below.

$$T_d = 2.78 + (0.912 \times IR) + \{\log(d) - 1.25\} \{-0.428 \times IR + 0.553 \times (1 - \text{day}) + 2.63 \times \sin(hr_{18} - 15.5)\} + 0.27 \times IR \times \sin(hr_{18} - 13.5) \quad \text{Equation 4}$$

Where;

$T_d$  = Pavement temperature at depth  $d$ , °C

$IR$  = Pavement surface temperature, °C

$\log$  = logarithm base 10

$d$  = depth at which material temperature is to be predicted, mm

1-day = Average air temperature the day before testing, °C

$\sin$  = sine function on an 18-hr clock system, with  $2\pi$  radians equal to one 18-hr cycle

$hr_{18}$  = Time of day, in a 24-hr clock system, but calculated using an 18-hr asphalt concrete (AC) temperature rise-and-fall time cycle

The surface temperatures recorded by the FWD at each 5m interval were averaged per experimental sub-section. This was seen as reasonable as the range between maximum and minimum temperatures recorded over the 350m long sub-section was small.

Once an average temperature within the asphalt material on the day of FWD testing per sub-section was determined, the asphalt temperature and dynamic modulus relationship depicted in Figure 6.11 for a specified loading frequency was used to estimate the stiffness of the asphalt layer in the field.

The relationship was extracted from asphalt master curves developed by the CSIR (Anochie-Boateng et al, 2011) as discussed above.

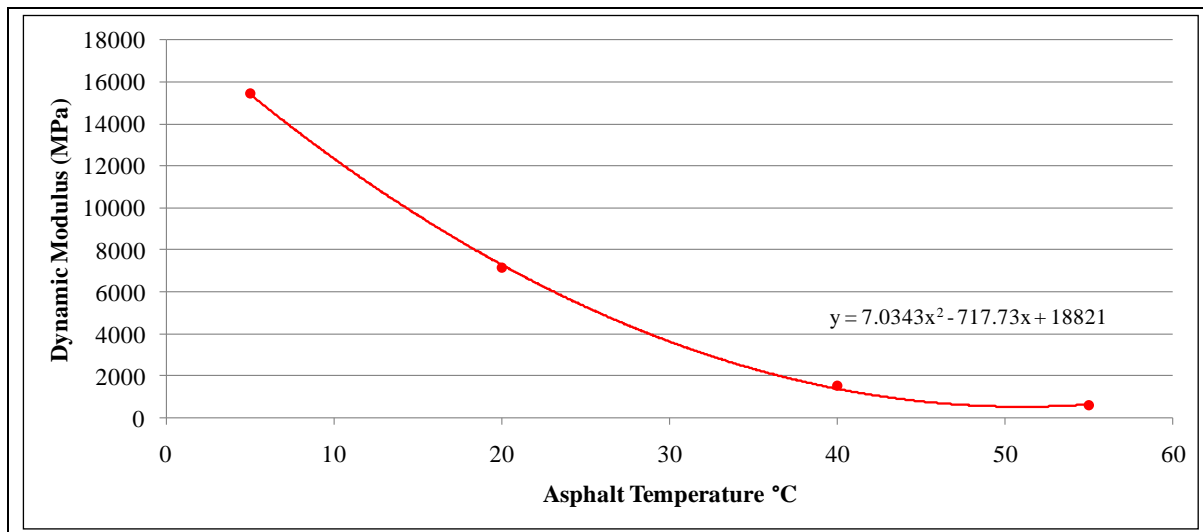


**Figure 6.11: Asphalt temperature – dynamic stiffness relationship at 5 Hz loading rate (CSIR)**

The back-calculation of FWD deflection bowls measured on asphalt surfaced sub-sections was carried out utilising backGAMES. The pavement structure model used in the back-calculation process fixed the asphalt stiffnesses to values determined by the procedure described above. By applying the above method greater confidence can be attributed to the accuracy of the back-calculated stiffnesses of the base, sub-base and subgrade layers.

#### 6.4.3 Correlation between stabilised base layer stiffness and deflection bowl parameters

In order to check the validity of the back-calculation process and the trends in stiffness values observed over the 360 day assessment period, the average back-calculated stiffnesses per sub-section were compared with the deflection parameters determined directly from the measured FWD deflection bowls. A full set of FWD deflection parameters for an experimental sub-section are attached in Addendum C. Figure 6.12 and Figure 6.13 below depict the trends in BLI and RoC along with the back-calculated stiffness of the 175mm BSM foam layer with 2% cement added in the southbound lane.

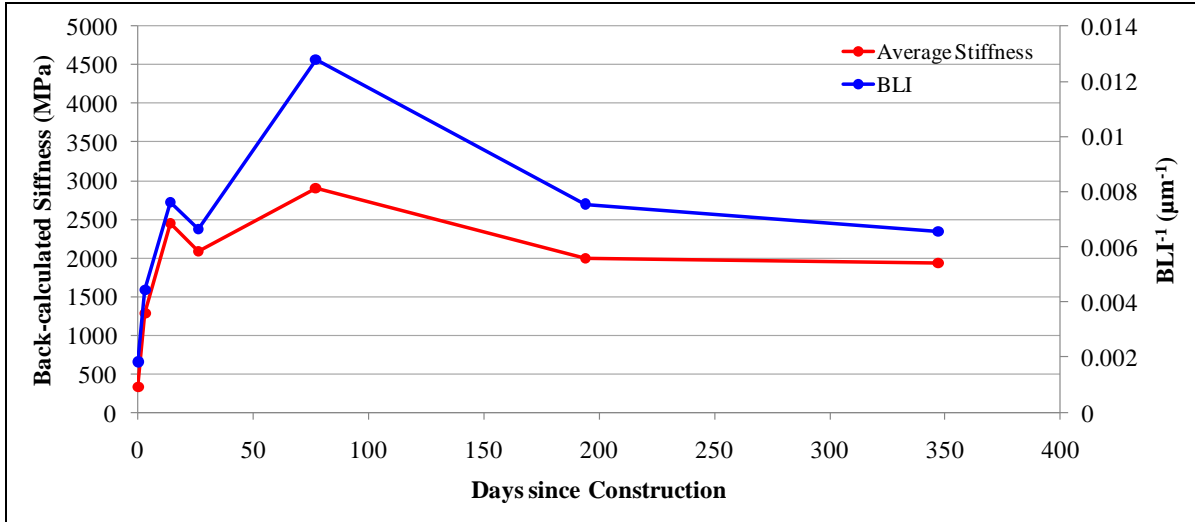


Figure 6.12: Base layer stiffness and BLI trend comparison – 175mm BSM foam 2% cement SB

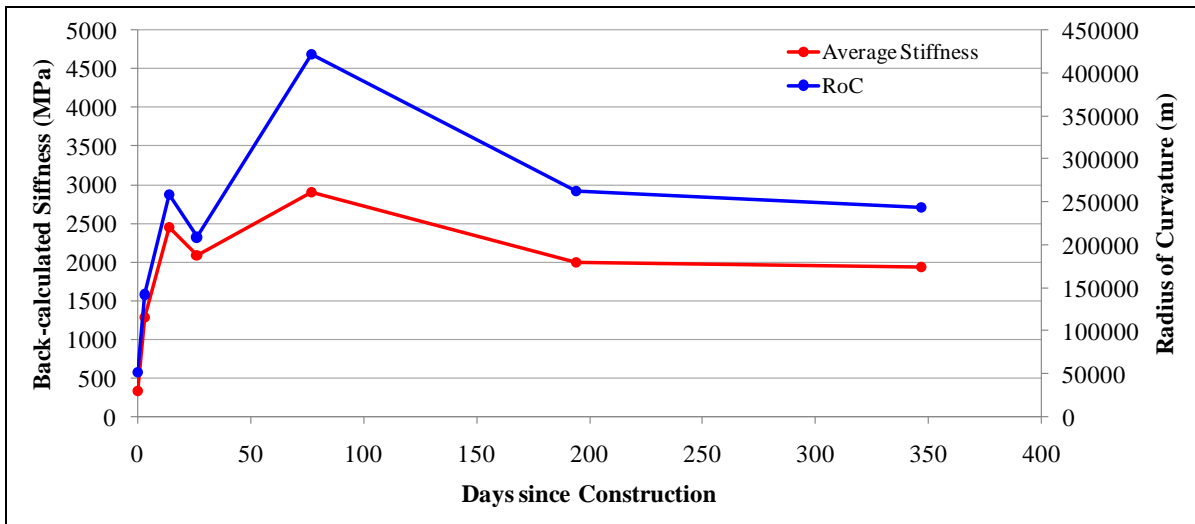


Figure 6.13: Base layer stiffness and RoC trend comparison – 175mm BSM foam 2% cement SB

In order to carry out a bulk assessment of the correlation between the average back-calculated stiffness and the average of deflection bowl parameters per sub-section, the correlation coefficient  $r$ , is used. For the purpose of the bulk correlation of average back-calculated base layer stiffness and deflection parameter, the RoC is utilised as the correlation is linear and thus allows for the easy assessment of correlation between trends for large amounts of data utilising the correlation coefficient. The relationship between the back-calculated base layer stiffness and BLI is a power function relationship, see Figure 6.14, and involves a more complex analysis to confirm correlation and hence is not utilised.

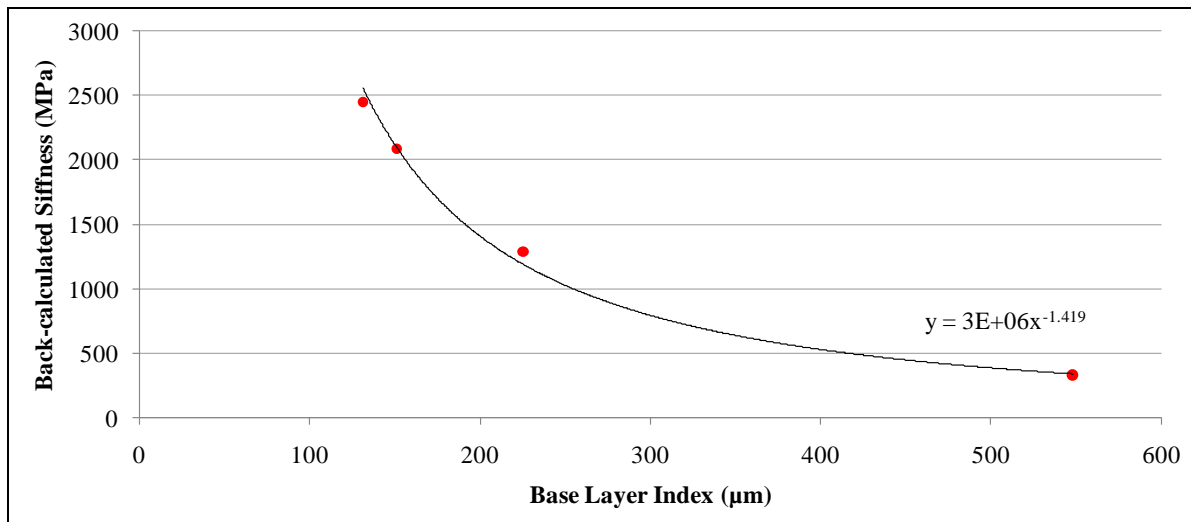


Figure 6.14: Power function relationship between back-calculated stiffness and BLI

Figure 6.15 illustrates the correlation between the average back-calculated base layer stiffness and the average RoC for the 175mm BSM foam layer with 2% cement added. Values determined for the pavement structures without bituminous surfacing are depicted as the correlation will be affected by the stiffening effects of the bituminous surfacing which cannot be removed from the RoC parameter, as is done within the back-calculation process to determine base layer stiffness. For the bulk correlation the surfaced pavement structure average back-calculated stiffness and average deflection bowl parameter correlation are reported separately to the correlation for the pavement structure without a surfacing layer.

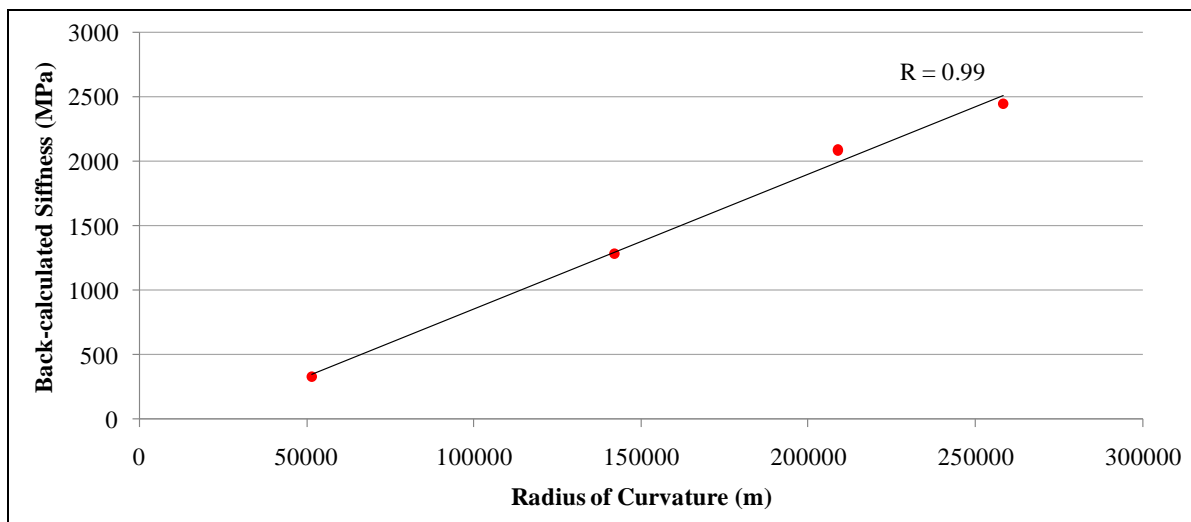


Figure 6.15: Average base layer stiffness to average RoC correlation - 175mm BSM foam 2% cement SB

Table 6.6 details the results of the correlation between the average back-calculated base layer stiffnesses and the average RoC per sub-section. A colour coding scheme is utilised to identify the degree of correlation between the base layer parameters, see Table 6.5.

**Table 6.5: Degree of correlation**

Category	R - value
Good	1.0
Fair	0.5
Poor	0.0

**Table 6.6: Correlation of average back-calculated base layer stiffness and average RoC**

Sub-section	Correlation co-efficient R		Surfacing
	Southbound	Northbound	
200mm C3-1 (2% c, 1% l)	1.0	1.0	N
	0.7	0.4	Y
200mm C3-2 (2% c, 1% l)	1.0	-	N
	0.3	-	Y
200mm ETB 3 (0.9%b, 1% c)	-	1.0	N
	-	1.0	Y
175mm BSM Emulsion (1% c, 2.4% b)	1.0	1.0	N
	1.0	1.0	Y
200mm BSM Emulsion (1% c, 2.4% b)	1.0	1.0	N
	1.0	1.0	Y
175mm BSM Emulsion (2% c, 2.4% b)	1.0	1.0	N
	1.0	1.0	Y
200mm BSM Emulsion (2% c, 2.4% b)	1.0	1.0	N
	1.0	1.0	Y
175mm BSM Foam (1% c, 2.4% b)	1.0	1.0	N
	1.0	0.9	Y
200mm BSM Foam (1% c, 2.4% b)	1.0	1.0	N
	1.0	1.0	Y
175mm BSM Foam (2% c, 2.4% b)	1.0	1.0	N
	1.0	1.0	Y
200mm BSM Foam (2% c, 2.4% b)	1.0	1.0	N
	1.0	1.0	Y

Table 6.6 above clearly shows that the correlation between the average back-calculated stiffness and average RoC per sub-section is represented by an R value of one in most cases showing a high degree of correlation. The most significant non-correlation is identified for the C3 layers with bituminous surfacing however this supposed non-correlation is due to the low variability in average stiffness values for the three average stiffness determinations made on the surfaced C3 sub-sections.

#### 6.4.4 Back-calculated stiffness and surface modulus correlation

The trend in pavement layer back-calculated stiffness through the depth of the pavement structure was compared against the surface modulus calculated for each deflection measured along the pavement surface by the FWD for an example sub-section. Assuming a 45° cone of load transfer through the pavement structure, geophone deflections along the pavement surface can be related to a pavement structure depth. The surface modulus calculated at each geophone position therefore relates to the strength of pavement material at an equivalent depth into the pavement structure as the geophone distance from the FWD load plate. By comparing the surface moduli calculated through the depth of

the pavement structure with the average back-calculated stiffnesses for the 175mm BSM foam with 1% cement sub-section in the northbound lane confidence in the back-analysis process is gained.

The surface modulus is calculated by the following equations:

At  $r = 0$ ,

$$SM_0 = 2\sigma_0(1 - \mu^2) \left( \frac{a}{d_0} \right) \quad \text{Equation 5}$$

Where;

$SM_0$  = Surface modulus directly beneath the load plate (MPa)

$\sigma_0$  = Peak stress beneath the load plate (MPa)

$\mu$  = Poisson's ratio, typically 0.35

$a$  = Load plate radius (mm)

$d_0$  = Deflection at load plate (mm)

At  $r = t$ ,

$$SM_t = \sigma_0(1 - \mu^2) \left( \frac{a^2}{rd_t} \right) \quad \text{Equation 6}$$

Where;

$SM_t$  = Surface modulus at depth  $t$  (MPa)

$\sigma_0$  = Peak stress beneath the load plate (MPa)

$\mu$  = Poisson's ratio, typically 0.35

$a$  = Load plate radius (mm)

$d_t$  = Deflection at position  $t$  (mm)

Figure 6.16 shows the plot of all surface modulus values, average surface modulus and average back-calculated layer stiffness through the depth of the pavement structure along 175mm BSM foam with 1% cement sub-section in the northbound lane. A good correlation between surface moduli and back-calculated pavement layer stiffness is observed giving confidence in the back-analysis process.

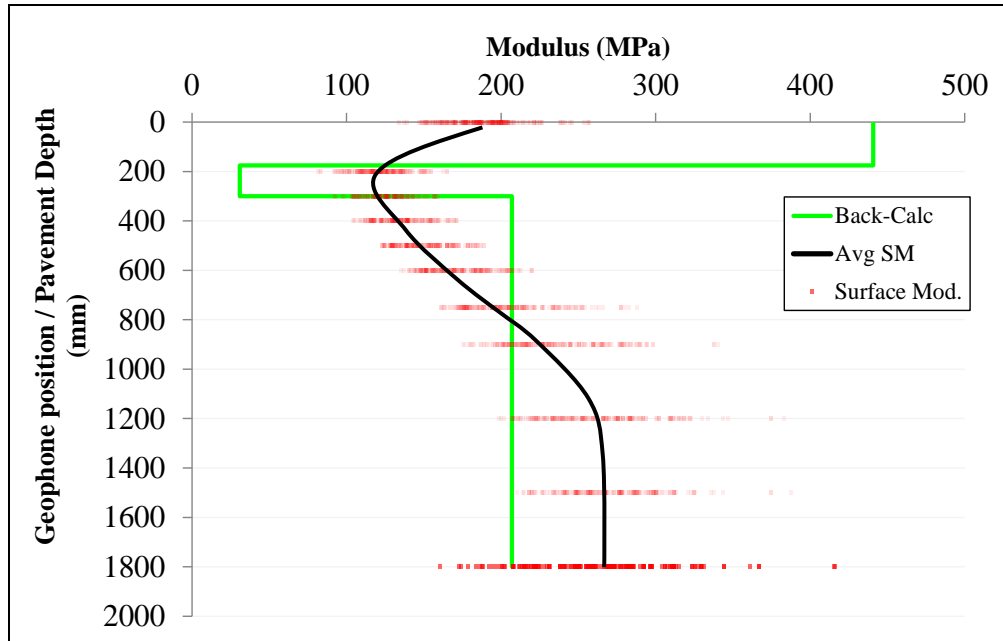


Figure 6.16: Correlation between back-calculated stiffness and surface modulus

#### 6.4.5 FWD rubber buffer temperature and stiffness

A theory was proposed that the temperature of the rubber buffers and hence subsequent variation in loading rate of the pavement during FWD testing may be affecting the observed FWD deflections and hence back-calculated layer stiffnesses (Kannemeyer, 2013). According to Dynatest, the manufacturers of the FWD utilised in the study presented here, once proper warm up drops are carried out before testing, the rubber buffer will reach a constant stiffness. Further investigation into this proposed phenomenon is required. Preliminary observations of air temperature data during FWD testing along the R35 experimental section, which is expected to correlate with the buffer temperature, indicate that there is no correlation between the observed stiffness variability and air temperature fluctuation at the time of FWD testing.

## CHAPTER 7 TRENDS IN STABILISED BASE LAYER STIFFNESS OVER TIME

This chapter illustrates and discusses the trends in average back-calculated stabilised base layer stiffness over time for each experimental sub-section's pavement structure model. The term stiffness utilised in this section refers to the stiffness determined through the back-analysis of FWD deflection bowls as discussed in Chapter 6.

A method of quantifying and visualising the trend in base layer stiffness was formulated in order to analyse the vast quantity of data. This chapter focuses on the average stiffness per stabilised material type, how it varies over time and factors influencing this variability. Theorised trends in stiffness development for each stabilised material type, discussed in Section 2.5, were compared to the actual stiffness trends observed.

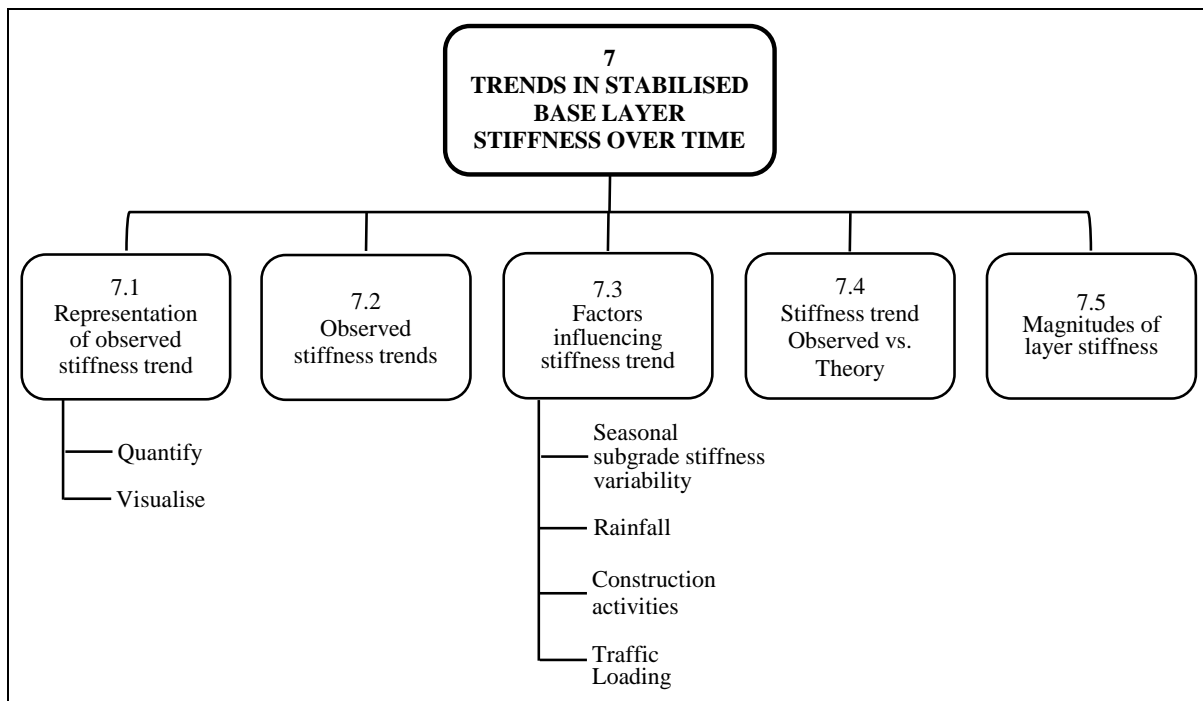


Figure 7.1: Outline of topics covered in Chapter 7

### 7.1 Representation of stabilised base layer stiffness trend over time

#### 7.1.1 Quantification of change in stiffness

The trend over time in average back-calculated stiffness of the stabilised base layers from the various experimental sub-sections were analysed by comparing the percentage change in stiffness between subsequent days of FWD measurement. The percentage change in stiffness identified whether the base layer stiffness had increased, decreased or remained stable between consecutive average stiffness determinations. The percentage change in average stiffness was determined by the following equation.



$$\% \text{StiffnessChange} = \frac{M_2 - M_1}{M_1} \times 100 \quad \text{Equation 7}$$

Where;

$M_1$  = Back-calculated stiffness at the start of the period

$M_2$  = Back-calculated stiffness at the end of the period

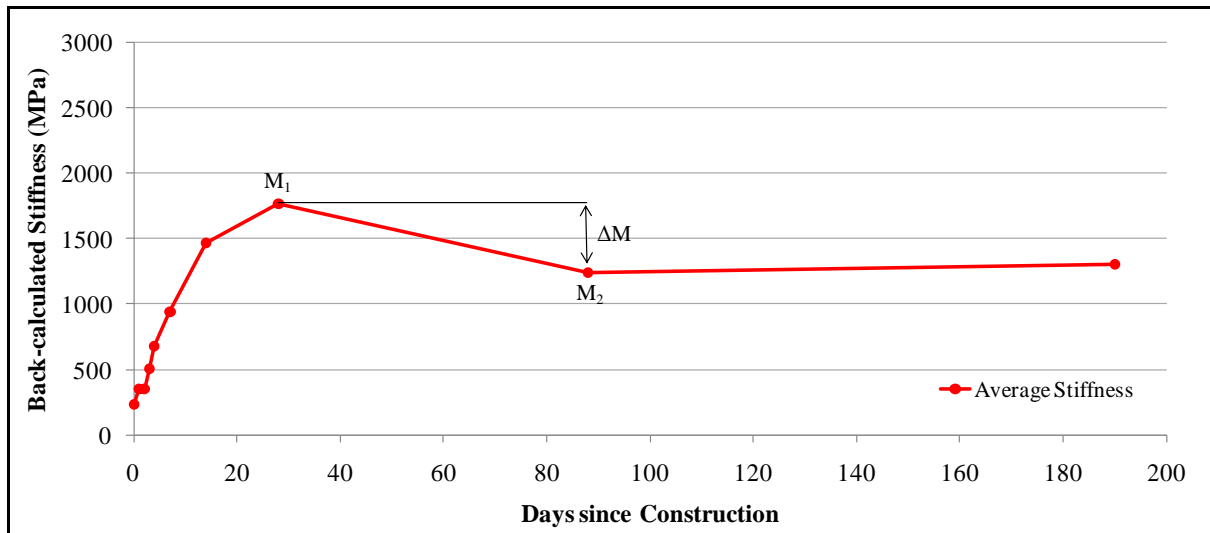


Figure 7.2: Depiction of parameters used in determination of percentage drop in stiffness

It is noted that this analysis method calculates the percentage change in stiffness between brief ‘snapshots’ of the stiffness profile of the stabilised layers. Variation in stiffness during the period between these ‘snapshots’ are not recorded because of the discrete FWD measurements. It is believed that the quantity of tests carried out during the initial 28 day FWD testing are substantial enough to have identified any significant variation in stiffness which may have occurred during the intervening period, hence a continuous plot through stiffness values is a reasonable estimation of the stiffness profile of the stabilised layer. For longer time periods of 90 and 180 days however, significant stiffness variation may have occurred and may not have been fully identified by the FWD tests carried out. This fact was considered when assessing possible trends in the stiffness of the pavement layers between values spaced by large time intervals.

## 7.1.2 Visualisation

### 7.1.2.1 Trend

In order to follow the trend in stiffness development over a 1 year period, graphs detailing the average, 95<sup>th</sup> and 5<sup>th</sup> percentiles of the back-calculated stiffness, determined from FWD deflection data measured along each experimental section at 5m intervals, are plotted with time. Also plotted are the complete sets of stiffness values calculated at each FWD test station at each temporal interval. This gives an indication as to the spread of stiffness values present along the length of each

Chapter 7 Trends in Stabilised Base Layer Stiffness over Time

experimental sub-section. Addendum D contains the stiffness plots for all experimental sub-sections displaying the average, 95<sup>th</sup> and 5<sup>th</sup> percentile back-calculated stiffnesses determined at each FWD testing day, spanning a period of approximately 360 days since the construction of the stabilised base layers. An example of this plot is shown below Figure 7.3.

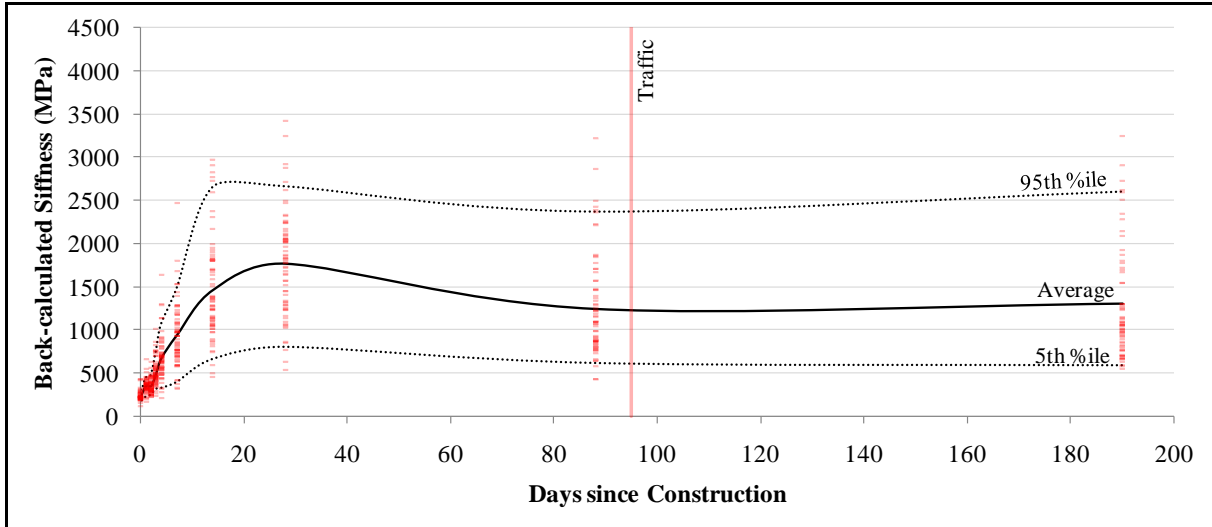


Figure 7.3: Typical plot of back-calculated stiffness trend

For the purposes of comparing the observed trend in stabilised base layer stiffness, the average base layer stiffness at each temporal location was plotted along with significant events occurring during the 360 day observation period. Significant events plotted include rainfall, surfacing layer construction activities and the opening of the experimental section to traffic. The average base layer stiffness was plotted to preserve the clarity of the graphical representation. An example of this plot is shown in Table 7.2. The complete set of average base layer stiffness plots for all material types is attached in Addendum E.

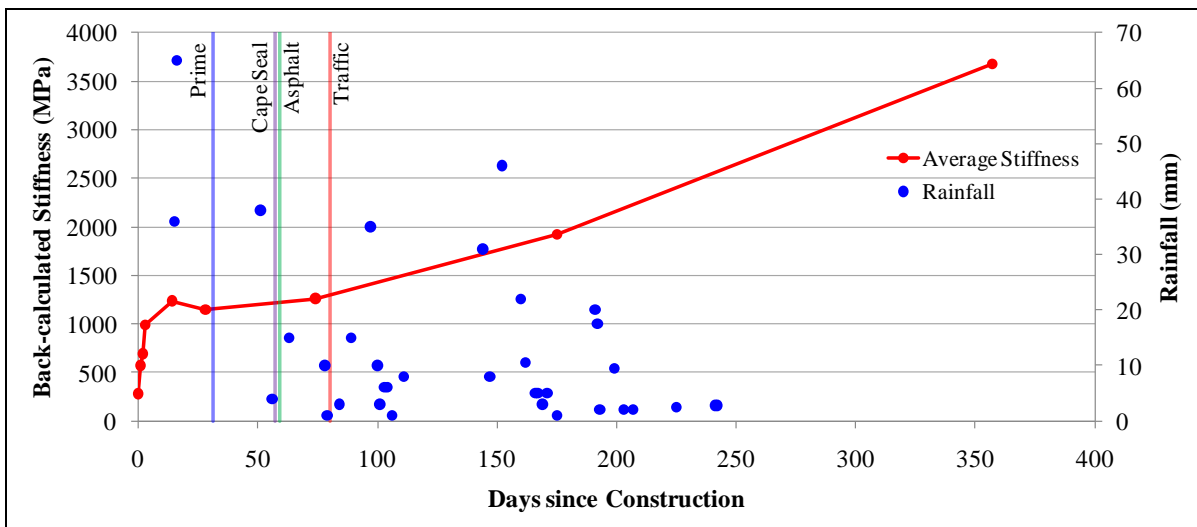


Figure 7.4: 175 mm bitumen emulsion (2.4%b, 2%c) NB - Rainfall and average base stiffness plot

Chapter 7 Trends in Stabilised Base Layer Stiffness over Time

For FWD testing subsequent to the initial 28 day period, the terms 90, 180 or 360 day FWD testing, refer to a general period describing the number of days since construction when the FWD testing of an experimental sub-section took place. It was not logistically feasible to measure each sub-section at exactly 360 days since its construction as each sub-section was constructed on a different day. Therefore FWD testing of the complete experimental section was carried out over a period which corresponded to 360 days since the construction of a sub-section within a few days. All data relating to FWD measurements will be plotted utilising its exact date but will be referred to in its general terms. The exact day since construction when FWD testing took place on each experimental sub-section is listed in Addendum A.

7.1.2.2 Quantified stiffness change

The percentage change in average base stiffness between each FWD test day was tabulated and the percentage change indicated by a colour coded system described in Table 7.1. Data relating to and quantifying the factors potentially influencing the change in base stiffness between the two stiffness determinations are then overlain to identify any possible correlations or patterns.

**Table 7.1: % Stiffness change - colour code**

Significant Increase	> 15%
Slight Increase	5% > or <= 15%
No change	+/- 5%
Slight Decrease	-5% < or >= -15%
Significant Decrease	< -15%

An example of the visualised percentage change in average base layer stiffness is depicted in Table 7.2. The diagram clearly indicates the extent of changes in base layer stiffness between FWD measurement days. These illustrations along with stiffness influencing factors are discussed in Section 7.3. Tables detailing the actual percentage change in average stiffness between each of the FWD test days are attached in Addendum F.

**Table 7.2: Visualisation of % change in average base layer stiffness**

Sub-section	Days since construction				
	0 - 28	28 - 90	90 - 180	180 - 360	
200mm C3-1 (2% c, 1% l)	Green	Green	Red	Green	Green
200mm C3-2 (2% c, 1% l)	Black	Green	Red	Blue	Red
175 Emulsion (1% c, 2.4% b)	Green	Green	Red	Red	Green
200 Emulsion (1% c, 2.4% b)	Green	Green	Red	Red	Green
175 Emulsion (2% c, 2.4% b)	Green	Green	Red	Red	Green
200 Emulsion (2% c, 2.4% b)	Green	Red	Green	Green	Red
175 Foam (1% c, 2.4% b)	Green	Green	Red	Red	Green
200 Foam (1% c, 2.4% b)	Green	Green	Red	Red	Green
175 Foam (2% c, 2.4% b)	Green	Green	Red	Red	Blue
200 Foam (2% c, 2.4% b)	Black	Green	Blue	Green	Red

## 7.2 Observed trends in base layer stiffness over time

### 7.2.1 Cement stabilised layers – 2% cement, 1% lime

Figure 7.5 below is a plot of the average base layer stiffness of cement stabilised base layers in both the northbound and southbound lanes of the experimental section over the 360 day observation period. Also plotted are significant events which occurred over the 360 day observation period. The symbology used to describe these events is explained in Table 7.3. The first set of events graphed relates to the southbound lane and the second set relates to the northbound lane. The average base layer stiffness trends for each sub-section plotted separately are attached in Addendum E.

**Table 7.3: Symbology used in stiffness trend plots**

Event	Symbology	
	Colour	Symbol
Rainfall	Blue	Points
Prime (P)	Blue	Vertical lines
Cape Seal (C)	Purple	Vertical lines
Asphalt (A)	Green	Vertical lines
Opening to traffic (T)	Red	Vertical lines

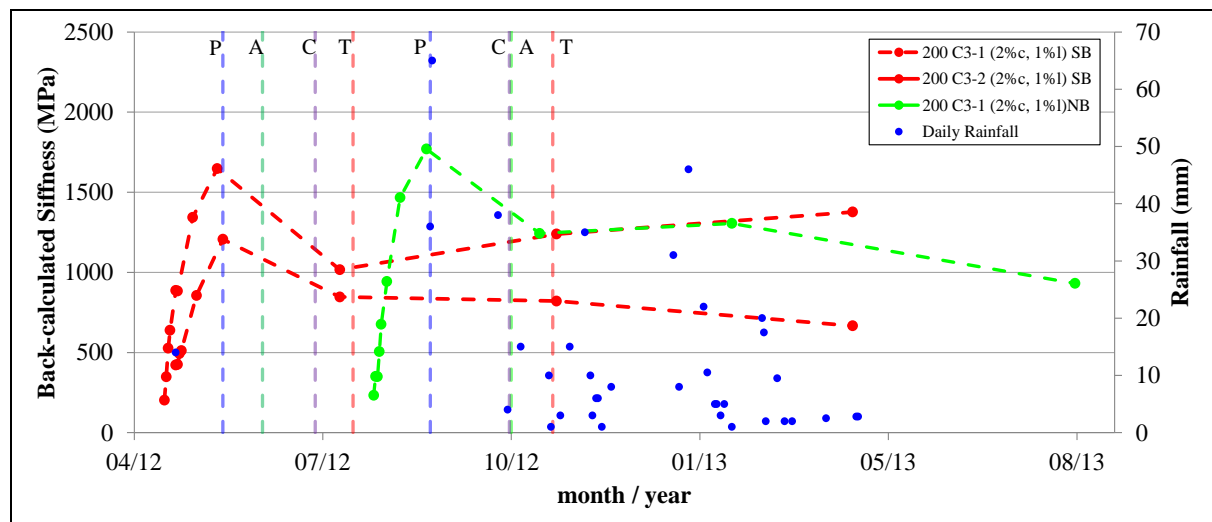


**Figure 7.5: Cement stabilised base layer average layer stiffness plot**

The average base layer stiffness trends for all cement stabilised materials show significant similarity over the 360 day observation period. The significant drop in base stiffness between day 28 and day 90 FWD testing coincided with bituminous surfacing construction activities. The damaging effects of this construction traffic may have had an influence on the cement and lime stabilised layer stiffness.

The majority of rainfall occurred between the 90, 180 and 360 day FWD testing however no significant effects on average base layer stiffness trend is observed.

## Chapter 7 Trends in Stabilised Base Layer Stiffness over Time

Subsequent to the opening of the experimental section to traffic no significant changes in trend of the cement stabilised layer stiffness are noted. Slight reductions in average stiffness occur for the C3-1 layer in the northbound and the C3-2 layer southbound between 180 and 360 day FWD testing. The C3-1 base layer in the southbound lane shows continued increase in stiffness subsequent to opening of the experimental section to traffic.

## 7.2.2 BSM Emulsion - 0.9% residual bitumen, 1% cement

The trend in average base layer stiffness for the BSM emulsion layer stabilised with 0.9% residual bitumen and 1% cement shows a stiffness increase during its curing phase, see Figure 7.5. A reduction in stiffness is noted subsequent to the application of the cutback bitumen prime and heavy rainfall. The average base layer stiffness remains relatively constant for the remainder of the observation period with a slight increase noted at 360 days.

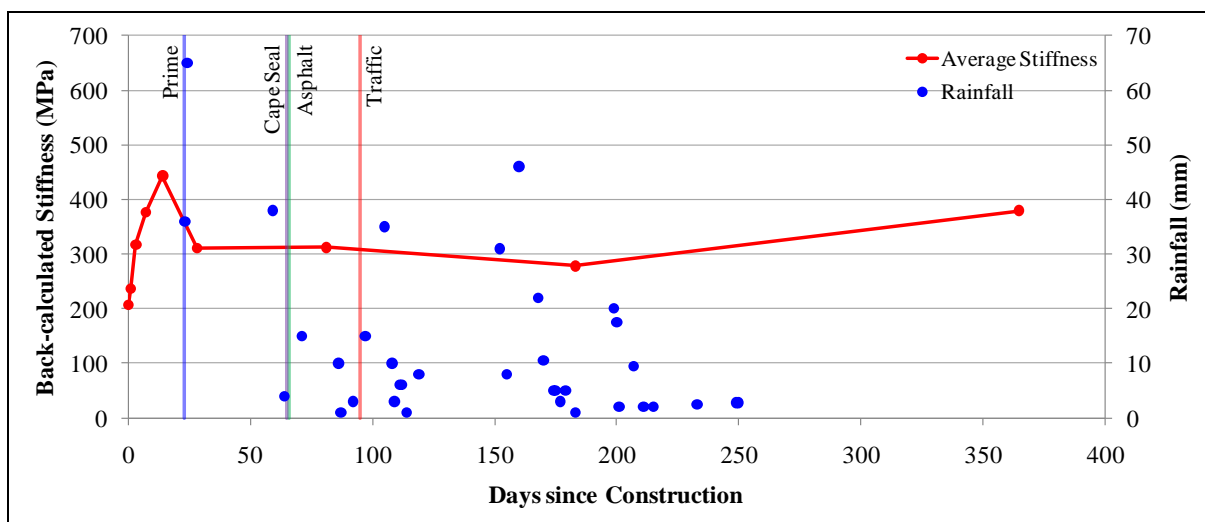


Figure 7.6: BSM Emulsion (0.9% residual bitumen and 1% cement) average layer stiffness plot

## 7.2.3 BSM Emulsion - 2.4% residual bitumen, 1% cement

The trends in average base layer stiffness of BSM emulsion layers stabilised with 2.4% residual bitumen and 1% cement are plotted in Figure 7.7. A clear correlation in stiffness trend is observed for these stabilised layers in both directional lanes. Subsequent to 28 days since construction of the stabilised base layers in both northbound and southbound lanes a reduction in base layer stiffness occurs.

Construction activities relating to the wearing coarse correlate with average stiffness reductions in both lanes.

The occurrence of heavy rainfall correlates with stiffness reduction in both northbound and southbound lanes. Increases in average base layer stiffness are observed in both lanes subsequent to

Chapter 7 Trends in Stabilised Base Layer Stiffness over Time

rainfall and the wet season. A significant increase in stiffness is observed in the northbound lane where FWD deflection measurements were taken outside of the wet season.

The opening of the experimental section to traffic does show a correlation with reductions in average base layer stiffness in the southbound lane however not in the north.

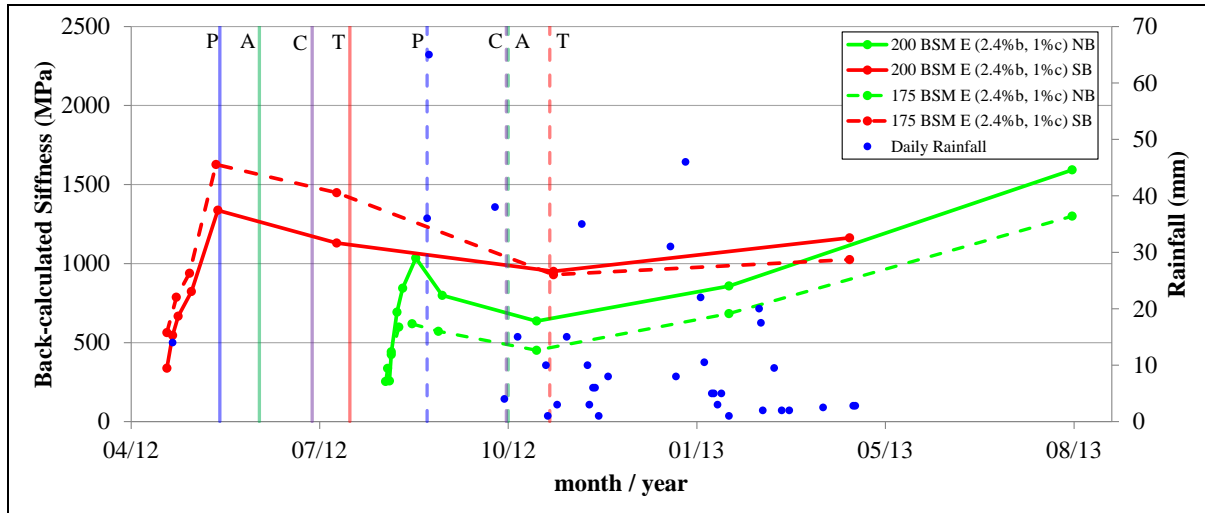


Figure 7.7: BSM Emulsion (2.4% residual bitumen and 1% cement) average layer stiffness plot

7.2.4 BSM Emulsion - 2.4% residual bitumen, 2% cement

The trends in average base layer stiffness for BSM emulsion materials stabilised with 2.4% residual bitumen and 2% cement indicate very different trends between both directional lanes over the 360 day observational period.

A significant reduction in average base layer stiffness occurs in the southbound lane between 90 and 180 days since construction. Significant rainfall is noted to have fallen during this period. Base layer stiffnesses in the northbound lane are seen to increase significantly up to 360 days since construction.

The application of prime to the 200 mm thick BSM emulsion layers is also seen to correlate with a significant but temporary reduction in base layer stiffness in the northbound and southbound lanes.

Chapter 7 Trends in Stabilised Base Layer Stiffness over Time

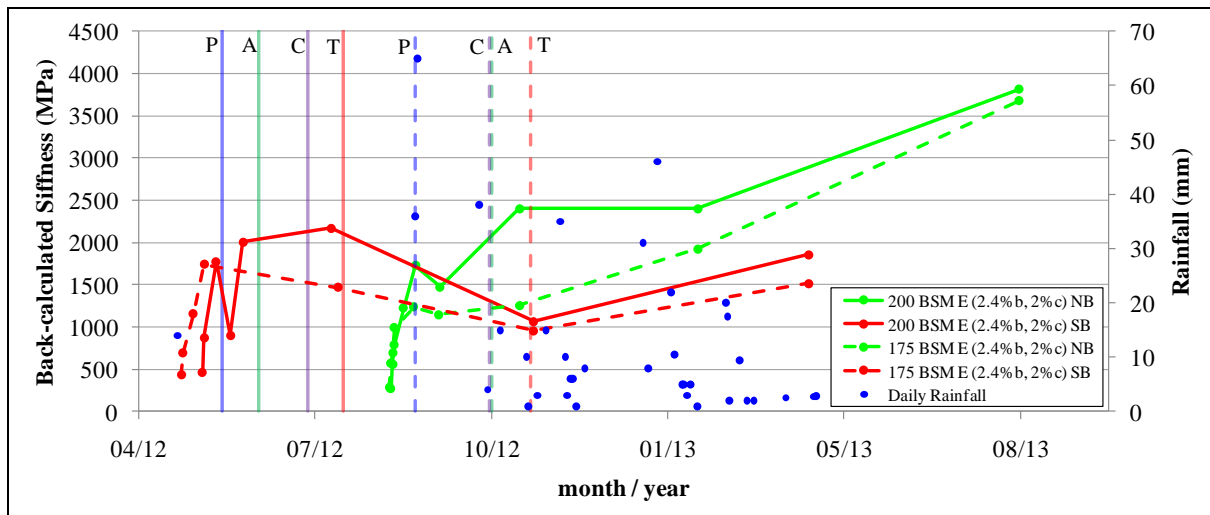


Figure 7.8: BSM Emulsion (2.4% residual bitumen and 2% cement) average layer stiffness plot

7.2.5 BSM Foam – 2.4% residual bitumen, 1% cement

Variable trends in average base layer stiffness are noted for BSM foam layers stabilised with 2.4% residual bitumen and 1% cement. In the southbound lane the 200 mm thick layer shows abnormally high stiffness values at 90 days since construction. A reason for this observation has not yet been confirmed however it is suspected to be due to the extremely low temperatures (5°C) experienced during FWD testing. Similar to BSM Emulsions in the southbound lane significant reductions in base layer stiffness are noted between 90 and 180 day stiffness determinations. Base layer stiffness values in the northbound lane show significant variability over the 360 day period however significant base layer stiffness increase is noted at 360 days after construction.

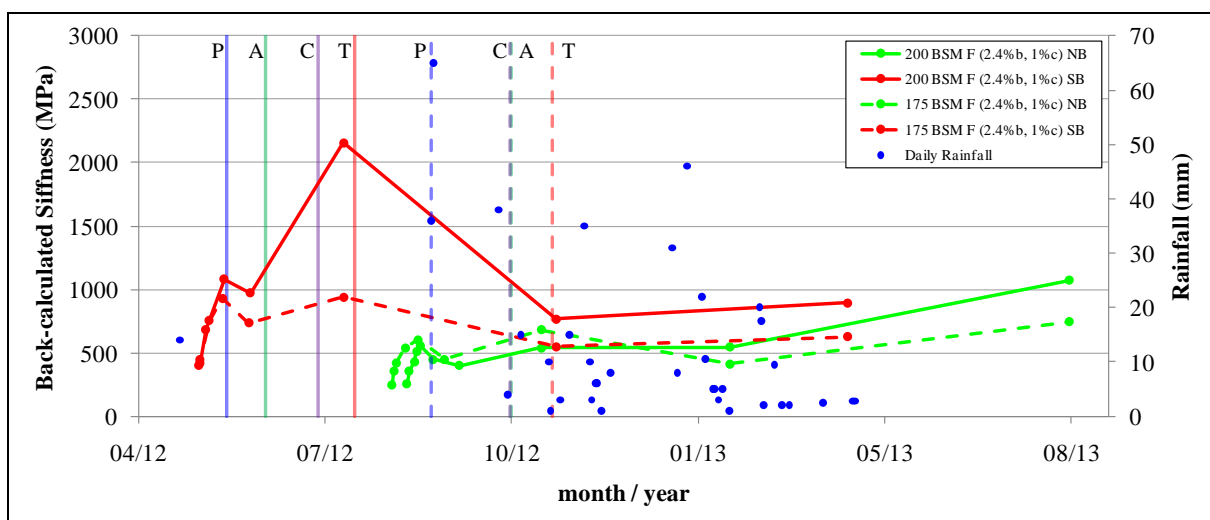


Figure 7.9: BSM Foam (2.4% residual bitumen and 1% cement) average layer stiffness plot

7.2.6 BSM Foam – 2.4% residual bitumen, 2% cement

BSM foam layers stabilised with 2.4% residual bitumen and 2% cement show similar trends in base layer stiffness compared with BSM emulsion layers with 2% cement added. In the southbound lane a

significant base layer stiffness reduction is observed coinciding with significant rainfall subsequent to 90 days since construction. The base layer stiffness remains constant up until 360 days since construction.

Base layer stiffness values in the northbound lane show a continuous increase in stiffness over the 360 day observation period. A reduction in stiffness is observed between 90 and 180 day stiffness determinations for the 175mm thick layer in the northbound lane however the overall trend indicates increasing base layer stiffness.

Temporary reductions in base layer stiffness are noted coinciding with the application of prime to the base layers in all but the 175 mm BSM foam layer in the northbound lane.

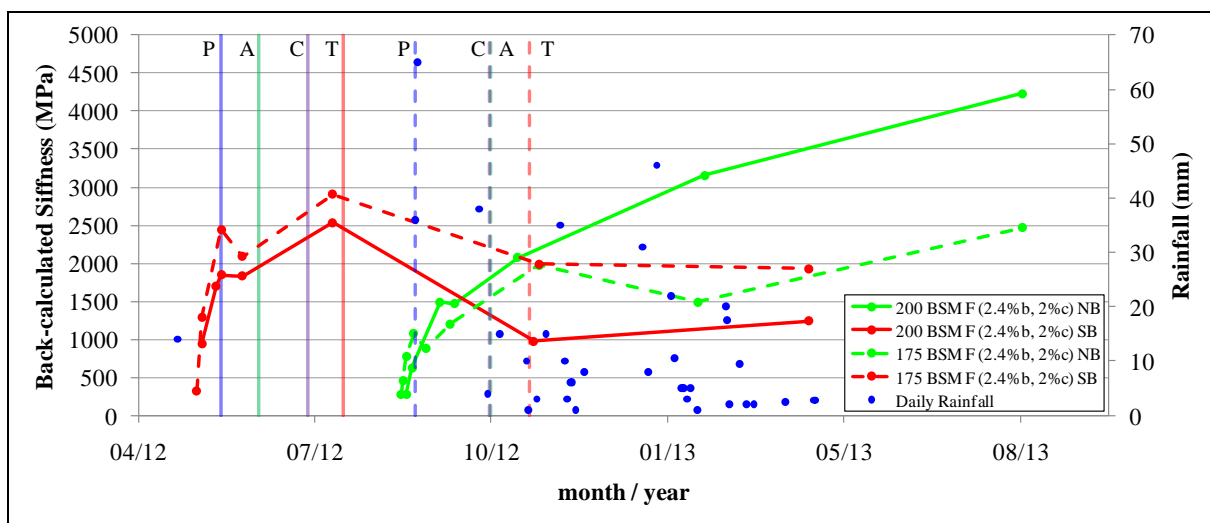


Figure 7.10: BSM Foam (2.4% residual bitumen and 2% cement) average layer stiffness plot

### 7.3 Identification of factors influencing observed trends

#### 7.3.1 Pavement layer seasonal moisture content and temperature fluctuation

As no long term moisture content data relating to the pavement layer materials were collected, daily rainfall records were used to identify temporal positions where the moisture content of the pavement layers may have increased due to moisture ingress from rainfall. Daily rainfall measurements were taken at the site laboratory approximately 5 km from the experimental section.

As illustrated in Figure 7.5 to Figure 7.10 reductions in stiffness of many of the stabilised base layers show a correlation with rainfall events occurring during the 360 day observation period. In order to summarise this observation colour-coded tables, detailed in Section 7.1.2.2, are used. Table 7.5 and Table 7.6 depict the correlation between reductions in base layer stiffness and rainfall occurrence for northbound and southbound lanes.



Chapter 7 Trends in Stabilised Base Layer Stiffness over Time

**Table 7.4: % Stiffness change - colour code**

Significant Increase	> 15%
Slight Increase	5% > or <= 15%
No change	+/- 5%
Slight Decrease	-5% < or >= -15%
Significant Decrease	< -15%

**Table 7.5: Correlation of average stiffness trend with rainfall (mm) - Southbound**

Sub-section	Days since construction			
	0 - 28	28 - 90	90 - 180	180 - 360
200mm C3-1 (2% c, 1% l)			172	274
200mm C3-2 (2% c, 1% l)			169	277
175 Emulsion (1% c, 2.4% b)			169	277
200 Emulsion (1% c, 2.4% b)			169	277
175 Emulsion (2% c, 2.4% b)			169	277
200 Emulsion (2% c, 2.4% b)			169	277
175 Foam (1% c, 2.4% b)			169	277
200 Foam (1% c, 2.4% b)			169	277
175 Foam (2% c, 2.4% b)			172	274
200 Foam (2% c, 2.4% b)			169	277

**Table 7.6: Correlation of average stiffness trend with rainfall (mm) - Northbound**

Sub-section	Days since construction			
	0 - 28	28 - 90	90 - 180	180 - 360
200mm C3-1 (2% c, 1% l)		158	224	61
200mm Emulsion (0.9% b, 1% c)	101	57	235	61
175 Emulsion (1% c, 2.4% b)	101	57	235	61
200 Emulsion (1% c, 2.4% b)	101	57	235	61
175 Emulsion (2% c, 2.4% b)	101	57	235	61
200 Emulsion (2% c, 2.4% b)	101	57	235	61
175 Foam (1% c, 2.4% b)	101	57	235	61
200 Foam (1% c, 2.4% b)	101	57	235	61
175 Foam (2% c, 2.4% b)	101	71	221	61
200 Foam (2% c, 2.4% b)	101	57	235	61

Table 7.5 and Table 7.6 indicate that many of the reductions in base layer stiffness correlate with a rainfall event. The correlating rainfall events represent the most intense periods of rainfall measured over the 360 day period.

This correlation is proposed to be due to pavement seasonal moisture condition variability. The effect of the degree of saturation of granular materials within pavement layers on the stiffness of those pavement layers is well understood, as discussed by Hicks and Monismith (1971).

It is unlikely that moisture content increase in the base layer due to rainfall has caused the observed base layer stiffness reduction. Two reasons for this observation are identified. The base layers are paved with a water proof new bituminous wearing course. In addition FWD measurements are taken a

Chapter 7 Trends in Stabilised Base Layer Stiffness over Time

distance of 2m inside the road centreline therefore at least 1.5m away from the pavement edge. Research has shown that the zone of seasonal variability in moisture contents within a pavement base layer exists up to 1.5m from the bituminous surfacing edge and typically 600 mm to 1000 mm for the bituminous surfacing edge (Emery, 1985).

The observed reduction in BSM layer stiffness is proposed to be due to the materials stress dependent characteristics responding to a reduction in stiffness of the supporting subgrade due to moisture content increase from rainfall induced moisture ingress. Figure 15 shows the plot of the stiffness trends for the 175 mm BSM emulsion layer with 1% cement added and the stiffness of its supporting subgrade over the 360 day observation period. The subgrade stiffness is represented by the deflection measured at the geophone 1800 mm from the load plate. An increase in deflection at the 1800mm geophone indicates a stiffness reduction of subgrade.

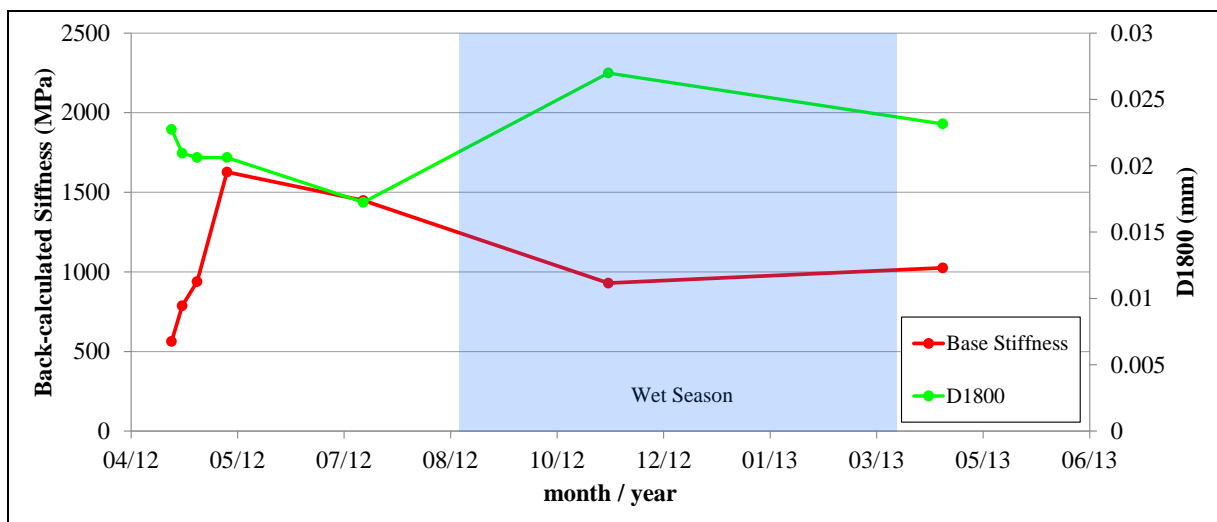


Figure 7.11: 175 mm BSM Emulsion (2.4%b, 1%c) base layer stiffness and 1800mm deflection - SB

Subgrade stiffness variability has been observed along the R35 experimental section over the 360 day observation period. Figure 7.12 plots the average of deflections measured at the FWD geophone positioned 1800mm from the load plate, per experimental sub-section, in the southbound lane. It is clear from Figure 7.12 that seasonal variability of the subgrade stiffness correlates with seasonal rainfall fluctuations. A sinusoidal subgrade stiffness model with period of 365 days fits the measured deflection data well further adding weight to the proposition that the observed stiffness variability may be due to seasonal pavement moisture content fluctuation. The form of the sine wave function takes the following form:

$$A \sin(\omega(t - \phi)) + K \tag{Equation 8}$$

Where;

$$A = (\text{Maximum Stiffness} + \text{Minimum Stiffness}) / 2$$

Chapter 7 Trends in Stabilised Base Layer Stiffness over Time

$$\omega = 1/\text{Period} = 1/365 \text{ cycles per day} = 2\pi/365 \text{ radians per day}$$

$\phi$  = Phase shift (Dependent upon climate)

K = Mean stiffness throughout 365 day cycle

**Table 7.7: D1800<sup>-1</sup> deflection variation - model parameters**

$\omega$ (rad/day)	A (MPa)	$\Phi$ (days)	Mean (MPa)
0.017	10	140	46

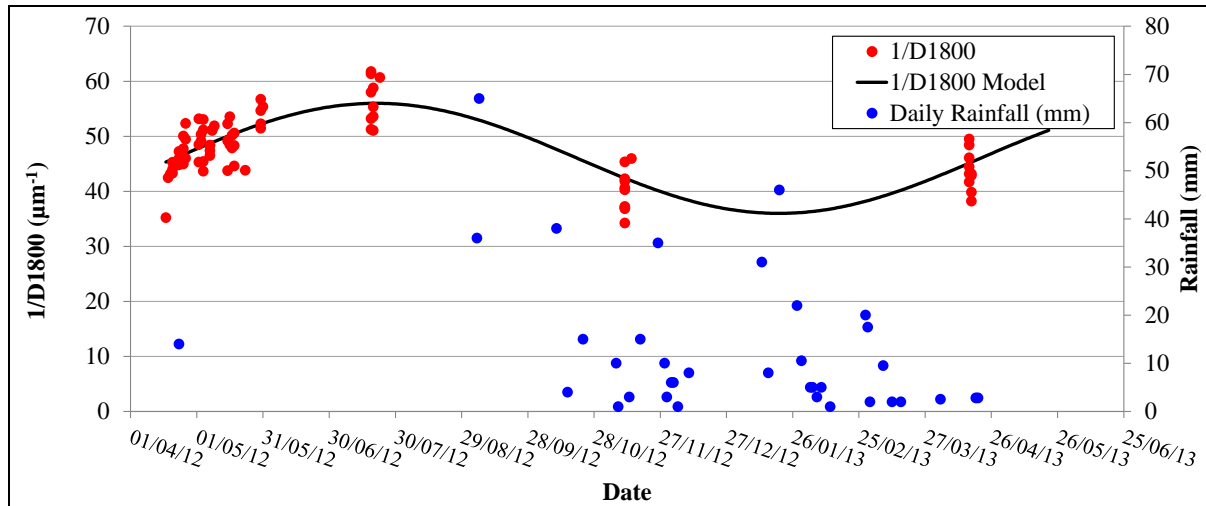


**Figure 7.12: Seasonal variability in subgrade stiffness correlating with seasonal rainfall pattern**

The variability observed and modelled in Figure 7.12 also correlated well with seasonal variability in air temperature. Figure 7.13 depicts the D1800 model created from actual FWD measurements on the southbound lane as well as the seven day moving average of air temperatures recorded at the site office within 5 kilometres of the experimental section during the 360 day observation period.

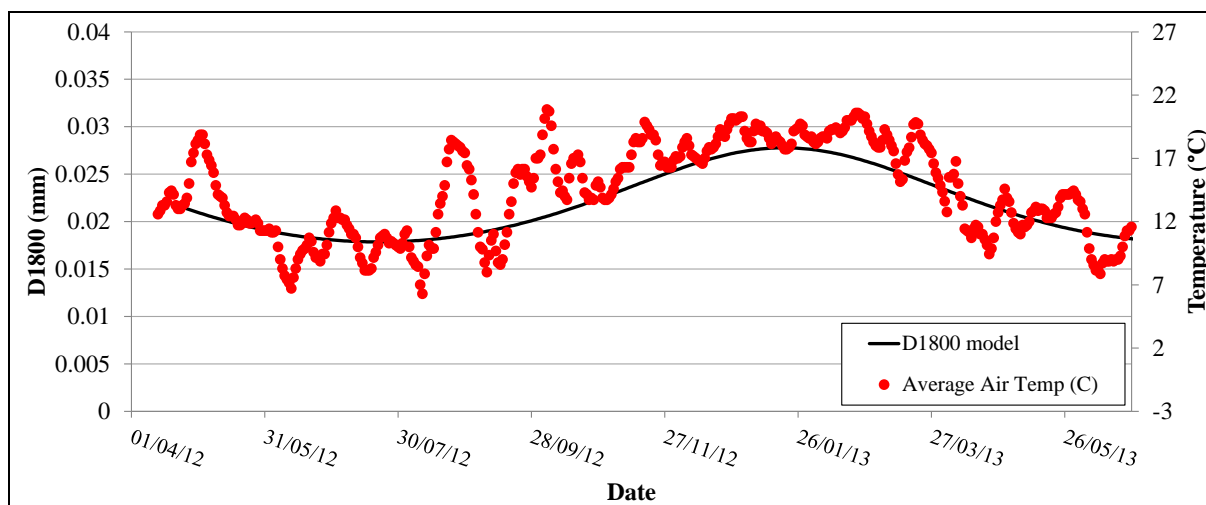


**Figure 7.13: Seasonal variability in air temperature correlating with D1800 model**

The subgrade seasonal stiffness variability beneath the cement stabilised materials in the southbound lane do not correlate with stiffness variability of cement stabilised layers themselves. This observation

conforms to the theory that cement stabilised layers are initially continuously bound and do not show stress dependent characteristics hence their resilient modulus will not be affected by the stiffness of supporting layers. Figure 17 depicts the trend in base layer stiffness the 200mm C3-1 layer along with its supporting subgrade stiffness, as indicated by the deflection measured at the 1800 mm geophone. No reduction in C-3 base layer stiffness is observed with significant increase of the average 1800mm geophone deflection measurement in line with season moisture variation. This indicates that the C3 layer is not affected by a reduction in stiffness of the supporting subgrade and may be bridging the reduced support.

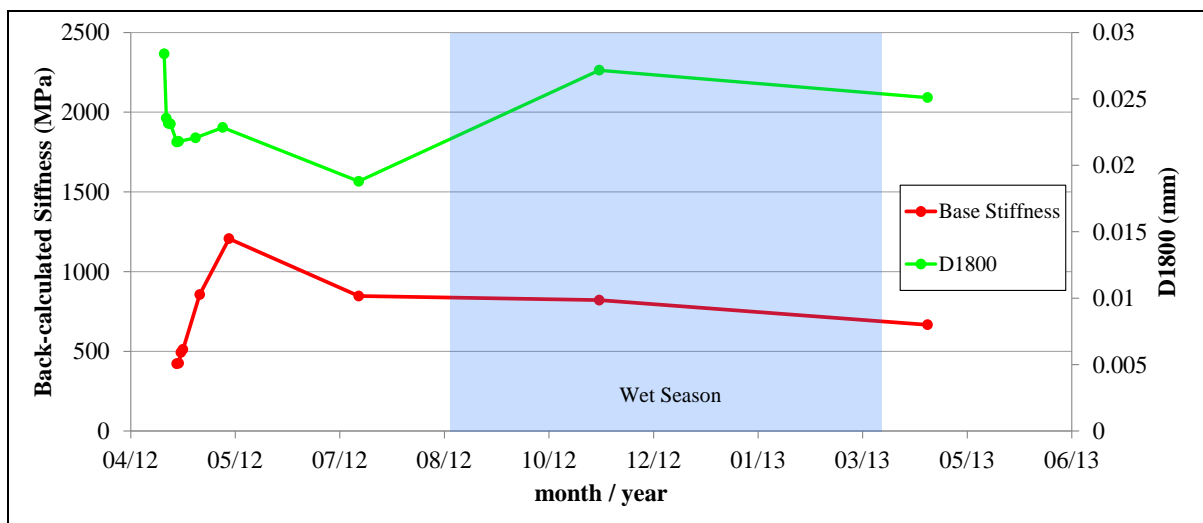


Figure 7.14: 200 mm C3-1 (2%c, 1%l) base layer stiffness and 1800mm deflection - SB

The above phenomenon proposed as a possible cause of the observed BSM base layer stiffness variability was observed in the southbound lane only.

### 7.3.2 Rainfall

In the northbound lane, BSM materials with 1% cement added showed an apparent correlation with southbound BSM layer seasonal stiffness variation as detailed in Section 7.3.1. This correlation is illustrated in Figure 7.15. However when examining the subgrade stiffness variability over the 360 day observation period in the northbound lane no seasonal variability was observed hence the subgrade support stiffness variability theory cannot be applied to the northbound lane. The plot of subgrade support stiffness as indicated by the deflection measurement 1800mm from the load plate is shown below in Figure 7.16.

It is proposed that the stiffness reductions observed on BSM base layers in the northbound lane are due to the direct application of moisture, in the form of rainfall, to these base layers before the construction of the bituminous surfacings. The occurrence of heavy rainfall before the construction of the asphalt and cape seal layers on the northbound experimental sub-sections is illustrated in Figure 7.15.

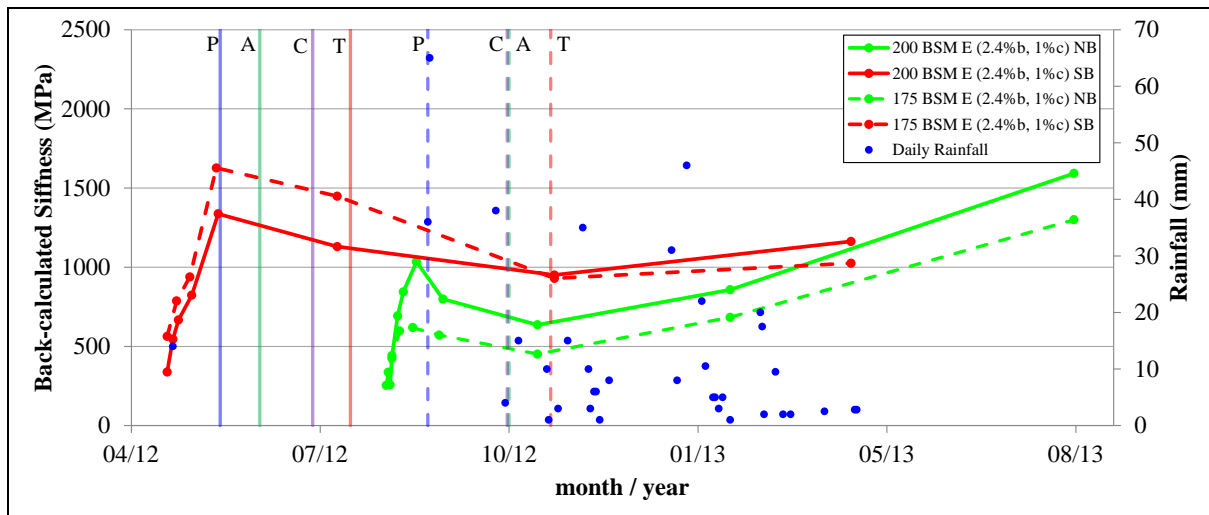


Figure 7.15: BSM Emulsion (2.4% residual bitumen and 1% cement) average layer stiffness plot

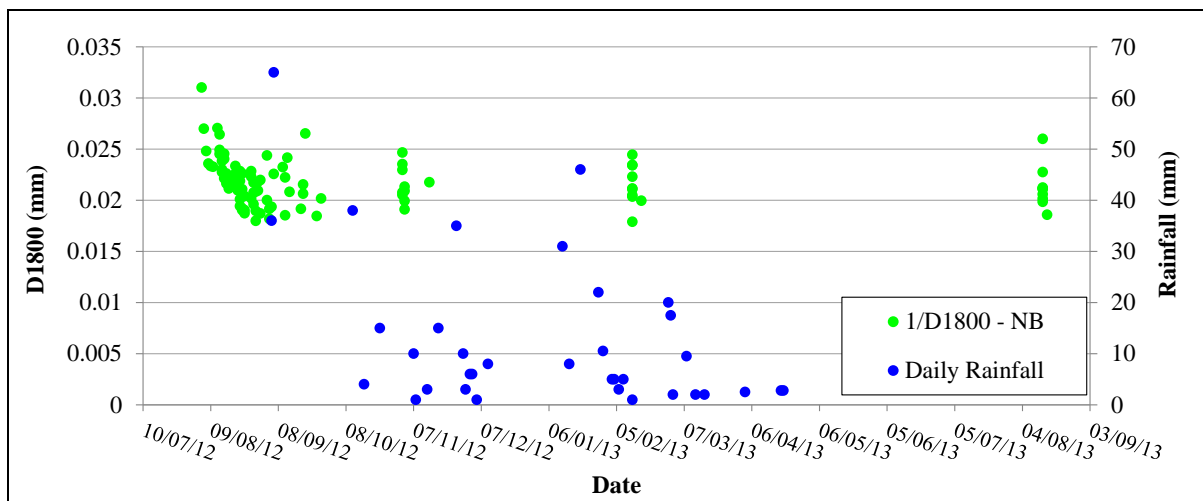


Figure 7.16: Plot of average geophone deflection measurements 1800mm from load plate - northbound

### 7.3.3 Construction Activity

Pavement surfacing activities on the experimental section include the following:

- COLAS MC 30 cut-back bitumen prime application
- S4 (19) Cape Seal
- 45mm AE-2 (Plastomer modified) asphalt with 13mm rolled in chips

From the depictions of stiffness trends detailed in Section 7.2 the correlation of reductions in base layer stiffness with surfacing layer construction activities was noted for a number of sub-sections. All cement stabilised base layer sub-sections showed a correlation between reductions in base layer stiffness and the construction of the surfacing layer. It is proposed that traffic due surfacing layer construction, in particular vibratory rollers, applying loads to the pavement structure have induced an early reduction in stiffness of the stiff, brittle cement stabilised layer.

Chapter 7 Trends in Stabilised Base Layer Stiffness over Time

The application of a cut-back bitumen prime was seen to correlate consistently with reductions in BSM base layer stiffness. It is proposed that the ingress of the prime into the BSM layer reduced the layer stiffness due to the bitumen softening effects of the cutter within the prime. Reductions in base layer stiffness of BSM layers were clearly observed where the application of the prime occurred between FWD measurements taken within a short time interval. Table 7.8 and Table 7.9 outline the subsections where the application of a prime correlated with a base layer stiffness reduction. Many of base layer stiffness reductions induced by prime application were observed to have been temporary with layer stiffnesses subsequently increasing.

**Table 7.8: Correlation of average stiffness trend with prime application - Southbound**

Sub-section	Days since construction			
	0 - 28	28 - 90	90 - 180	180 - 360
200mm C3-1 (2% c, 1% l)		Prime		
200mm C3-2 (2% c, 1% l)		Prime		
175 Emulsion (1% c, 2.4% b)		Prime		
200 Emulsion (1% c, 2.4% b)		Prime		
175 Emulsion (2% c, 2.4% b)		Prime		
200 Emulsion (2% c, 2.4% b)		Prime		
175 Foam (1% c, 2.4% b)		Prime		
200 Foam (1% c, 2.4% b)		Prime		
175 Foam (2% c, 2.4% b)		Prime		
200 Foam (2% c, 2.4% b)		Prime		
Expected Trend				

**Table 7.9: Correlation of average stiffness trend with prime application- Northbound**

Sub-section	Days since construction			
	0 - 28	28 - 90	90 - 180	180 - 360
200mm C3-1 (2% c, 1% l)		Prime		
200mm Emulsion (0.9% b, 1% c)		Prime		
175 Emulsion (1% c, 2.4% b)		Prime		
200 Emulsion (1% c, 2.4% b)		Prime		
175 Emulsion (2% c, 2.4% b)		Prime		
200 Emulsion (2% c, 2.4% b)		Prime		
175 Foam (1% c, 2.4% b)		Prime		
200 Foam (1% c, 2.4% b)		Prime		
175 Foam (2% c, 2.4% b)		Prime		
200 Foam (2% c, 2.4% b)		Prime		

7.3.4 Traffic

As noted in Section 4.2, data providing insight to traffic characterisation and quantification was limited for the R35 experimental section at the time of compiling this thesis. The influence of traffic loading on the stiffness of the stabilised base layers was investigated by comparing the percentage change in average base layer stiffness between consecutive FWD test days and the periods where traffic loads were applied to the experimental pavement structure. Table 7.10 and Table 7.11 show the

Chapter 7 Trends in Stabilised Base Layer Stiffness over Time

colour coded correlation tables for both southbound and northbound lanes and the periods where the experimental section was subjected to traffic loads.

A strong correlation between reductions in base layer stiffness and the opening of the experimental section to traffic is noted in the southbound lane. A poor correlation exists in the northbound lane. It is proposed that the stiffness trends observed on the R35 experimental section are not significantly due to the damaging effects of traffic. This is based on the observation that the majority of the experimental sub-sections showed an increase in stiffness between day 180 and day 360, subsequent to the significant base layer stiffness reductions coinciding with traffic loading on the experimental section. If reductions in base layer stiffness were due to traffic load damage it is unlikely that the damaged pavement materials would subsequently repair themselves and increase in stiffness to the extent observed.

**Table 7.10: Correlation of average stiffness trend with prime application - Southbound**

Sub-section	Days since construction			
	0 - 28	28 - 90	90 - 180	180 - 360
200mm C3-1 (2% c, 1% l)	Green	Green	Red	Traffic
200mm C3-2 (2% c, 1% l)	Black	Green	Red	Traffic
175 Emulsion (1% c, 2.4% b)	Green	Green	Red	Traffic
200 Emulsion (1% c, 2.4% b)	Green	Green	Red	Traffic
175 Emulsion (2% c, 2.4% b)	Green	Green	Red	Traffic
200 Emulsion (2% c, 2.4% b)	Green	Red	Light Green	Traffic
175 Foam (1% c, 2.4% b)	Green	Green	Red	Traffic
200 Foam (1% c, 2.4% b)	Green	Green	Red	Traffic
175 Foam (2% c, 2.4% b)	Green	Green	Red	Traffic
200 Foam (2% c, 2.4% b)	Green	Green	Red	Traffic
Expected Trend	Green	Light Green	Blue	Blue

**Table 7.11: Correlation of average stiffness trend with prime application- Northbound**

Sub-section	Days since construction			
	0 - 28	28 - 90	90 - 180	180 - 360
200mm C3-1 (2% c, 1% l)	Green	Green	Red	Traffic
200mm Emulsion (0.9% b, 1% c)	Green	Green	Red	Traffic
175 Emulsion (1% c, 2.4% b)	Green	Green	Red	Traffic
200 Emulsion (1% c, 2.4% b)	Green	Green	Red	Traffic
175 Emulsion (2% c, 2.4% b)	Green	Green	Red	Traffic
200 Emulsion (2% c, 2.4% b)	Green	Green	Red	Traffic
175 Foam (1% c, 2.4% b)	Green	Green	Red	Traffic
200 Foam (1% c, 2.4% b)	Green	Green	Red	Traffic
175 Foam (2% c, 2.4% b)	Green	Green	Red	Traffic
200 Foam (2% c, 2.4% b)	Green	Green	Red	Traffic

### 7.4 Observed and theorised stabilised material stiffness trends

Theories relating to the development of stabilised pavement layer stiffness were discussed in Section 2.5. These theories will be compared with the actual, observed stiffness trends of stabilised pavement layers along the experimental section.

#### 7.4.1 Cement stabilised material stiffness trends – theory versus actual

Figure 7.17 depicts a proposed correlation between the cement stabilised stiffness development theory presented in Section 2.5 and the observed cement stabilised pavement layer stiffness trend observed on the experimental section. It is proposed that the initial reduction in cement stabilised layer stiffness observed on the experimental section and attributed to construction traffic loads correlates to the pre-cracked phase stiffness reduction proposed by the SAMDM theory. Subsequent to this pre-cracked phase slight change in stiffness is observed in both the theoretical and actual base layer stiffness trends as the experimental section has been exposed to normal traffic loads for a period of less than one year. The above analysis indicates that a good correlation between theoretical and observed base layer stiffness trends for cement stabilised materials exists.

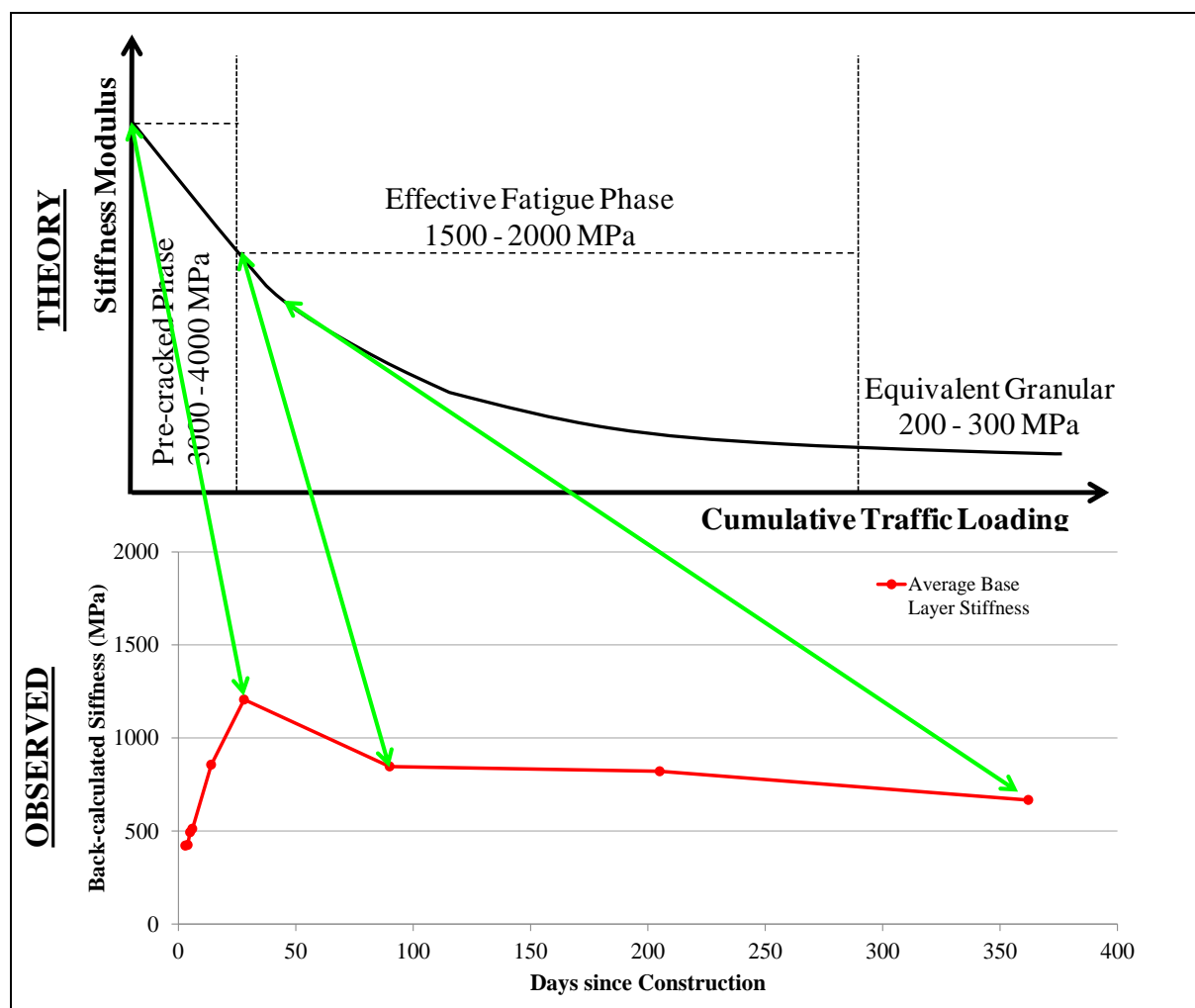


Figure 7.17: Cement stabilised pavement layer stiffness development - theory versus observed



Chapter 7 Trends in Stabilised Base Layer Stiffness over Time

7.4.2 BSM stiffness trends – theory versus actual

7.4.2.1 *Continuously bound theory*

Trends in stiffness observed for BSM base layers along the experimental section are compared with theories relating to their stiffness development discussed in Section 2.5. Figure 7.18 depicts the continuously bound BSM theory compared with the stiffness trend observed for the 175 mm BSM emulsion sub-section with 2% cement added in the southbound lane. The theory predicting stiffness reduction soon after traffic (construction and normal) is replicated by the experimental sub-section up until 180 days after construction however the subsequent stiffness increase at 360 days after construction is not predicted by the theory. The observation of an increase in BSM layer stiffness at 360 days since construction for the majority of BSM layers along the experimental section contradicts the continuously bound theory a continuous reduction in stiffness over time is expected.

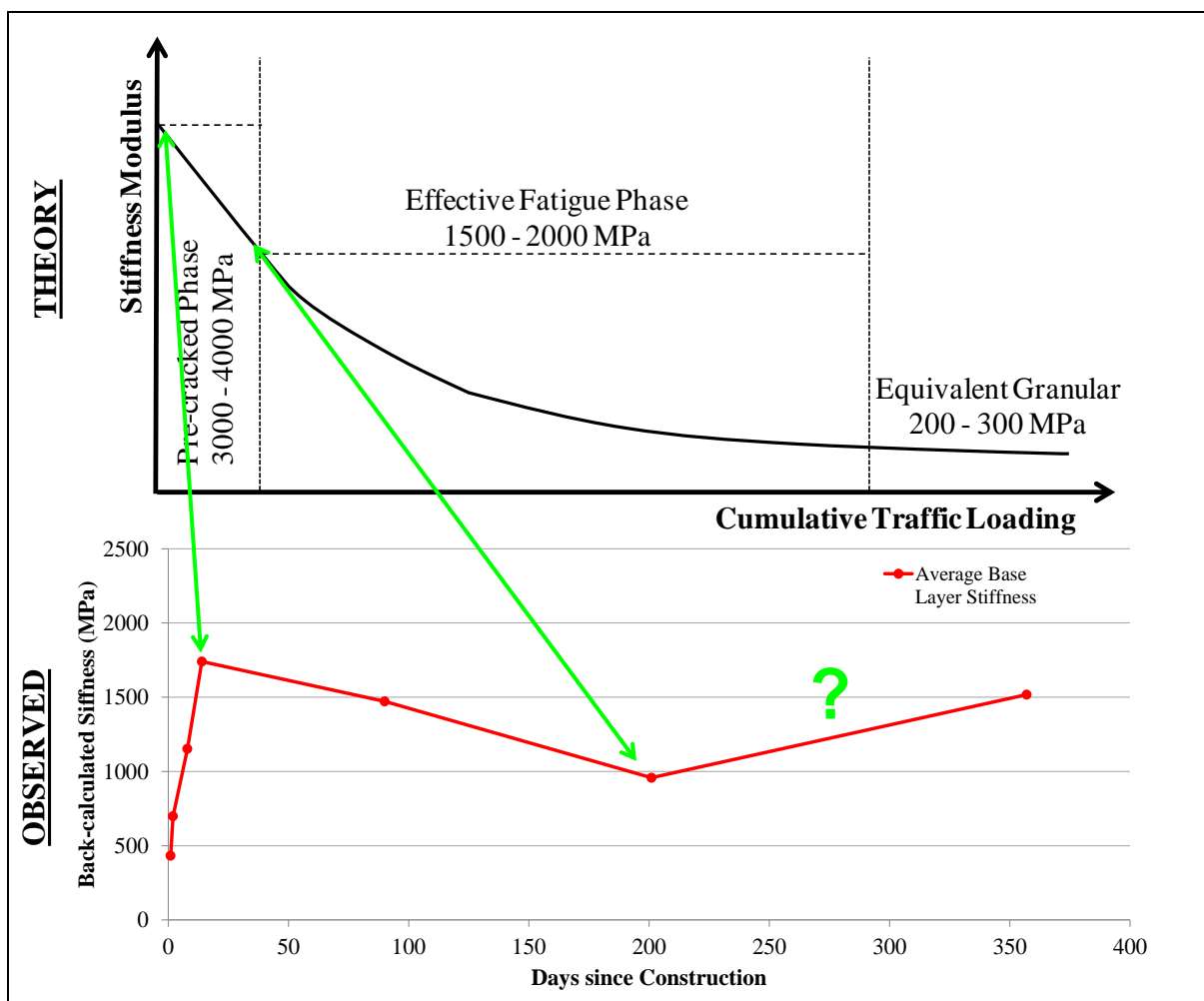


Figure 7.18: Continuously bound theory versus observed - 175mm BSM foam (2.4%b, 2%c) SB

7.4.2.2 *Non-continuously bound theory*

The granular, non-continuously bound material stiffness development theory for BSMs is compared with the observed trend in stiffness for the 175 mm BSM emulsion sub-section with 2% cement added

## Chapter 7 Trends in Stabilised Base Layer Stiffness over Time

in the southbound lane. The comparison is shown graphically in Figure 7.19. The stiffness reduction observed from 28 to 180 days after the base layer construction is not predicted by the non-continuously bound BSM theory which predicts continuous curing over the initial service life of the BSM layer. Subsequent to 180 days since construction a stiffness increase is observed indicating that some curing may still be taking place.

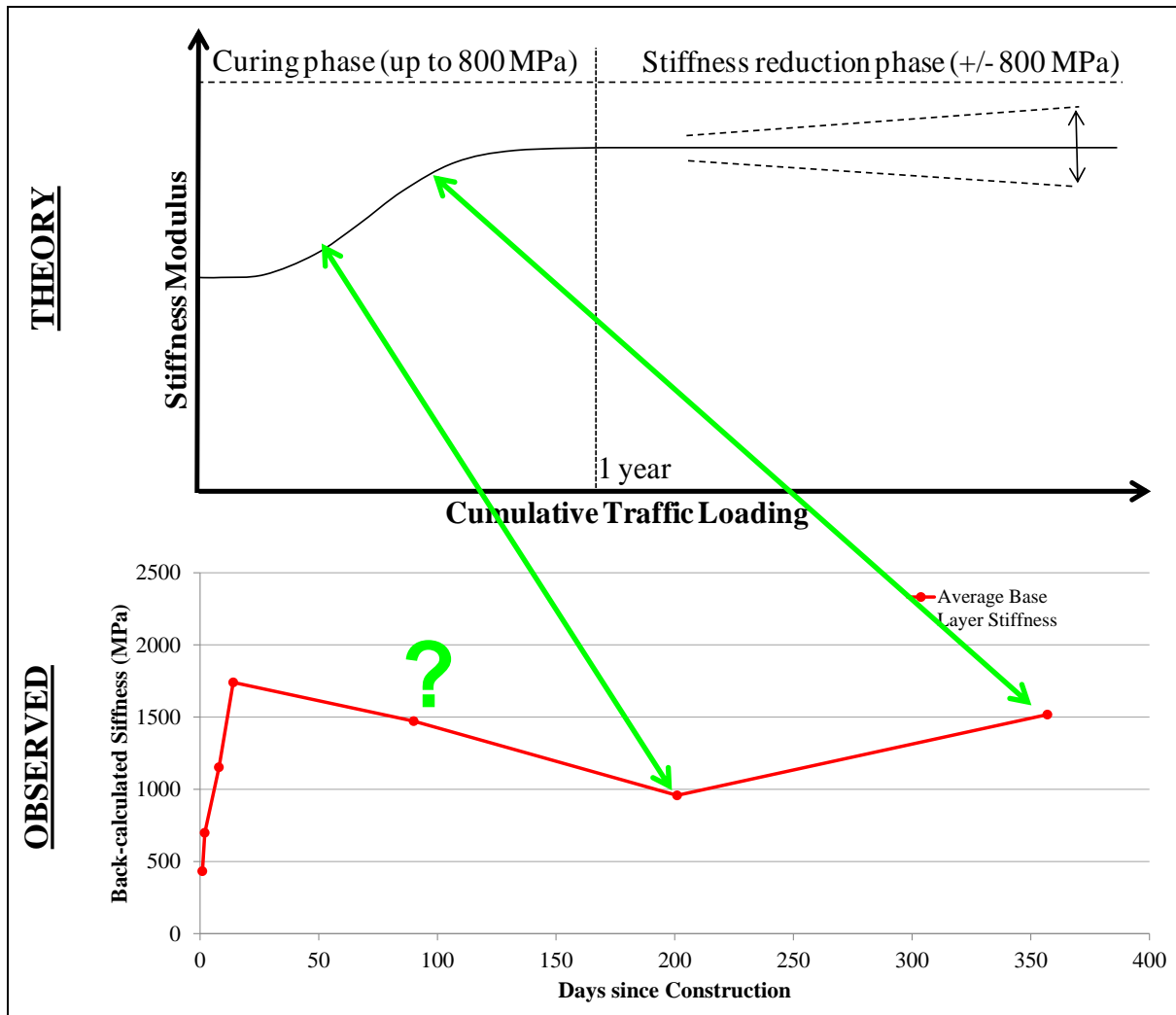


Figure 7.19: Non-continuously bound BSM theory versus observed – 175mm BSM foam (2.4%b, 2%c) SB

Continuous curing over the 360 day observation period is more evident on BSM sub-sections in the northbound lane. BSMs with 2% cement added in the northbound lane show significant curing throughout the observation period. This stronger correlation between the theory and experimental section observations is shown in Figure 7.20 where the 200 mm BSM foam with 2% cement added is compared with the non-continuously bound BSM stiffness development theory.

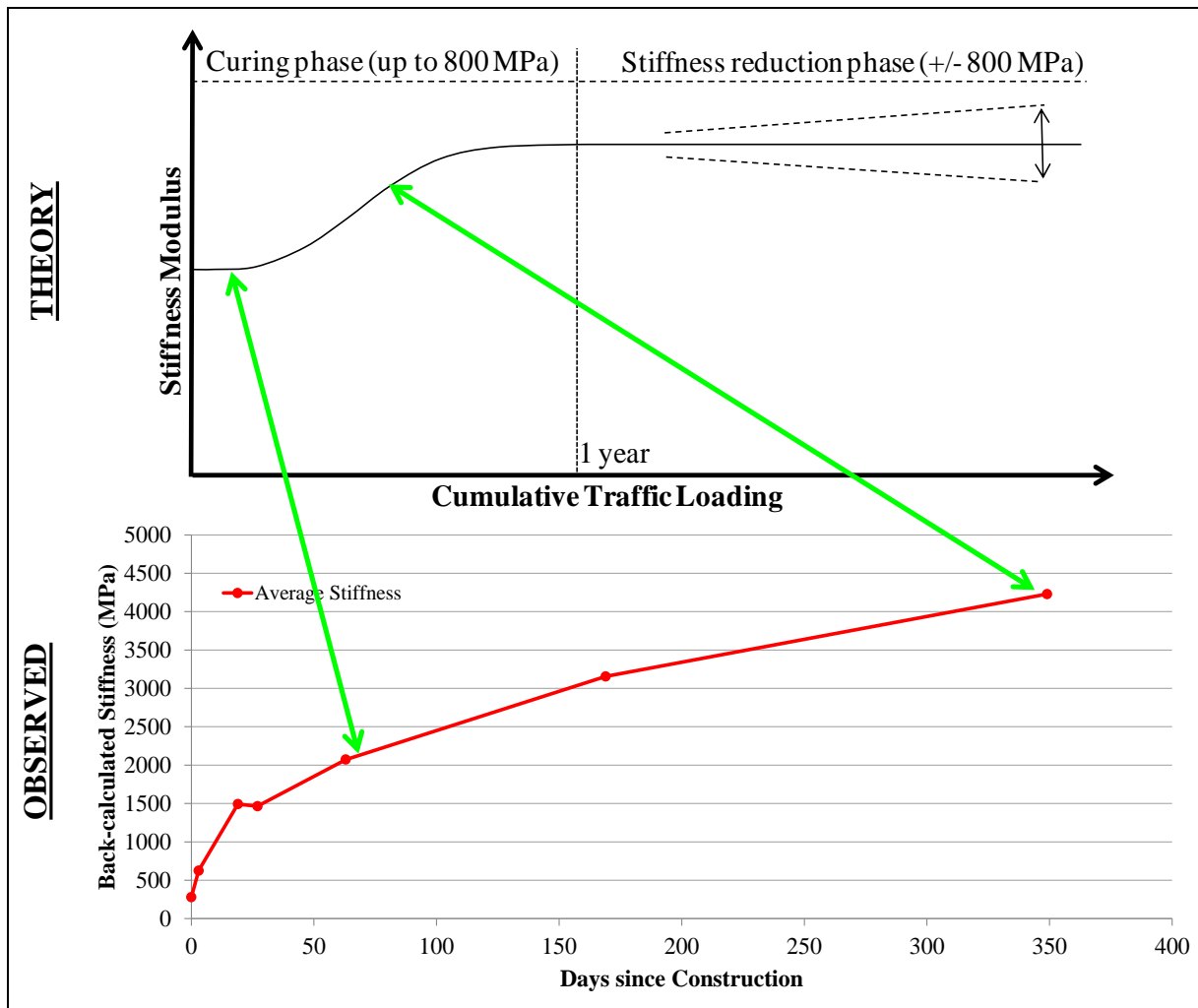


Figure 7.20: Non-continuously bound theory versus observed – 200mm BSM foam (2.4%b, 2%c) NB

The non-continuously bound material stiffness development theory for BSMs corresponds with the observed curing and increasing layer stiffness trends observed in the northbound lane with exception of the temporary stiffness reductions. The theory however does not correlate with BSM stiffness trend observations on the southbound lane.

### 7.5 Magnitudes of base layer stiffness observed

Figure 7.21 illustrates the magnitude of the stiffness of all base layer material types, in both the northbound and southbound lanes, for selected temporal locations during the 360 day period. The red bars indicated the maximum average base layer stiffness occurring during the whole observation period. This value gives an indication as to the maximum stiffness the various stabilised base layers achieved over the 360 day observation period.

The minimum average base layer stiffness occurring over the period, subsequent to 28 days since construction of the layer is shown as blue bars. These stiffness magnitudes indicate the lowest stiffness values occurring, outside of the initial curing period, over the 360 day observation period.

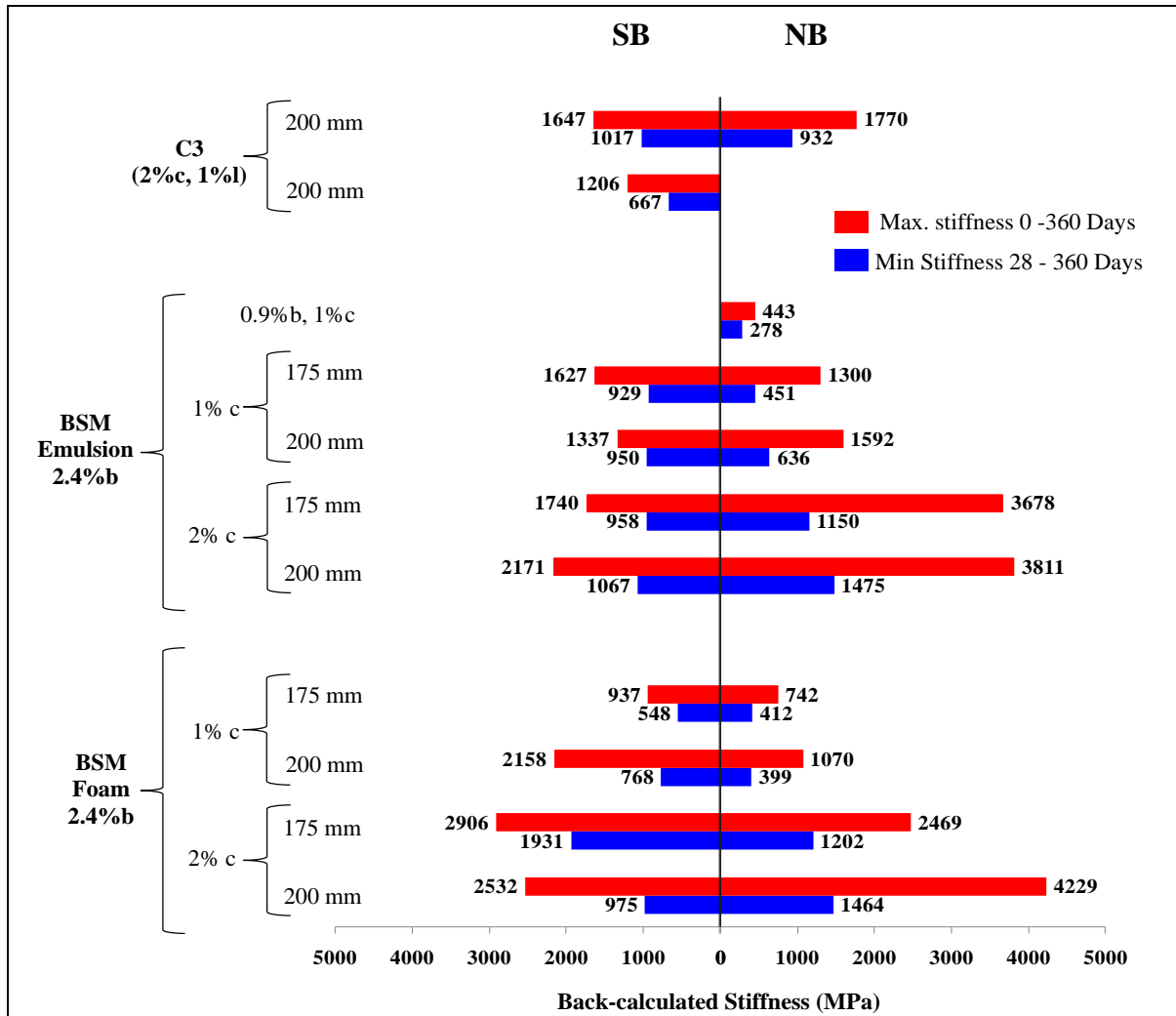


Figure 7.21: Summary of average back-calculated base layer stiffnesses – northbound and southbound

## 7.6 Conclusion

### 7.6.1 Trends in stabilised material stiffness over time and related influencing factors

It is concluded that the trend in stabilised base layer stiffness over time varies dependent upon the stabilised pavement material type and the influence of external factors on the stabilised materials stiffness. Table 7.12 below summarises the experimental sub-sections and the factors proposed as influencing the stabilised base layer stiffness over the 360 day observation period.

**Table 7.12: Summary of factors influencing stabilised base layer stiffness**

Sub-section	Constr. Traffic		Prime		Seasonal variability		Rainfall		Traffic	
	SB	NB	SB	NB	SB	NB	SB	NB	SB	NB
200mm C3-1 (2% c, 1% l)	Y	Y								
200mm C3-2 (2% c, 1% l)	Y									
200mm ETB 3 (0.9%b, 1%c)		Y								
175mm BSM Emulsion (1%c, 2.4%b)					Y			Y		
200mm BSM Emulsion (1%c, 2.4%b)					Y			Y		
175mm BSM Emulsion (2%c, 2.4%b)					Y			Y		
200mm BSM Emulsion (2%c, 2.4%b)			Y	Y	Y			Y		
175mm BSM Foam (1%c, 2.4%b)			Y		Y			Y		
200mm BSM Foam (1%c, 2.4%b)			Y		Y			Y		
175mm BSM Foam (2%c, 2.4%b)			Y		Y			Y		
200mm BSM Foam (2%c, 2.4%b)			Y		Y					

Detail on how each proposed influencing factor affects the stabilised base layer stiffness is summarised:

- (i) **Construction traffic** - Heavy steel drum vibratory compaction equipment, used for the construction of the bituminous surface layer, is proposed to have induced damage, during asphalt compaction, within the cement stabilised materials due to its brittle, continuously bound stabilised material state.
- (ii) **Prime** - The application of prime, especially to BSM layers, is proposed to have reduced the stiffness of the bitumen within the BSM layers due to the content of paraffinic, bitumen softening cutters within the prime applied.
- (iii) **Seasonal Variability** - BSMs in the southbound lane show significant correlation with seasonal variation in subgrade support stiffness over the 360 day observation period. It is proposed that the stress dependent nature of the BSM material and variability in support has induced the variability observed in stabilised base layer stiffness.
- (iv) **Rainfall** – In the northbound lane BSM layers received a direct application of rainfall during the period where no bituminous surfacing layers had been constructed. It is proposed that the

## Chapter 7 Trends in Stabilised Base Layer Stiffness over Time

reduction in stiffness observed, significantly on BSMs with 1% cement added, was due to this direct application moisture from rainfall.

- (v) **Traffic** – No evidence of a reduction in stabilised base layer stiffness on any experimental sub-section due to the damaging effects of traffic loading was identified.

### 7.6.2 Correlation of observed and theorised stabilised layer stiffness trends

Cement stabilised materials show a reasonable correlation with the theory proposed by the SAMDM.

The observations made with respect to the correlation of the observed trends in BSM layer stiffness and those proposed by current theories show limited correlation. The continuously bound stiffness development theory for BSMs was contradicted by the stiffness trends observed for most BSM materials with 1% or 2% cement added. The contradiction occurs due to the BSM layer stiffness increase observed towards the end of the observation period.

The correlation between the non-continuously bound BSM theory and observed BSM layer stiffness trends is also not consistent throughout the experimental section. A number of experimental sub-sections show significant reductions in layer stiffness 90 days after construction. This is contradictory to the continuously bound theory which predicts continuous curing of the BSM layer throughout the initial service life of the BSM layer.

It seems theories relating to BSM layer stiffness development have not captured the temporal variability in layer stiffness which is being observed in the field for in-situ recycled BSMs.

### 7.6.3 Stiffness magnitudes per material type

It is clear from Figure 7.21 that BSMs with 2% cement added show the highest stiffness values over the 360 day observation period. It is also noted BSM emulsions with 1% cement added show similar maximum average stiffness values to purely cement stabilised materials. BSM foam layers with 1% cement added show lower maximum values over the observation period. As discussed previously the BSM foam layer with 1% cement added in the southbound lane showed abnormally high stiffness values at day 90 testing.

The trend in minimum average stiffness values occurring over the observation period also corresponds with that observed for the maximum values per material type. BSMs with 2% cement added show the highest minimum stiffness values over the 360 day period. BSM emulsions with 1% cement and cement stabilised materials show similar lower stiffness values over the observation period with BSM foam layers with 1% cement added showing lower minimum stiffness values.

## Chapter 7 Trends in Stabilised Base Layer Stiffness over Time

The BSM emulsion with 0.9% residual bitumen and 1% cement showed the lowest maximum and minimum average stiffness values of all material types.

## CHAPTER 8 PRELIMINARY MODELS OF STABILISED MATERIAL CURING AND LAYER STIFFNESS VARIABILITY

From the base layer stiffness trends observed in Section 7.2 it is obvious that the variability in pavement layer stiffness is complex and influenced by many factors throughout its construction and service life. As is the case with most pavement engineering experimental observations of a complex nature, a simplification of the observations is required in order to incorporate them within the a usable pavement design process.

This chapter will propose models for two significant observations made from the average base layer stiffness plots of the various stabilised material types displayed in Section 7.2. The chapter layout is outlined in Figure 8.1.

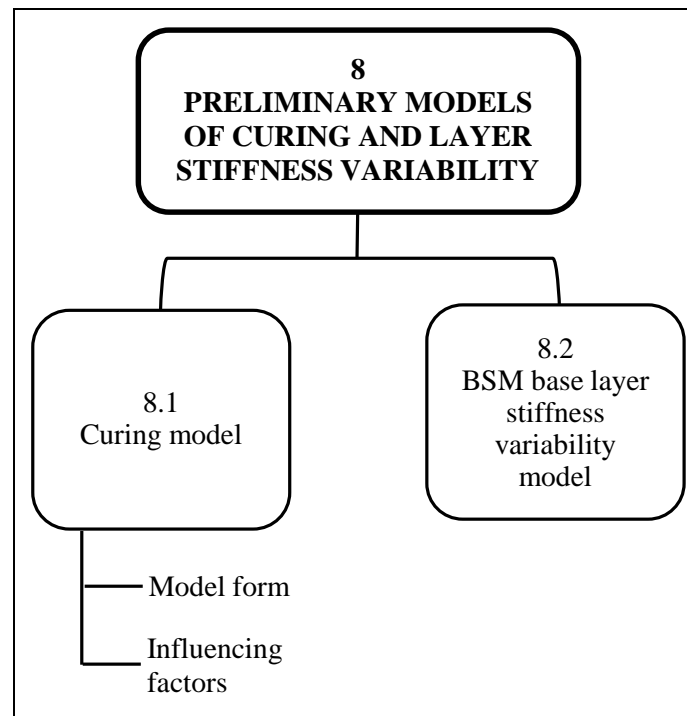


**Figure 8.1: Outline of Chapter 8**

The development of base layer stiffness during the initial 28 day curing period, for all stabilised material types, will be modelled. No loading from either construction or normal traffic was applied to the experimental section during this period therefore the stiffness trends observed represent the stiffness development within a material due solely to the materials properties and the curing process taking place within.

The seasonal variability of BSM layer stiffness is the second material characteristic for which models were developed. No model is proposed for cement stabilised materials due to the observation that the cement stabilised material showed no variability in line with seasonal rainfall and temperature variability.



## 8.1 Curing stiffness model

### 8.1.1 Model formulation

The curing period modelled spans the initial 28 days since construction for all stabilised pavement layers. The model takes the form described by Equation 7:

$$M_r = k_1 t^{k_2} \quad \text{Equation 9}$$

Where:

$k_1, k_2$  = model constants

$t$  = time in days

While this model is similar in form to the  $k$ - $\theta$  model used to describe the resilient modulus of stress dependent granular materials, its selection is based purely on the fact it provides a good fit to measured stiffness data during stabilised material curing. The above curing model parameters were adjusted to create a best fit to the average back-calculated stiffness values for each sub-section base layer over the 360 day observation period. Two examples of such models are depicted in Figure 8.2 and Figure 8.3 and the full list of model parameters per sub-section shown in Table 8.1. Figure 8.3 shows the deviation from the curing stiffness model at 28 days after construction due to the application of prime to the base layer. In order to create a simplified curing model, influences on stiffness which were seen as abnormal and temporary were removed and a standardised conceptualisation of curing stiffness development models for the various stabilised materials were formed. The abnormal and temporary influences identified in this study were:

- Stiffness reduction due to prime application
- Stiffness reduction due rain induced increases in moisture content of the unsealed base layer

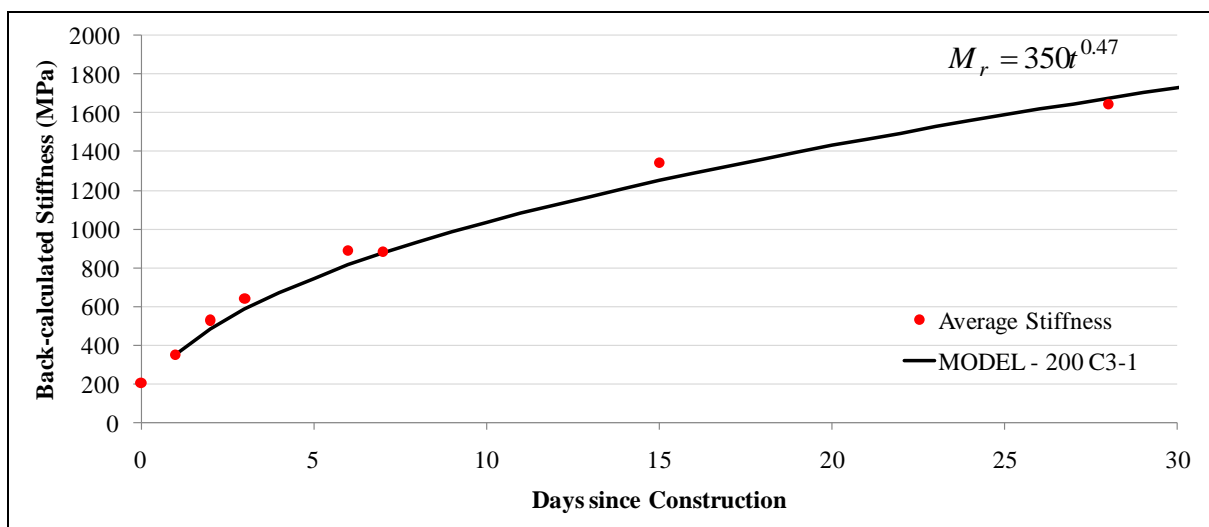


Figure 8.2: Curing stiffness model - 200mm C3-1 (2% c, 1% l) Southbound

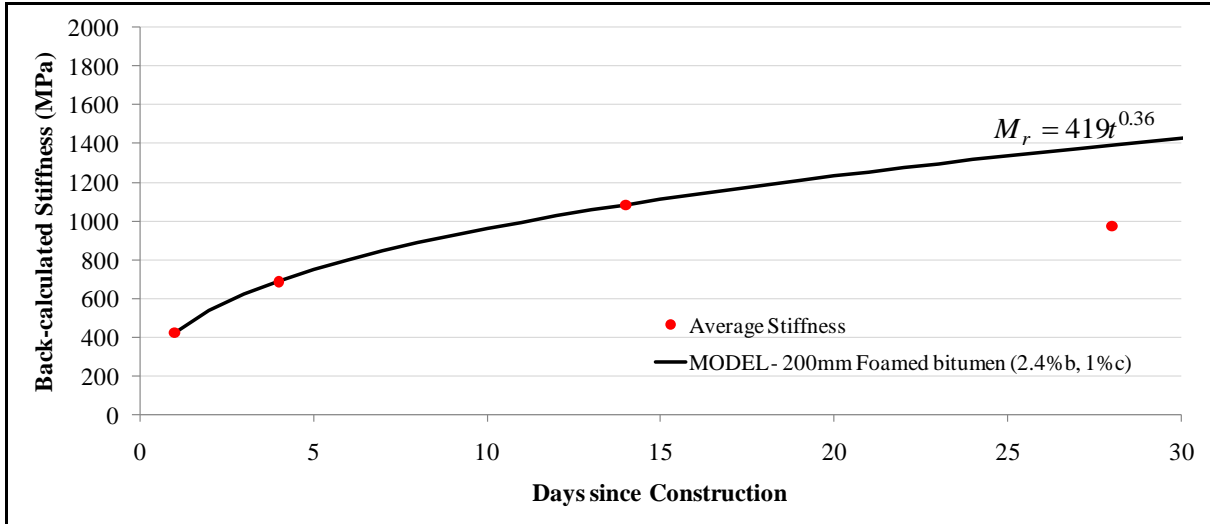


Figure 8.3: Curing average stiffness model - 200 Foamed bitumen (2.4%b, 1%c) Southbound

Table 8.1: Curing model parameters and 28 day model stiffness

Sub-section	Curing model parameters				28 day model stiffness (MPa)	
	k1		k2		SB	NB
	SB	NB	SB	NB	SB	NB
200mm C3-1 (2%c, 1%l)	350	350	0.47	0.51	1676	1915
200mm C3-2 (2%c, 1%l)	220	-	0.51	-	1204	-
200mm Bitumen Emulsion (0.9%b, 1%c)	-	235	-	0.25	-	541
175mm Bitumen Emulsion (2.4%b, 1%c)	320	336	0.46	0.26	1482	799
200mm Bitumen Emulsion (2.4%b, 1%c)	337	441	0.38	0.33	1196	1324
175mm Bitumen Emulsion (2.4%b, 2%c)	432	569	0.52	0.32	2443	1653
200mm Bitumen Emulsion (2.4%b, 2%c)	873	559	0.35	0.43	2802	2343
175mm Foamed Bitumen (2.4%b, 1%c)	380	354	0.33	0.21	1141	713
200mm Foamed Bitumen (2.4%b, 1%c)	419	357	0.36	0.23	1391	768
175mm Foamed Bitumen (2.4%b, 2%c)	790	454	0.43	0.45	3311	2034
200mm Foamed Bitumen (2.4%b, 2%c)	720	420	0.37	0.4	2470	1593

It can be seen from Figure 8.2 and Figure 8.3 that the  $k_1$  parameter relates to the stiffness achieved by the stabilised material one day after its construction and the  $k_2$  parameter describes the rate of increase in stiffness from the 1 day stiffness to 28 days since the base layer construction. After the 28 day period the proposed model begins to dramatically overestimate the measured stiffness of the stabilised material. It is assumed that the curing process has slowed significantly after 28 days since construction and factors such as traffic loading and the environment are primarily influencing the stiffness behaviour of the stabilised layer. Figure 8.4 shows the modelled 28-day stiffness values for each stabilised material type.

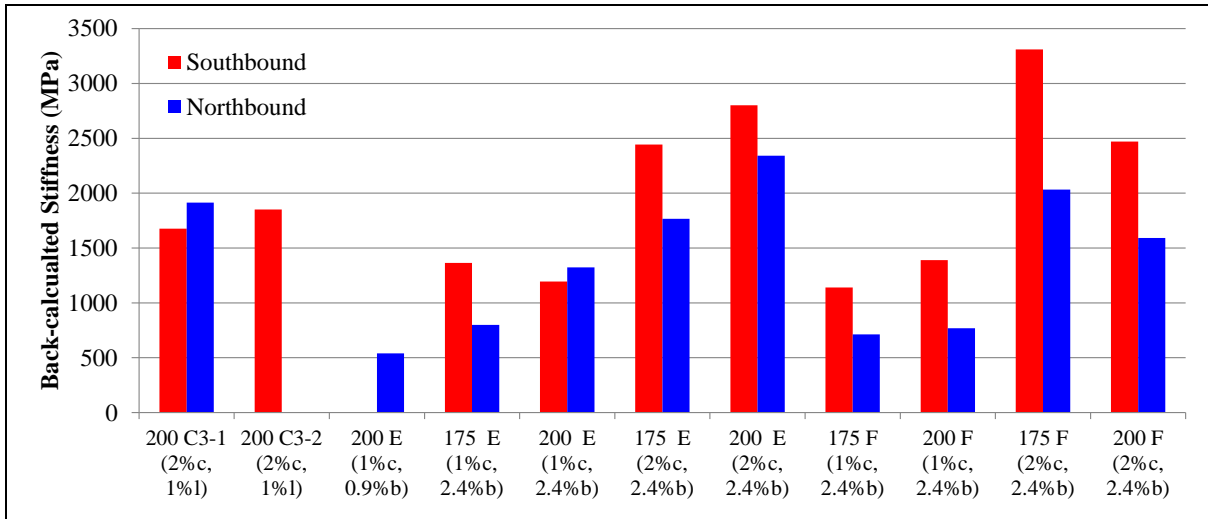


Figure 8.4: 28 day modelled base layer stiffnesses

### 8.1.2 Factors influencing curing

The k parameters of the proposed models, shown in Table 8.1, were compared with various factors which are known to affect the development of stiffness of stabilised materials during curing. Data collected from the field during the same period of time the FWD measurements, whose related stiffness values were utilised in creating the curing model were collected, are utilised in the analysis. Curing influencing factors investigated were:

- Air temperature
- Moisture content
- Design cement content
- Design bitumen content

As we now have a parametric model estimating the development of average stiffness over time for various stabilised pavement materials, it was possible to estimate the rate of change in stiffness of a stabilised material at any time over the initial 28 day period. In order to investigate the various effects the influencing factors described above may have on the curing of a stabilised material, the rate of change in stiffness at the time of measurement of the influencing factors and the influencing factor measurement are compared. The determination of the rate of change in stiffness at any point in time was determined by differentiating the curing models detailed in Section 8.1. The rate of change in stiffness takes the form described below:

$$\frac{dM_r}{dt} = k_1 k_2 t^{k_2 - 1} \tag{Equation 10}$$

Where:

$M_r$  = Back-calculated stiffness

$k_1, k_2$  = Model parameters related to stabilised material properties

t = time in days

8.1.2.1 Air Temperature

It is well known that the temperature of the environment in which the curing of cement and lime stabilised materials and BSMs takes place has an effect on the rate of curing of those materials. No reliable source of temperature data from within the stabilised material base layers, during the course of the initial 28 day curing period, was available. An attempt was therefore made to compare the curing model parameters determined for each material type in the directional lane with the average of daily average temperatures over the curing period. As can be seen from Figure 8.5 to Figure 8.8 below no correlation is observed between the characterisation of stabilised material curing and the average daily average air temperature over its curing period.

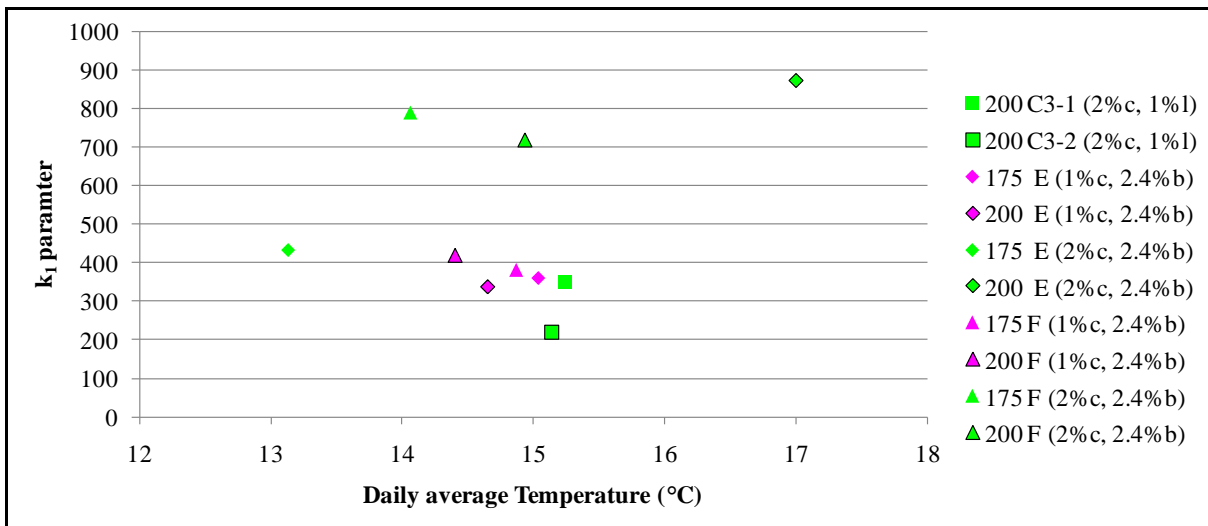


Figure 8.5: Curing model parameter  $k_1$  versus curing period average daily temperature – southbound

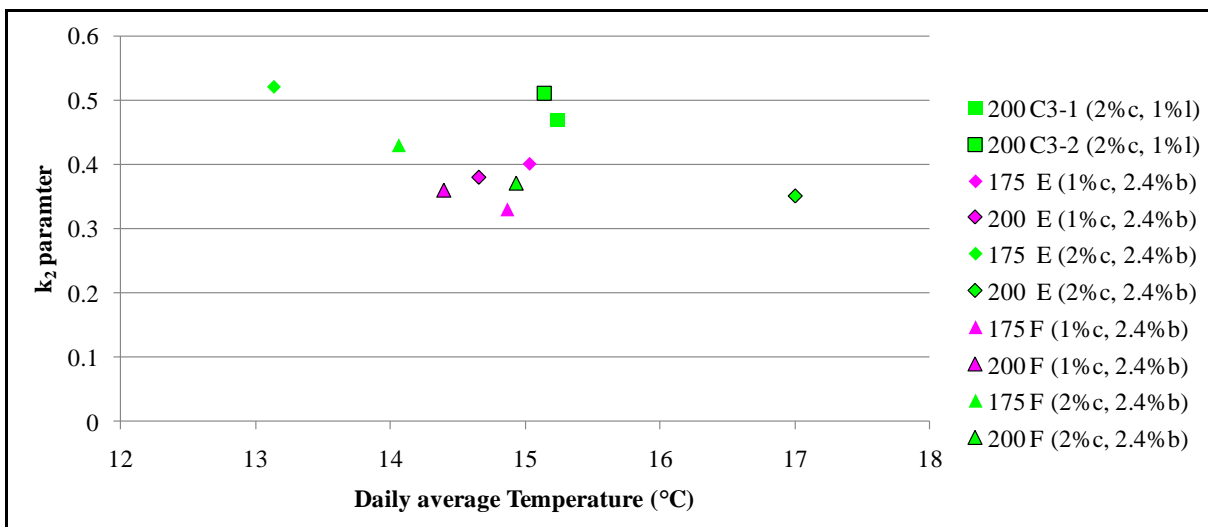


Figure 8.6: Curing model parameter  $k_1$  versus curing period average daily temperature – northbound

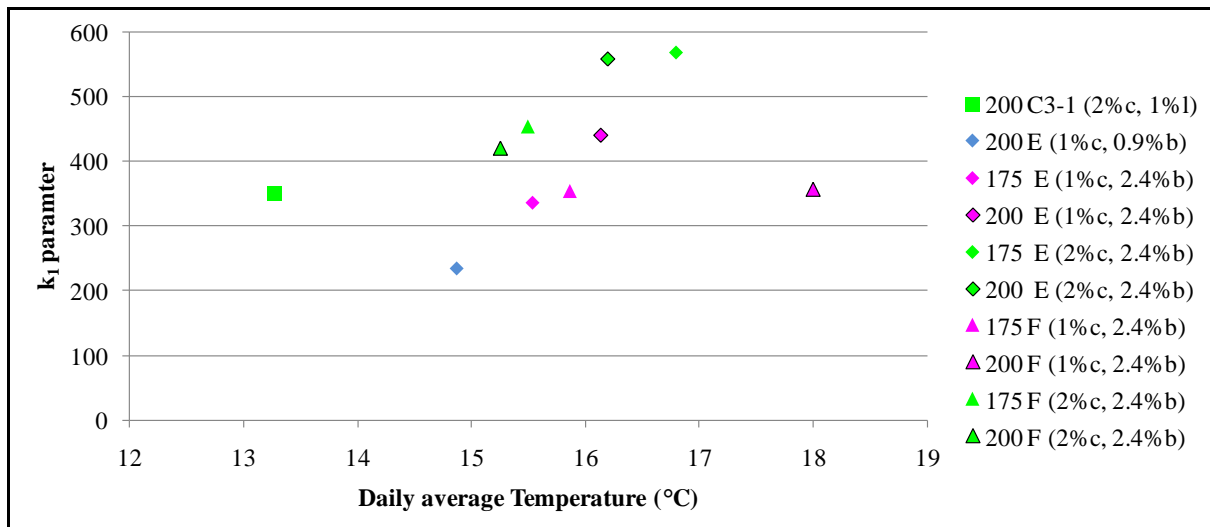


Figure 8.7: Curing model parameter  $k_2$  versus curing period average daily temperature – southbound

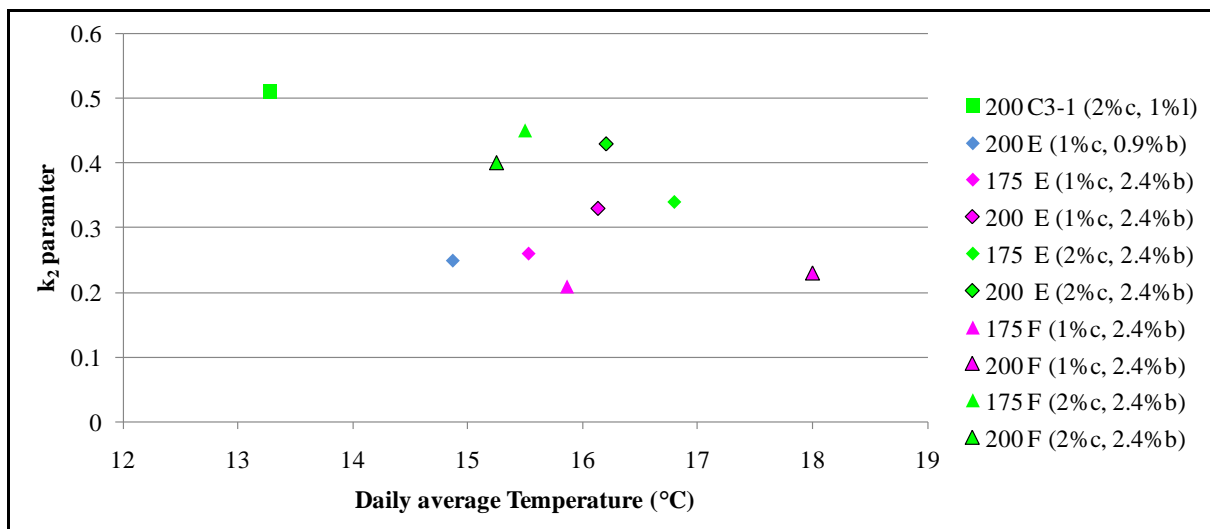


Figure 8.8: Curing model parameter  $k_2$  versus curing period average daily temperature - northbound

### 8.1.2.2 Moisture Content

The moisture content of the stabilised base layers were recorded a number of times throughout the initial 28-day curing period. In Figure 8.9 the average moisture content per stabilised layer material at a point in time is plotted against the rate of change in stiffness of the stabilised pavement layer material at the time of moisture content measurement. While a clear relationship per stabilised material is not evident it can be seen that the rate of stiffness change decreases along with moisture content reduction.

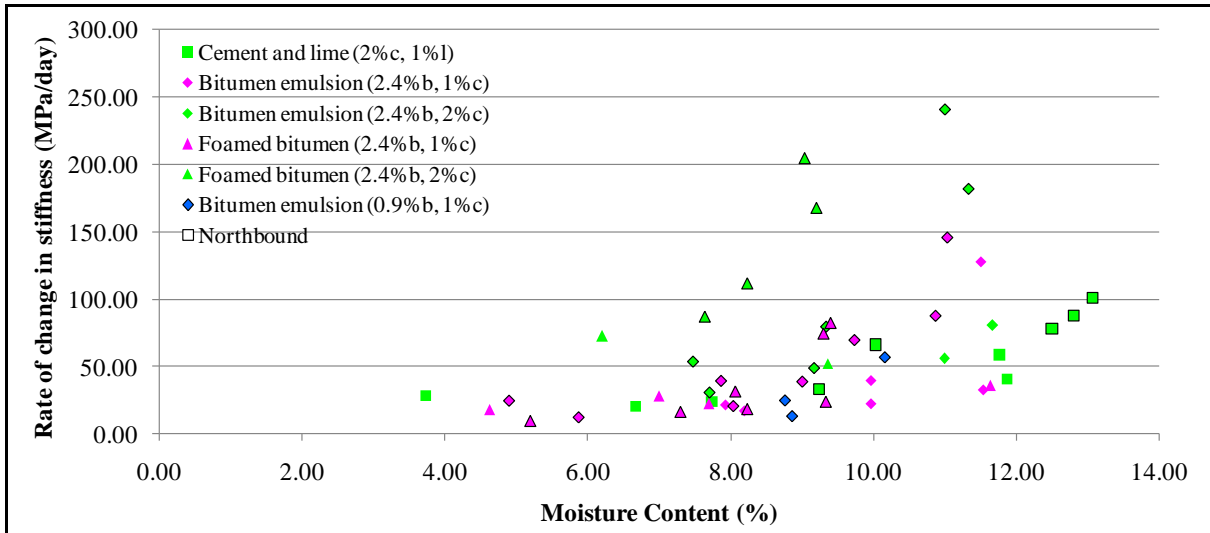


Figure 8.9: Rate of stiffness gain at a specific time versus moisture content - southbound and northbound

The above analysis does not confirm whether the reduction in rate of stiffness gain and reduction in moisture content is a causal relationship and may be incidental to the fact that the amount of cement available for the cement hydration reaction reduces as the curing period progresses. It does seem however that the BSM sub-sections in the northbound lane show a greater increase in stiffness per day for the same moisture content when compared with sub-sections in the southbound lane.

### 8.1.2.3 Design residual bitumen content

The rate and magnitude of the increase in stiffness of the stabilised pavement layers discussed here can be inferred from the model parameters  $k_1$  and  $k_2$ . By plotting the model parameters against the bitumen contents of each stabilised material an indication of the effect of this material design parameter on the curing performance of the stabilised materials in the field can be observed.

Figure 8.10 and Figure 8.11 depict the model constant  $k_1$  plotted against the bitumen content of each material.

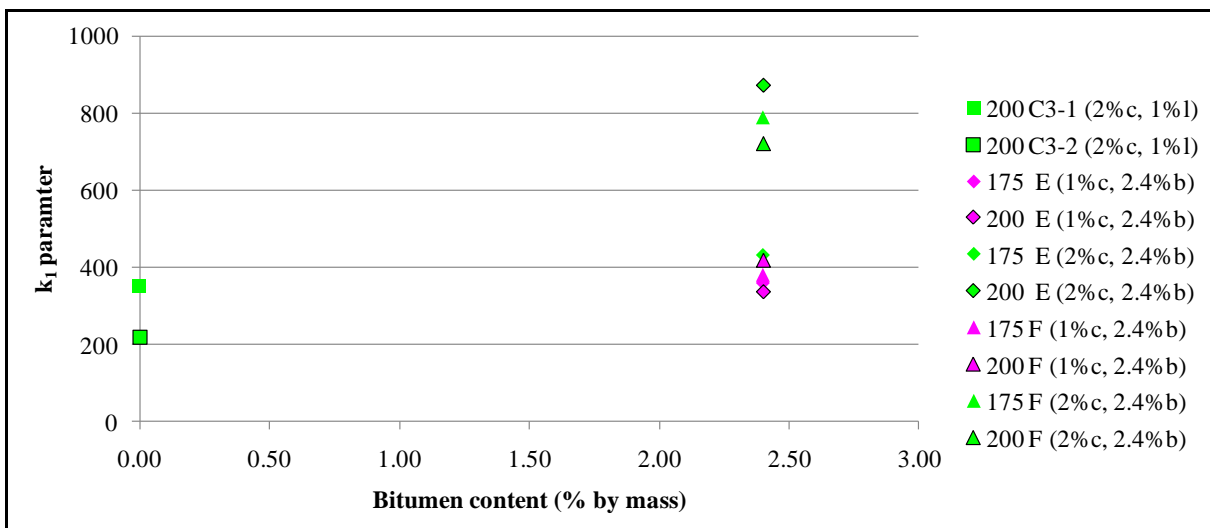


Figure 8.10: Curing model parameter  $k_1$  versus bitumen content – southbound

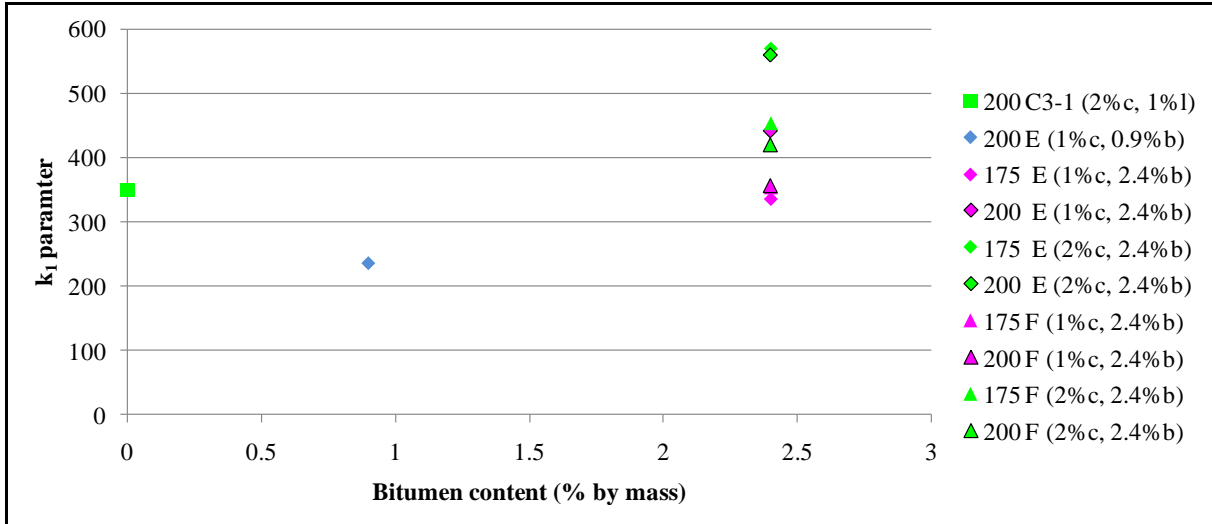


Figure 8.11: Curing model parameter  $k_1$  versus bitumen content – northbound

The curing model parameter  $k_1$  relates to the stiffness of a stabilised material 1 day after its construction. The observation that cement stabilised materials consistently show low  $k_1$  values compared to BSMs with 2.4% residual bitumen is made. A separation within BSMs with 2.4% residual bitumen contents based on cement content is also noted. The BSM emulsion with 0.9% residual bitumen and 1% cement formed the curing model with the lowest  $k_1$  parameter value.

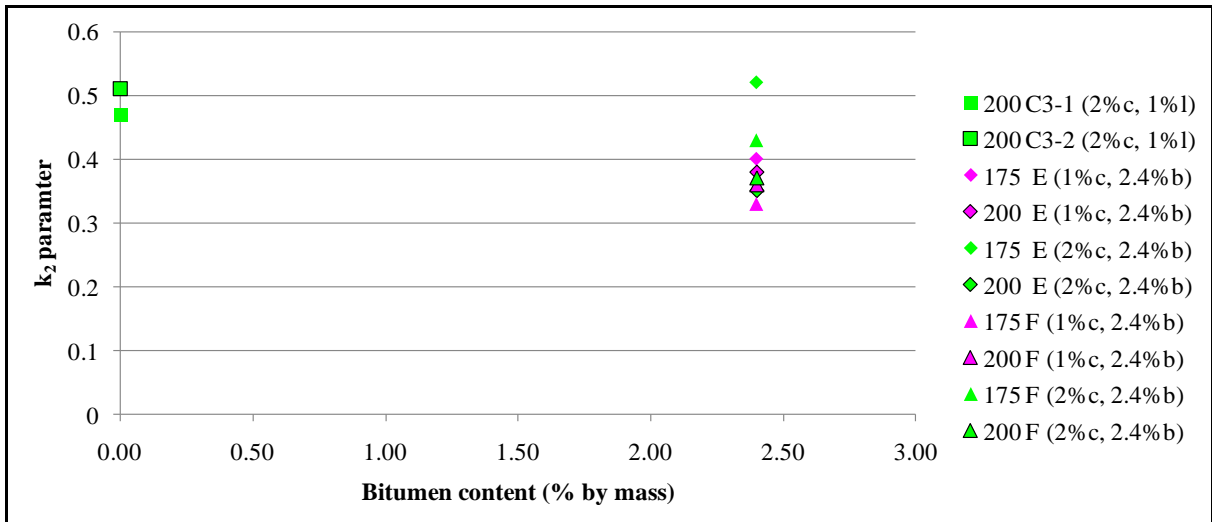


Figure 8.12: Curing model parameter  $k_2$  versus bitumen content - southbound

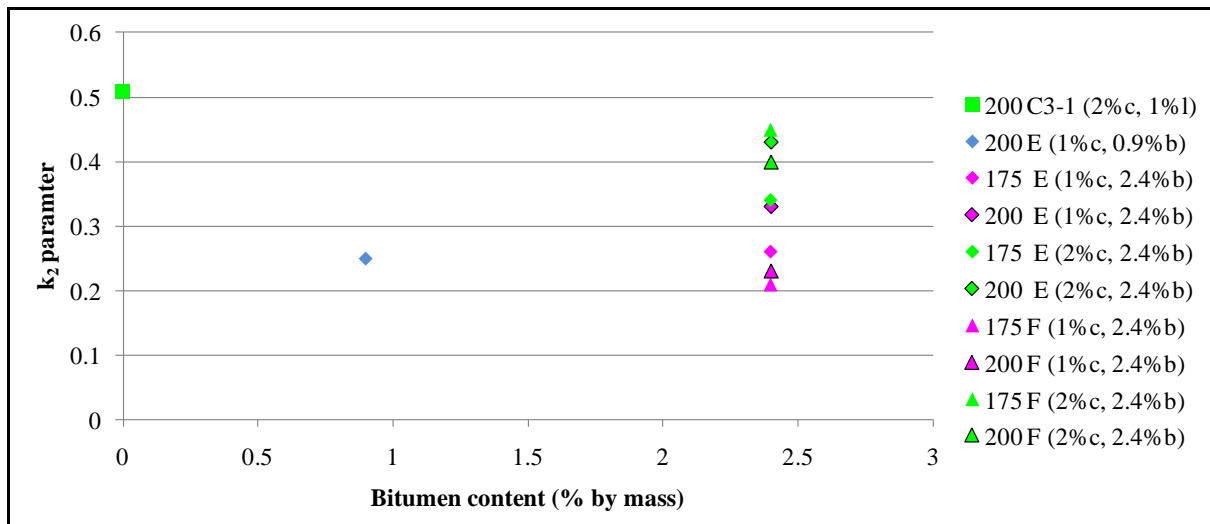


Figure 8.13: Curing model parameter  $k_2$  versus bitumen content – northbound

Figure 8.12 and Figure 8.13 above describe the relationship between the  $k_2$  curing model parameter and the bitumen contents for the experimental sub-sections in the northbound and southbound lanes. The  $k_2$  parameter relates to the rate of stiffness increase from the stabilised layer stiffness 1 day after construction. The above graphs indicate that cement stabilised materials, with no residual bitumen content, create curing models with the highest  $k_2$  parameter. A wide range of  $k_2$  parameter values relate to materials with a residual bitumen content of 2.4%. Within the cluster of materials with residual bitumen contents of 2.4% a trend, based on cement content, is observed, significantly in the northbound lane.

#### 8.1.2.4 Design cement content

Figure 8.14 and Figure 8.15 depict the relationship between the  $k_1$  curing model parameter and the design cement content of each stabilised material type per sub-section. No clear trend between the curing model  $k_1$  parameter and design cement content is noted. In both directional lanes materials with 1% cement and a number materials with 2% cement added show similar  $k_1$  parameter values. The largest  $k_1$  parameter values occur within curing models of BSMs with 2% cement added.



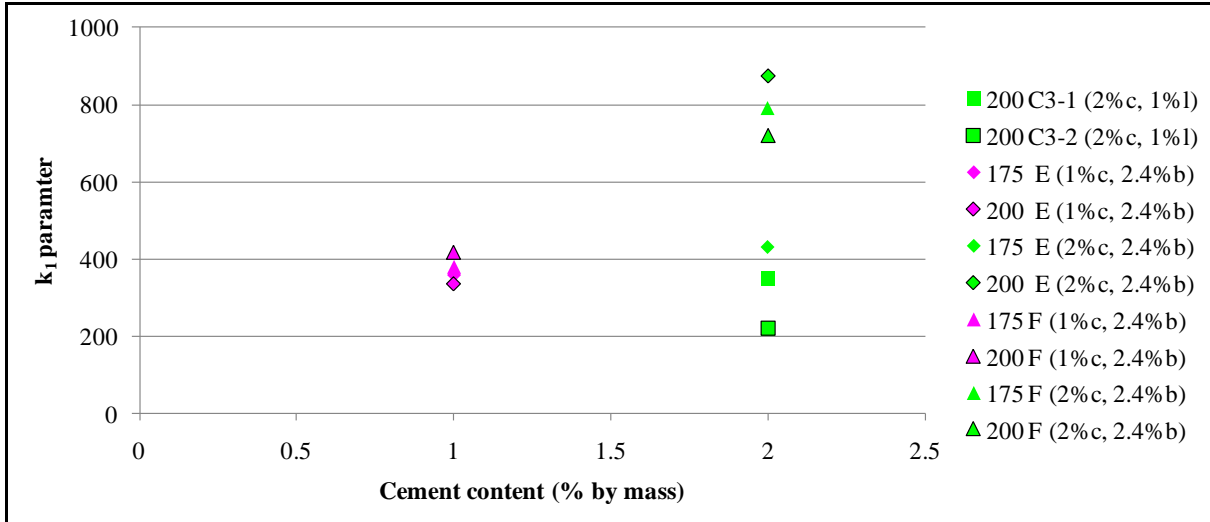


Figure 8.14: Curing model parameter  $k_1$  versus cement content – southbound

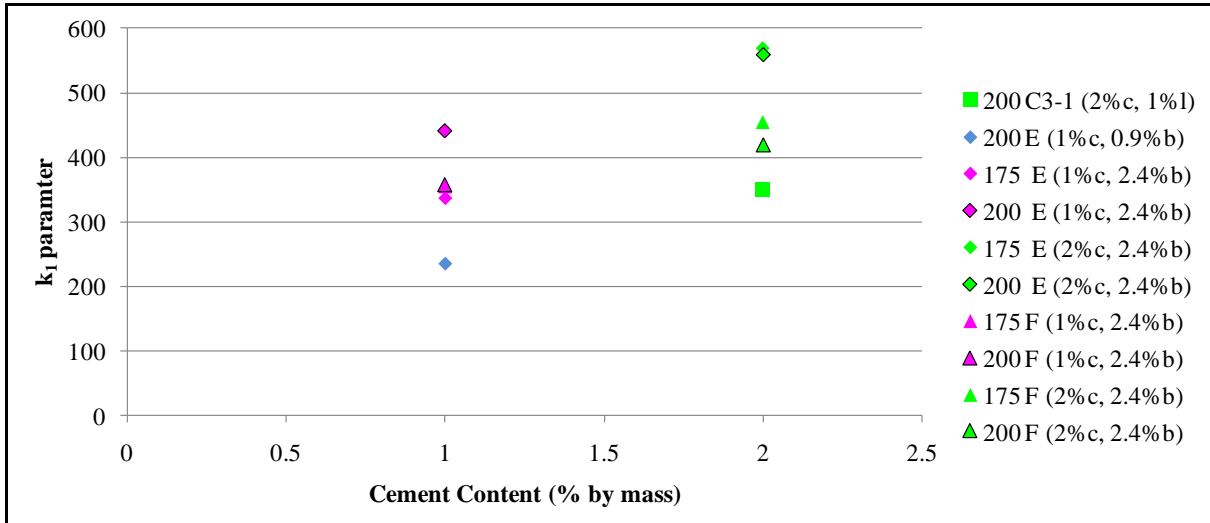


Figure 8.15: Curing model parameter  $k_1$  versus cement content – northbound

Figure 8.16 and Figure 8.17 depict the  $k_2$  curing model parameters for sub-sections in the southbound and northbound experimental sub-sections. The general trend of higher  $k_2$  parameter for materials stabilised with 2% cement is observed on both directional lanes. Exceptions to this observed trend are the 200mm BSM materials with 2% added in the southbound lanes. A greater correlation with the proposed trend is seen in the northbound direction. The cement and lime stabilised materials show consistently higher  $k_2$  values in both directions. This observation indicates that the materials with 2% cement added show higher rates of stiffness increase compared with those which have 1% cement added.

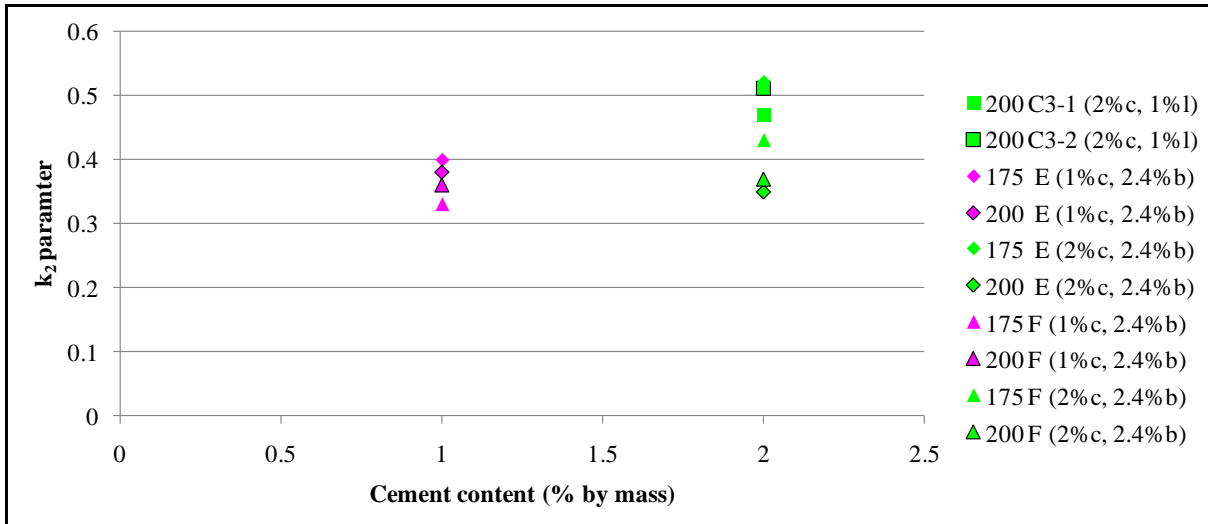


Figure 8.16: Curing model parameter  $k_2$  versus cement content – southbound

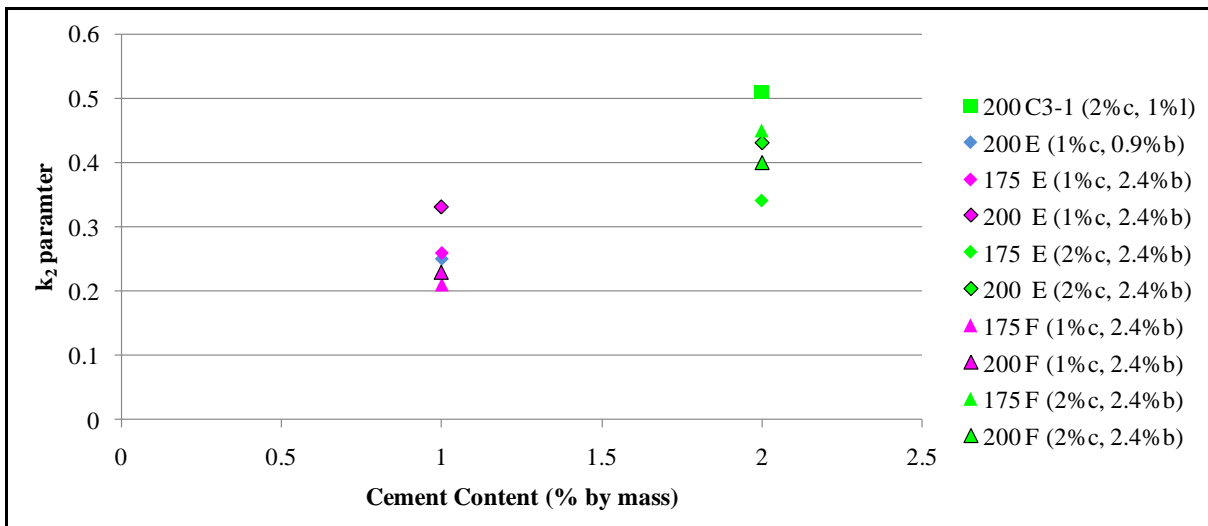


Figure 8.17: Curing model parameter  $k_2$  versus cement content – northbound

### 8.1.3 Plot of $k_1$ versus $k_2$

When the  $k_1$  and  $k_2$  parameters from the curing models for all sub-sections in both the northbound and southbound lanes are plotted against each other Figure 8.18 is created. While the boundaries between the various material types are not wide or definitive, the stabilised materials do show a clear tendency towards a certain  $k_1$ - $k_2$  parameter combination based upon their design cement and bitumen contents. The stabilised material types and the zones of the  $k_1$  and  $k_2$  parameter plot within which they fall are indicated in Figure 8.18. Taking into account the significant variability in base layer stiffness existing within each sub-section, the pattern depicted in Figure 8.18 by the model parameters, based on average stiffness values, succeed in identifying the varying curing characteristics by material type.

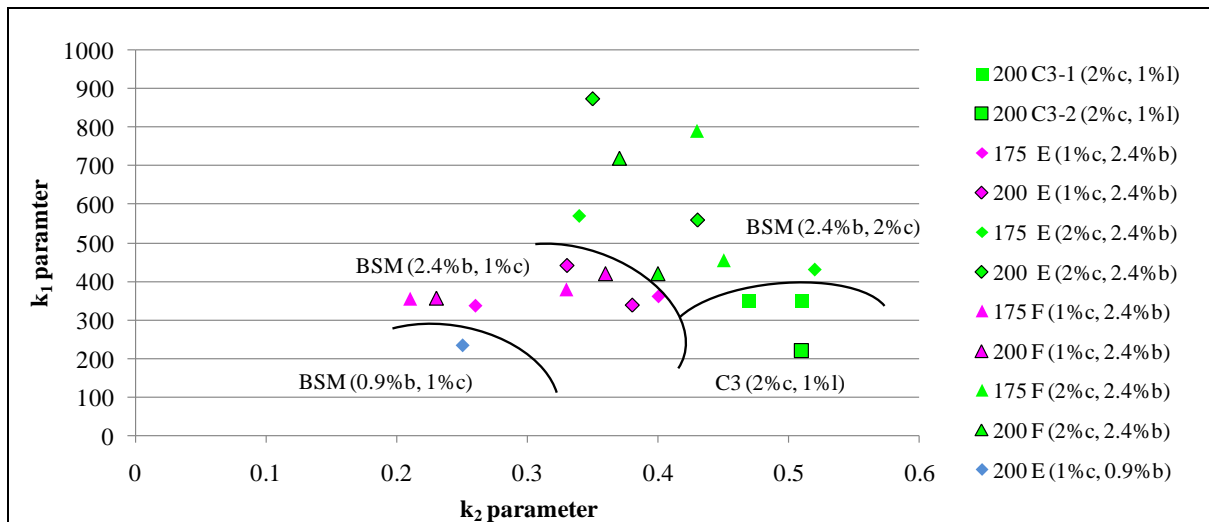


Figure 8.18: Curing model parameter plot -  $k_1$  versus  $k_2$

Cement and lime stabilised materials tend toward a lower initial stiffness ( $k_1$ ) with a high rate of stiffness gain ( $k_2$ ). BSMs with 1% cement added tend toward a similar or slightly higher initial stiffness than cement stabilised materials with a lower rate of stiffness gain.

BSMs with 2% cement added either show a combination of high initial stiffness and rate of stiffness increase similar to that of BSMs with 1% added, or else show an initial stiffness similar to that of BSMs with 1% cement and a rate of stiffness increase similar to that of cement stabilised materials. This observation indicates that the BSMs with 2% cement added, constructed along this experimental section, may show curing characteristics similar to BSMs with 1% cement added with higher initial stiffness or characteristics similar to that of cement stabilised materials with low initial stiffness and high rate of stiffness increase.

The observation that each stabilised material type may have a characteristic layer stiffness increase curve during curing may be useful in the construction of stabilised pavement layers. The quality control process for pavement construction could utilise the LFWD to determine this characteristic curing curve for the constructed material and compare with typical  $k_1$  and  $k_2$  values for the material type specified in the design of the pavement to be constructed. Further research into the characteristic curing curves of various materials under various conditions would however be required.

## 8.2 Seasonal variability in stabilised base layer stiffness

From the analysis in Chapter 7 there is evidence that the stiffness of many of the stabilised base layers are showing seasonal variability similar to that observed in the subgrade layers. In order to model this observation, the fitting of sinusoidal functions, in the same manner as utilised in the analysis of subgrade layers in Section 7.3.1 was carried out. The sine function parameters for each stabilised material type, along with the  $R^2$  fit of each model produced, are tabulated in Table 8.2. The reduction

in layer stiffness of these materials due to traffic loading induced damage is not considered as no indication of such damage is apparent, as discussed in section 7.3.4.

All purely cement and lime stabilised sub-sections do not follow the proposed sinusoidal stiffness variation pattern. This could be an indication of the low susceptibility of cement stabilised materials to seasonal variations in support stiffness while the material remains in a continuously bound condition. Once the cement stabilised material begins to breakdown due to fatigue, as proposed by current theories discussed in Section 2.5.1, it is expected the material will show greater dependency on its support stiffness.

Table 8.2 indicates that five of the BSM sub-sections show a reasonable fit, as identified by the  $R^2$  value; however when one looks at the actual plots the sinusoidal models show a reasonable correlation with the pattern of stiffness observed along the BSM sub-sections. It is believed that the  $R^2$  parameter for models fitted to actual average back-calculated stiffness values with low variance will produce an  $R^2$  value indicating poor fit. Taking the variation in stiffness along each sub-section, inaccuracies within the back-calculation method and the possibility of deterioration or further curing within the BSM materials into account the sinusoidal models give a reasonable representation of the seasonal variation in BSM layer stiffness. As discussed previously BSM foam layers with 1% cement added, in the southbound lane, showed an abnormally high average stiffness value for 90 day FWD test measurements into which further investigation is required.

**Table 8.2: Sinusoidal stabilised base layer seasonal stiffness variation model parameters - southbound**

Section	Seasonal variation sinusoidal model parameters				
	$\Omega$ (rads/day)	A (MPa)	$\Phi$ (days)	Mean (MPa)	$R^2$
200 C3-1 (2% <i>c</i> , 1% <i>l</i> )	0.017	300	-140	1350	0.00
200 C3-2 (2% <i>c</i> , 1% <i>l</i> )	0.017	20	-140	830	0.00
175 E (2.4% <i>b</i> , 1% <i>c</i> )	0.017	380	-140	1100	0.97
200 E (2.4% <i>b</i> , 1% <i>c</i> )	0.017	150	-140	1000	0.00
175 E (2.4% <i>b</i> , 2% <i>c</i> )	0.017	400	-140	1100	0.00
200 E (2.4% <i>b</i> , 2% <i>c</i> )	0.017	800	-140	1500	0.66
175 F (2.4% <i>b</i> , 1% <i>c</i> )	0.017	280	-140	650	1.00
200 F (2.4% <i>b</i> , 1% <i>c</i> )	0.017	200	-140	860	0.00
175 F (2.4% <i>b</i> , 2% <i>c</i> )	0.017	650	-140	2250	0.88
200 F (2.4% <i>b</i> , 2% <i>c</i> )	0.017	800	-140	1200	0.79

Figure 8.19 and Figure 8.20 depict sinusoidal models which show poor and good fit to their selected data-sets respectively. The full set of seasonal stiffness variation models for the southbound lane can be found in Addendum G.

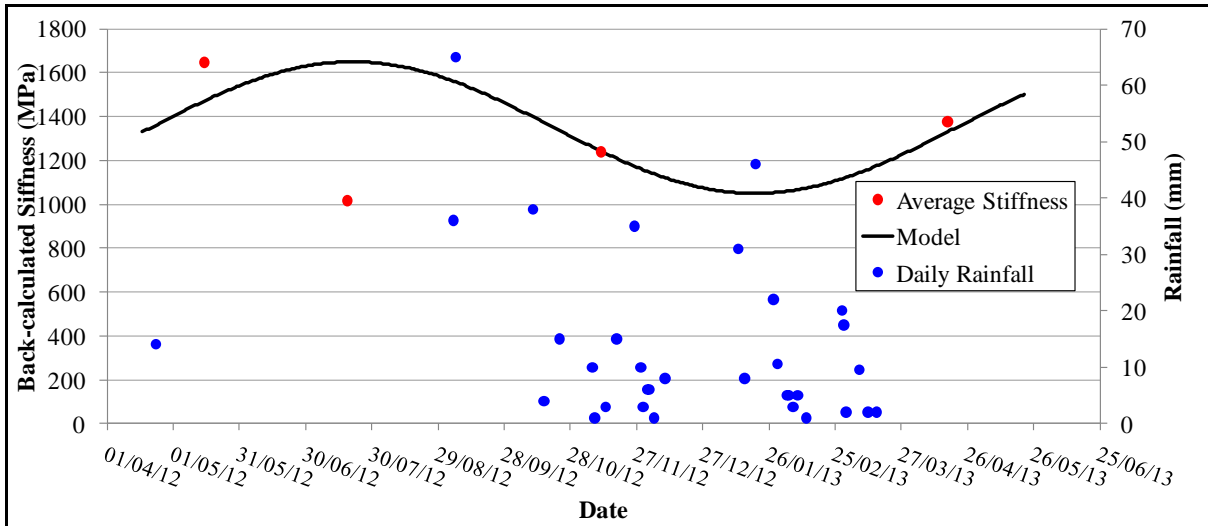


Figure 8.19: 200mm C3-1 (2%c, 1%l) - Seasonal stiffness variation model

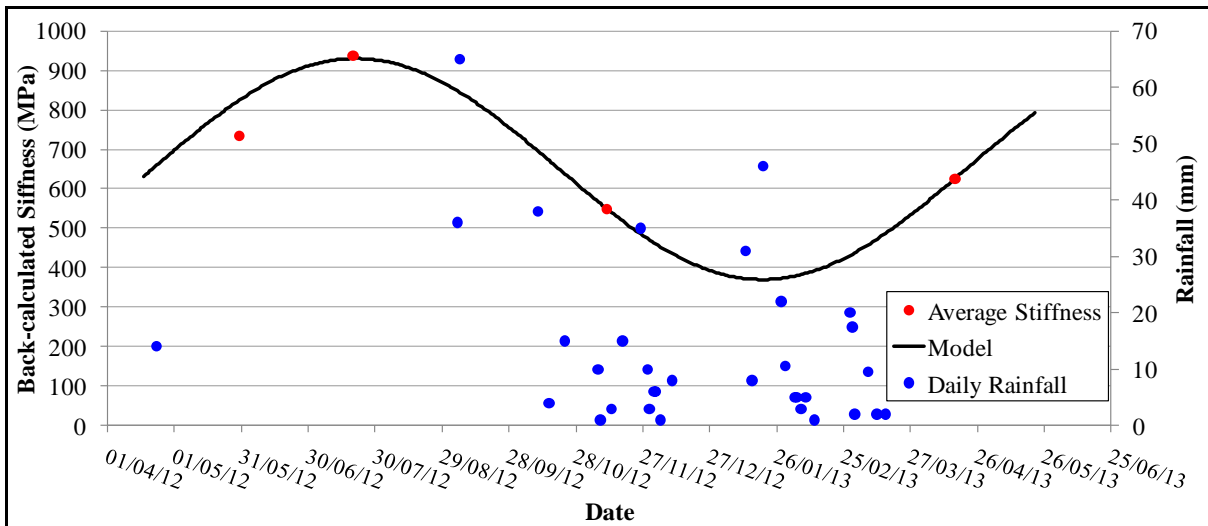


Figure 8.20: 175mm Foamed bitumen (2.4%b, 1%c) - Seasonal variation model

The fitting of sinusoidal model to the variability in average back-calculated stiffness is by no means definitive. Deflection data for a greater period of time will be required to develop or verify the proposed model and the reduction in stiffness due to damaging effects of traffic loading.

### 8.3 Conclusions

The selected curing model form describes satisfactorily the trend in average stiffness of the stabilised base layers over the initial 28 day curing period. The developed curing model k parameters show a significant correlation with stabilised material type identified by its design cement and residual bitumen contents. It was proposed that characteristic curing curves, following the model form proposed here, be developed for various material types. The Light Falling Weight Deflectometer (LFW) could then be utilised on site as a quality control test procedure to ensure the construction of a specific material type by comparing the required materials characteristic curing curve and that occurring on site.

The models describing the temporal variability in base layer stiffness over time utilising a sinusoidal model show reasonable levels of correlation with actual stabilised base layer stiffness values for some sub-sections. A number of sub-sections show no correlation however. The validity of this proposed model and the intimation that base layer stiffness is varying in a sinusoidal, seasonal manner will require further long term experimental section FWD testing and base layer stiffness determinations.

## CHAPTER 9 SPATIAL VARIABILITY OF STABILISED BASE LAYER STIFFNESS

The variability in back-calculated base layer stiffness along the length of each experimental sub-section is discussed in this chapter. This spatial variability over time is depicted utilising two plotting techniques. Summary statistics are used to quantify the variability in stiffness per sub-section over time. The structure of this chapter is displayed in Figure 9.1

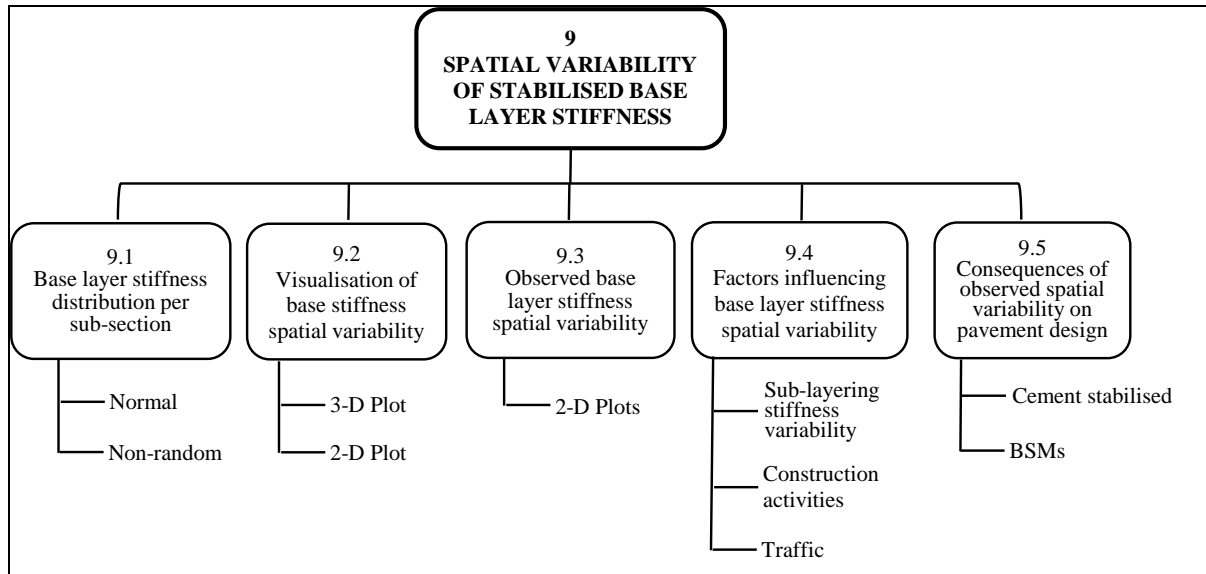


Figure 9.1: Outline of Chapter 9

### 9.1 Stabilised base layer stiffness distribution per sub-section

Figure 9.2 depicts a scatter plot of the stabilised base layer stiffness values determined along the 200 mm BSM foam with 2% cement sub-section in the southbound lane. It is clear from this plot that the variation in stiffness is not random and varies based on spatial position.

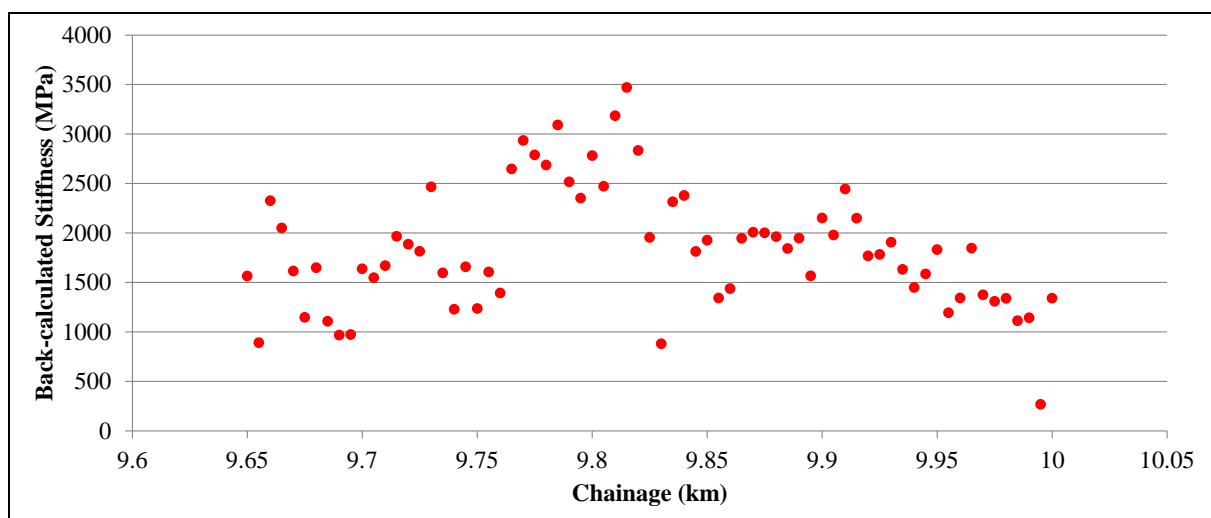


Figure 9.2: Scatter plot – 200mm BSM Foam (2.4%b, 1%c) day 25 southbound

The cumulative sum of deviations plot of base layer stiffness for the same sub-section is depicted in Figure 9.3. The cumulative sum plot visualises spatial locations where consecutively similar stiffness values occur. The similarity in stiffness is identified by the linearity in the cumulative sum plot. The cumulative sum of deviations was determined by the following equation:

$$S_i = x_i - \bar{x} + S_{i-1} \quad \text{Equation 11}$$

Where,

$S_i$  = Cumulative sum at chainage i

$x_i$  = Stiffness value at chainage i

$\bar{x}$  = Mean base layer stiffness for the sub-section

$S_{i-1}$  = Cumulative sum at chainage i-1

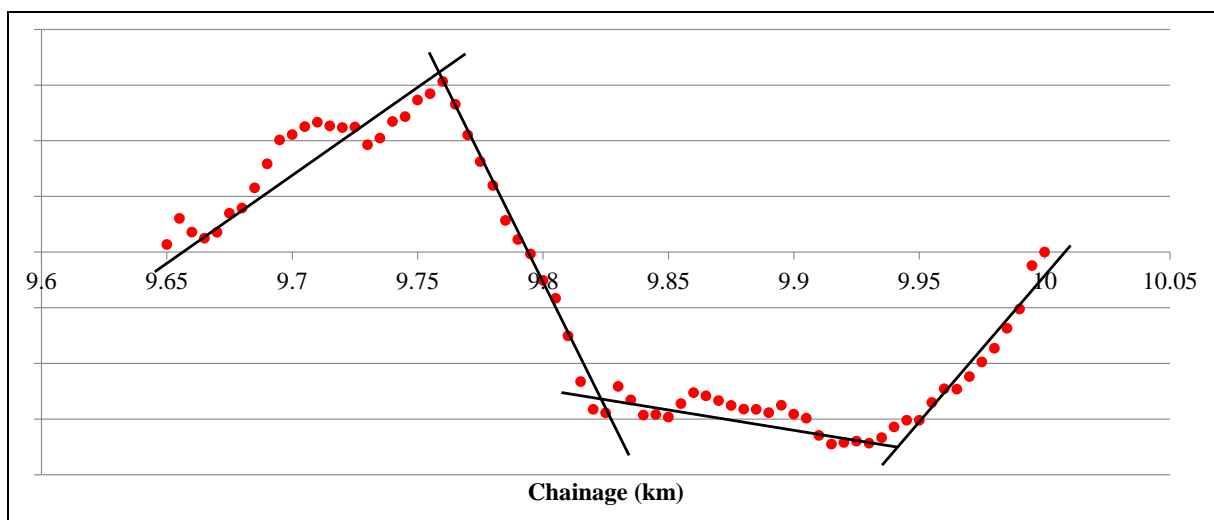


**Figure 9.3: Cumulative sum plot 200mm BSM Foam (2.4%b, 1%c) day 25 southbound**

It can be clearly seen that a number of subdivisions within the sub-section show linearity in the cumulative sum plot. This provides further indication that the observed variability in base layer stiffness is spatial and not random about a mean value.

It is therefore concluded that the stiffness data collected cannot be considered to fit a normal distribution. Further investigation into the stabilised pavement layers material properties and the determination of the cause of the observed spatial variability is required before the layer stiffness data can be fit to a normal distribution. It is only at this point that adequate knowledge into the behaviour of the stabilised material will have been achieved and its incorporation into pavement modelling techniques feasible.

Unfortunately due to the limited data relating to stabilised material properties such as moisture content, binder content, material grading and actual layer thickness available at the time of compiling this thesis, no investigations into the correlation between stabilised material properties and observed



stabilised base layer stiffness variability was possible. Therefore the observed variability in stabilised base layer stiffness per sub-section is depicted visually as it occurred in the field.

## 9.2 Visualisation of stabilised base layer stiffness spatial variability

### 9.2.1 3-D plotting

Three dimensional (3-D) plots of the back-calculated stabilised base layer stiffness of each experimental sub-section, in both the northbound and southbound lanes were created to visually portrait the spatial variability in stiffness of the base layer along the length of a sub-section and the change in spatial variability over time. Figure 9.4 depicts such a 3-D plot for the 200 mm C3-2 base layer in the southbound lane. The axes are labelled within Figure 9.4 identifying the parameters plotted. It must be noted that the time or days since construction axis is not scalar. This non-scalar representation was implemented to allow for the plotting of the stiffness values temporally within a reasonable plot area.

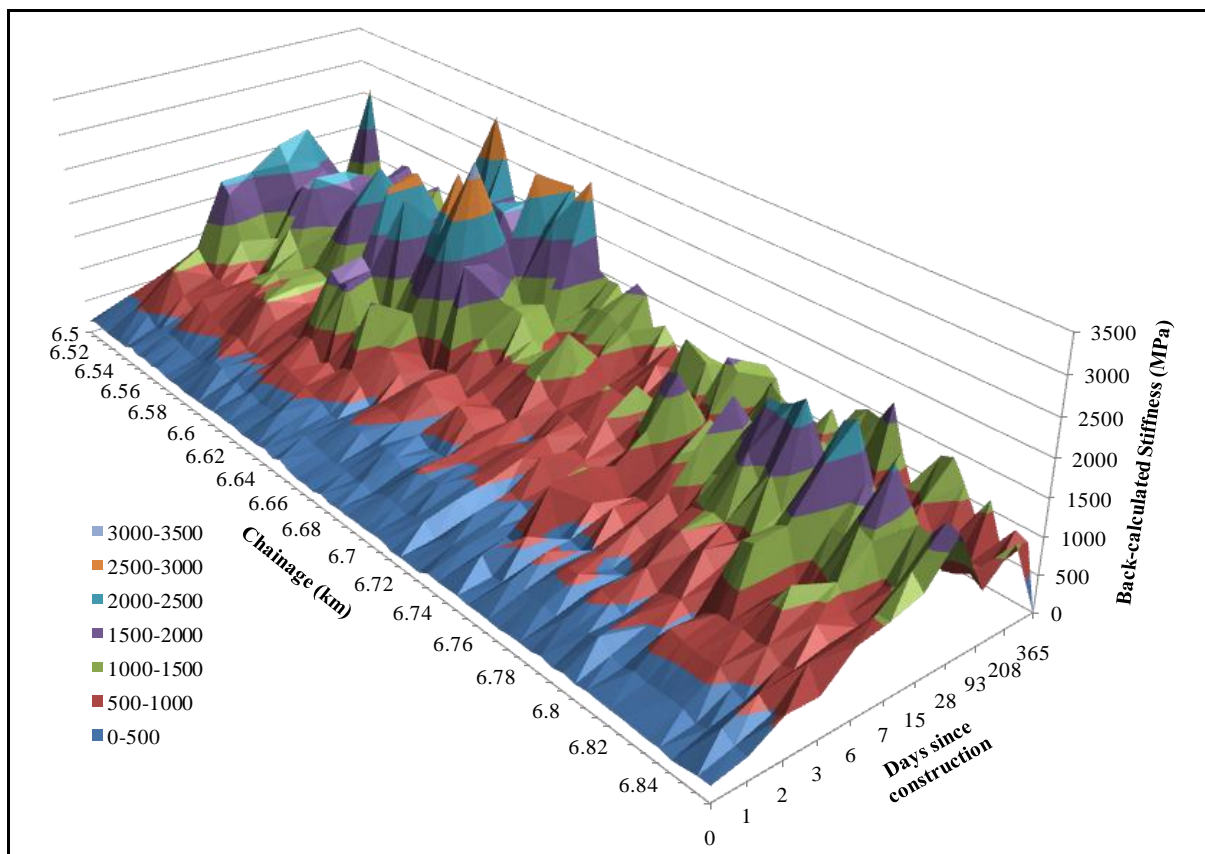


Figure 9.4: 3-D spatial base layer stiffness profile - 200mm C3-1, 2% cement and 1% lime SB

## 9.2.2 2-D plotting

For the analysis carried out in this chapter “heat” maps are utilised to depict the spatial and temporal variability of the back-calculated stiffness of each experimental sub-section determined at various temporal positions. An example of such a “heat” map is shown in Figure 9.6. The time variable, as quantified by the number of days since construction of the base layer, varies in the vertical direction. The chainage position along the length of the road varies in the horizontal direction. The stiffness back-calculated at a specific spatial and temporal position is depicted by colour. The colour range and related back-calculated stiffness is depicted in Figure 9.5.

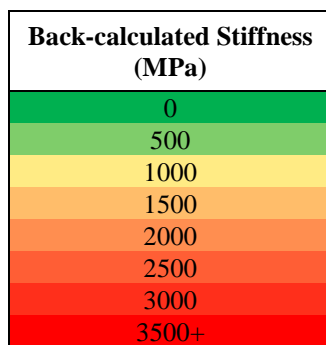


Figure 9.5: Back-calculated stiffness colour range

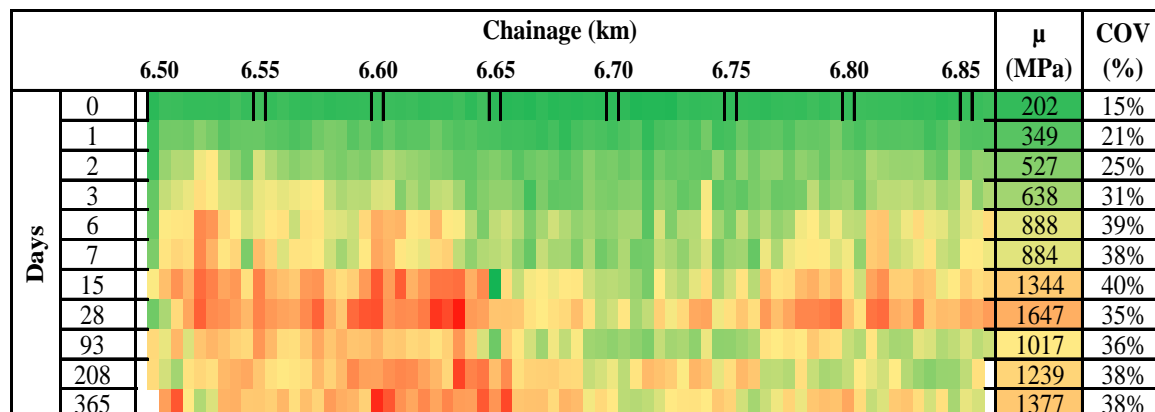


Figure 9.6: Base layer spatial stiffness profile – 200 mm C3-1 2% cement, 1% lime

Along with the visual depiction of the temporal and spatial variation in base layer stiffness, summary statistics are tabulated beside each “heat” map visualisation. The average and co-efficient of variation (CoV) of the back-calculated base layer stiffness of each sub-section, at each temporal location, is shown. The CoV of a sample is calculated by dividing the sample mean by the sample standard deviation. Also listed is the Pearson’s  $r$  value or correlation co-efficient which is used to identify the correlation in spatial stiffness variation between two sets of stiffness data. The value of this determination is discussed in the following section.

### 9.2.3 Spatial stiffness profile variability over time

In order to illustrate the change in stabilised base layer spatial stiffness profile with time the sample correlation coefficient  $r$  is utilised to quantify the correlation between the stiffness distributions at each temporal interval. The sample correlation coefficient is determined by the following relationship:

$$r = \frac{\sum_{i=1}^n (X_i - \bar{X})(Y_i - \bar{Y})}{\sqrt{\sum_{i=1}^n (X_i - \bar{X})^2} \sqrt{\sum_{i=1}^n (Y_i - \bar{Y})^2}} \quad \text{Equation 12}$$

Where:

$r$  = sample correlation coefficient

$X_i$  =  $i^{\text{th}}$  value from X sample

$\bar{X}$  = Mean of X sample

$Y_i$  =  $i^{\text{th}}$  value from Y sample

$\bar{Y}$  = Mean of Y sample

$n$  = sample size

An  $r$  value of 1 indicates a perfect linear correlation while 0 represents no correlation between two stiffness distributions. An example of the correlation between two base layer stiffness distributions for the 200 mm C3-1 sub-section in the southbound lane, determined at different times, is discussed below. Figure 9.7 depicts the scatter plot of the 200mm C3-1 base layer in the southbound lane at 7 and 15 days after its construction. It can be seen that the variation in stiffness along the length of the sub-section is similar for both days of stiffness determination. By plotting the stiffness values determined at the same spatial location on different days since construction against one another, Figure 9.8 is created. The correlation coefficient  $r$  indicates the degree of correlation between both distributions. For the example depicted in Figure 9.8 the  $r$  value determined was 0.8 representing a good correlation. The range of  $r$  values observed and the determination of good, fair and poor correlation in spatial stiffness variability of different data sets from differing temporal locations are depicted in Addendum H. Their value range, degree of correlation and the related colour coding is depicted in Table 9.1. The value of making this determination is the summarisation of visually

assessing and comparing the spatial variability in stiffness of a sub-section over time. While the method is not perfect it is robust enough to give indications as to the degree of change in the stabilised base layer stiffness profile over time for each experimental sub-section.

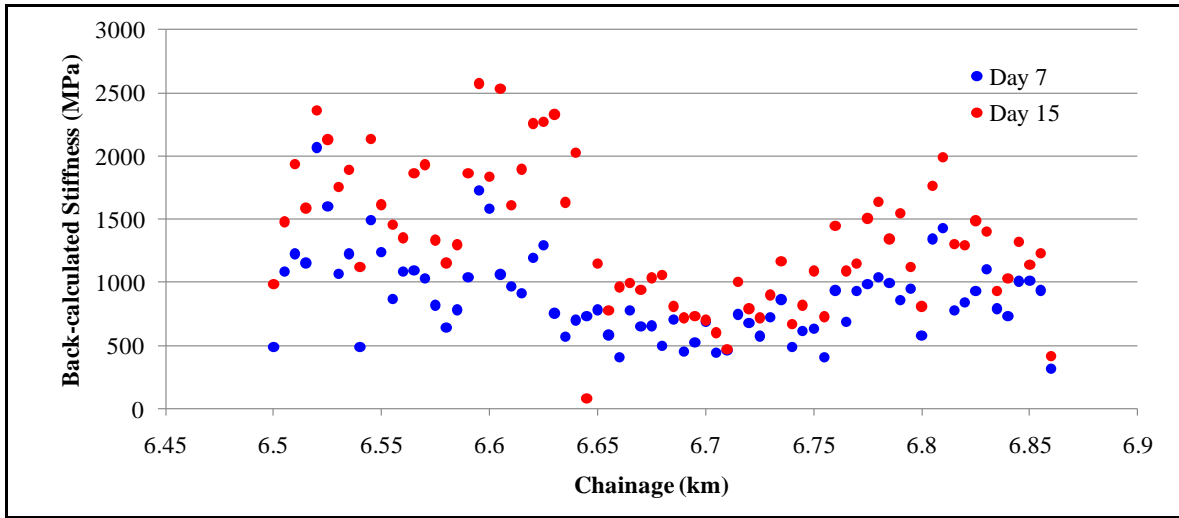


Figure 9.7: Scatter plot - 200 C3-1 day 7 and day 15 southbound

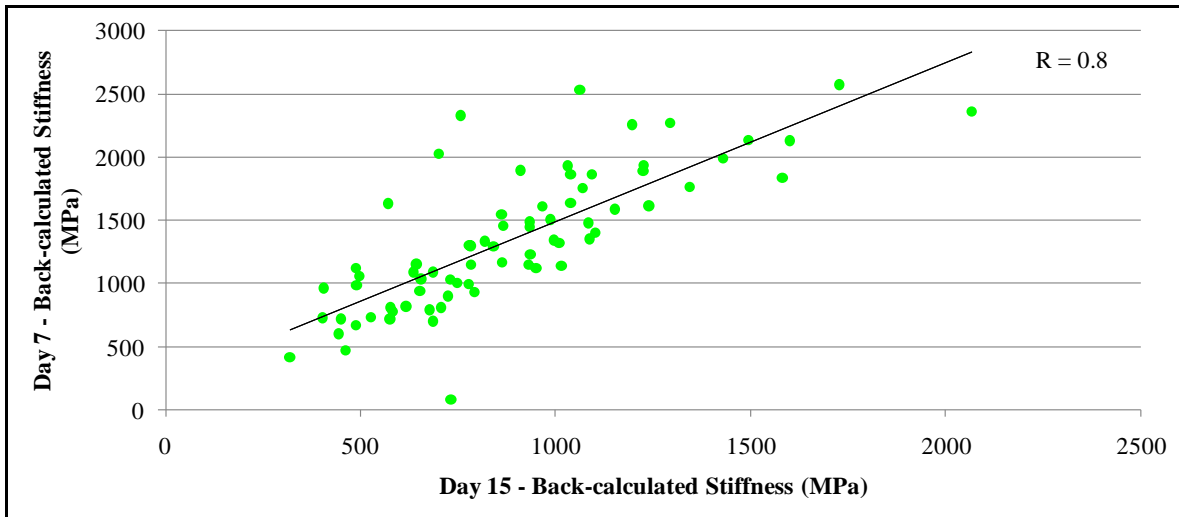


Figure 9.8: 200mm C3-1 day 7 versus day 15 southbound

Table 9.1: Degree of spatial trend correlation

Category	R - value
Good	1.0
Fair	0.5
Poor	0.0

Days	Spatial stiffness profile correlation									
0	0.5	0.5	0.5	0.5	0.5	0.6	0.5	0.4	0.1	0.2
	1	0.6	0.6	0.6	0.5	0.5	0.5	0.5	0.0	0.0
		2	0.7	0.7	0.7	0.6	0.4	0.5	-0.1	0.0
			3	0.7	0.8	0.6	0.5	0.6	0.0	0.1
				6	0.8	0.8	0.7	0.6	0.2	0.2
					7	0.8	0.6	0.6	0.0	0.2
						15	0.8	0.8	0.4	0.4
							28	0.7	0.3	0.2
								93	0.4	0.4
									208	0.5
										365

Figure 9.9: Correlation of base layer stiffness trends – 200mm C3-2 Southbound

### 9.3 Observed base layer stiffness spatial variability over time

The stabilised base layer stiffness spatial variability observed along each sub-section is illustrated using the method of 2-D graphical representation described in Section 9.2.2. The average and CoV of base layer stiffness values and correlation co-efficient  $r$  relating to the continuity of the spatial stiffness trend over time are shown for each sub-section over the 360 day observation period. The complete set of 2-D base layer stiffness plots showing the observed spatial variability for each sub-section in both the northbound and southbound lanes are attached in Addendum I.

Figure 9.11 illustrates the spatial variability in base layer stiffness observed along the BSM emulsion sub-section stabilised with 2.4% residual bitumen and 1% cement. It is clear from this 2-D plot example that significant variability in stiffness occurs along the length of the sub-section. High levels of variability are observed throughout the experimental section with no sub-section or material type showing uniform levels of base layer stiffness along the length of the sub-section. The non-random nature of the stiffness variability can also be observed from these 2-D plots. CoVs are observed to increase over time, typically to levels in the order of 40% thus indicating the high levels of variability in base layer stiffness reached.

Back-calculated Stiffness (MPa)
0
500
1000
1500
2000
2500
3000
3500+

Figure 9.10: Back-calculated stiffness colour range

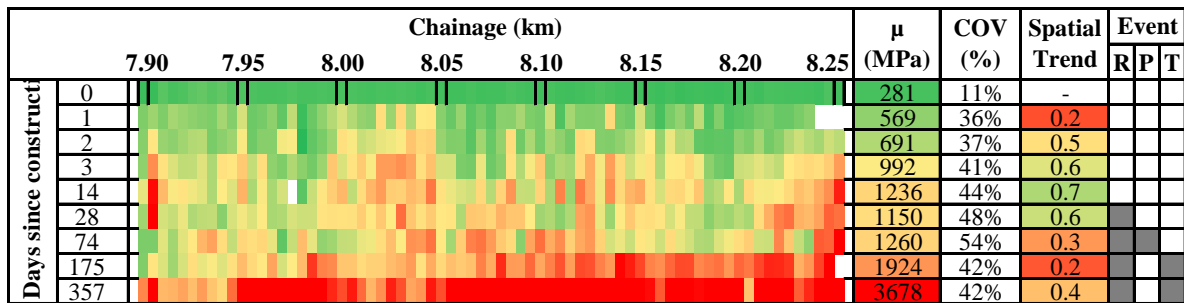


Figure 9.11: Spatial variability in layer stiffness - 175mm BSM Emulsion (2.4%b, 2%c) Northbound

The comparison between consecutive days base layer stiffness distributions is assessed based on the correlation co-efficient calculated from two consecutive stiffness distributions. The colour coding of the correlation co-efficient assists with indicating the continuation of the same base layer stiffness spatial variation pattern over time.

Also noted was the influence of events occurring throughout the observation period, these include rainfall, construction activities and the opening of the experimental section to traffic. Factors identified as possibly influencing the observed trend in average stiffness, as identified in Chapter 7, were also compared with the spatial variation of base layer stiffness along the length of each sub-section. These events include rainfall (R), prime application (P) and traffic loading (T). Their occurrence is also indicated on the 2-D plots. The possible influence of these events on the spatial variability in base layer stiffness observed is investigated in the next section.

## 9.4 Factors influencing base layers stiffness spatial variability

### 9.4.1 Support stiffness variability

#### 9.4.1.1 Sub-base

No correlation between the back-calculated base layer stiffnesses and the under lying sub-base layer stiffness is noted. Figure 9.12 depicts the plot of the base layer stiffnesses for the 200mm BSM emulsion sub-section with 1% cement added in the southbound lane, 78 days after construction, on the x-axis with the back-calculated sub-base layer stiffnesses plotted on the y-axis. The absence of a correlation between the base and sub-base layer stiffness trends, as identified in Figure 9.12, indicates that sub-base support is not influencing the observed stabilised base layer variability.

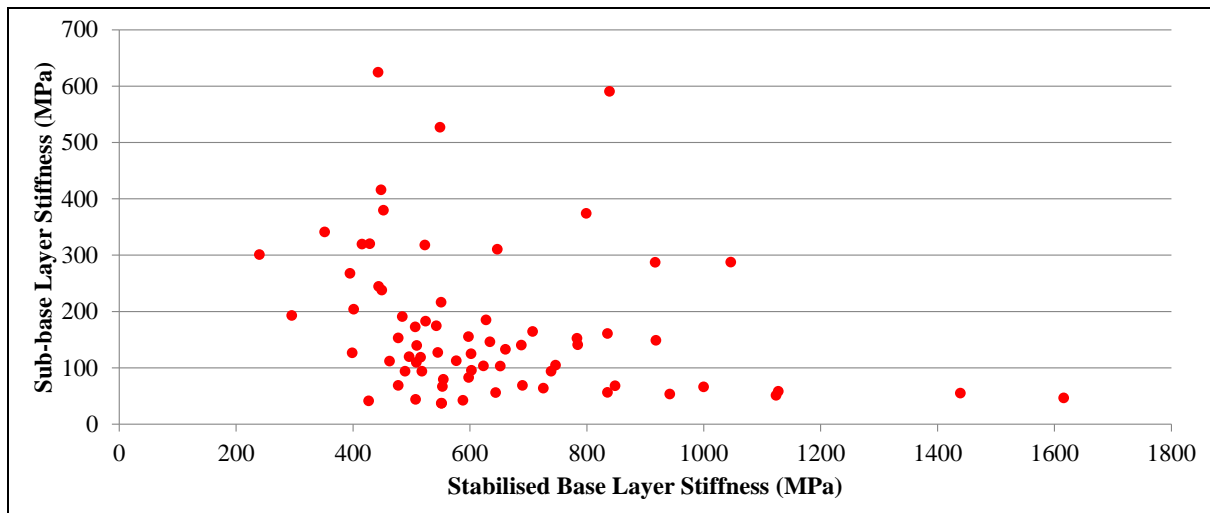


Figure 9.12: Correlation between base and sub-base layer stiffness - 200mm BSM emulsion 2.4%b, 1%c

#### 9.4.1.2 Subgrade

No relationship between the stabilised base layer stiffness and combined subgrade stiffness is observed for the 200mm BSM emulsion layer with 1% cement added in the southbound lane at 78 days after construction. The plot of the base stiffness and combined subgrade stiffness illustrate this conclusion.

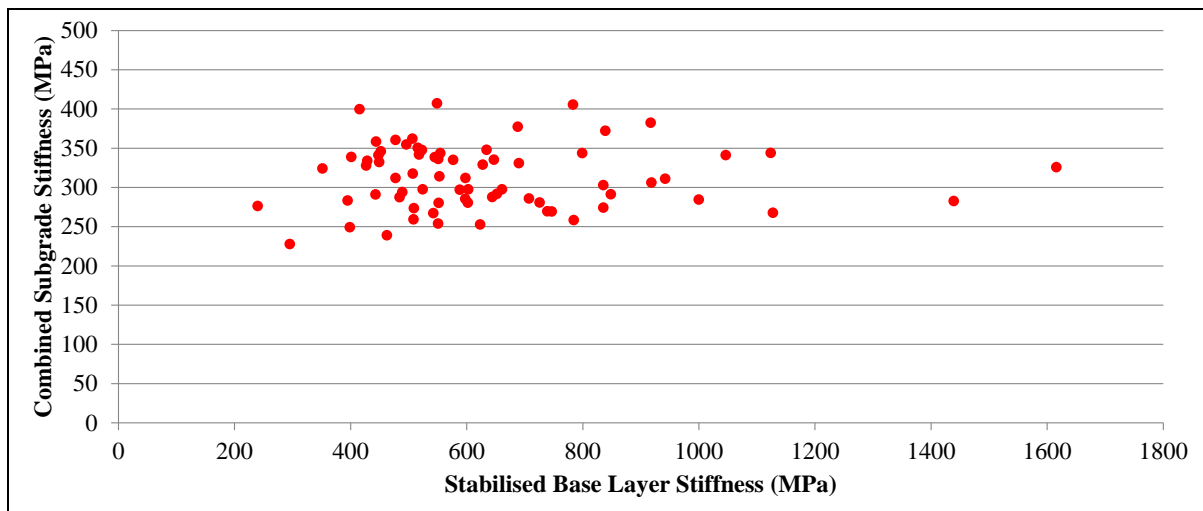


Figure 9.13: Correlation between base and subgrade layer stiffness - 200mm BSM emulsion 2.4%b, 1%c

It is clear from the above figures that there is no evidence to suggest that sub-layer beneath the stabilised base layer is influencing the base layer stiffnesses observed along the experimental sub-section shown above. The same observation is made throughout the experimental section in both the northbound and southbound lanes.

#### 9.4.2 Rainfall, prime application and traffic

Colour coded tables depicting the degree of correlation between consecutive stiffness distributions over time and per sub-section were used to identify if factors such as rainfall, the opening of the

experimental section to traffic or construction activities such as prime application had an influence on the spatial stiffness profile observed along the length of each sub-section. Table 9.2 depicts the colour code and related correlation co-efficient values used in the graphical representation. Figure 9.14 depicts an example of the coded plot of correlation coefficients between stiffness distributions for each experimental sub-section at various times over the 360 day observation period in the southbound lane. The occurrence of prime application within the observation period for each sub-section is shown in this example. It is clear for Figure 9.14 that there is no correlation between the application of prime to the base layer and changes to the spatial base layer stiffness profile during the 360 day observation period.

**Table 9.2: Degree of spatial trend correlation**

Category	R - value
Good	1.0
Fair	0.5
Poor	0.0

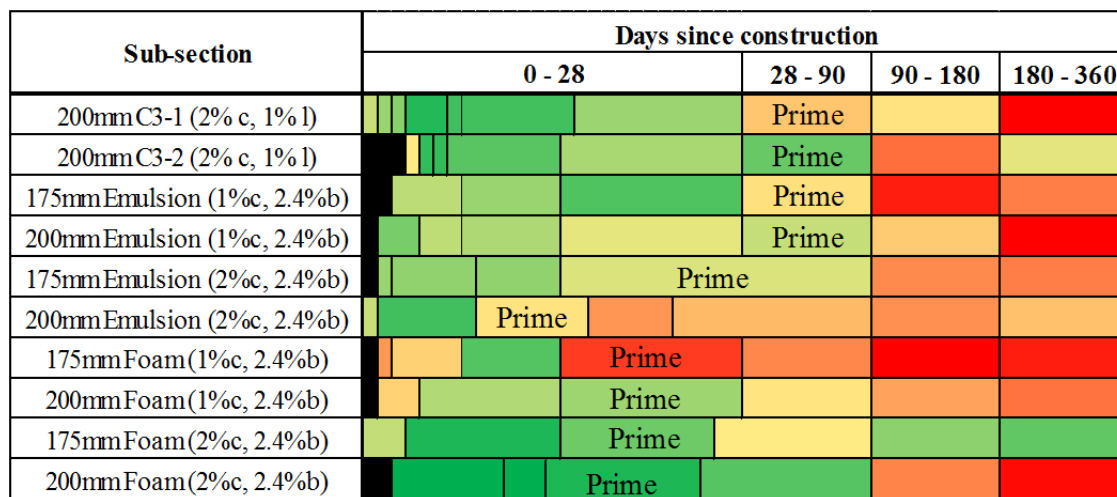


**Figure 9.14: Correlation between prime application and changes in spatial stiffness profile SB**

The complete set of colour coded correlation tables is attached in Addendum J. No clear correlation between changes in spatial stiffness profile and rainfall, traffic or prime application events is identified by these graphical representations. What can be observed however is that the majority of significant changes to the spatial stiffness profile occur either in the early stages of the curing period, where significant curing of the stabilised base material is occurring or else subsequent to 14 days after base layer construction where the combined effects of rainfall, prime application and traffic loading are influencing the spatial base layer stiffness profile.

**9.5 Effects of base layer stiffness spatial variability on pavement design**

As detailed in Section 9.1, the variability in back-calculated base layer stiffness observed along the length of a sub-section was not due to the random variability. The variability observed is spatial and



due to the varying material properties of the base layer constructed along the length of a sub-section. In order to quantify the effects of this variability in base layer stiffness within a pavement design scenario, a structural and bearing capacity analysis of two experimental sub-sections was carried out. The actual stiffness data collected along the experimental section was used to show the resultant bearing capacity variability of the experimental pavement structure using current South African Mechanistic-Empirical Design Method (SAMDM) deterioration models.

A standard axle of 80kN load, with a dual wheel half axle was applied to the pavement to determine the selected pavement structure bearing capacities. The wheel spacing on a half axle was set at 350mm and with tyre pressures at 850kPa.

#### 9.5.1 Variability in pavement life of cement stabilised base layers

Base layer stiffness data from the 200mm C3-1 cement stabilised sub-section in the northbound lane is used in the analysis presented here. The cement stabilised fatigue model within the South African Mechanistic-Empirical Design Method (SAMDM) (Theyse et al 1996) was used to estimate the number of load repetitions of the selected standard axle to fatigue failure of the C3 layer. An equivalent granular phase, utilised within the SAMDM (1995) was not implemented in this study.

The 90<sup>th</sup>, median and 10<sup>th</sup> percentile bearing capacities determined from the distribution of pavement layer back-calculated stiffnesses along the selected cement stabilised experimental sub-section are shown in Figure 9.15. The level of variability in bearing capacity calculated is significant. For a Category B road a 90<sup>th</sup> percentile level of reliability is required for pavement design. If the experimental sub-section analysed is assumed to be a category B road the 90<sup>th</sup> percentile bearing capacity would equate to 40,000 standard axle load repetitions. If the sub-section had been designed for this bearing capacity half the length of the sub-section would have been over designed by a factor of 4 when the variability in layer stiffness is incorporate within the design process. As a result of this variability and the wide range of pavement bearing capacities occurring in reality, the performance of the stabilised pavement material becomes difficult to predict. Also a pavement structure which is over designed by a factor of 4 over 50% of its length represents an inefficient use of resources.

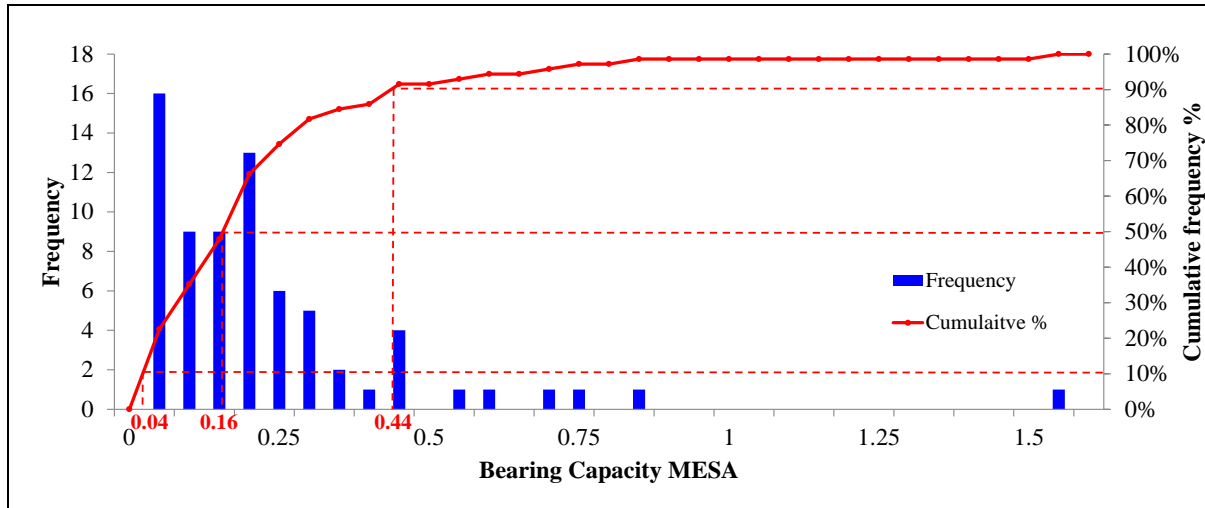


Figure 9.15: Distribution of bearing capacities of 200 mm C3-1 Northbound

### 9.5.2 Variability in pavement life of CIPR BSM materials

The 90<sup>th</sup>, 10<sup>th</sup> and median base layer stiffness pavement structures were analysed to give an indication of the variability in performance of the BSM emulsion with 1% cement in the northbound lane. The deviator stress ratio (DSR) response parameter of the BSM base layer, under the standard 80kN axle load, is used to determine the performance of the three pavement structures analysed. The DSR is used due to the theory that BSM materials perform as a granular, non-continuously bound material. The deviator stress ratio gives an indication of the stress condition within the BSM base layer which would induce rapid shear deformation within the material. Shear deformation of a pavement layer material equates to the occurrence of rutting of the pavement in reality. DSR is determined as follows:

$$\text{DeviatorStressRatio}(SR) = \frac{\sigma_1 - \sigma_{2,3}}{\sigma_{1f} - \sigma_{2,3}} \quad \text{Equation 13}$$

$\sigma_1$  = Principal stress 1 (kPa)

$\sigma_{1f}$  = Principal stress at failure (kPa) =  $((1 + \sin\phi)\sigma_{2,3} + 2c\cos\phi)/(1 - \sin\phi)$

$\sigma_{2,3}$  = Principal confining stresses 2, 3 (kPa)

$c$  = cohesion (kPa)

$\phi$  = angle of internal friction (°deg)

Figure 9.16 displays the principal stresses occurring on an element within a pavement structure beneath a wheel load. The lines of action of the principal stresses are not always parallel and orthogonal to the wheel load. Dependent upon the wheel load configuration or position in relation to the element observed, the line of action of the principal stresses on an element, in relation to the pavement structure surface, will vary.

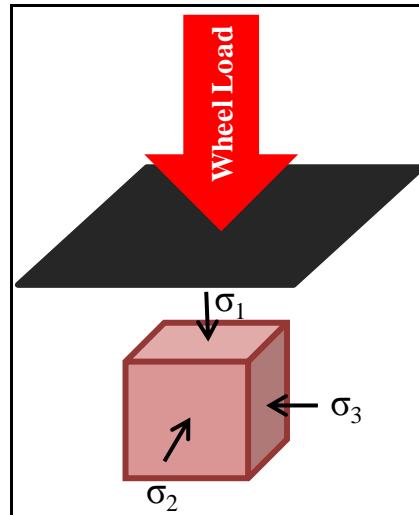


**Figure 9.16: Depiction of Principal Stresses**

The principal normal stress at failure,  $\sigma_{1f}$ , is determined utilising Mohr's Circle and typical values of cohesion and angle of internal friction measured by monotonic tri-axial tests on cores taken from the R35 experimental site. It was assumed in the analysis that the stiffer material related to higher cohesion and angles of internal friction and lower stiffness values corresponded with lower shear parameter values. The determination of the pavement response was carried out using BISAR. The pavement structures modelled and resultant critical DSRs are tabulated below. Figure 9.18 depicts the DSR determined at one quarter depths in the 200mm thick base layer for the three pavement structure scenarios.

	Layer D (mm)	90th %ile		Median		10th %ile	
		Mr (MPa)	SR	Mr (MPa)	SR	Mr (MPa)	SR
Asphalt	45	3500	-	3500	-	3500	-
In-situ recycled BSM	200	554	1.19	811	0.77	1377	0.49
Broken - down C3 / 4	100	25	-	32	-	44	-
Subgrade	$\infty$	216	-	360	-	291	-

**Figure 9.17: SR analysis pavement structure and results**

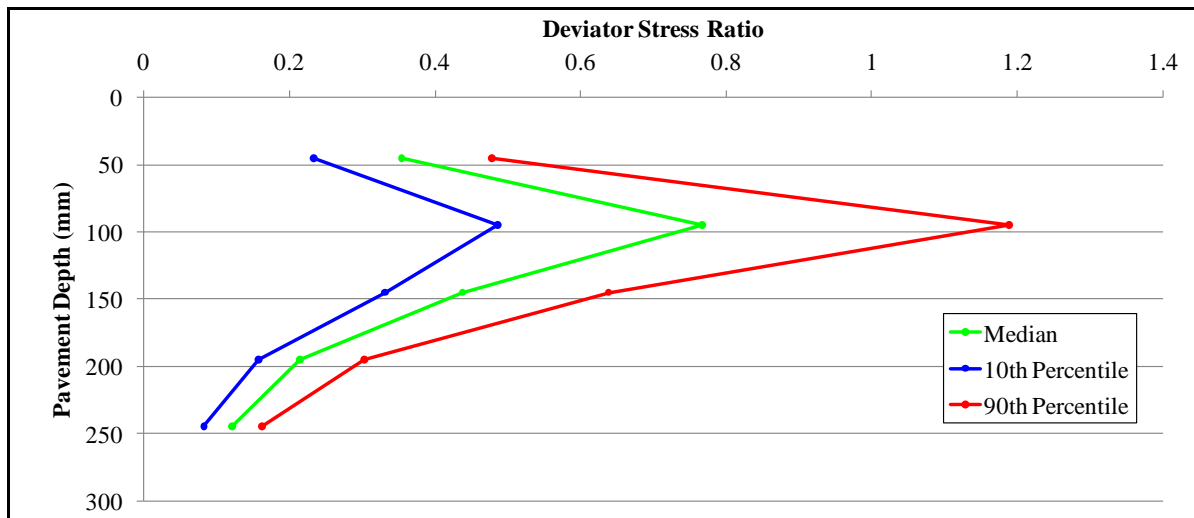


Figure 9.18: Variation in SR versus depth in pavement structure

The wide range in SR values indicates the large variability in material performance. While SR is typically material dependent, values greater than 0.6 indicate significant risk of rapid permanent deformation (Ebels, 2008). Applying the hypothetical scenario utilised in Section 9.5.1, if the variability in material stiffness was utilised in a pavement design of a Category B road (90% reliability), at least half the length of the pavement structure would be over designed by an SR factor of 1.5, which relates to a wide range of rates of permanent deformation in the stabilised material. This level of variability makes it difficult to reliably predict the performance of the stabilised material and provides for uneconomical pavement designs.

## 9.6 Conclusions

The CIPR and stabilisation of existing pavement structures along the experimental section has constructed stabilised base layers which have significantly varying levels of stiffness. From stiffness data collected along the experimental section CoVs per experimental sub-section of up to 40% were determined at a point in time. This level of variability is significant and is put into perspective when the bearing capacities provided by the varying pavement structure is considered. The over design of 50% of a cement stabilised sub-section by a factor of 4 was determined for one pavement design scenario analysed which incorporated the observation base layer stiffness variability.

A relationship between stabilised base layer stiffness and supporting sub-base and combined sub-grade layer stiffness was not identified. A correlation between the occurrence of traffic loading, rainfall and construction activity on the spatial stiffness profile was not found.

In order to determine cause of the observed variability in base layer stiffness further high density testing of the stabilised material will be required. Required testing would include material gradings, binder content and moisture content.

## CHAPTER 10 CORRELATION BETWEEN BASE LAYER STIFFNESS AND ENGINEERING TEST RESULTS

During the construction of each experimental sub-section, stabilised pavement material samples were taken at a number of locations from behind the recycling machine. The stabilised material samples were utilised to create specimens and subsequently tested to determine the stabilised materials UCS and ITS. Background to these test methods are discussed in Chapter 5. The quality control tests carried out determined the following material parameters:

- Indirect Tensile Strength (ITS) – 150mm diameter dry specimens cured for 28 days
- Unconfined Compressive Strength (UCS) – 150mm diameter soaked specimens cured for 28 days

ITS testing is an indirect method of measuring the flexibility of a stabilised material. UCS determines the compressive strength of a stabilised material. The theory of elasticity utilised in determining the stresses and strains within a pavement layer indicates that both compressive and tensile forces can occur within a pavement layer. This chapter, as outlined in Figure 10.1, will compare the site laboratory ITS and UCS values with base layer stiffness at the specific locations where UCS and ITS tests were carried out along the experimental section.

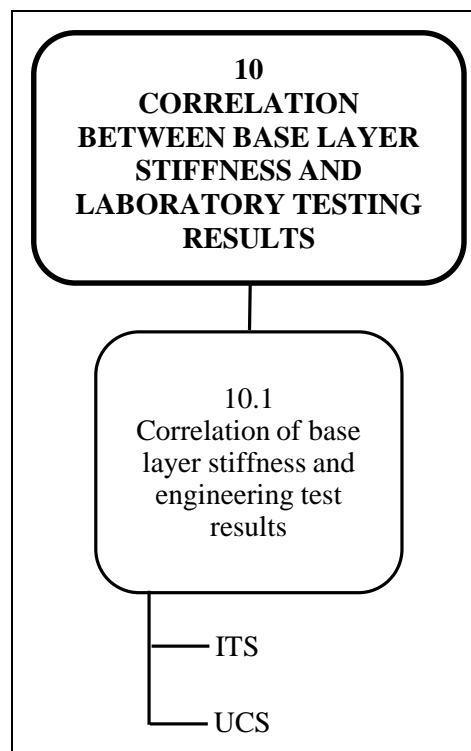


Figure 10.1: Outline of Chapter 10

### 10.1 Correlation of base layer stiffness with engineering tests

The ITS and UCS determined from specimens sampled at specific spatial locations will be compared with the average of base layer stiffnesses within 10 metres of the spatial location where samples for the engineering tests were taken. The maximum of average base layer stiffness values occurring over the 360 day observation period is used in the analysis. The maximum values are used as this is expected to give the best indication of the stiffness capabilities of the stabilised material and preventing the use of stiffness values which have been influenced by seasonal pavement stiffness variability and prime application.

#### 10.1.1 Indirect Tensile Strength (ITS)

##### 10.1.1.1 Southbound

Figure 10.2 depicts the correlation between ITS and the localised base layer stiffness values for cement and lime treated materials. A poor correlation between ITS values and the localised base layer stiffness values is observed. While both materials were constructed to the same design with respect to cement contents at 2% and lime at 1%, the C3-2 material shows lower stiffness and ITS values in general.

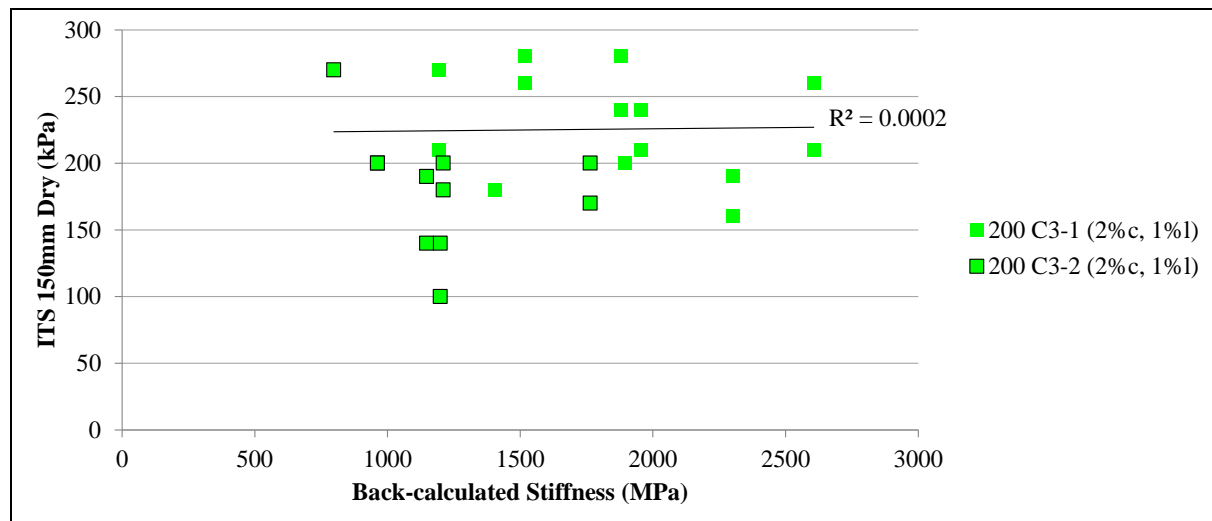


**Figure 10.2: Correlation of cement stabilised material ITS and base layer stiffness - southbound**

Figure 10.3 depicts the relationship between ITS test results and localised back-calculated stiffness values for BSMs stabilised with bitumen emulsion. No clear correlation between ITS and stiffness is observed. The ITS values increase with stabilised material cement contents however this trend is not observed for base layer stiffness values. A strong overlap between base layer stiffness values for the 175 mm BSM emulsion layer with 1% cement added and BSM emulsion layers with 2% cement added is noted.

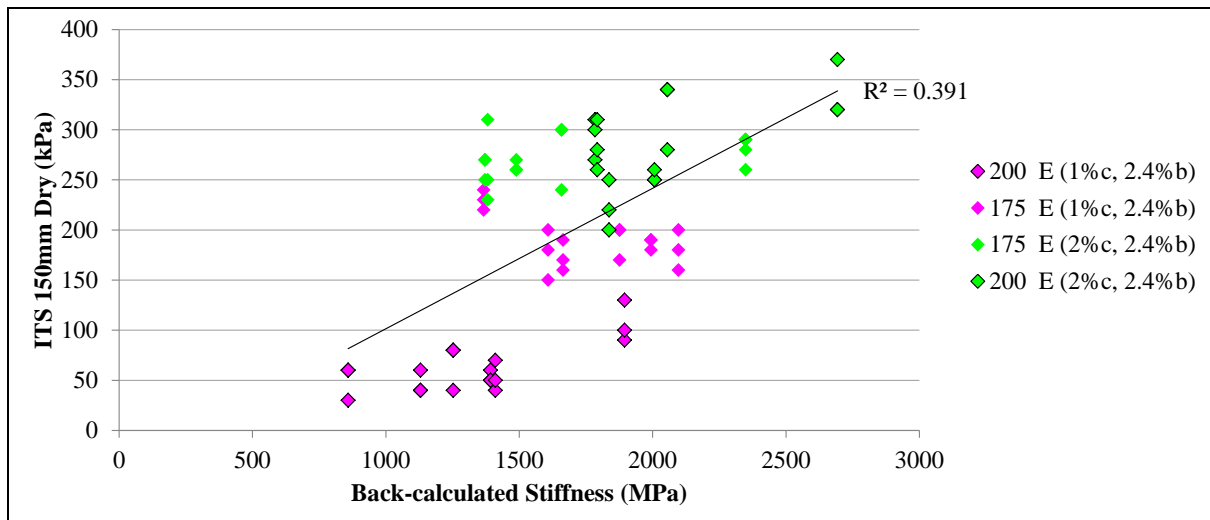


Figure 10.3: Correlation of BSM emulsion ITS and base layer stiffness – southbound

Figure 10.4 depicts ITS and localised base layer stiffness values for BSM foam sub-sections. No correlation between ITS and base layer stiffness is observed. In contrast to the bitumen emulsion materials, ITS values do not increase with increasing cement content. The localised base layer stiffness values do however show a general increase with increasing cement content.

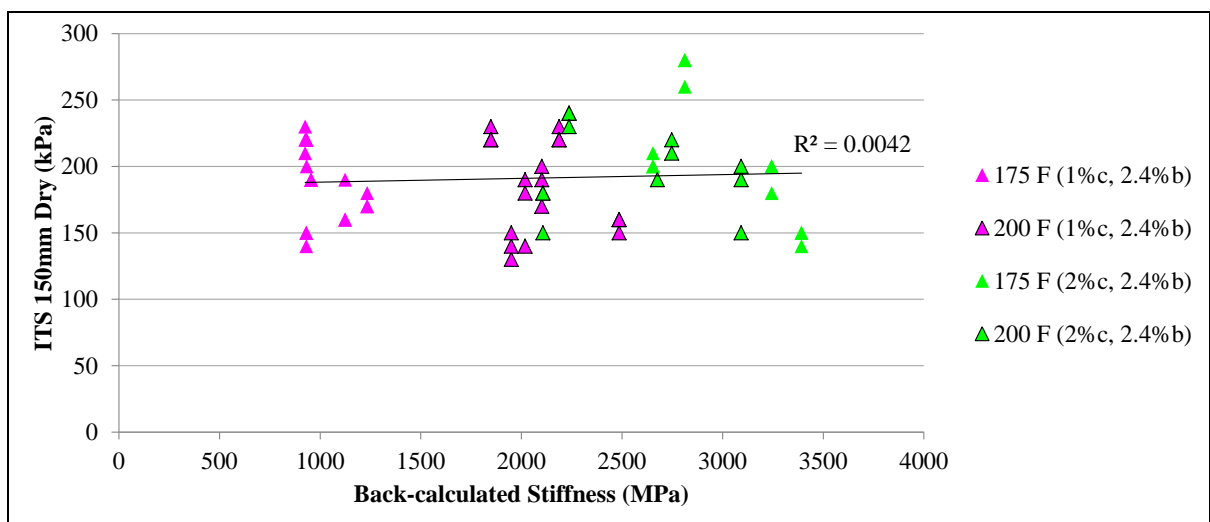


Figure 10.4: Correlation of BSM foam ITS and base layer stiffness – southbound

#### 10.1.1.2 Northbound

No ITS tests were carried out on samples of stabilised materials during the construction of the cement stabilised base layers in the northbound lane.

Figure 10.5 illustrates the correlation between ITS and localised base layer stiffness values for BSM emulsion sub-sections. A weak linear relationship, as indicated by the  $R^2$  value, is observed between ITS and base layer stiffness values. ITS and base layer stiffness values tend to increase with increasing levels of cement content. The BSM material stabilised with 0.9% bitumen emulsion and 1% cement show the lowest combination of ITS and base layer stiffness. BSM emulsions with 2%

cement added show higher stiffness values spread over a wide range. ITS values for BSM emulsions with 2% cement added are in a similar range to BSM emulsion layers with 1% cement added.

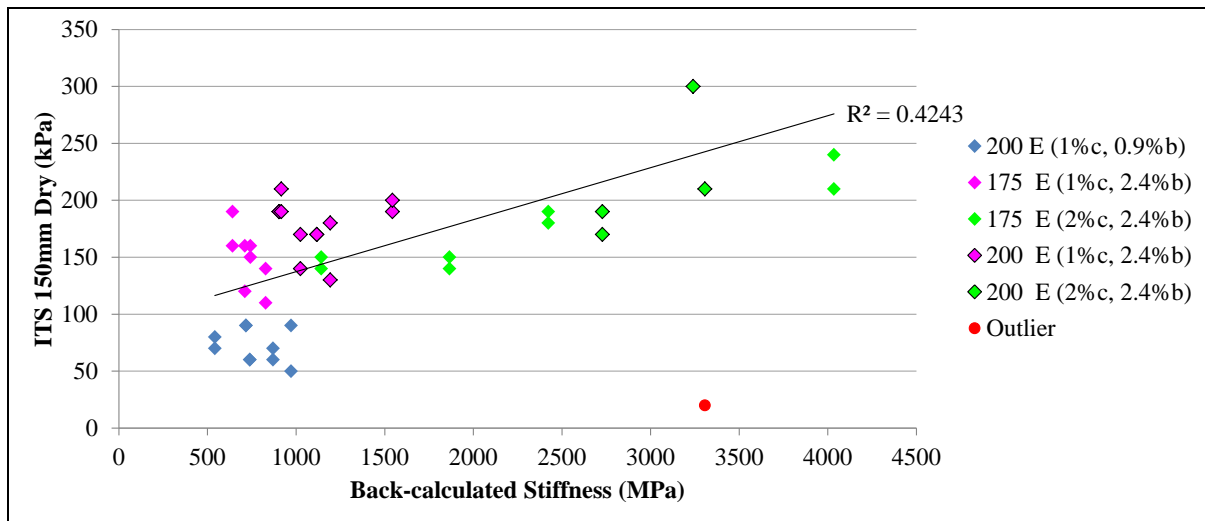


Figure 10.5: Correlation of BSM emulsion ITS and base layer stiffness – northbound

Figure 10.6 depicts the ITS and localised base layer stiffness relationship for BSMs stabilised with foamed bitumen. A relatively good linear correlation is observed with BSM foam layers containing lower cement contents showing lower ITS and base layer stiffness combinations when compared to BSMs with higher cement contents. A wide range of base layer stiffness values for BSM foam layers with 2% cement added is noted

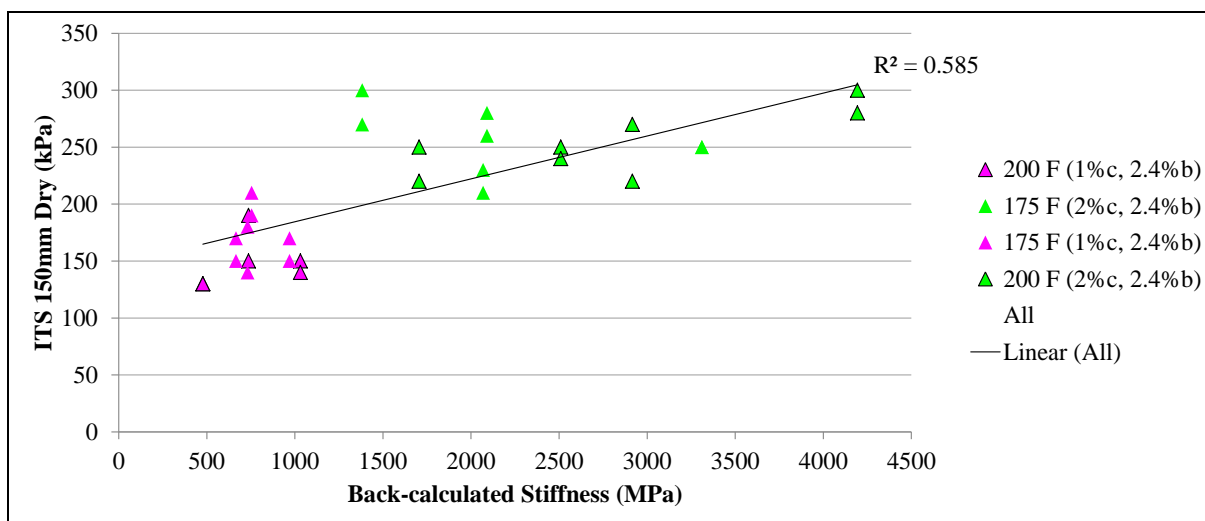
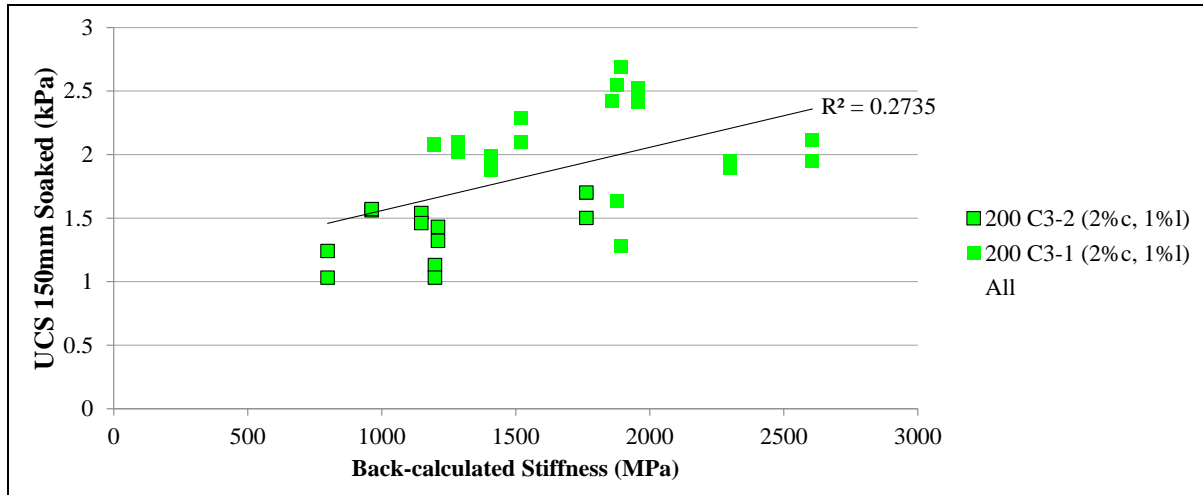


Figure 10.6: Correlation of BSM foam ITS and base layer stiffness – northbound



## 10.1.2 Unconfined compressive Strength (UCS)

## 10.1.2.1 Southbound



**Figure 10.7: Correlation of cement stabilised material UCS and base layer stiffness – southbound**

Figure 10.7 depicts the correlation between UCS and localised base layer stiffness values for cement and lime stabilised materials in the southbound lane. A wide spread of stiffness and UCS values were measured for the stabilised material which were designed to have the same cement and lime contents. The C3-2 material, in comparison to the C3-1 material, in general show base layer stiffness and UCS values in the lower ranges of the values observed. This is in agreement with the ITS and stiffness correlation discussed in section 10.1.1.1. The cause of the low strength values for the C3-2 cement stabilised layer was not found.

## 10.1.2.2 Northbound

As is depicted in Figure 10.8 no correlation between UCS and localised base layer stiffness values is evident for cement and lime stabilised materials in the northbound lane. The data set available however is too small to make a definitive observation on correlation.

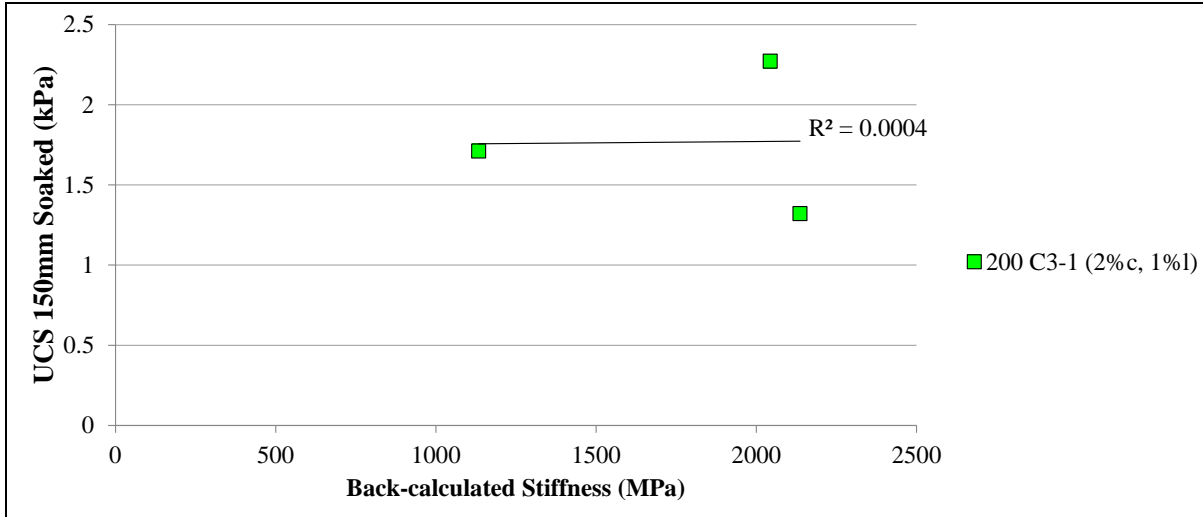


Figure 10.8: Correlation of cement stabilised material UCS and base layer stiffness – northbound

Figure 10.9 depicts the relationship between UCS values and localised back-calculated base layer stiffness for BSM emulsion layers. A poor correlation exists between the measured material properties. A rational spread of data exists with material containing higher levels of cement showing higher stiffness however the UCS values do not indicate any clear increase in with increasing cement contents.

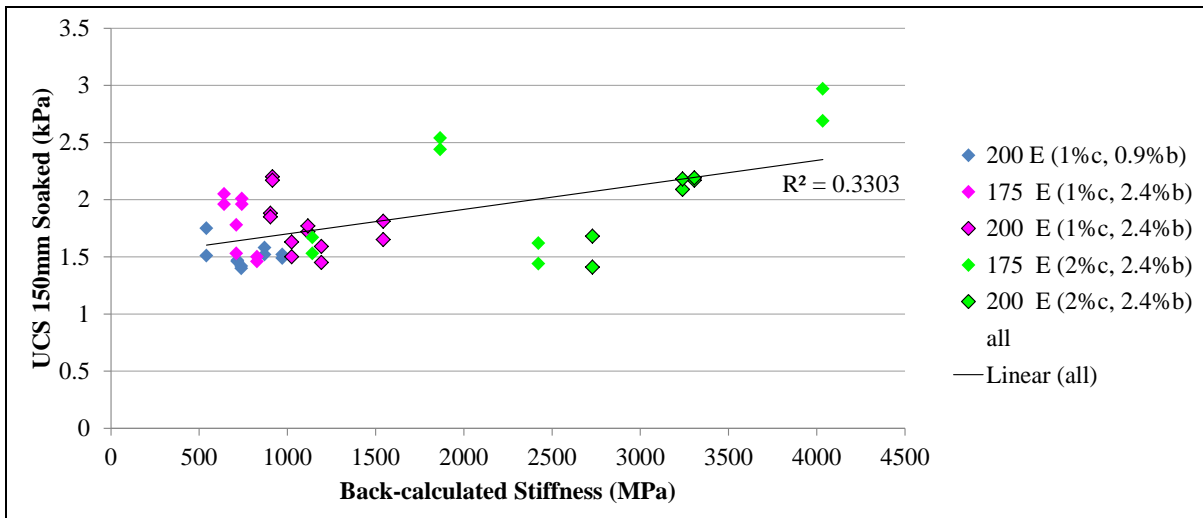


Figure 10.9: Correlation of BSM emulsion UCS and base layer stiffness – northbound

Figure 10.10 shows the plot of UCS versus BSM foam base layer stiffnesses. A reasonable correlation exists between UCS and base layer stiffness values. As base layer stiffness increases UCS values are seen to also increase. The spread of stiffness values which correlate with a narrow band of UCS values makes the relationship questionable.

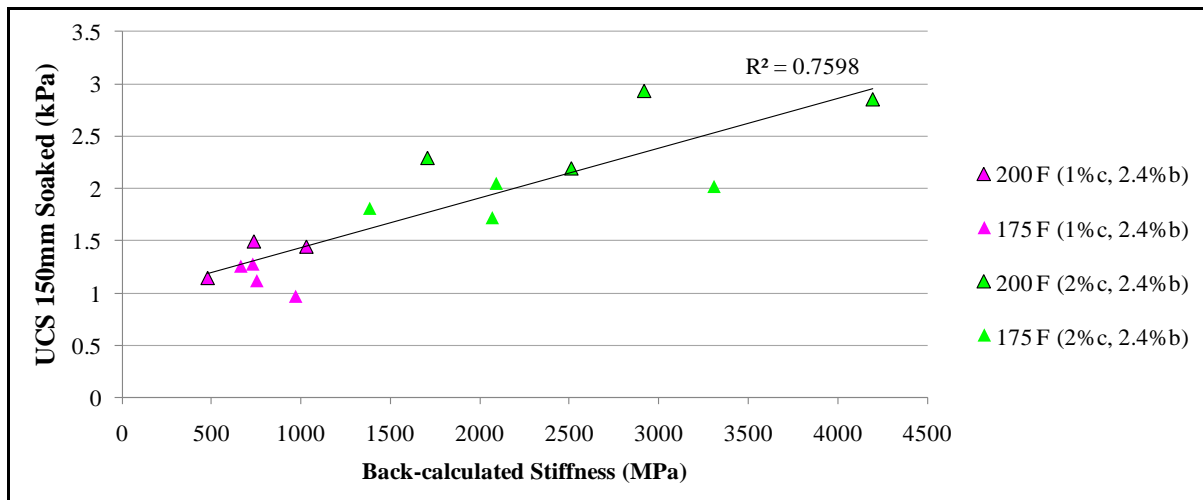


Figure 10.10: Correlation of BSM foam UCS and base layer stiffness – northbound

## 10.2 Conclusions

No clear correlation between engineering tests and back-calculated base layer stiffness was observed consistently along the experimental section. BSM foam layers in the northbound lane showed reasonable correlation of ITS and UCS values with base layer stiffnesses, as indicated by  $R^2$  values of 0.59 and 0.76 for ITS and UCS values respectively. The general impression however is that engineering tests show little correlation with stiffness values determined from the back-calculation of FWD measured deflection bowls.

From the above conclusion the use of engineering tests to solely determine the structural adequacy of a pavement material to be constructed (mix design) or which has been constructed (construction quality control) could be questioned. If the design procedure of a pavement structure uses the stiffness of the pavement layers as a critical design input, a method of measuring the possible layer stiffness provided by the material (mix design) and the actual layer stiffness constructed in the field (construction quality control) is required.

**CHAPTER 11 CONCLUSIONS AND RECOMMENDATIONS**

To conclude this thesis the objectives set out in Chapter 1 are re-visited and reconciled with a summary of the results from analyses and conclusions presented in the preceding chapters. Recommendations are made with respect to acquiring additional information and testing which will support conclusions made in this thesis and further our knowledge on the behaviour of the stabilised pavement materials considered. Figure 11.1 outlines the structure of Chapter 11.

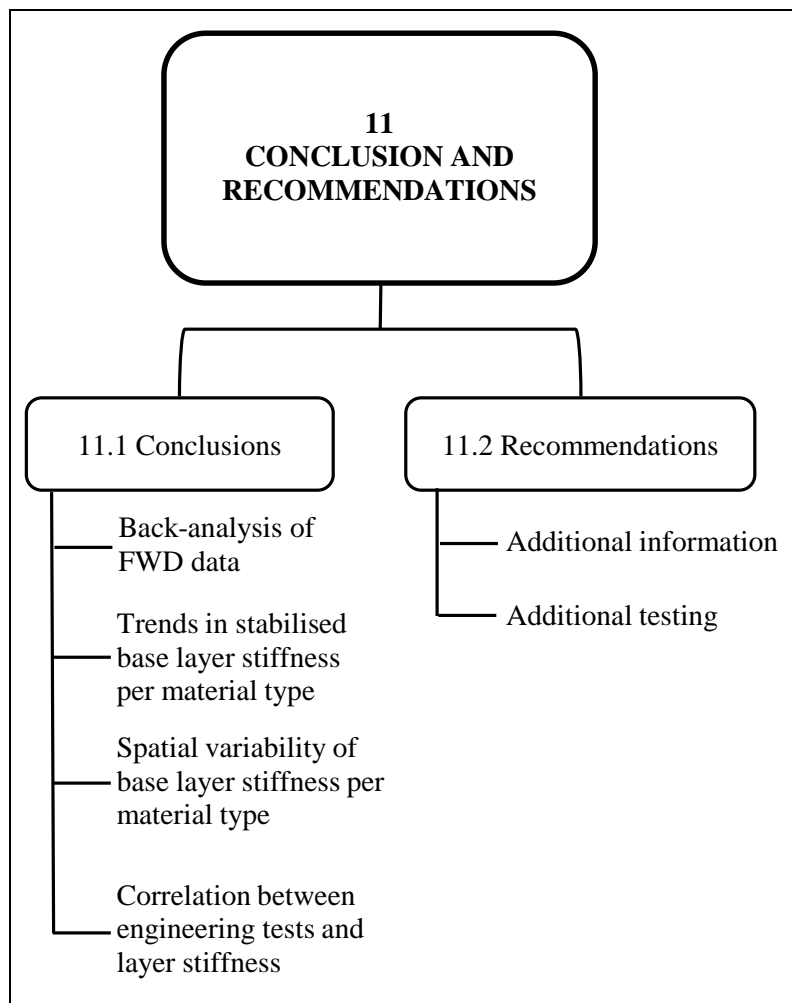


**Figure 11.1: Outline of Chapter 11**

**11.1 Conclusions****11.1.1 Back-analysis of FWD data**

1. A simplified pavement structure is utilised within the back-analysis of FWD deflection data. This allowed for an efficient analysis process by ignoring the complex pavement sub-structure identified by test pits. The effects of this assumption on the back-calculated base layer stiffnesses was negligible with an increase of 6% in base layer stiffness determined between the utilisation of actual and simplified pavement structure models.

2. The effect of back-calculated asphalt layer stiffness variability on back-calculated base layer stiffness was shown to be significant. To remove this inaccuracy in base layer stiffness determination, asphalt layers stiffness was estimated outside of the back-calculation process using experimental data. This asphalt stiffness was then fixed within the back-calculation pavement structure model for the back-analysis of FWD data and the determination of stabilised base layer stiffnesses.
3. The comparison of trends in RoC and back-calculated base layer stiffness over time for each experimental sub-section indicated the reliability of the back-calculation process. A high degree of correlation existed between trends in RoC and base layer stiffness over time for all stabilised material sub-sections.

### 11.1.2 Trends in back-calculated base layer stiffness per sub-section over time

#### 11.1.1.1 *Cement and lime stabilised materials*

1. A significant reduction in base layer stiffness correlated consistently with the effects of bituminous surfacing construction on cement stabilised material sub-sections. It is proposed that the load applied to the pavement structure by asphalt compaction equipment damaged the supporting cement stabilised base layer.
2. Base layer stiffness trend remained relatively flat when traffic loading was applied.
3. No correlation between observed seasonal rainfall and temperature fluctuations and cement stabilise base layer variability was observed.
4. The continuously bound nature of cement stabilised material was indicated by the absence of a correlation between base layer stiffness and seasonal variability in subgrade support stiffness in the southbound lane.
5. A good correlation between theories relating to the stiffness development of cement stabilised materials and the trends observed along the experimental section were made.
6. Cement stabilised pavement layers showed average stiffness values per sub-section between 600 MPa and 1800 MPa over the 360 day observation period. Expected layer stiffness for cement stabilised materials range between 1500 MPa and 2000 MPa according to the SAMDM (Theyse et al, 1996).

*11.1.1.2 BSM pavement layers*

1. BSM emulsion and BSM foam pavement layers showed similar trends in back-calculated layer stiffness over the 360 day observation period.
2. Trends in BSM layer stiffness in the southbound lane showed significant correlation with seasonal rainfall and temperature fluctuation.
3. Trends in BSM layer stiffness in the southbound lane showed significant correlation with seasonal subgrade stiffness variability. This correlation is proposed to be due to the stress dependent character of BSM materials responding to variability in support stiffness.
4. BSM emulsion and foam layers with 1% cement added in the northbound lane show reductions in layer stiffness when moistened due to the direct application of rainfall before bituminous surfacing construction.
5. BSM emulsion and foam layers with 2% cement added in the northbound show a generally continuous increase in layer stiffness over the 360 day observation period.
6. The application of prime on BMS layer was shown to conclusively induce a temporary reduction in BSM layer stiffness. This is proposed to be due to the softening of the bitumen within the layer by the paraffinic cutters within the prime applied.
7. A poor correlation between theories relating to the stiffness development of BSM materials and the trends observed along the experimental section were made. The extent of variability observed along the experimental section was not captured by current theories.
8. BSM emulsion layers with 1% cement added showed average layer stiffness values per subsection between 400 MPa and 1700 MPa over the 360 day observation period. Expected layer stiffness for BSM materials with 1% cement added would be approximately 800 MPa (Ebels, 2008).
9. BSM emulsion layers with 2% cement added showed average layer stiffness values per subsection between 900 MPa and 3900 MPa over the 360 day observation period. Typical stiffness values for BSM materials with 2% cement are not readily available as these BSM materials are not typically constructed.
10. BSM foam layers with 1% cement added showed average layer stiffness values per subsection between 400 MPa and 1100 MPa over the 360 day observation period. Expected layer stiffness for BSM materials with 1% cement added would be approximately 800 MPa (Ebels, 2008).

11. BSM foam layers with 2% cement added showed average layer stiffness values per sub-section between 900 MPa and 4300 MPa over the 360 day observation period. Typical stiffness values for BSM materials with 2% cement are not readily available as these BSM materials are not typically constructed.

#### 11.1.2 Spatial variability in back-calculated base layer stiffness

1. Significant spatial variability of stabilised base layer back-calculated stiffness was observed along all experimental sub-sections. CoVs of up to 40% were determined for many sub-sections at a point in time.
2. The variability in stabilised base layer stiffness observed was not random about a mean value nor conforming to a normal distribution. The base layer stiffness variability observed was spatial and is dependent upon a stabilised material property which has yet to be determined.
3. Incorporating the observed base layer stiffness variability within a pavement design scenario with a requirement for a 90<sup>th</sup> percentile design reliability would produce a pavement design in which half of the projects length is over designed by a factor of 4. The levels of pavement layer stiffness and subsequent bearing capacity variability provide for unpredictable and uneconomical pavement designs.

#### 11.1.3 Correlation between back-calculated base layer stiffness and engineering test results

1. No clear correlation between back-calculated base layer stiffness and engineering test results was observed along the experimental section. BSM foam materials in the northbound lane showed reasonable  $R^2$  values of 0.59 and 0.76 for ITS Dry and UCS soaked test results on 150 mm diameter samples cured for 28 days.

## 11.2 Recommendations

A number of recommendations are made with respect to additional materials testing which would assist in further substantiating the analyses and conclusions made in this study.

### 11.2.1 Stabilised base layer moisture content and temperature measurement

The continuous measurement of temperature and moisture within the pavement structure layers at a number of locations along each sub-section would assist in clarifying and adding weight to the primary claim of this study that seasonal moisture and temperature variability and subsequent subgrade stiffness variability are affecting the observed stabilised base layer stiffness.

These material properties could be determined by the installation of Time Domain Reflectometry (TDR) sensors within the granular and stabilised material. These sensor collected data continuously and data can be extracted by an external cable connection to a laptop.

### 11.2.2 Stabiliser content determination

Another observation of this study is that the variability in back-calculated stiffness is possibly due to variability in stabilisation along the length of a sub-section. It would therefore be useful to have either an accurate pre-determination or post-determination of the stabiliser content and distribution within each sub-section.

Pre-stabiliser content determination would involve sampling and quantifying the spread of cement at a number of points along a sub-section before CIPR took place. The bitumen content input to the pavement during CIPR would have to be monitored, recorded and measurements spatially located.

Post-stabiliser content determination would involve back-titration to estimate cement contents within the stabilised materials and bitumen extraction utilising solvents such as toluene to estimate residual bitumen contents. The post determination methods are difficult to perform and not recommended. Bitumen extractions were attempted on a number of sub-sections; however the results were voided due to the presence of bitumen from recycled existing bituminous surfacings in addition to the bitumen added for stabilisation. The bitumen content results were hence much greater than anticipated and disregarded.

### 11.2.3 Pavement layer thickness determination

The addition of accurate pavement layer thicknesses to the back-analysis process would increase the accuracy of the pavement layer stiffness values determined. The most accurate method to determine pavement layer thicknesses would be to dig test-pits and measure the pavement structure first hand. However due to the destructive nature of test pitting, Ground Penetrating Radar (GPR) could be used, with proofing by selective test pitting. The used of GPR to determine consecutive granular layer thicknesses can be challenging if the dielectric constant of consecutive layers of pavement material do not vary significantly.



## BIBLIOGRAPHY

- Anochie-Boateng, J., O'Connell, J., Denneman, E., & Verhaeghe, B. (2011). Resilient Response Characterisation of Hot-mix Asphalt Mixes for a New South African Pavement Design Method. *10th Conference on Asphalt Pavements*. South Africa.
- Asphalt Academy. (2009). *Technical Guidance: Bitumen Stabilised Materials TG 2*. Pretoria.
- AusStab. (2012). *Technical Note No.5 Cement Stabilisation Practice*. Pavement Recycling and Stabilisation Association.
- CSRA. (1985). *TRH 14 - Guidelines for Road Construction Materials*. Pretoria: South Africa.
- Ebels, L. J. (2008). *Characterisation of Material Properties and Behaviour of Cold Bituminous Mixtures for Road Pavements*. PhD Dissertation, University of Stellenbosch, Stellenbosch.
- Emery, S. J. (1988). *The Prediction of Moisture Content in Untreated Pavement Layers and an Application to Design in Southern Africa*. Pretoria: CSIR.
- Jenkins, K. J. (2000). *Mix Design Considerations for Cold and Half-Warm Bituminous Mixes with Emphasis on Foamed Bitumen*. PhD Dissertation, University of Stellenbosch, Stellenbosch.
- Jooste, F., & Long, F. (2007). *Summary of LTPP Emulsion and Foamed Bitumen Treated Sections*. Pretoria: CSIR.
- Jordaan, J. (2011). Behaviour of an emulsion treated base (ETB) layer as determined from Heavy Vehicle Simulator (HVS) testing. *Conference on Asphalt Pavements for South Africa CAPSA 2011*. Kwa-zulu Natal, South Africa.
- Kannemeyer, L. (2013). personal communication.
- Leyland, R. C., & Paige-Green, P. (2013). *Investigation into use of intelligent compaction as a possible quality control tool and general compaction process aid*. Pretoria: SANRAL.
- Liebenberg, J. J. (2003). *A Structural Design Procedure for Emulsion Treated Pavement Materials*. MEng Thesis, University of Pretoria, Pretoria, South Africa.
- Loizos, A., & Papavasiliou, V. (2007). Evaluation of Foamed Asphalt Cold In-place Pavement Recycling using Non-destructive Techniques. *International Conference of Pavement and Soil Materials ICACPSEM*. Athens, Greece.
- Long, F. M., Thesye, H. L., & Ventura, D. F. (2004). *Characterisation of Foamed Bitumen Treated Materials from HVS Test Sections*. Pretoria: CSIR.

- Loulizi, A., Flintsch, G., Al-Qadi, I., & Mokarem, D. (2006). Comparing Resilient Modulus and Dynamic Modulus of Hot-Mix Asphalt as Material Properties for Flexible Pavement Design. *Journal of the Transportation Research Board*, 161-170.
- Lukanen, E. O., Stubstad, R. N., & Briggs, R. C. (1998). *Research Report FHWA-RD-98-085 - Temperature Predictions and Adjustment Factors for Asphalt Pavements*. McLean, VA: Federal Highway Administration.
- Maina, J. W., & Matsui, K. (2004). Developing Software for Elastic Analysis of Pavement Structure Responses to Vertical and Horizontal Loadings. *Transportation Research Records*, No. 1896, (pp. 107 - 118).
- Maina, J. W., Denneman, E., & De Beer, M. (2008). Introduction of new road pavement response modelling software by means of benchmarking. *27th Annual South African Transport Conference*. Pretoria.
- Modelling and Analysis Systems CC. (2005). *Automated Back-calculation Tutorial*. Cullinan: MAS.
- Oh, J., Fernando, E., & Lee, S. H. (March 2012). Correlation of Asphalt Concrete Layer Moduli Determined from Laboratory and Non-Destructive Field Tests. *Journal of Transportation Engineering*, Vol. 138, No. 3 : pp. 361-370.
- Role of Portland Cement in Concrete*. (2013). Retrieved 08 15, 2013, from Portland Cement Association: <http://www.cement.org/>
- Romanoschi. (2003). [www.ctre.iastate.edu/pubs/midcon2003/RomanoschiFoamed.pdf](http://www.ctre.iastate.edu/pubs/midcon2003/RomanoschiFoamed.pdf). Retrieved 08 05, 2013
- Theyse, H. L. (2013). *Design of experimental sections - R35 Bethal, km 5.5 to 10.0*. Pretoria: South African National Roads Agency.
- Theyse, H. L. (2004). *First level Analysis Report: HVS Testing of the foamed-bitumen-treated crushed stone base on the slow lane of the southbound carriageway of the N7 near Cape Town*. Pretoria: CSIR.
- Theyse, H. L., de Beer, M., & Rust, F. C. (1996). *Overview of the South African Mechanistic Pavement Design Method*. Washington D.C.: Transportation Research Board.
- van Niekerk, A. A. (2002). *Mechanical Behaviour and Performance of Granular Bases and Sub-bases in Pavements*. PhD Thesis, Delft University of Technology, Delft, Netherlands.

Weinert, H. (1984). Climate and the Durability of South African Road Aggregates. *Bulletin of the International Journal of Geology* , 463-466.

**ADDENDUM A**  
**FWD Testing Days**

<b>Northbound</b>		
<b>Sub-Section</b>	<b>Day</b>	<b>Date</b>
200 mm C3-1 (2% c, 1% l)	-1	05 August 2012
	0	06 August 2012
	1	07 August 2012
	2	08 August 2012
	3	09 August 2012
	4	10 August 2012
	7	13 August 2012
	14	20 August 2012
	28	03 September 2012
	88	02 November 2012
	190	12 February 2013
200 mm Emulsion (0.9% b, 1% c)	-1	12 August 2012
	0	13 August 2012
	1	14 August 2012
	3	16 August 2012
	7	20 August 2012
	14	27 August 2012
	28	10 September 2012
	81	02 November 2012
	183	12 February 2013
175 mm Emulsion (1% c, 2.4% b)	-1	13 August 2012
	0	14 August 2012
	1	15 August 2012
	3	17 August 2012
	7	21 August 2012
	14	28 August 2012
	28	11 September 2012
	80	02 November 2012
	182	12 February 2013
200 mm Emulsion (1% c, 2.4% b)	-1	15 August 2012
	0	16 August 2012
	0	16 August 2012
	1	17 August 2012
	4	20 August 2012
	7	23 August 2012
	14	30 August 2012
	28	13 September 2012
	78	02 November 2012
	180	12 February 2013
175 mm Emulsion (2% c, 2.4% b)	-1	20 August 2012
	0	21 August 2012
	1	22 August 2012
	2	23 August 2012
	3	24 August 2012

<b>Northbound</b>		
<b>Sub-Section</b>	<b>Day</b>	<b>Date</b>
175 mm Emulsion (2%c, 2.4%b)	14	04 September 2012
	28	18 September 2012
	74	03 November 2012
	175	12 February 2013
200 mm Emulsion (2%c, 2.4%b)	-1	21 August 2012
	0	22 August 2012
	1	23 August 2012
	2	24 August 2012
	7	29 August 2012
	14	05 September 2012
	28	19 September 2012
	73	03 November 2012
	174	12 February 2013
175 mm Foam (1%c, 2.4%b)	-1	14 August 2012
	0	15 August 2012
	1	16 August 2012
	2	17 August 2012
	7	22 August 2012
	14	29 August 2012
	28	12 September 2012
	80	03 November 2012
	181	12 February 2013
200 mm Foam (1%c, 2.4%b)	-1	22 August 2012
	0	23 August 2012
	1	24 August 2012
	4	27 August 2012
	5	28 August 2012
	7	30 August 2012
	14	06 September 2012
	28	20 September 2012
	72	03 November 2012
	173	12 February 2013
175 mm Foam (2%c, 2.4%b)	-1	27 August 2012
	0	28 August 2012
	1	29 August 2012
	3	31 August 2012
	7	04 September 2012
	14	11 September 2012
	29	26 September 2012
	78	14 November 2012
	168	12 February 2013
200 mm Foam (2%c, 2.4%b)	0	31 August 2012
	3	03 September 2012

<b>Northbound</b>		
<b>Sub-Section</b>	<b>Day</b>	<b>Date</b>
200 mm Foam (2%c, 2.4%b)	19	19 September 2012
	27	27 September 2012
	63	02 November 2012
	169	16 February 2013

<b>Southbound</b>			
<b>Sub-Section</b>	<b>Day</b>	<b>Date</b>	
200 mm C3-1 (2% c, 1% l)	0	17 April 2012	
	1	18 April 2012	
	2	19 April 2012	
	3	20 April 2012	
	6	23 April 2012	
	7	24 April 2012	
	15	02 May 2012	
	28	15 May 2012	
	93	19 July 2012	
	208	11 November 2012	
	365	17 April 2013	
200 mm C3-2 (2% c, 1% l)	3	23 April 2012	
	4	24 April 2012	
	5	25 April 2012	
	6	26 April 2012	
	14	04 May 2012	
	28	18 May 2012	
	90	19 July 2012	
	205	11 November 2012	
		362	17 April 2013
	175 mm Emulsion (1%c, 2.4%b)	2	20 April 2012
7		25 April 2012	
14		02 May 2012	
28		16 May 2012	
92		19 July 2012	
207		11 November 2012	
		364	17 April 2013
200 mm Emulsion (1%c, 2.4%b)		1	20 April 2012
	4	23 April 2012	
	7	26 April 2012	
	14	03 May 2012	
	28	17 May 2012	
	91	19 July 2012	
	206	11 November 2012	
		363	17 April 2013
175 mm Emulsion (2%c, 2.4%b)	1	25 April 2012	
	2	26 April 2012	
	8	02 May 2012	
	14	08 May 2012	
	90	23 July 2012	
	201	11 November 2012	
		357	16 April 2013
	200 mm Emulsion (2%c, 2.4%b)	0	07 May 2012
1		08 May 2012	



<b>Southbound</b>		
<b>Sub-Section</b>	<b>Day</b>	<b>Date</b>
200 mm Emulsion (2% <i>c</i> , 2.4% <i>b</i> )	8	15 May 2012
	16	23 May 2012
	23	30 May 2012
	73	19 July 2012
	188	11 November 2012
	344	16 April 2013
175 mm Foam (1% <i>c</i> , 2.4% <i>b</i> )	1	03 May 2012
	2	04 May 2012
	7	09 May 2012
	14	16 May 2012
	28	30 May 2012
	79	20 July 2012
	193	11 November 2012
	349	16 April 2013
200 mm Foam (1% <i>c</i> , 2.4% <i>b</i> )	1	04 May 2012
	4	07 May 2012
	14	17 May 2012
	27	30 May 2012
	78	20 July 2012
	192	11 November 2012
	348	16 April 2013
175 mm Foam (2% <i>c</i> , 2.4% <i>b</i> )	0	04 May 2012
	3	07 May 2012
	14	18 May 2012
	26	30 May 2012
	77	20 July 2012
	194	14 November 2012
	347	16 April 2013
200 mm Foam (2% <i>c</i> , 2.4% <i>b</i> )	2	07 May 2012
	10	15 May 2012
	13	18 May 2012
	25	30 May 2012
	76	20 July 2012
	190	11 November 2012
	346	16 April 2013

## **ADDENDUM B**

### **R35 Experimental Section Layout**

**R35 Experimental Section Pavement Design and Layout**

**Southbound Lane**

Layer design properties	km 5.5	45 mm Asphalt	km 5.833	km 6.166	km 6.5	km 6.85	km 7.2	km 7.55	km 7.9	km 8.25	km 8.6	km 8.95	km 9.3	km 9.65	km 10
		G1 (1)	G1 (2)	Cape Seal	G1 (3)	200 mm C3-1 subbase	200 mm C3-2 subbase	200 mm C3-2 base	175 mm BSM Emulsion	200 mm BSM Emulsion	175 mm BSM Emulsion	200 mm BSM Emulsion	175 mm BSM Foam	200 mm BSM Foam	200 mm BSM Foam
	% by mass content	2	2	2	2	2	2	2	1	2	2	1	1	2	2
		1	1	1	1	1	1	1	0	0	0	0	0	0	0
Residual Bitumen	0	0	0	0	0	0	2.4	2.4	2.4	2.4	2.4	2.4	2.4	2.4	2.4

**Northbound Lane**

Layer design properties	km 5.5	45 mm Asphalt	km 5.925	km 6.5	km 6.85	km 7.2	km 7.55	km 7.9	km 8.25	km 8.6	km 8.95	km 9.3	km 9.65	km 10
		G1 (1)	G1 (2)	Cape Seal	200 mm C3-1 subbase	200 mm C3-2 subbase	200 mm C3-1 base	175 mm BSM Emulsion	200 mm BSM Emulsion	175 mm BSM Emulsion	200 mm BSM Emulsion	175 mm BSM Foam	200 mm BSM Foam	200 mm BSM Foam
	% by mass content	2	2	2	2	2	2	1	2	2	1	1	2	2
		1	1	1	1	1	1	0	0	0	0	0	0	0
Residual Bitumen	0	0	0	0	0	0.9	2.4	2.4	2.4	2.4	2.4	2.4	2.4	2.4

Surfacing Extents			
Asphalt		Cape Seal	
Start (km)	End (km)	Start (km)	End (km)
5.5	6.166	6.166	6.68
6.68	7.03	7.03	7.38
7.38	7.73	7.73	8.08
8.08	8.43	8.43	8.78
8.78	9.13	9.13	9.48
9.48	9.83	9.83	10

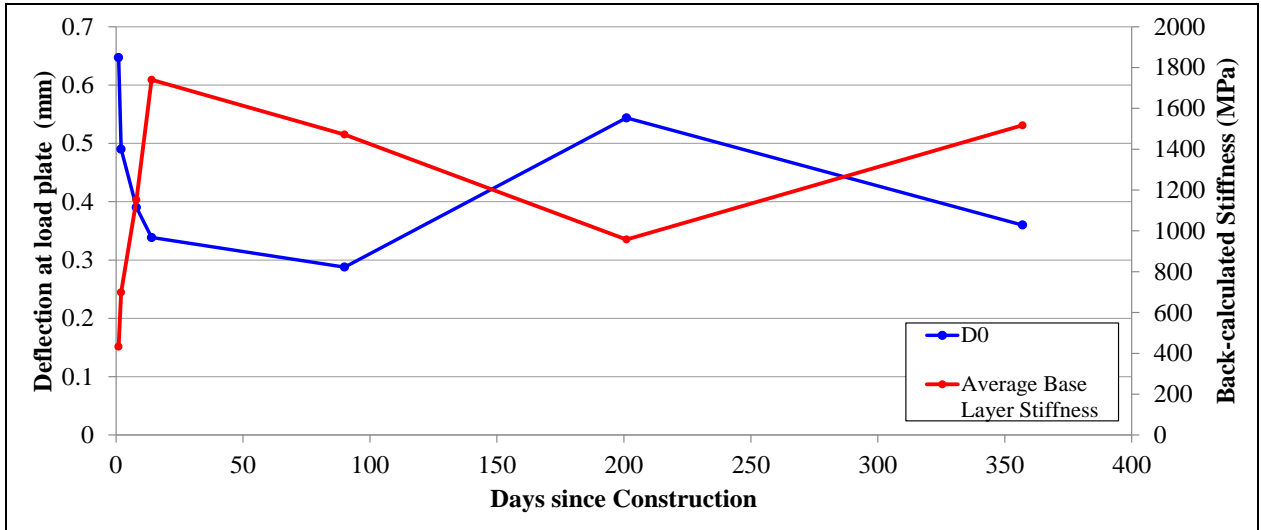
## **ADDENDUM C**

### **FWD Deflection Bowl Parameter Example**

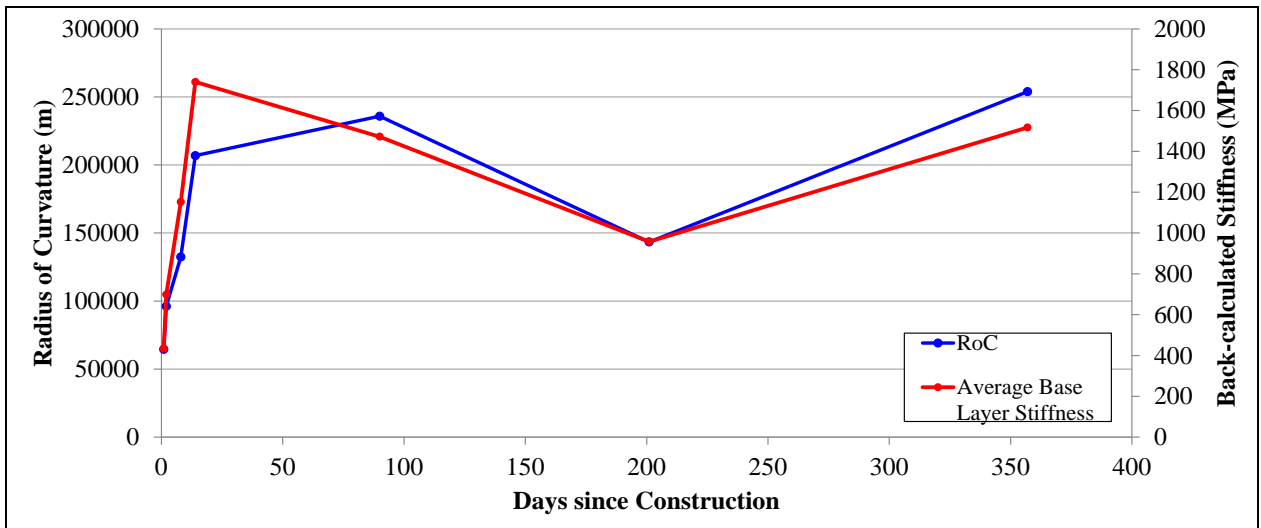
#### **Sub-section**

**175 mm BSM EMULSION (2.4% Residual Bitumen 1% cement)**

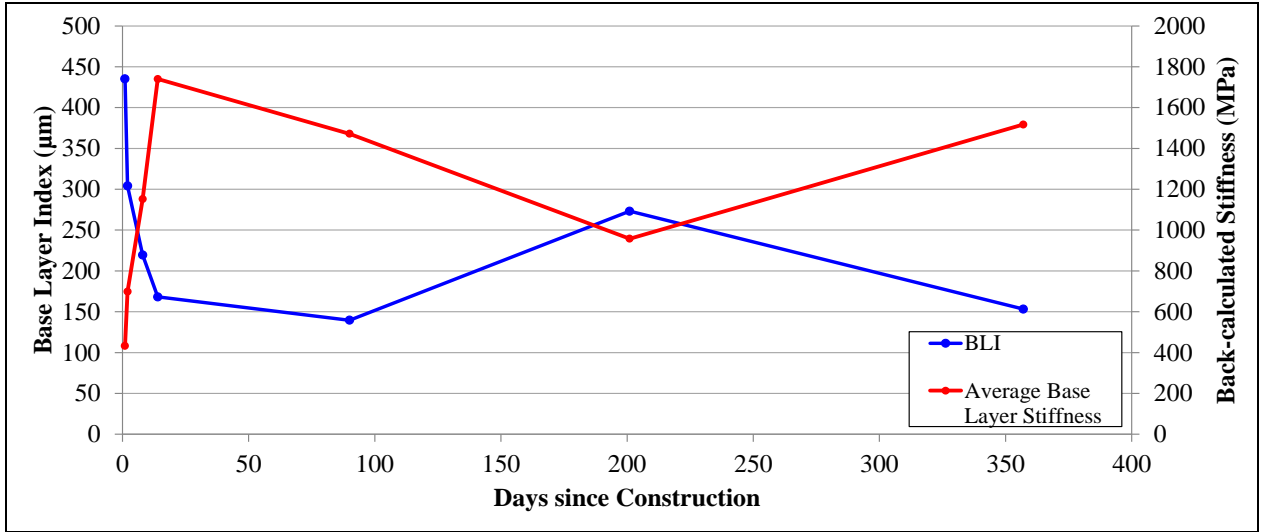
**Deflection at Load Plate**



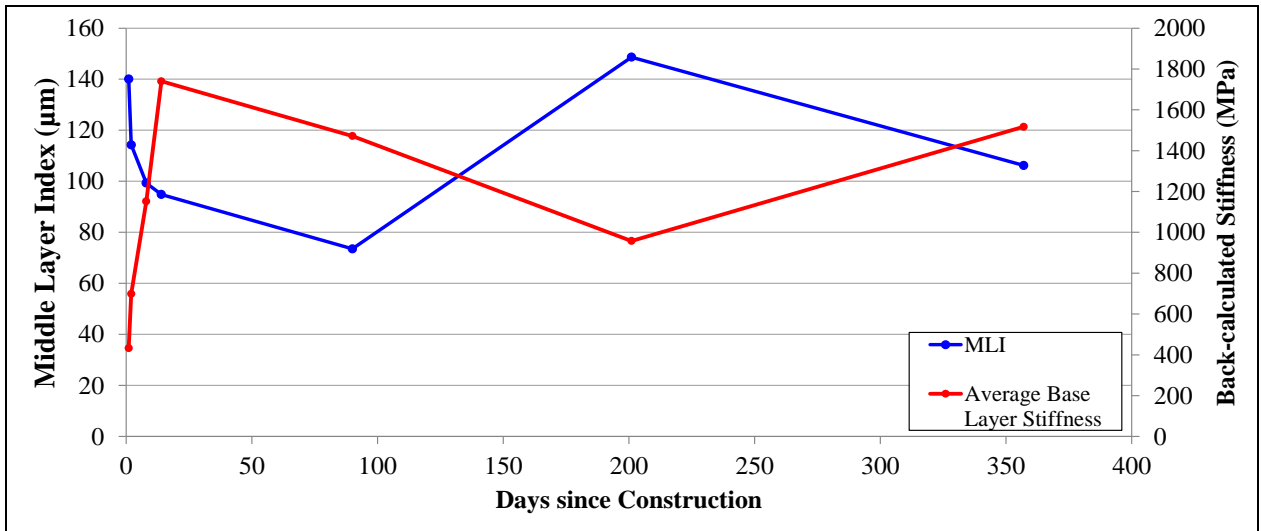
**Radius of Curvature**



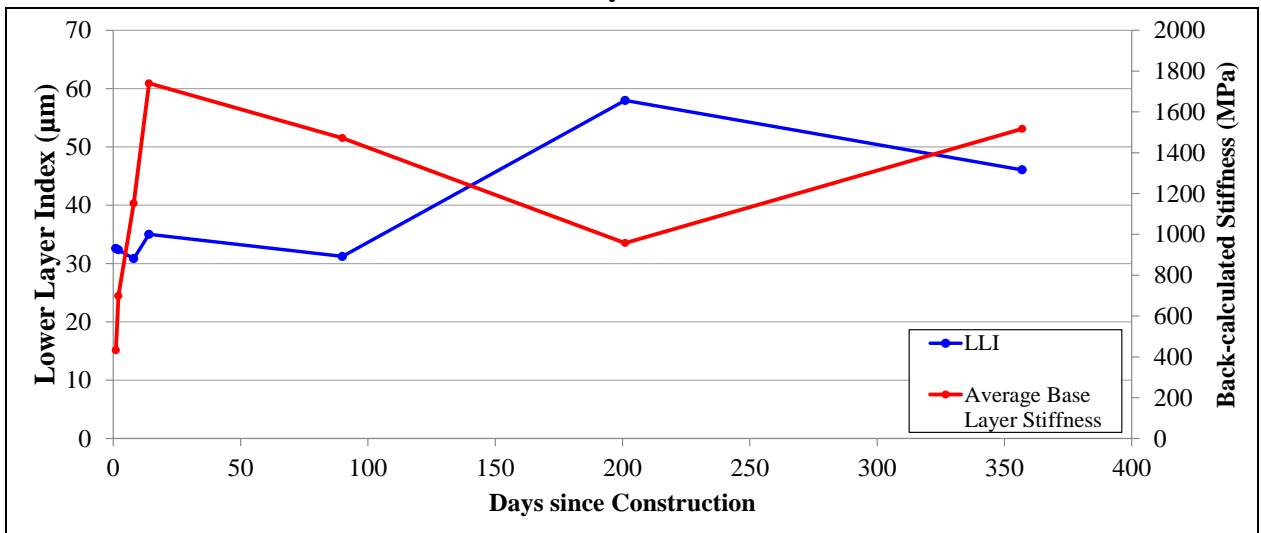
**Base Layer Index**



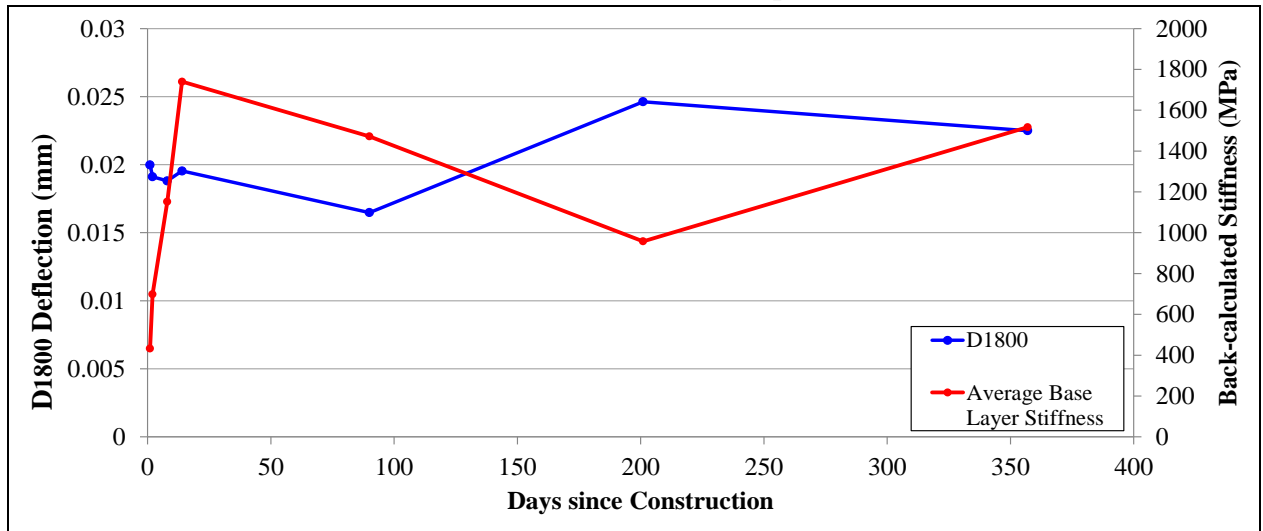
**Middle Layer Index**



**Lower Layer Index**



**Deflection at Far (1800mm) Geophone**



## **ADDENDUM D**

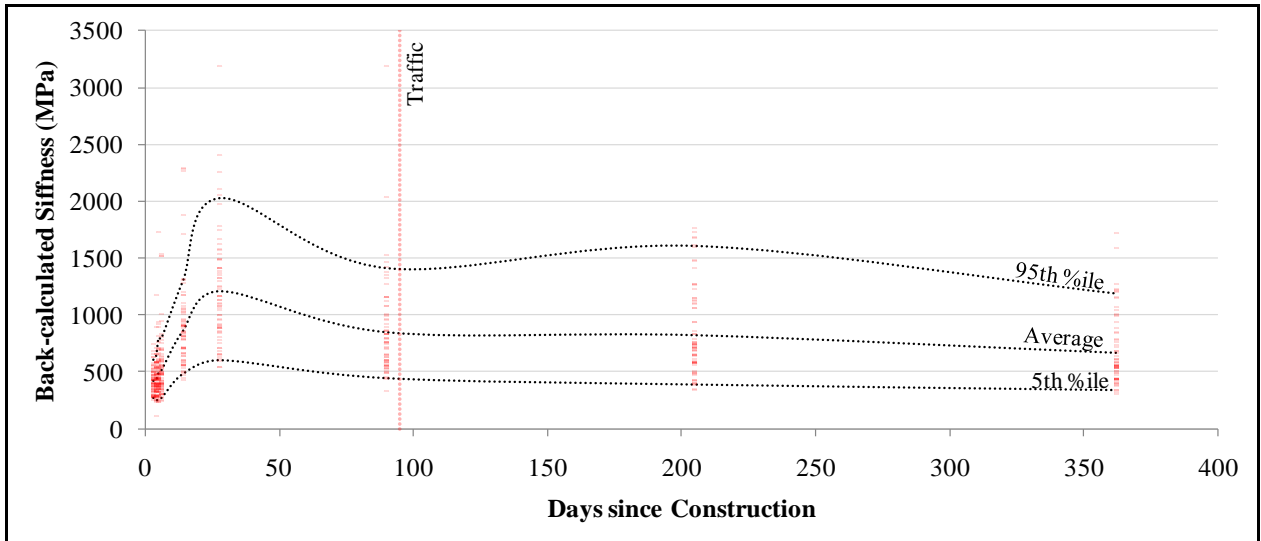
# **Complete Back-calculated Base Layer Stiffness Trend Plots**



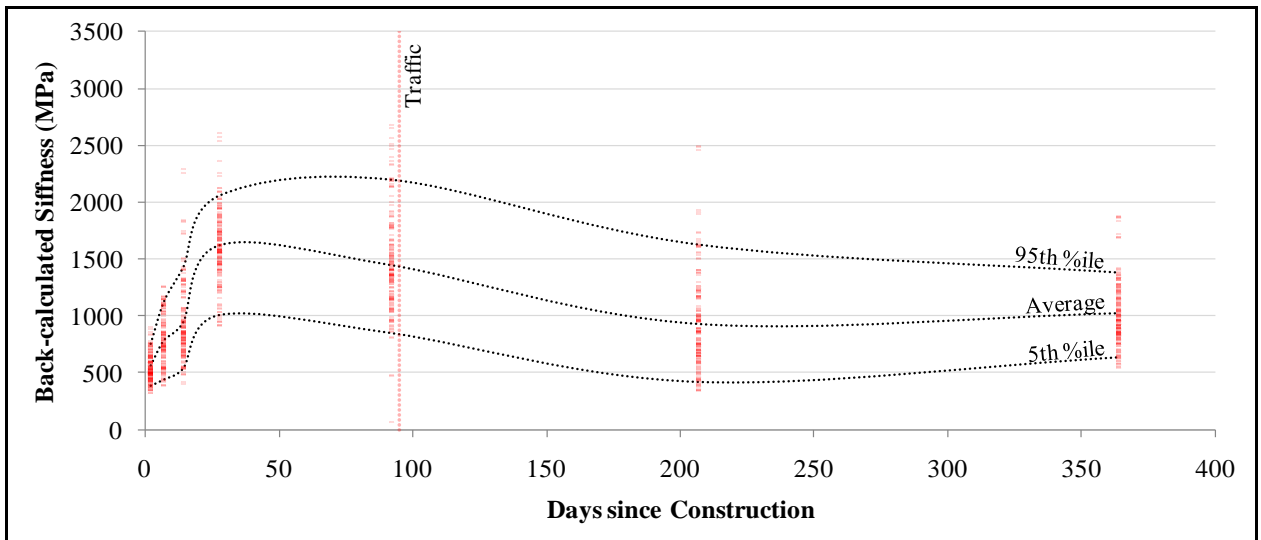
## SOUTHBOUND

### BACK-CALCULATED BASE LAYER STIFFNESS TRENDS

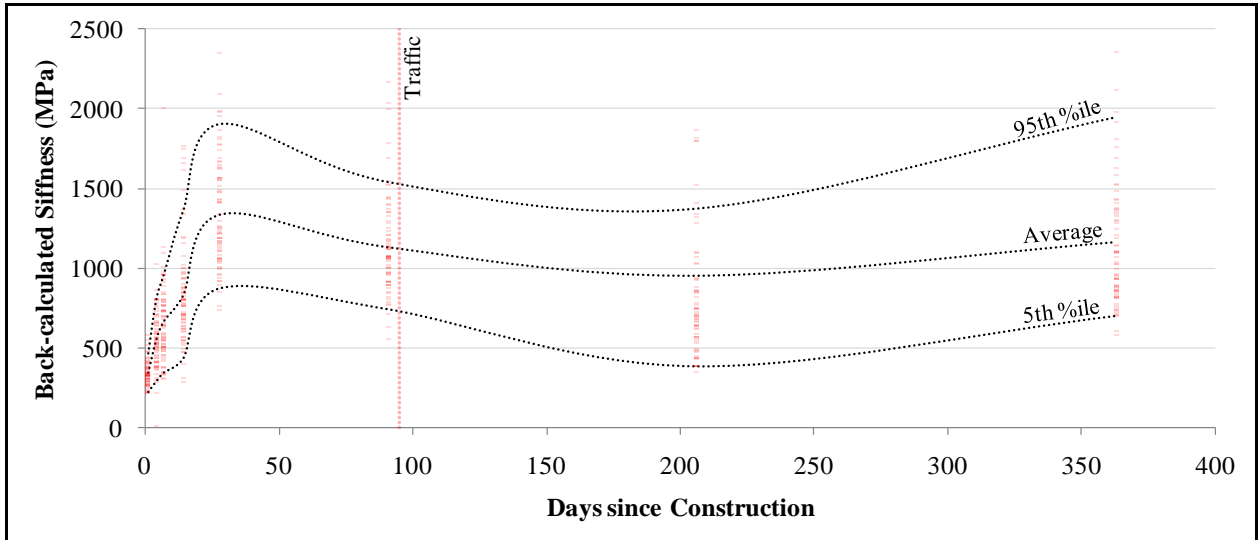
#### 200 mm C3-1 km 6.5 to km 6.85



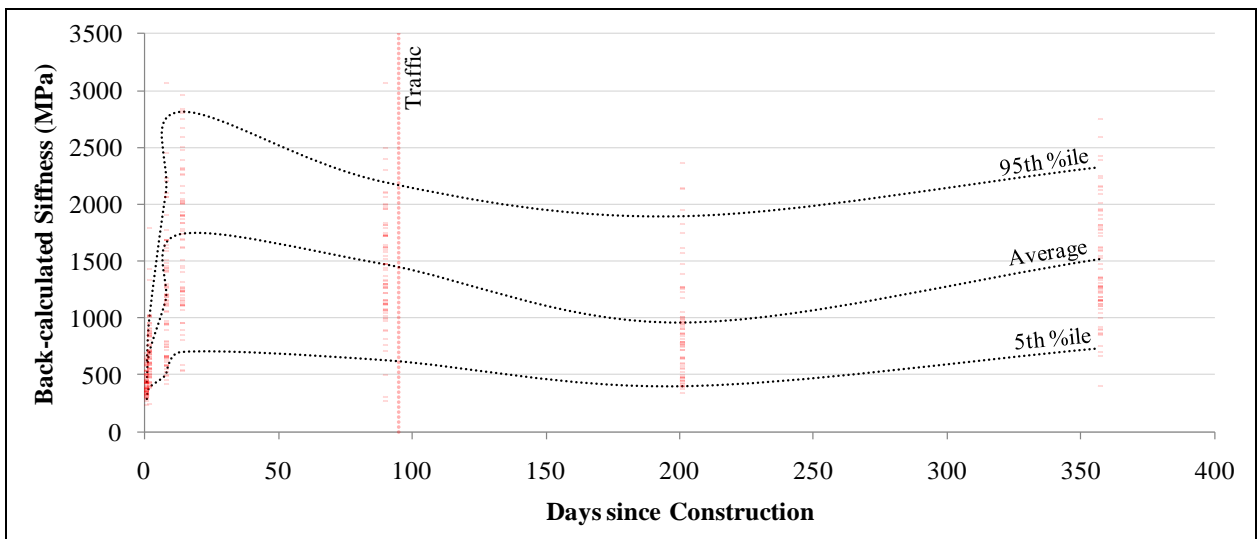
#### 200 mm C3-2 km 6.85 to km 7.2



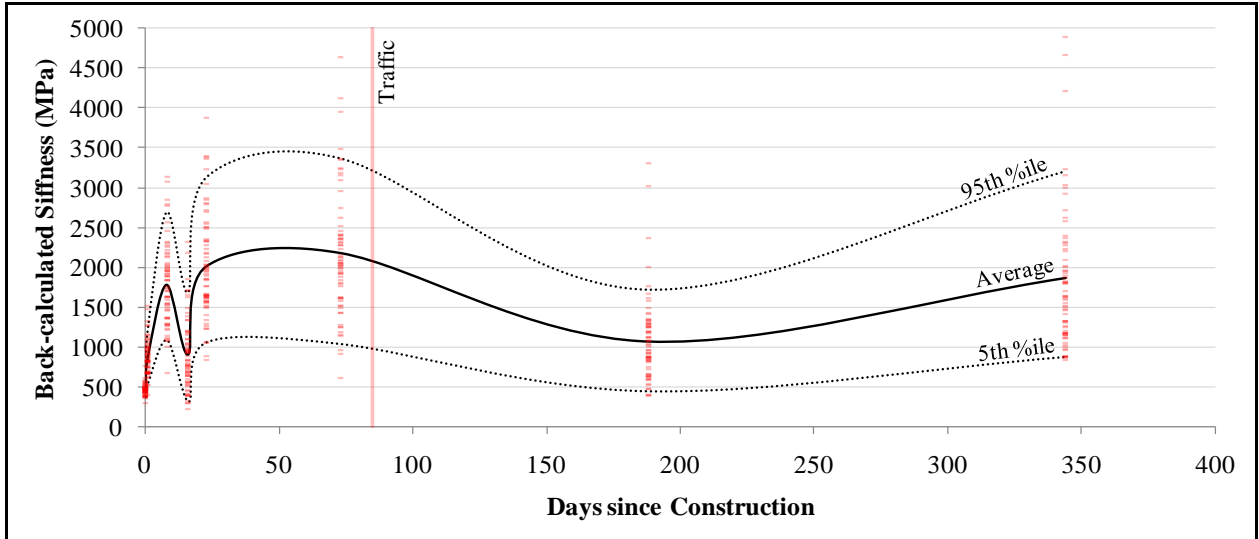
**175 mm Bitumen Emulsion (2.4%b, 1%c) km 7.2 to km 7.55**



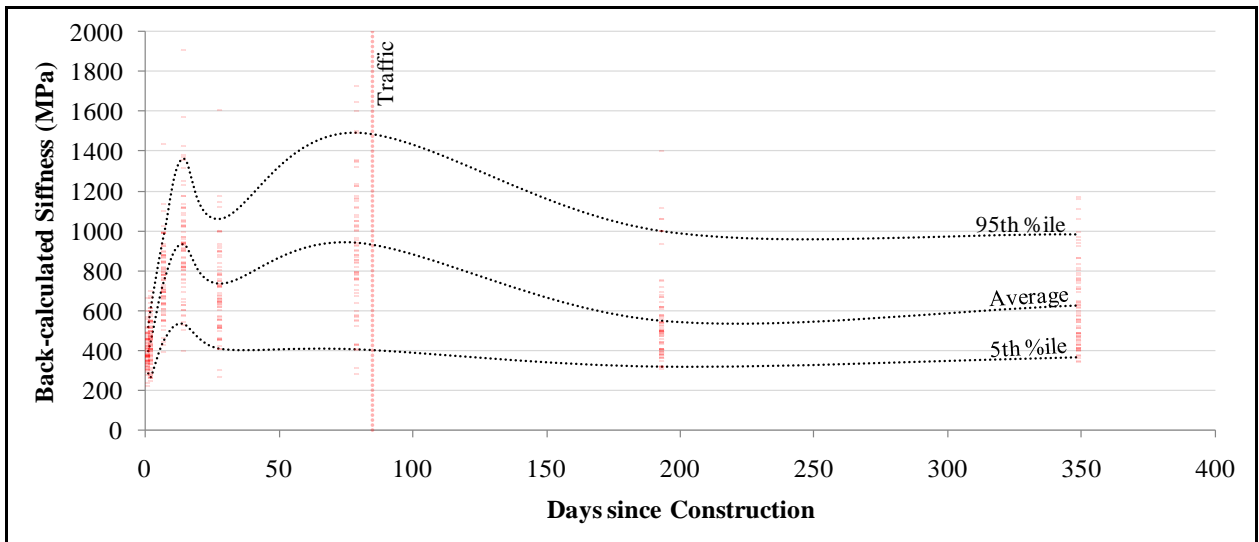
**200 mm Bitumen Emulsion (2.4%b, 1%c) km 7.55 to km 7.9**



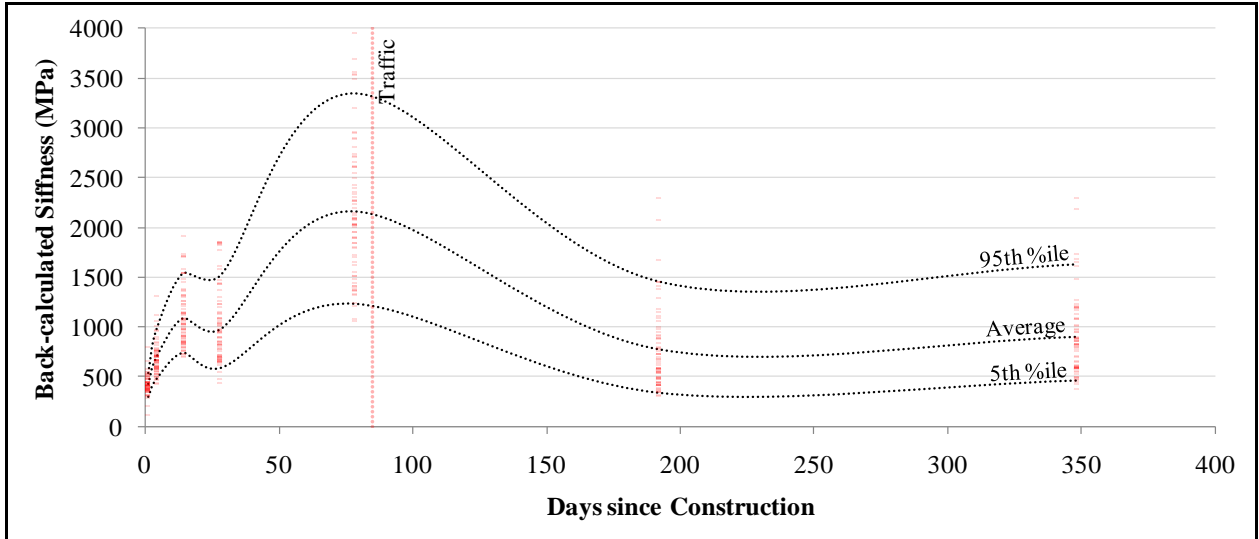
**175 mm Bitumen Emulsion (2.4%b, 2%c) km 7.9 to km 8.25**



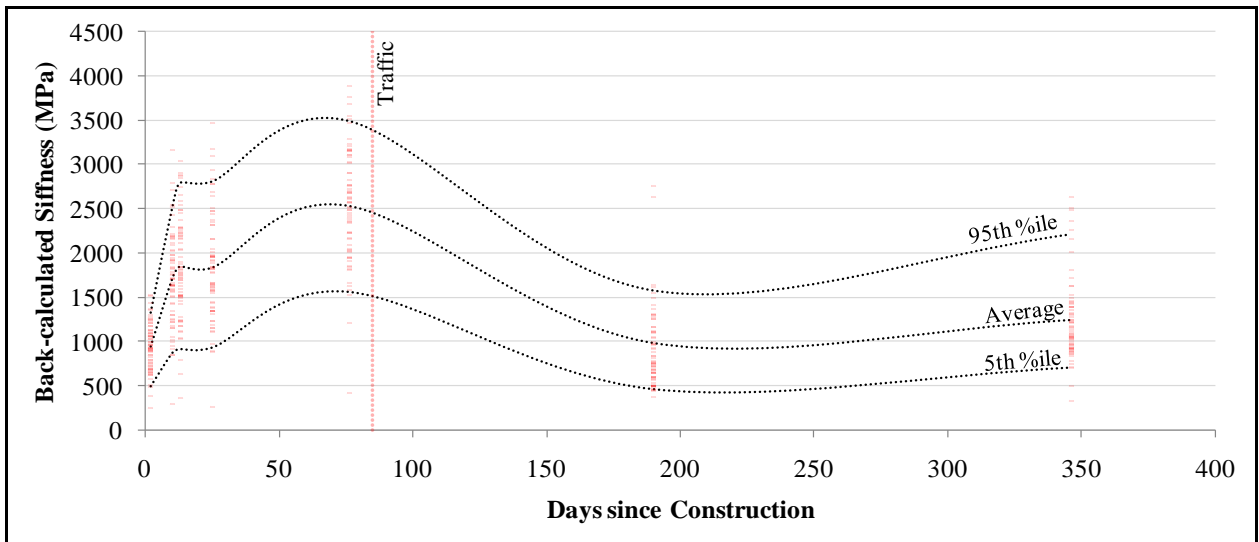
**200 mm Bitumen Emulsion (2.4%b, 2%c) km 8.25 to km 8.6**



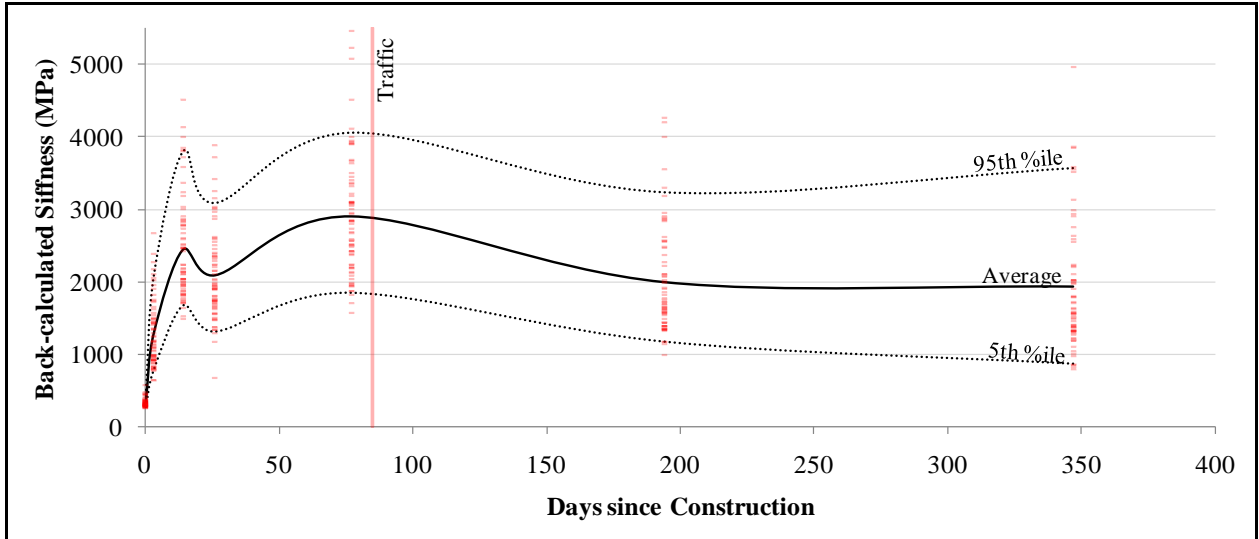
**175 mm Foamed Bitumen (2.4%b, 1%c) km 8.6 to km 8.95**



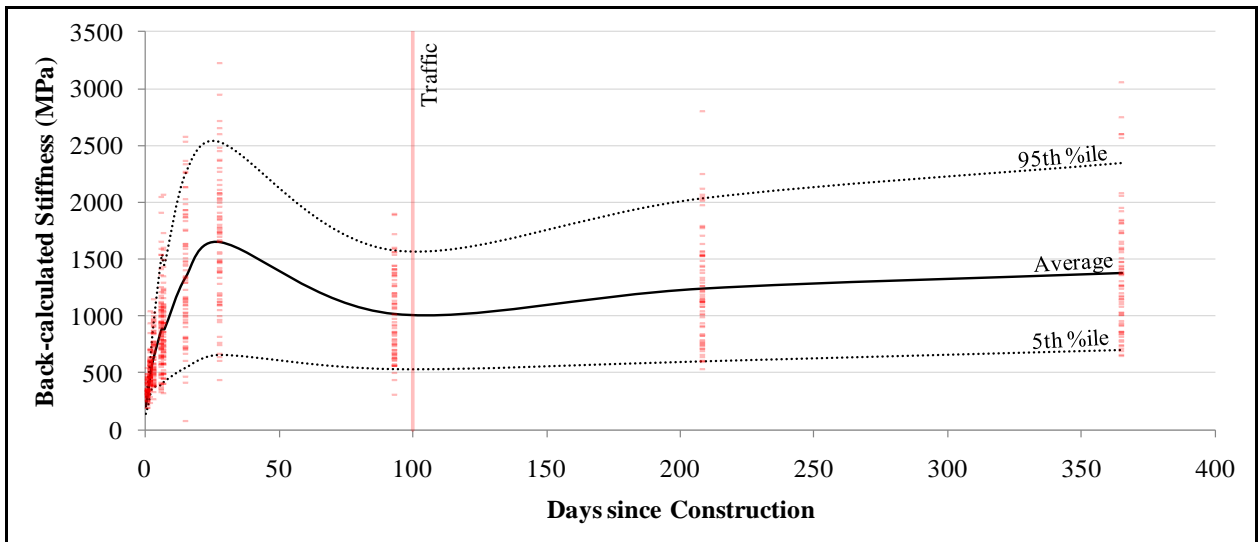
**200 mm Foamed Bitumen (2.4%b, 1%c) km 8.95 to km 9.3**



**175 mm Foamed Bitumen (2.4%b, 2%c) km 9.3 to km 9.65**



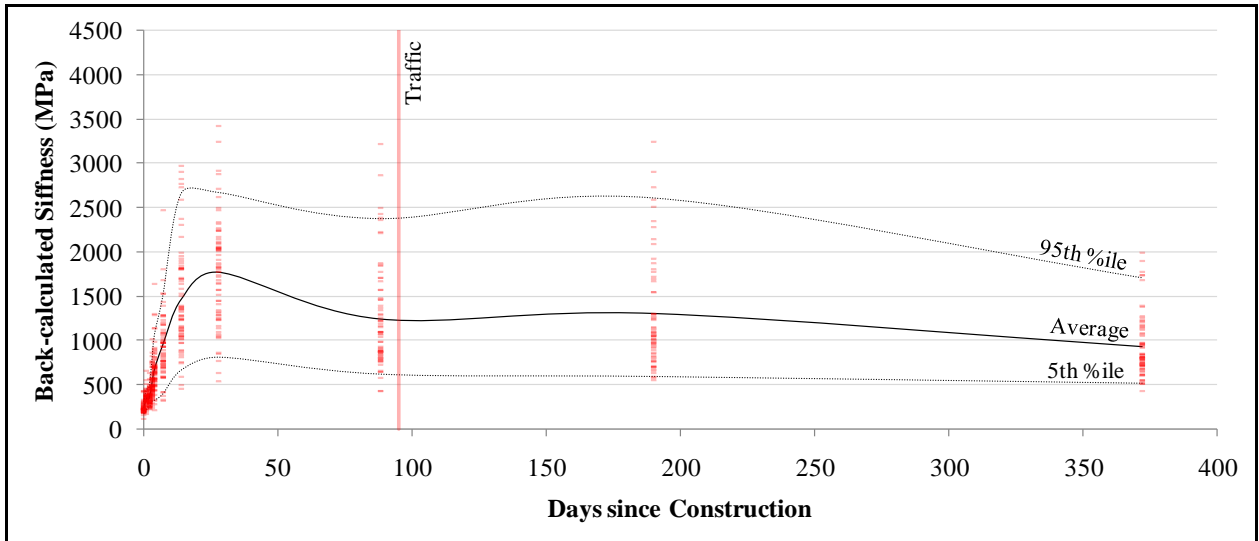
**200 mm Foamed Bitumen (2.4%b, 2%c) km 9.65 to km 10**



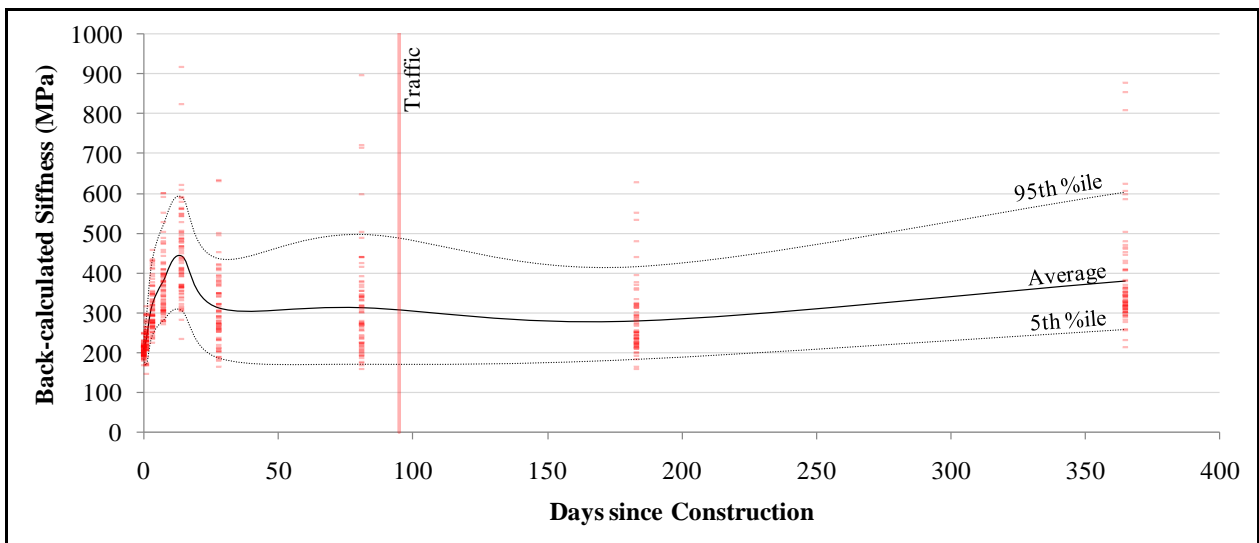
## NORTHBOUND

### BACK-CALCULATED BASE LAYER STIFFNESS TRENDS

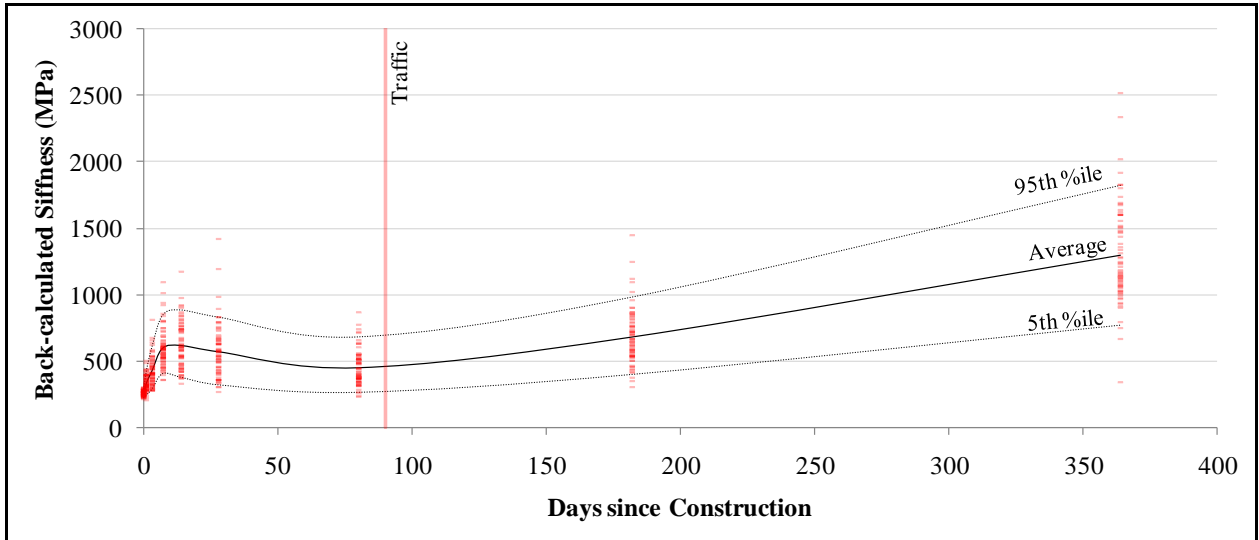
#### 200 mm C3-1 km 6.5 to km 6.85



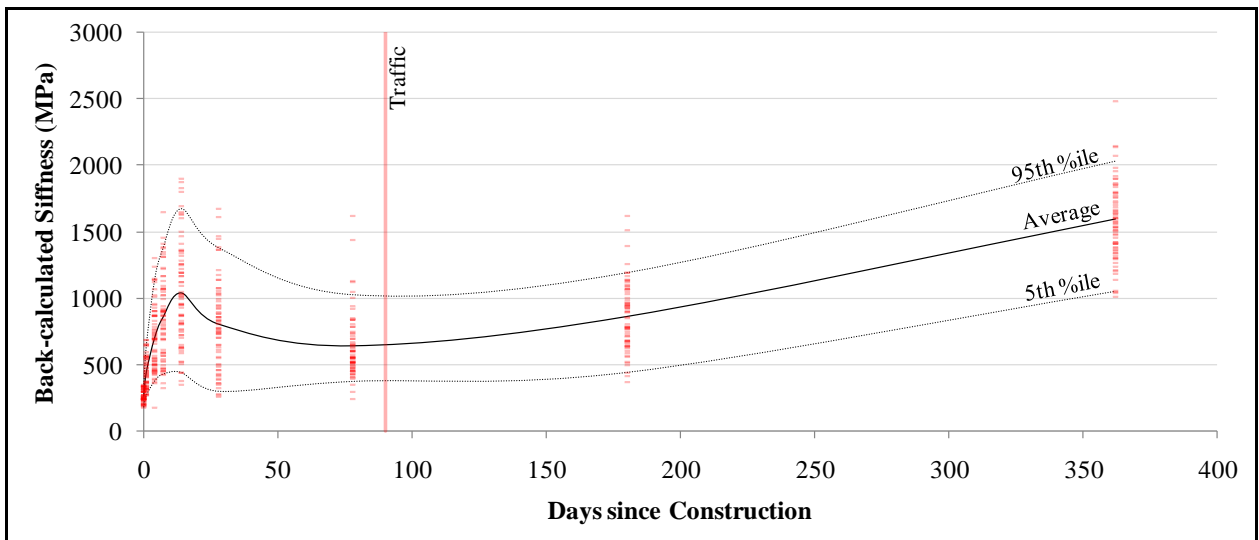
#### 200 mm Bitumen Emulsion (0.9%b, 1%c) km 6.85 to km 7.2



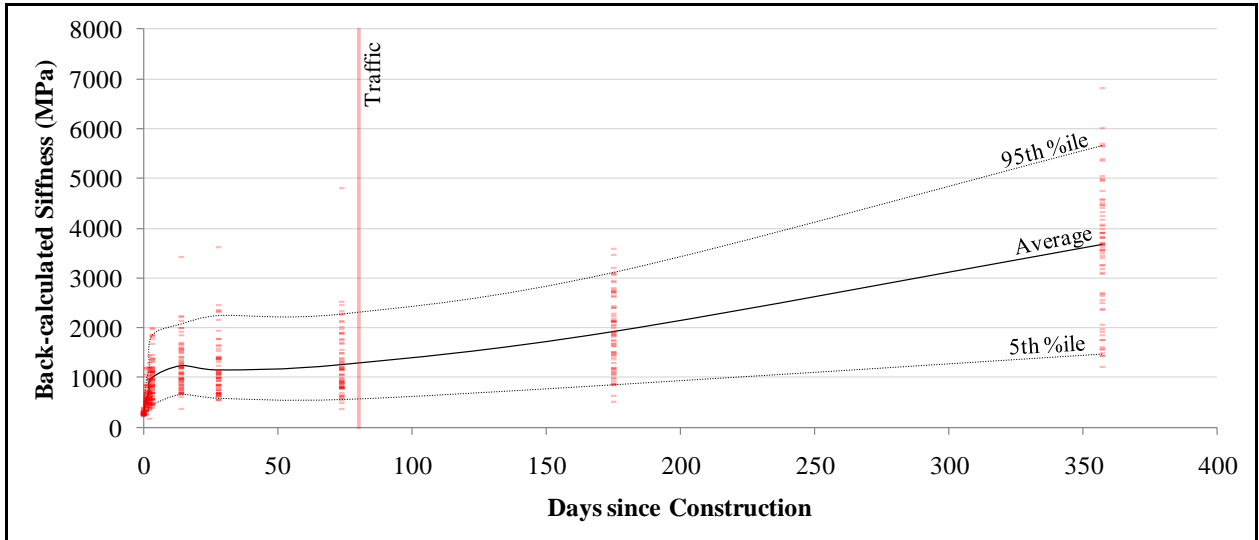
**175 mm Bitumen Emulsion (2.4%b, 1%c) km 7.2 to km 7.55**



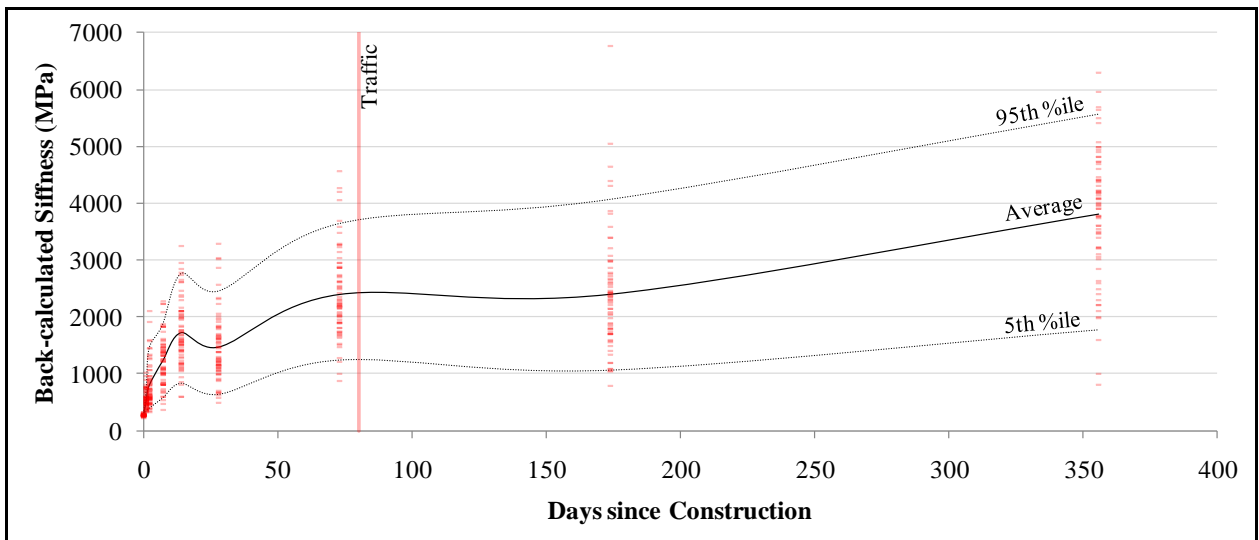
**200 mm Bitumen Emulsion (2.4%b, 1%c) km 7.55 to km 7.9**



**175 mm Bitumen Emulsion (2.4%b, 2%c) km 7.9 to km 8.25**

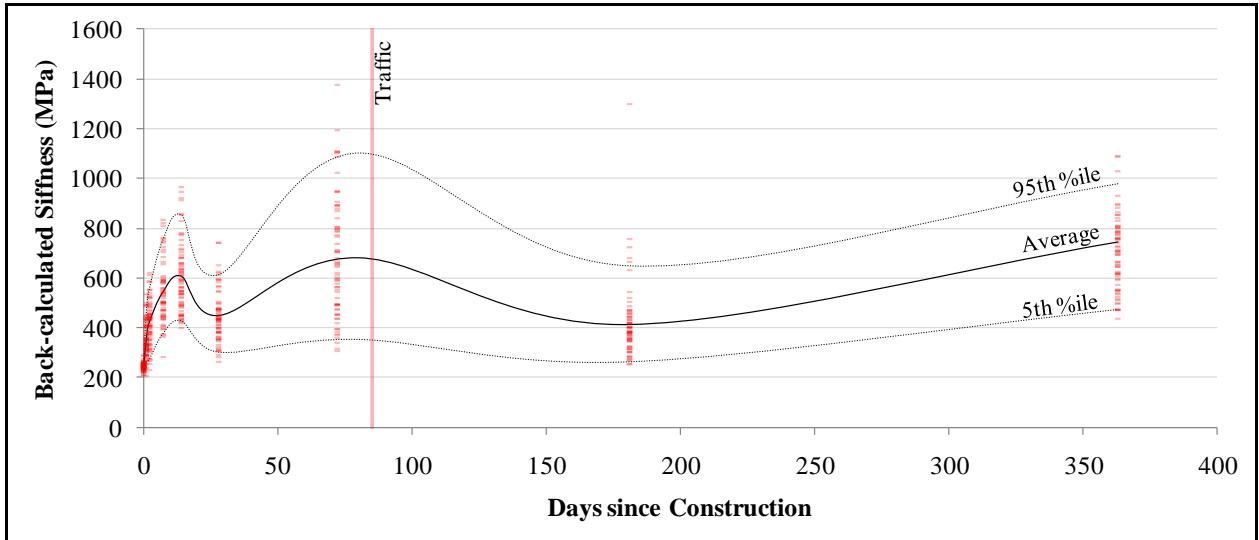


**200 mm Bitumen Emulsion (2.4%b, 2%c) km 8.25 to km 8.6**

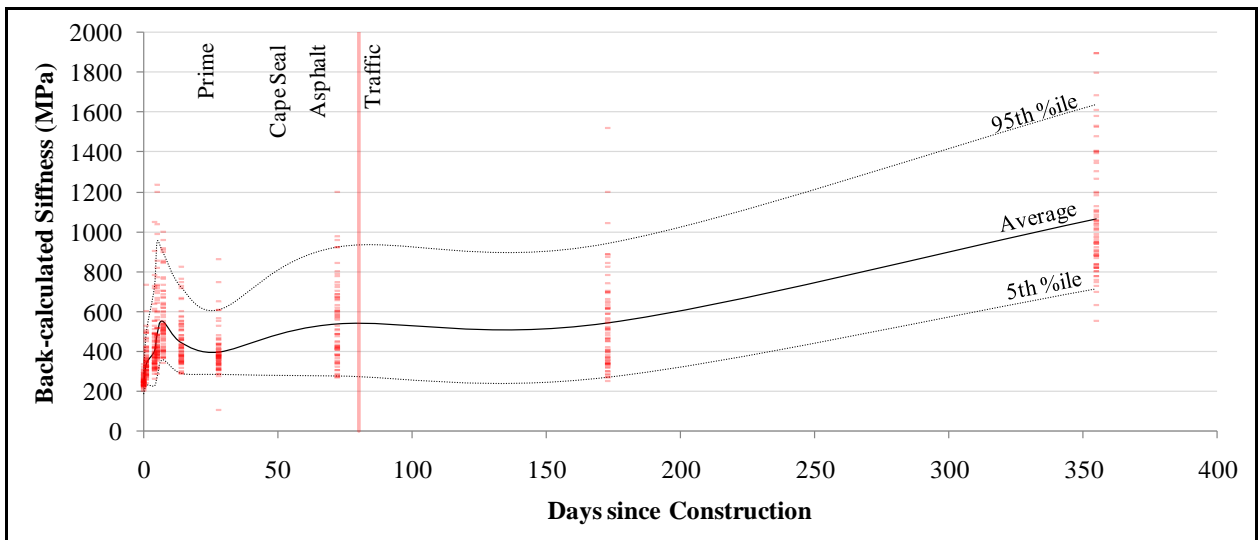




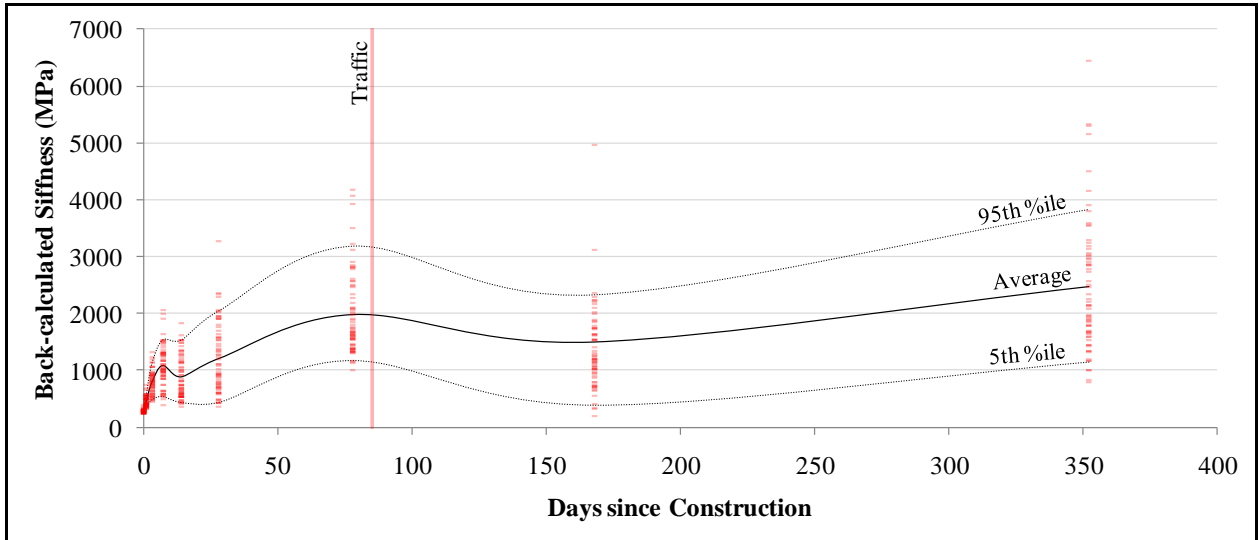
**175 mm Foamed Bitumen (2.4%b, 1%c) km 8.6 to km 8.95**



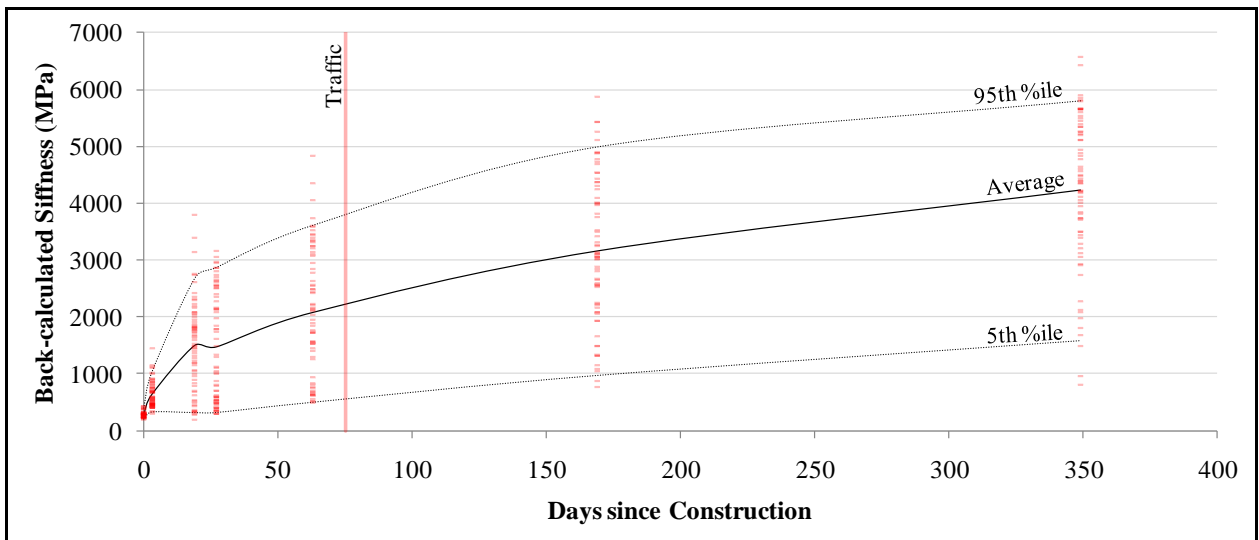
**200 mm Foamed Bitumen (2.4%b, 1%c) km 8.95 to km 9.3**



**175 mm Foamed Bitumen (2.4%b, 2%c) km 9.3 to km 9.65**



**200 mm Foamed Bitumen (2.4%b, 2%c) km 9.65 to km 10**

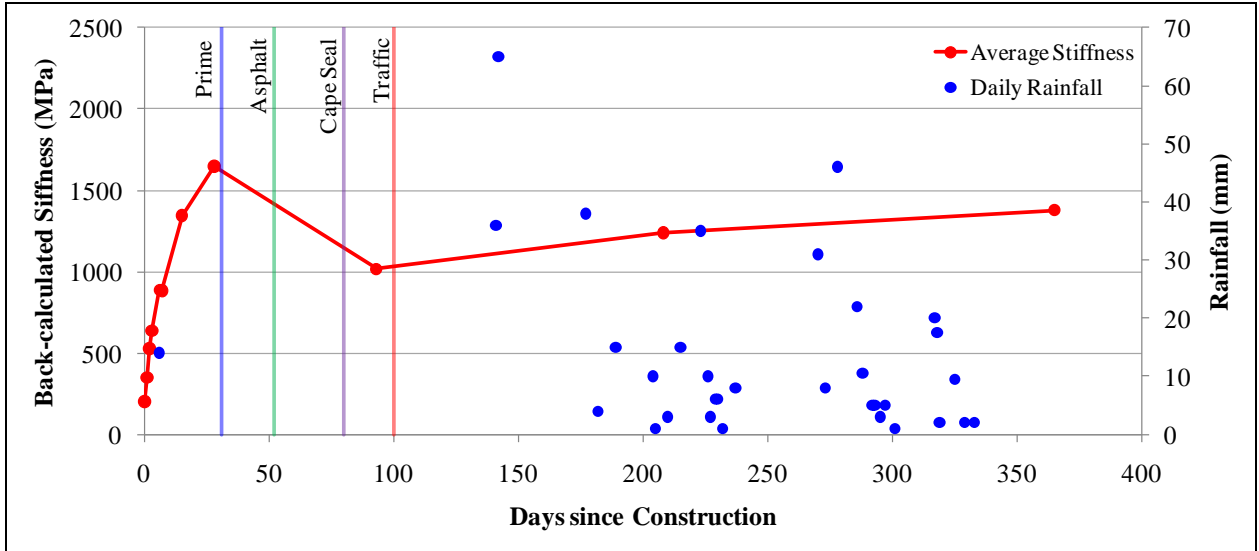


## **ADDENDUM E**

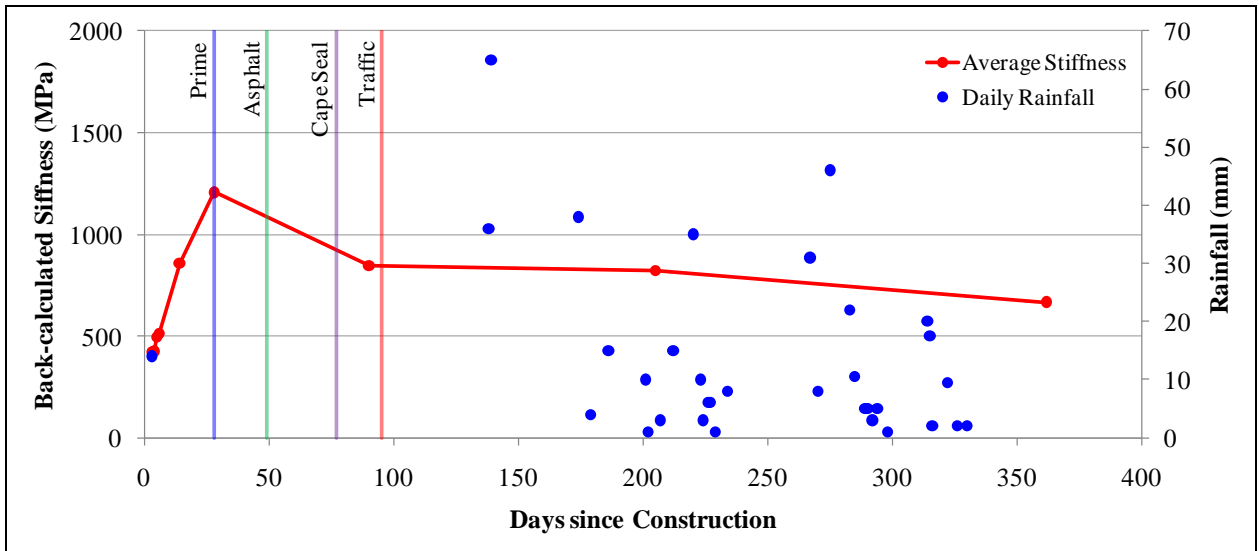
# **Average Back-calculated Base Layer Stiffness Trend Plots**

**SOUTHBOUND**

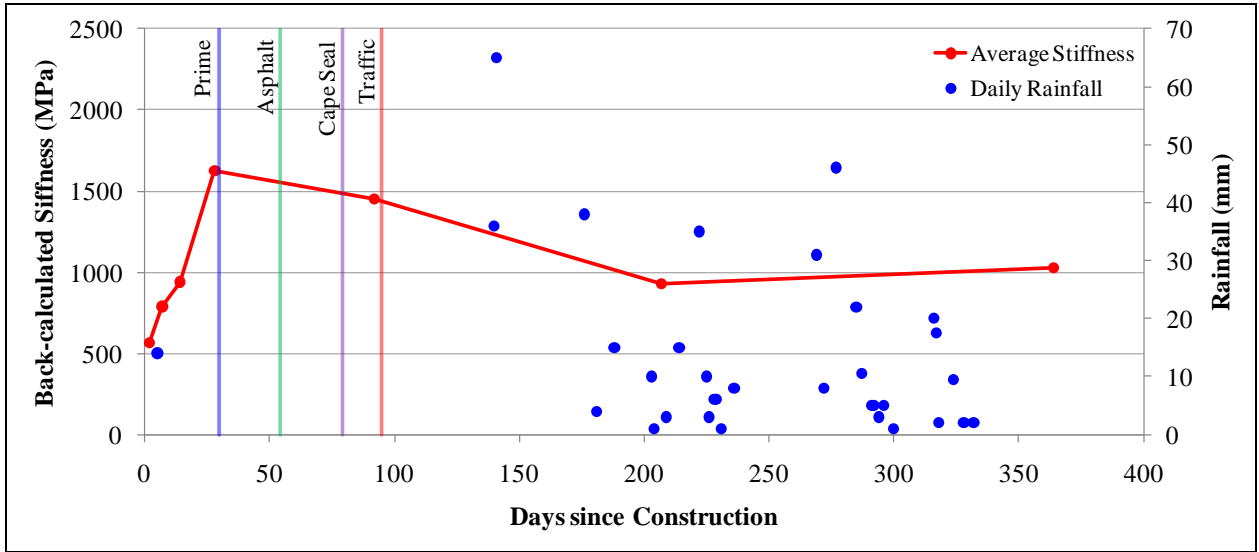
**200mm C3 – 1 (2% cement, 1% lime)**



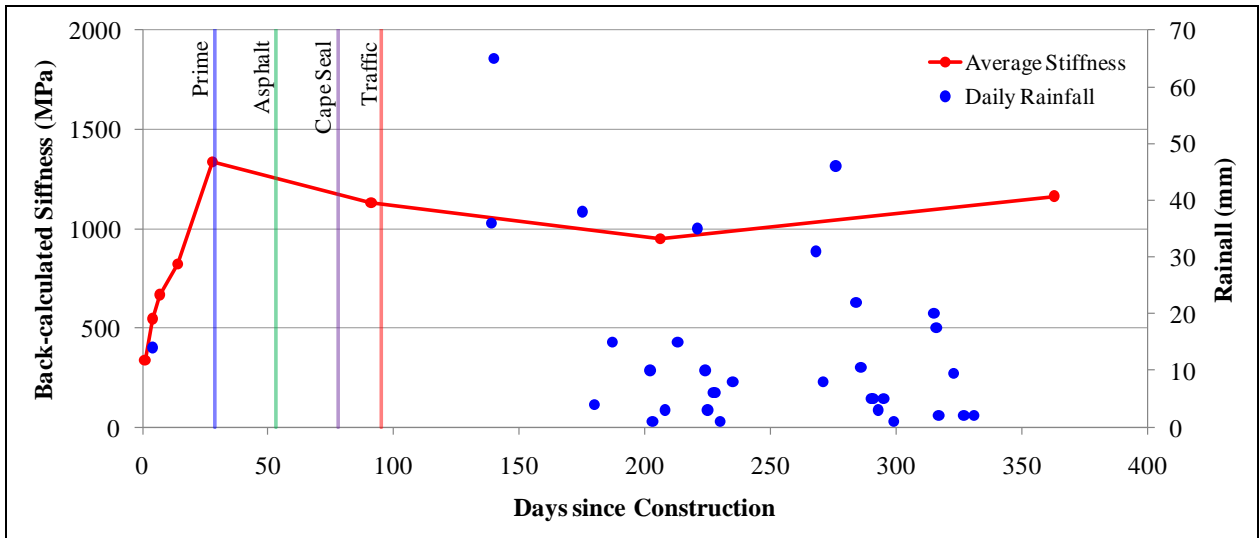
**200mm C3 – 2 (2% cement, 1% lime)**



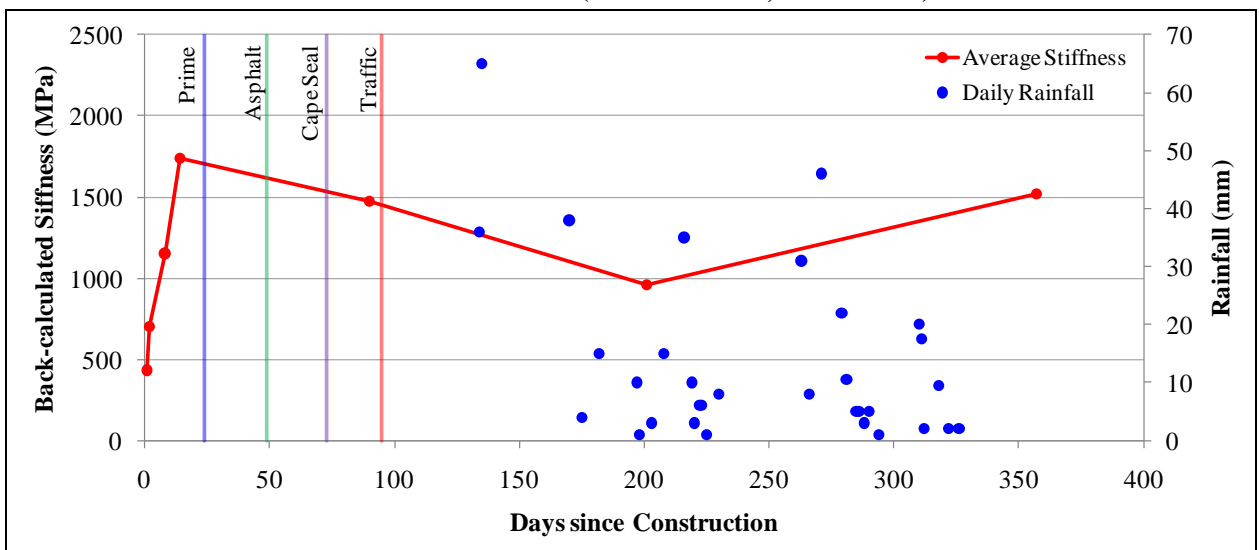
**175mm BSM Emulsion (2.4% bitumen, 1% cement)**



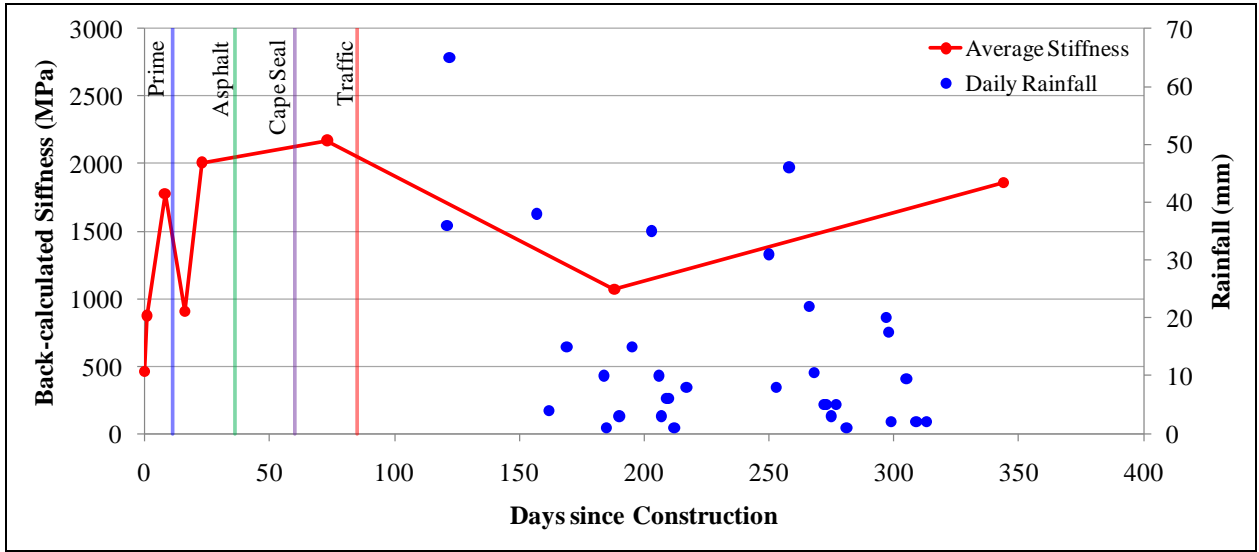
**200mm BSM Emulsion (2.4% bitumen, 1% cement)**



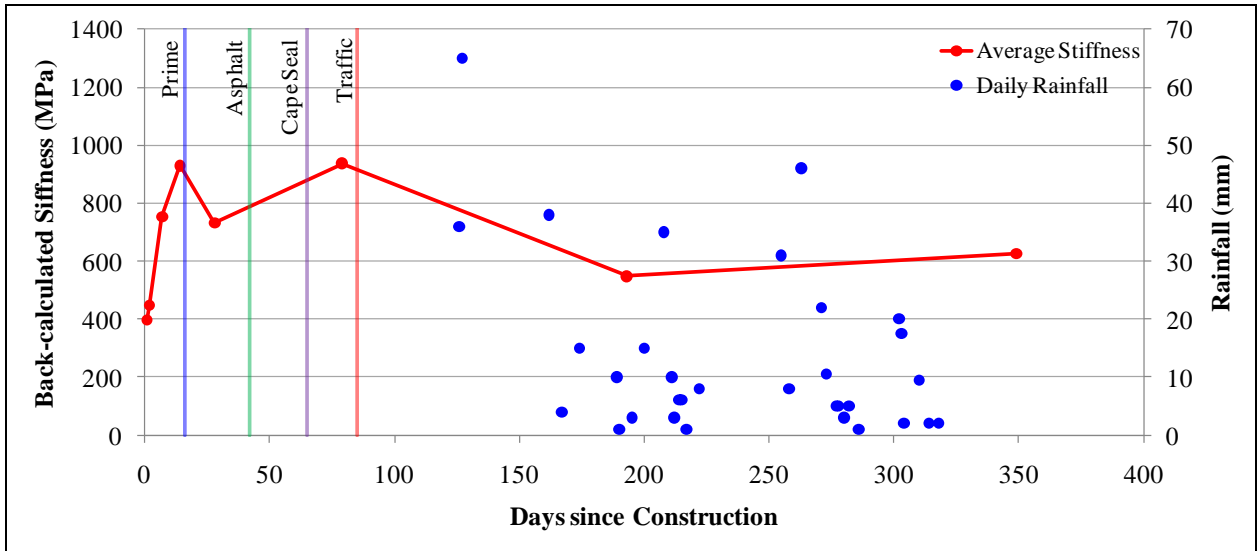
**175mm BSM Emulsion (2.4% bitumen, 2% cement)**



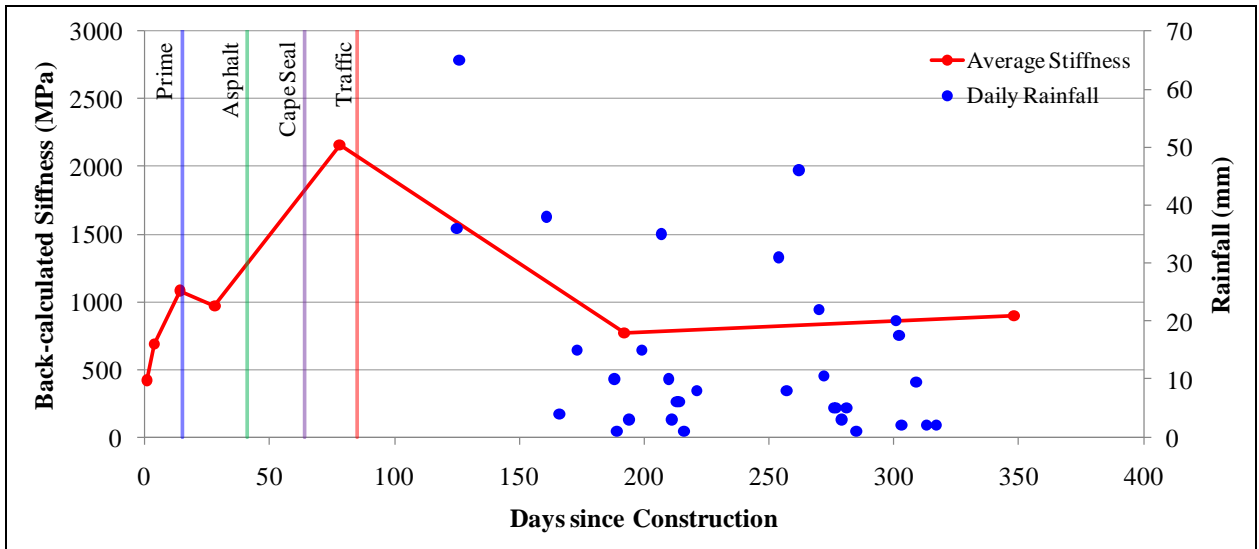
**200mm BSM Emulsion (2.4% bitumen, 2% cement)**



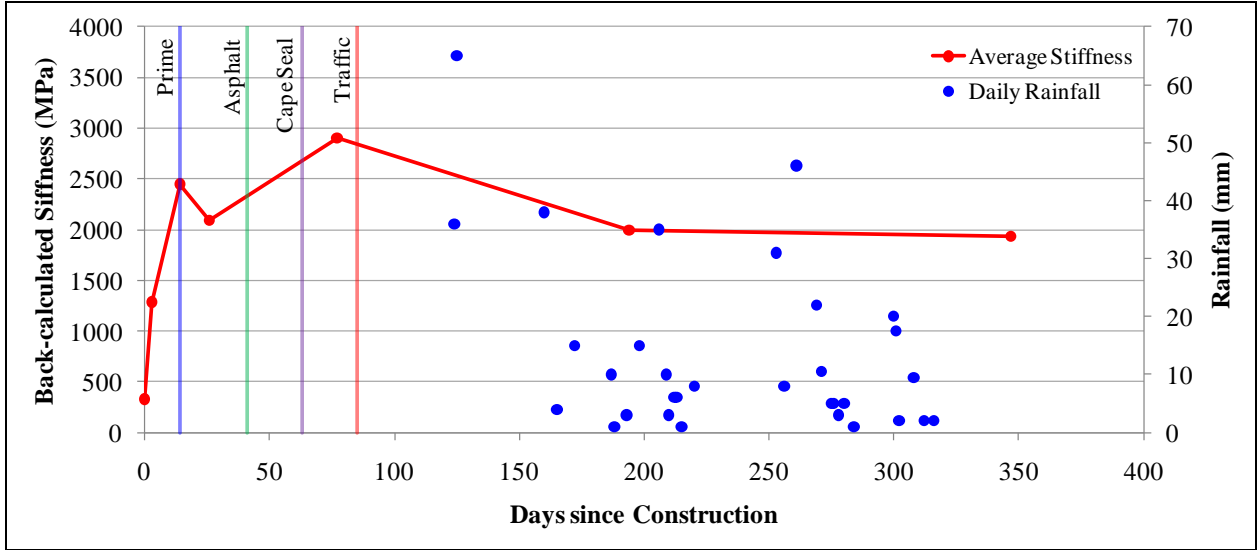
**175mm BSM Foam (2.4% bitumen, 1% cement)**



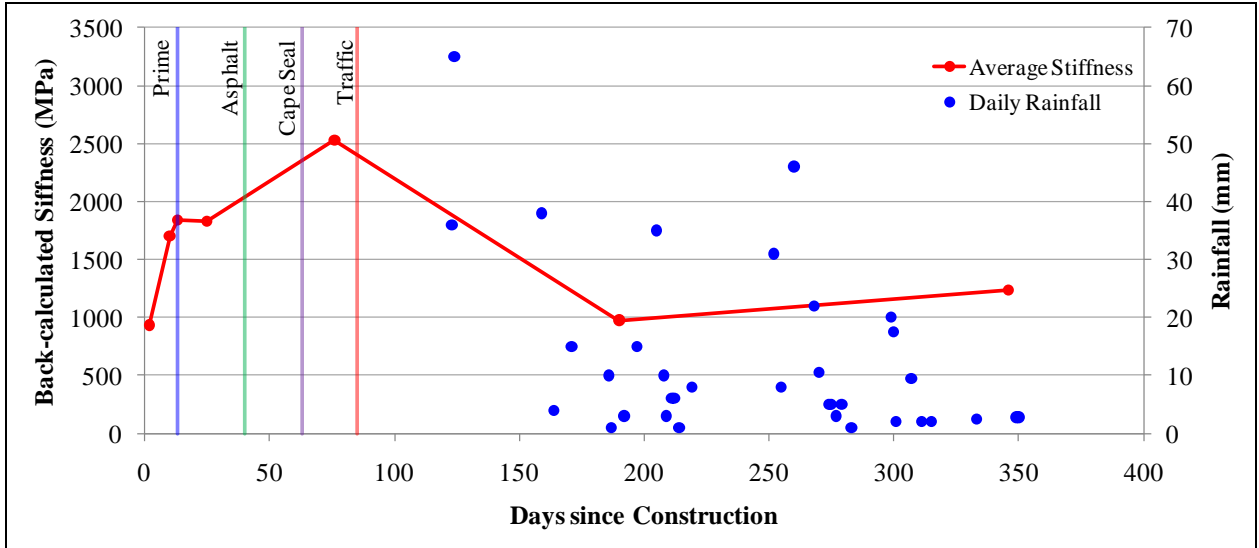
**200mm BSM Foam (2.4% bitumen, 1% cement)**



**175mm BSM Foam (2.4% bitumen, 2% cement)**

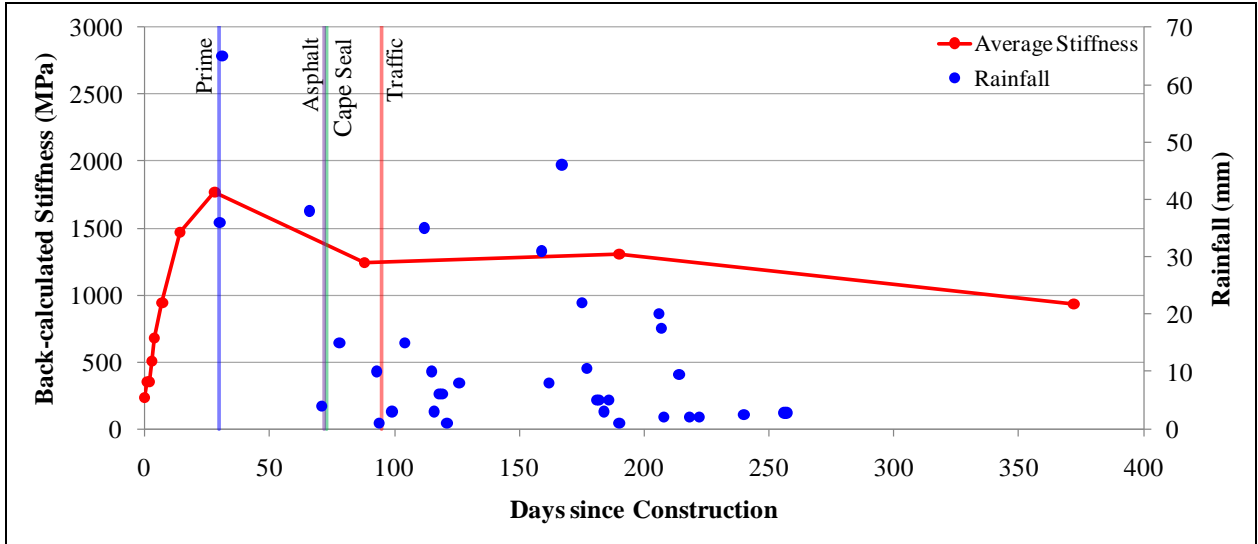


**200mm BSM Foam (2.4% bitumen, 2% cement)**

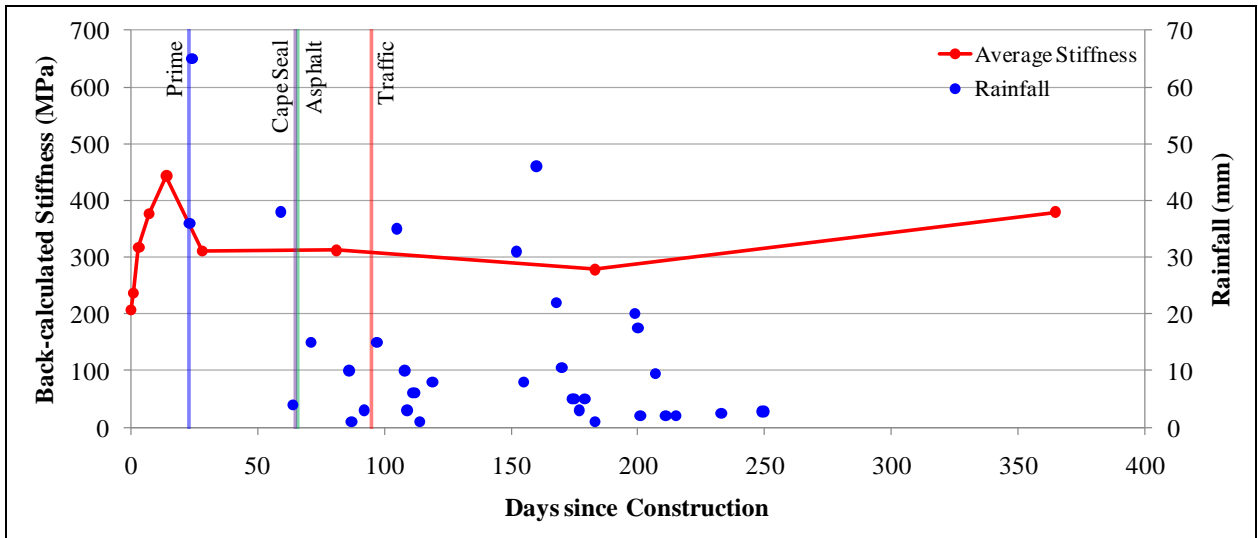


**NORTHBOUND**

**200mm C3 – 1 (2% cement, 1% lime)**

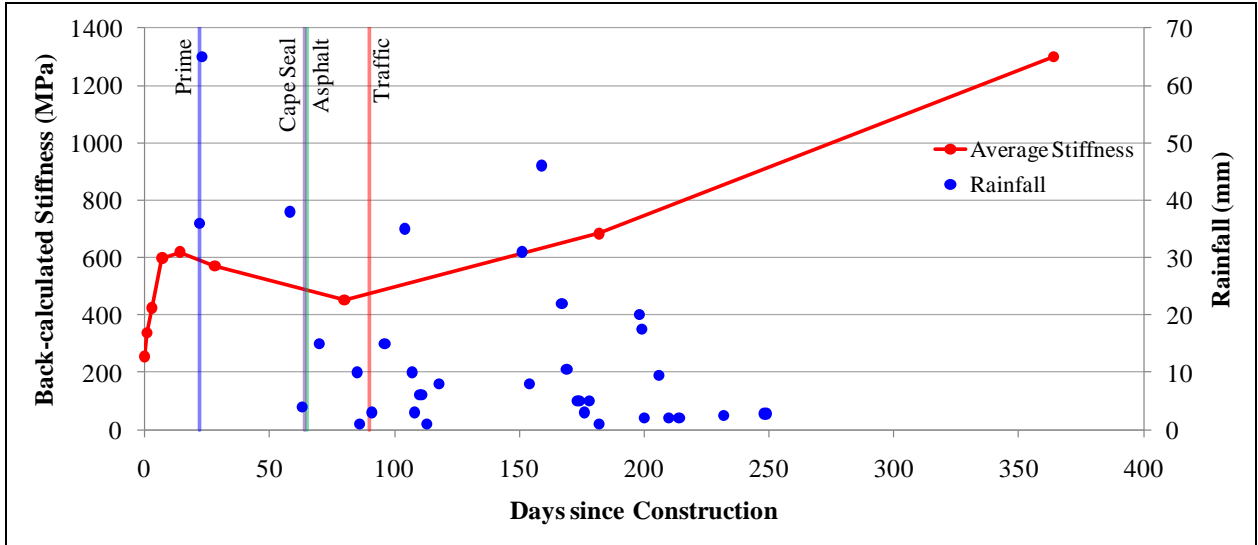


**200mm BSM Emulsion (0.9% residual bitumen, 1% cement)**

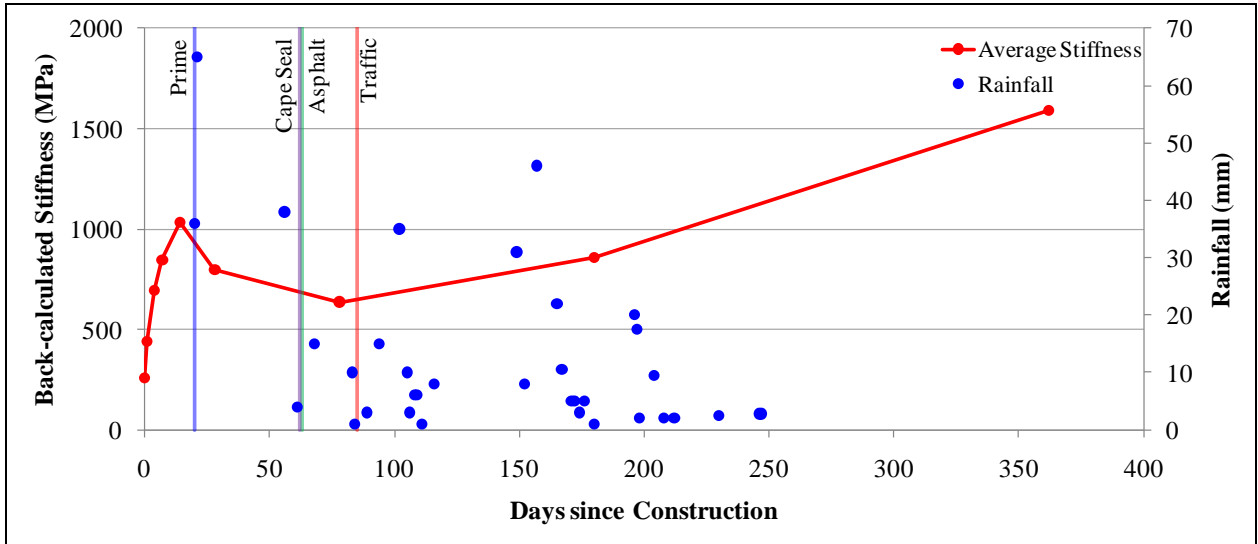




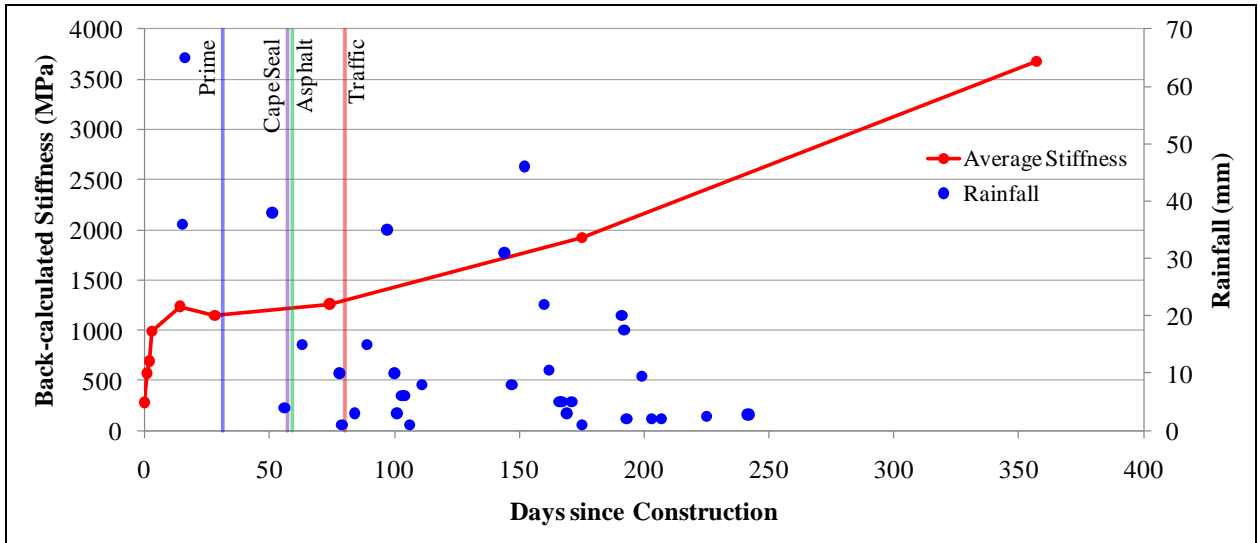
**175mm BSM Emulsion (2.4% bitumen, 1% cement)**



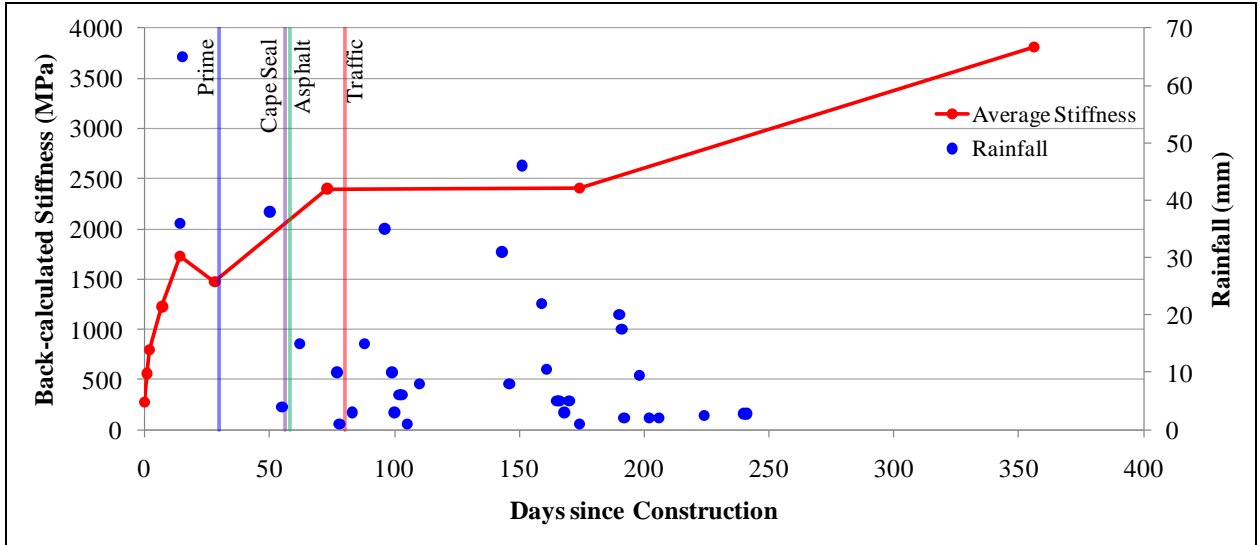
**200mm BSM Emulsion (2.4% bitumen, 1% cement)**



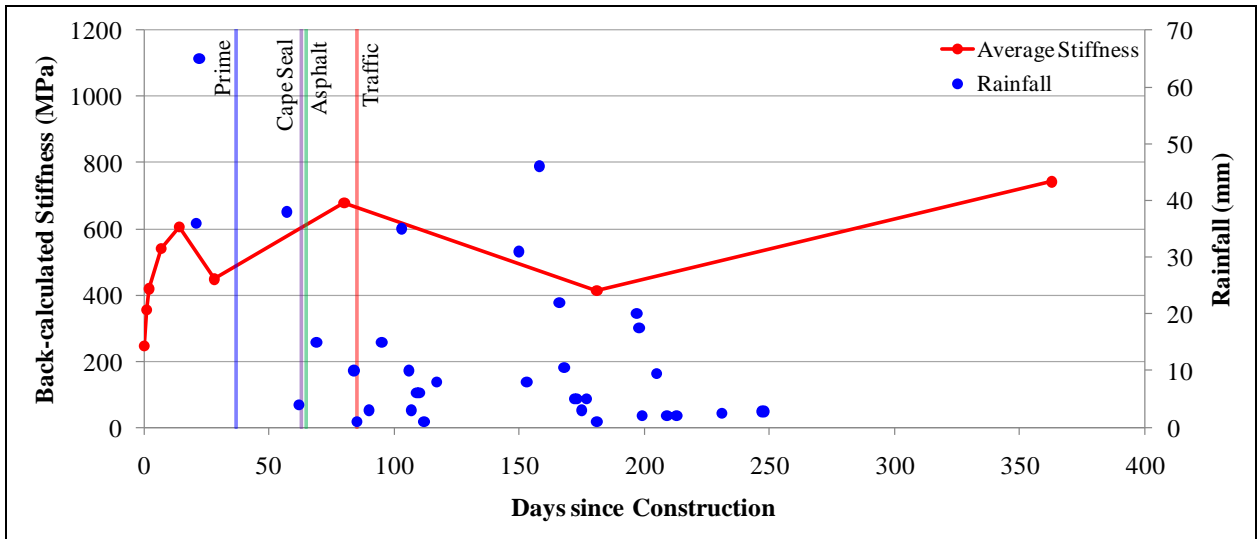
**175mm BSM Emulsion (2.4% bitumen, 2% cement)**



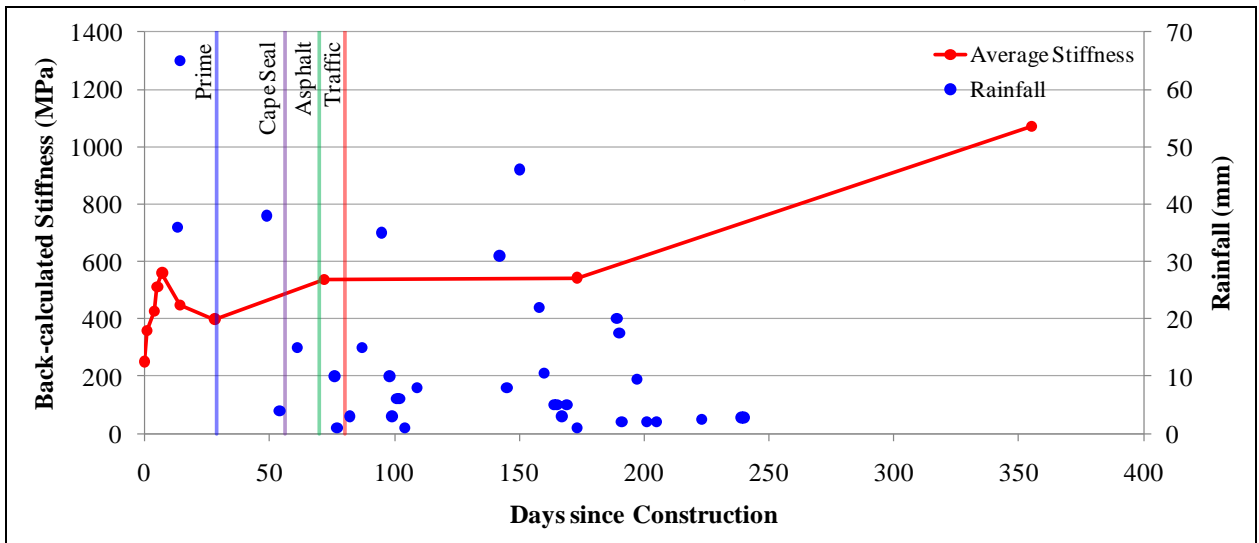
**200mm BSM Emulsion (2.4% bitumen, 2% cement)**



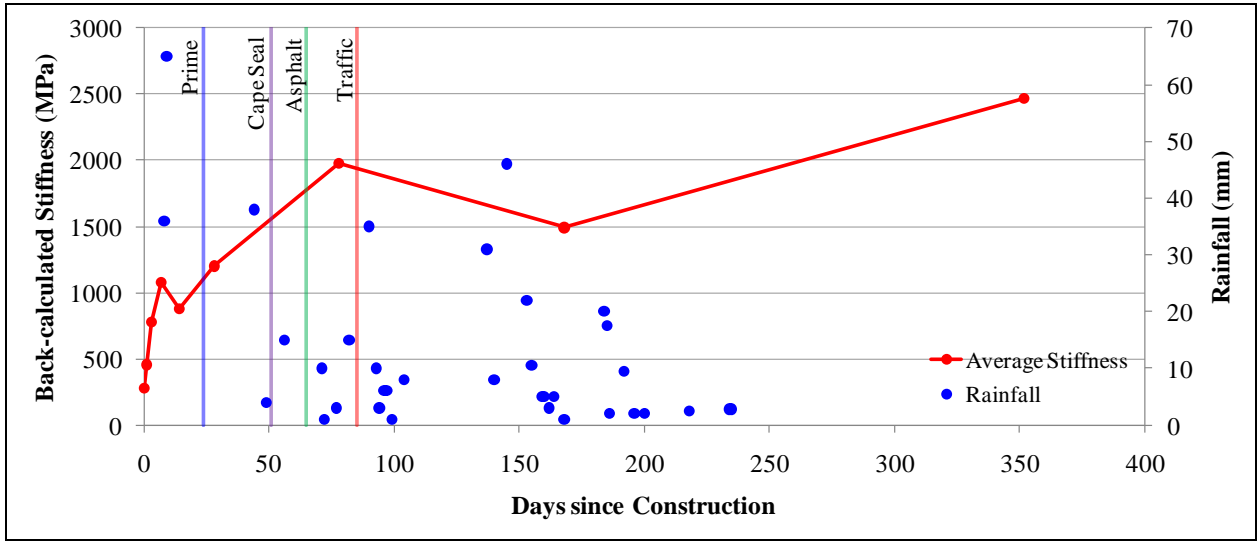
**175mm BSM Foam (2.4% bitumen, 1% cement)**



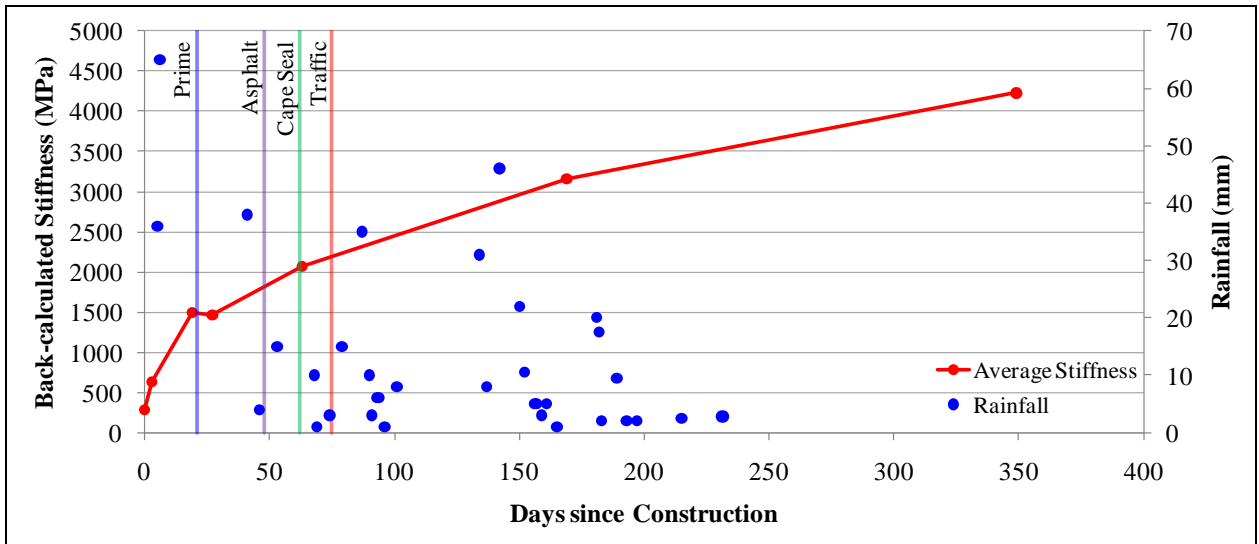
**200mm BSM Foam (2.4% bitumen, 1% cement)**



**175mm BSM Foam (2.4% bitumen, 2% cement)**



**200mm BSM Foam (2.4% bitumen, 2% cement)**



## **ADDENDUM F**

### **% Change in Average Base Layer Stiffness with Time**

**PERCENTAGE CHANGE IN AVERAGE BASE STIFFNESS BETWEEN FWD TEST DAYS  
SOUTHBOUND**

Sub-section	Days since construction											
	0 - 28							28 - 90	90 - 180	180 - 360		
200mm C3-1 (2% c, 1% l)	0 - 1	1 - 2	2 - 3	3 - 6		6 - 7	7 - 15	15 - 28	28 - 93	93 - 208	208 - 365	
	74%	52%	21%	39%		0%	54%	20%	-38%	21%	11%	
200mm C3-2 (2% c, 1% l)				3 - 4	4 - 5	5 - 6	6 - 14		14 - 28	28 - 90	90 - 205	205 - 362
				2%	16%	4%	67%		40%	-30%	-3%	-19%
175 Emulsion (1%c, 2.4%b)			2 - 7			7 - 14		14 - 28	28 - 92	92 - 207	207 - 364	
			42%			19%		73%	-9%	-37%	10%	
200 Emulsion (1%c, 2.4%b)		1 - 4		4 - 7		7 - 14	14 - 28	28 - 91	91 - 206	206 - 363		
		64%		23%		23%	64%	-16%	-17%	22%		
175 Emulsion (2%c, 2.4%b)		1 - 2	2 - 8			8 - 14		14 - 90		90 - 201	201 - 357	
		64%	69%			51%		-16%		-35%	57%	
200 Emulsion (2%c, 2.4%b)	0 - 1	1 - 8				8 - 16		16 - 23	23 - 73	73 - 188	188 - 344	
	92%	104%				-49%		122%	8%	-51%	74%	
175 Foam (1%c, 2.4%b)		1 - 2	2 - 7			7 - 14		14 - 28	28 - 79	79 - 193	193 - 349	
		16%	71%			24%		-21%	28%	-42%	14%	
200 Foam (1%c, 2.4%b)		1 - 4		4 - 14			14 - 28	28 - 78	78 - 192	192 - 348		
		67%		58%			-9%	121%	-64%	16%		
175 Foam (2%c, 2.4%b)		0 - 3		3 - 14			14 - 26	26 - 77	77 - 194	194 - 347		
		314%		90%			-14%	39%	-32%	-4%		
200 Foam (2%c, 2.4%b)			2 - 10			10 - 13	13 - 25	25 - 76	76 - 190	190 - 346		
			82%			9%	-1%	39%	-62%	26%		

**PERCENTAGE CHANGE IN AVERAGE BASE STIFFNESS BETWEEN FWD TEST DAYS NORTHBOUND**

Sub-section	Days since construction									
	0 - 28							28 - 90	90 - 180	180 - 360
200mm C3-1 (2% c, 1% l)	0 - 1	1 - 2	2 - 3	3 - 4	4 - 7	7 - 14	14 - 28	28 - 88	88 - 190	
	50%	0%	44%	34%	39%	56%	21%	-30%	5%	-29%
200mm Emulsion (0.9% b, 1% c)	0 - 1	1 - 3		3 - 7		7 - 14	14 - 28	28 - 81	81 - 183	
	14%	34%		19%		18%	-30%	0%	-11%	37%
175 Emulsion (1% c, 2.4% b)	0 - 1	1 - 3		3 - 7		7 - 14	14 - 28	28 - 80	80 - 182	
	32%	26%		41%		3%	-8%	-21%	51%	90%
200 Emulsion (1% c, 2.4% b)	0 - 1	1 - 4		4 - 7		7 - 14	14 - 28	28 - 78	78 - 180	
	71%	57%		22%		23%	-23%	-20%	35%	86%
175 Emulsion (2% c, 2.4% b)	0 - 1	1 - 2	2 - 3	3 - 14			14 - 28	28 - 74	74 - 175	
	103%	21%	44%	25%			-7%	10%	53%	91%
200 Emulsion (2% c, 2.4% b)	0 - 1	1 - 2	2 - 7			7 - 14	14 - 28	28 - 73	73 - 174	
	103%	43%	54%			41%	-15%	63%	0%	59%
175 Foam (1% c, 2.4% b)	0 - 1	1 - 2	2 - 7			7 - 14	14 - 28	28 - 80	80 - 181	
	44%	18%	29%			12%	-26%	52%	-17%	80%
200 Foam (1% c, 2.4% b)	0 - 1	1 - 4		4 - 5	5 - 7	7 - 14	14 - 28	28 - 72	72 - 173	
	42%	19%		20%	9%	-20%	-11%	35%	1%	97%
175 Foam (2% c, 2.4% b)	0 - 1	1 - 3		3 - 7		7 - 14	14 - 28	28 - 78	78 - 168	
	62%	71%		39%		-18%	37%	64%	-24%	65%
200 Foam (2% c, 2.4% b)	0 - 3		3 - 19				19 - 27	27 - 63	63 - 169	
	123%		139%				-2%	42%	52%	34%

## **ADDENDUM G**

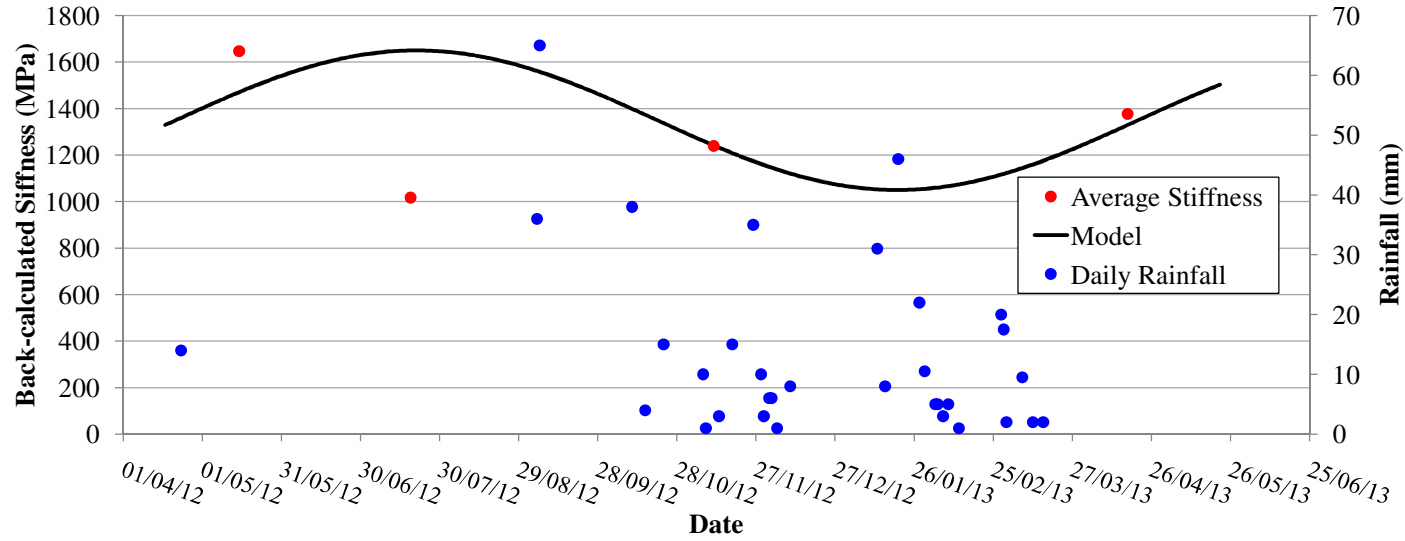
# **Base Layer Stiffness Seasonal Variation Models – Southbound**

**SUGGESTED BASE LAYER STIFFNESS SEASONAL VARIATION MODELS - SOUTHBOUND**

**MODEL 200 C3-1 (2%c, 1%I)**

Freq	A	Phi	Mean
0.017214	300	-140	1350
365			

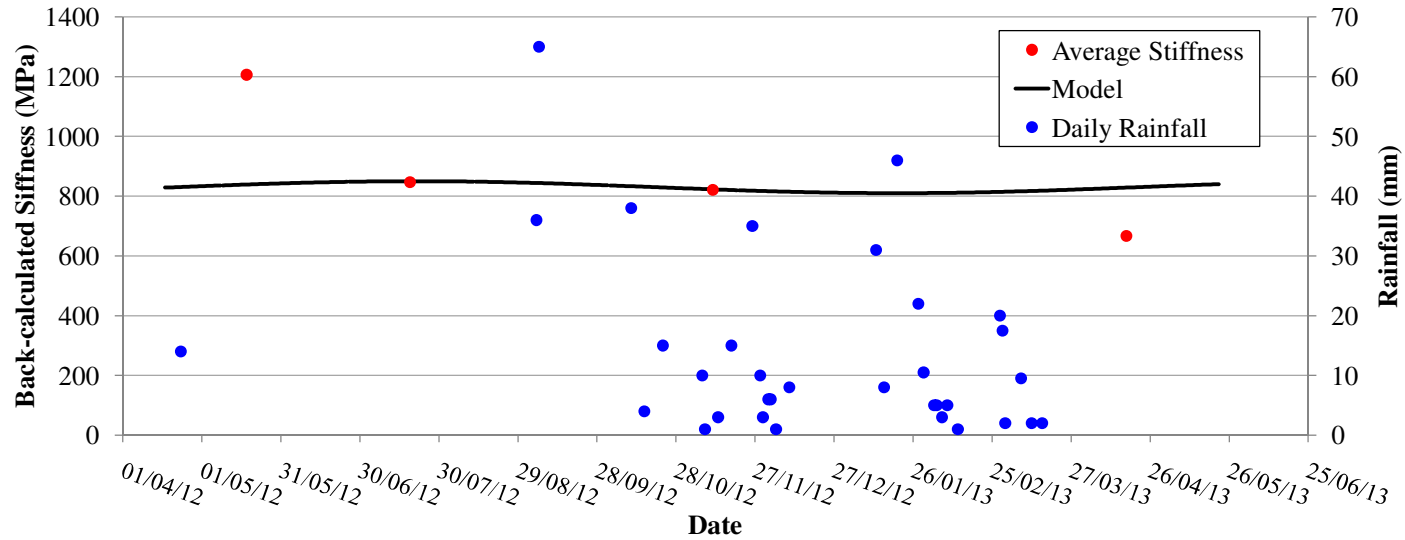
R 2 = -5.10508



**MODEL 200 C3-2 (2%c, 1%I)**

Freq	A	Phi	Mean
0.017214	20	-140	830
365			

R 2 = -0.38124

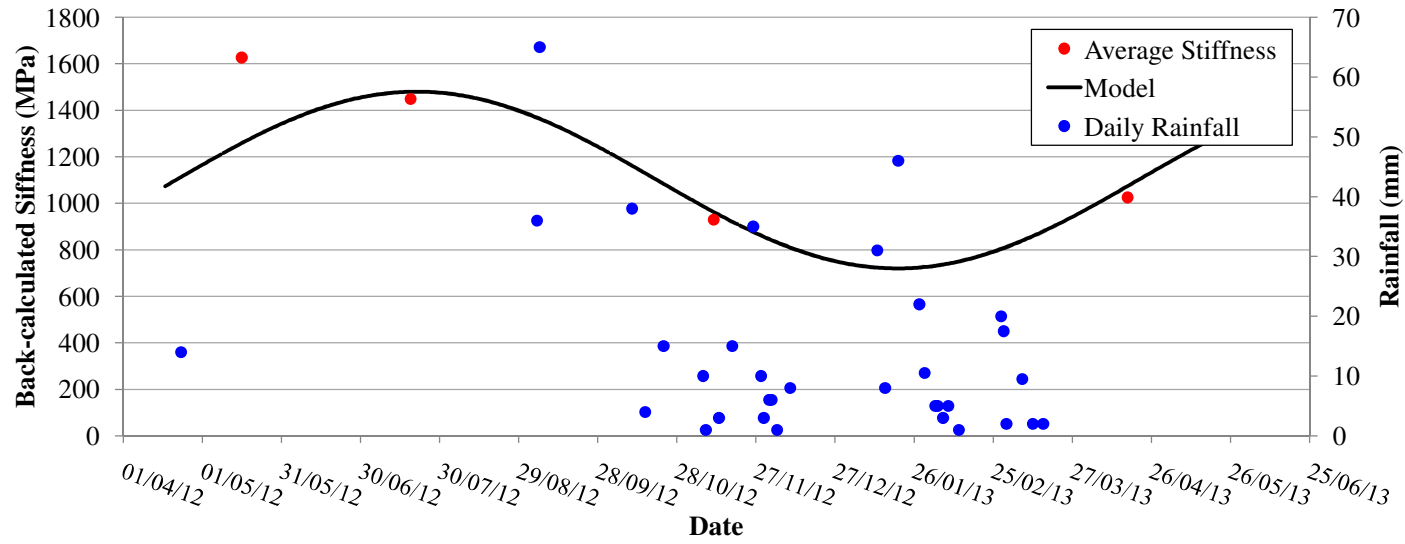




MODEL 175 E (2.4%b, 1%c)

Freq	A	Phi	Mean
0.017214	380	-140	1100
365			

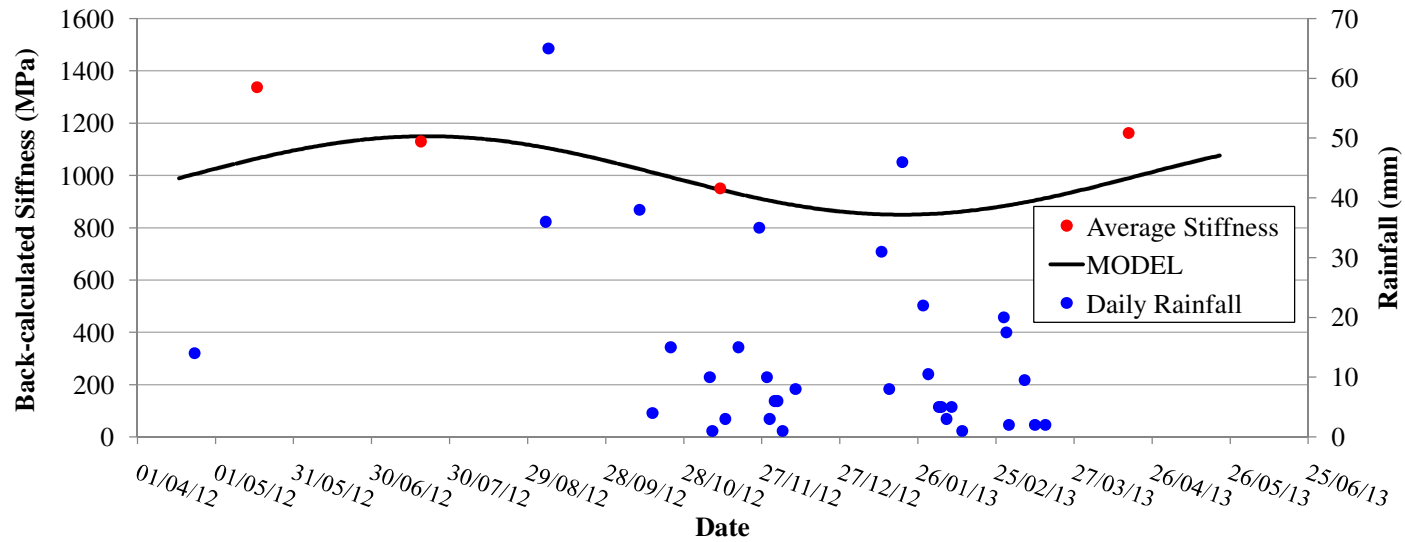
R 2 = 0.970875



MODEL 200 E (2.4%b, 1%c)

Freq	A	Phi	Mean
0.017214	150	-140	1000
365			

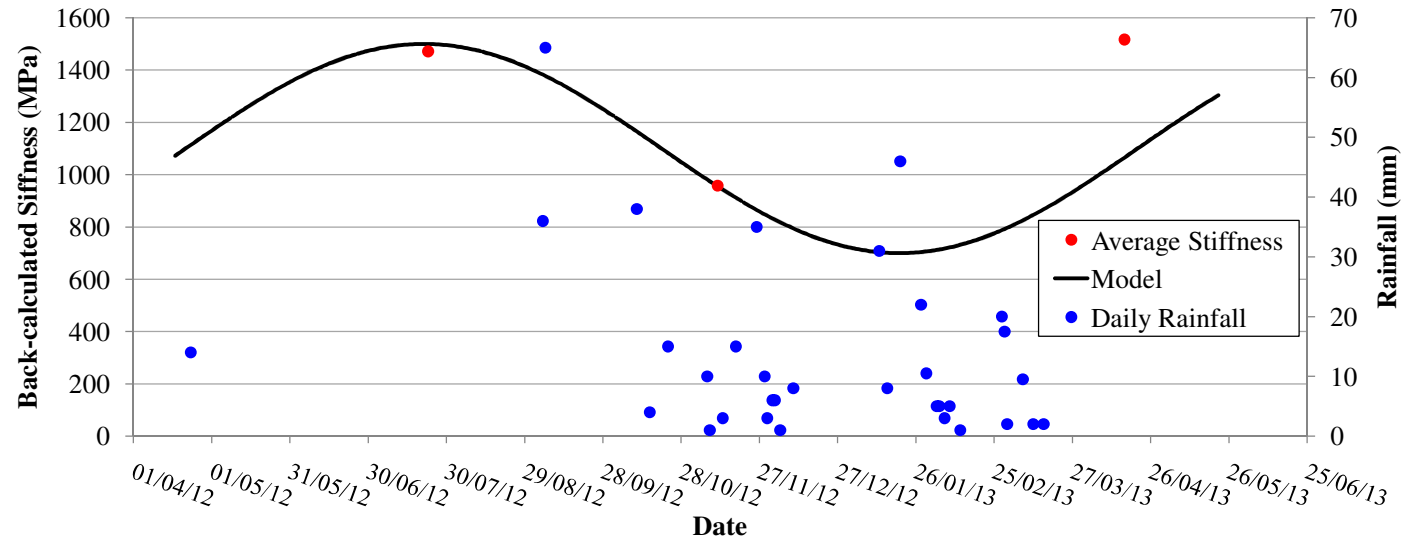
R 2 = -0.16394



MODEL 175 E (2.4%b, 2%c)

Freq	A	Phi	Mean
0.017214	400	-140	1100
365			

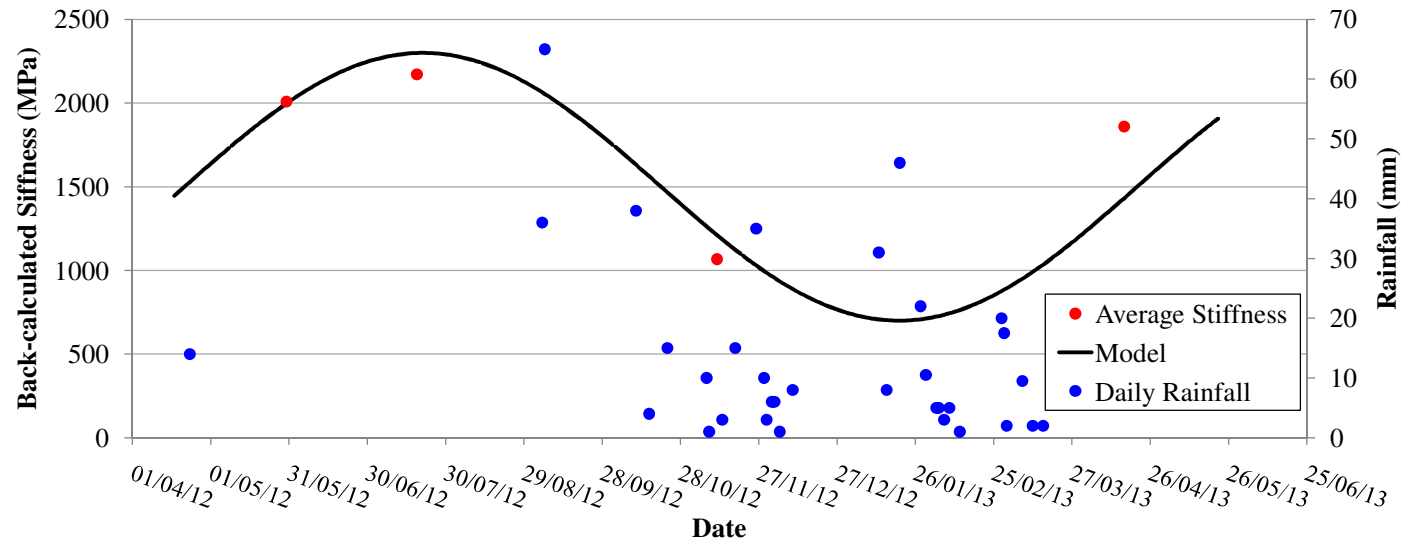
R<sup>2</sup> = -0.06023



MODEL 200 E (2.4%b, 2%c)

Freq	A	Phi	Mean
0.017214	800	-140	1500
365			

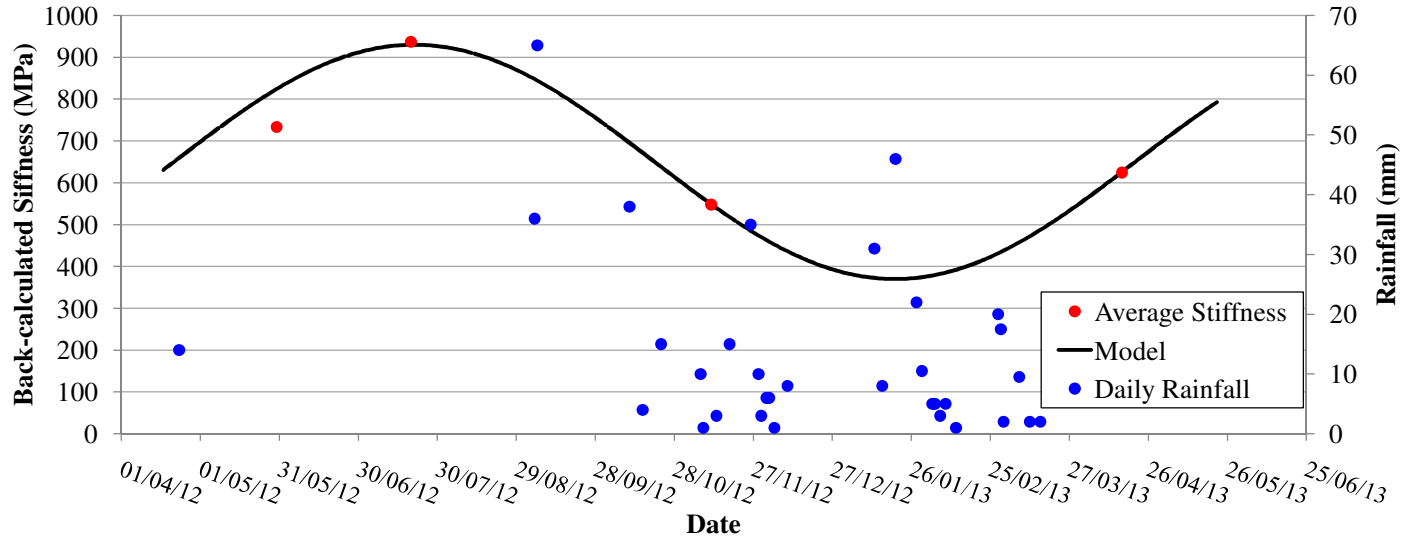
R<sup>2</sup> = 0.659041



MODEL 175 F (2.4%b, 1%c)

Freq	A	Phi	Mean
0.017214	280	-140	650
365			

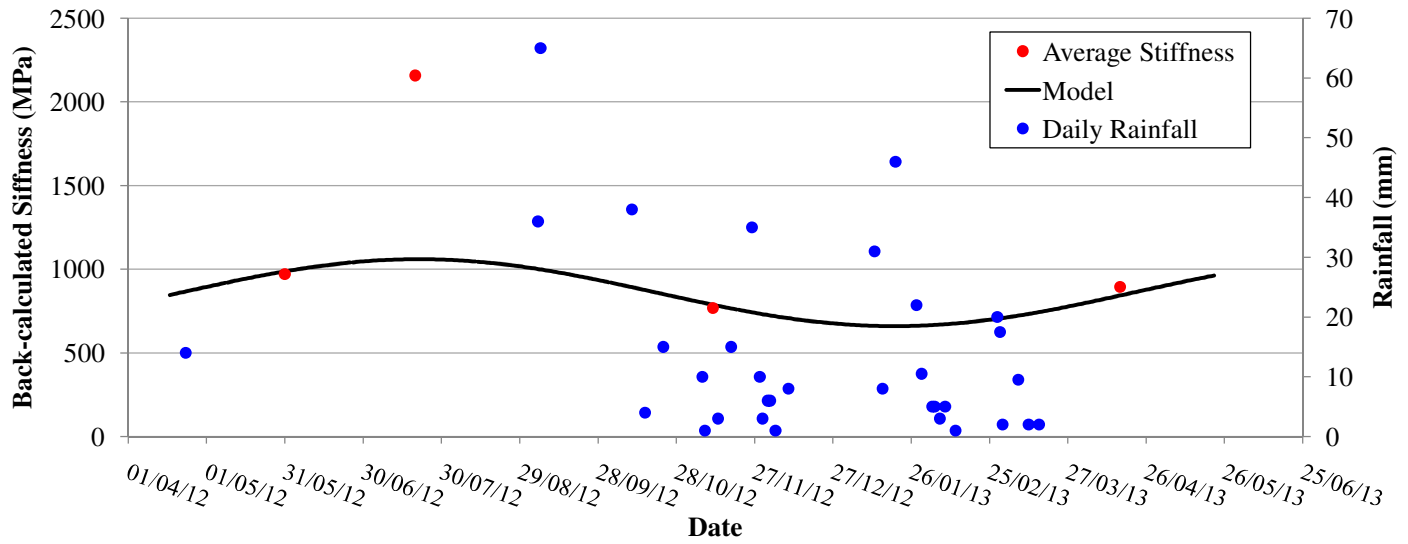
R 2 = 0.999373



MODEL 200 F (2.4%b, 1%c)

Freq	A	Phi	Mean
0.017214	200	-140	860
365			

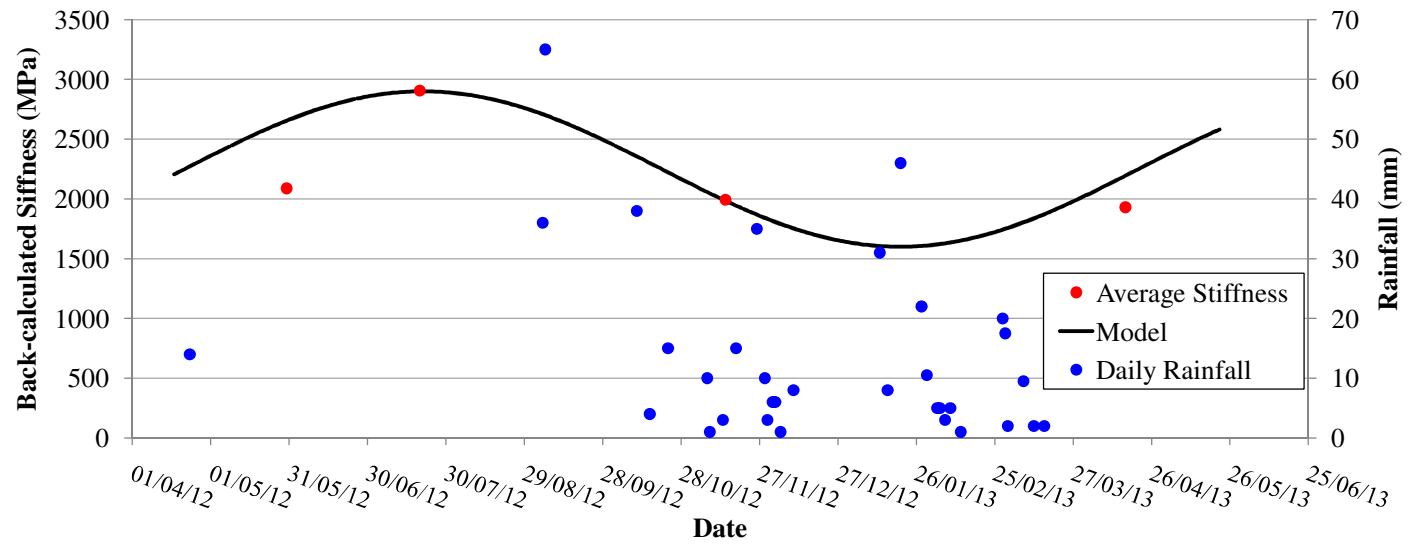
R 2 = -0.0226



MODEL 175 F (2.4%b, 2%c)

Freq	A	Phi	Mean
0.017214	650	-140	2250
365			

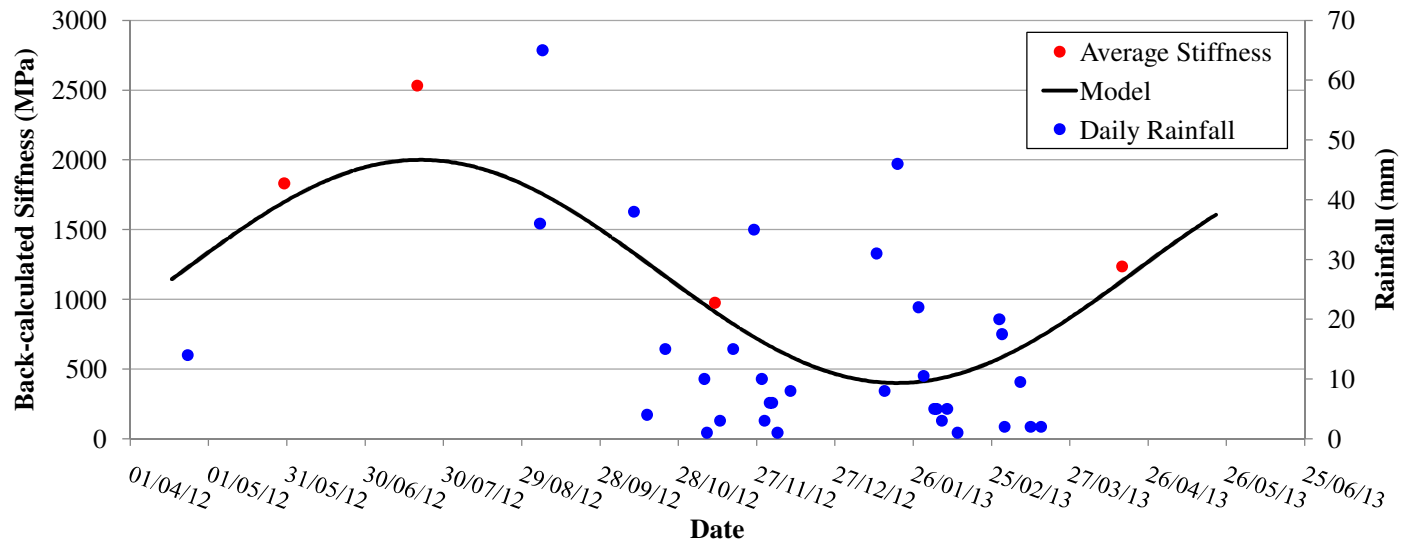
R<sup>2</sup> = 0.883307



MODEL 200 F (2.4%b, 2%c)

Freq	A	Phi	Mean
0.017214	800	-140	1200
365			

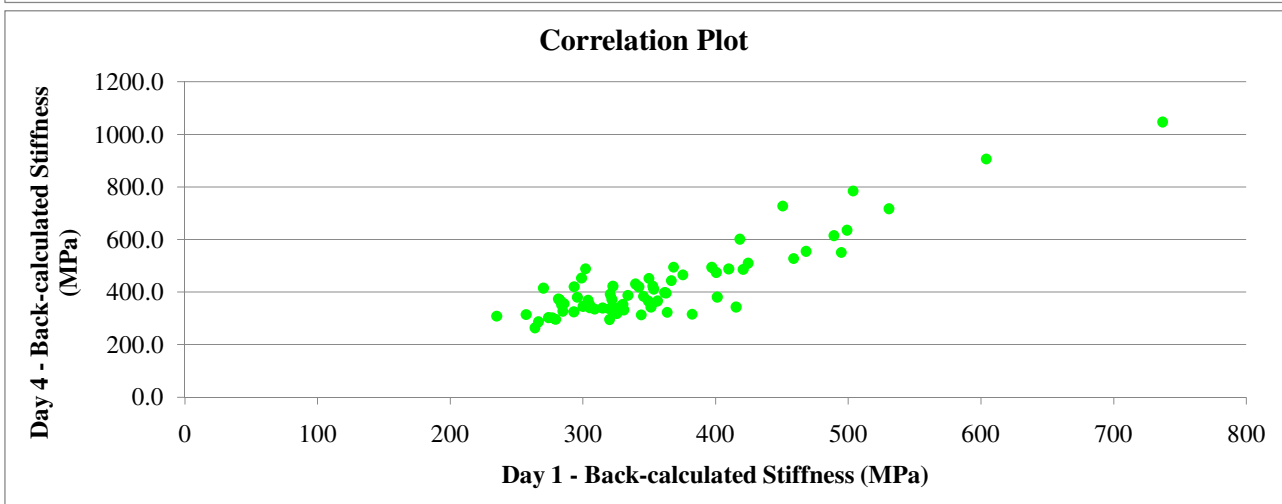
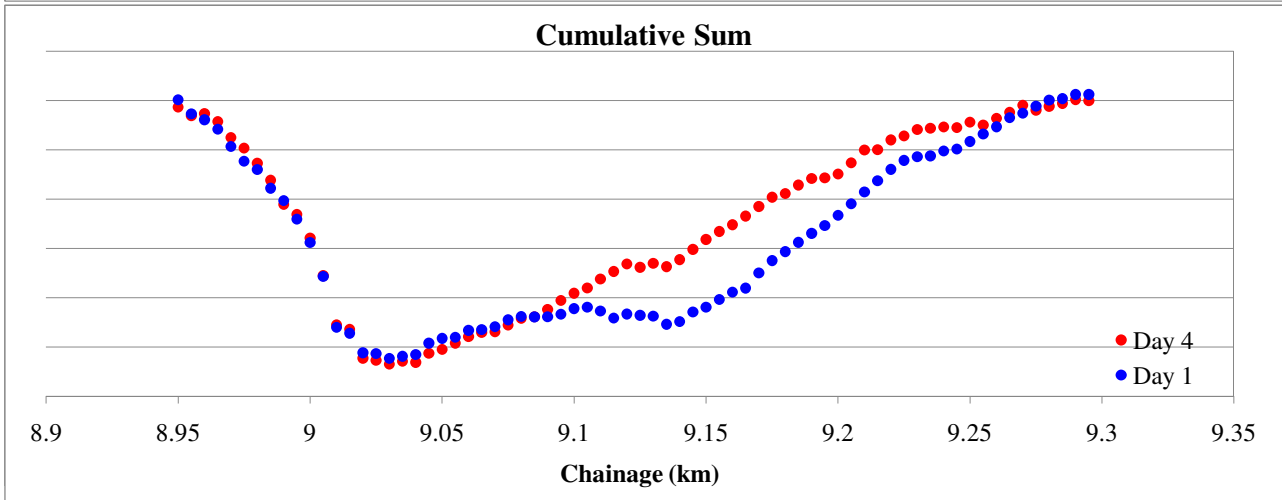
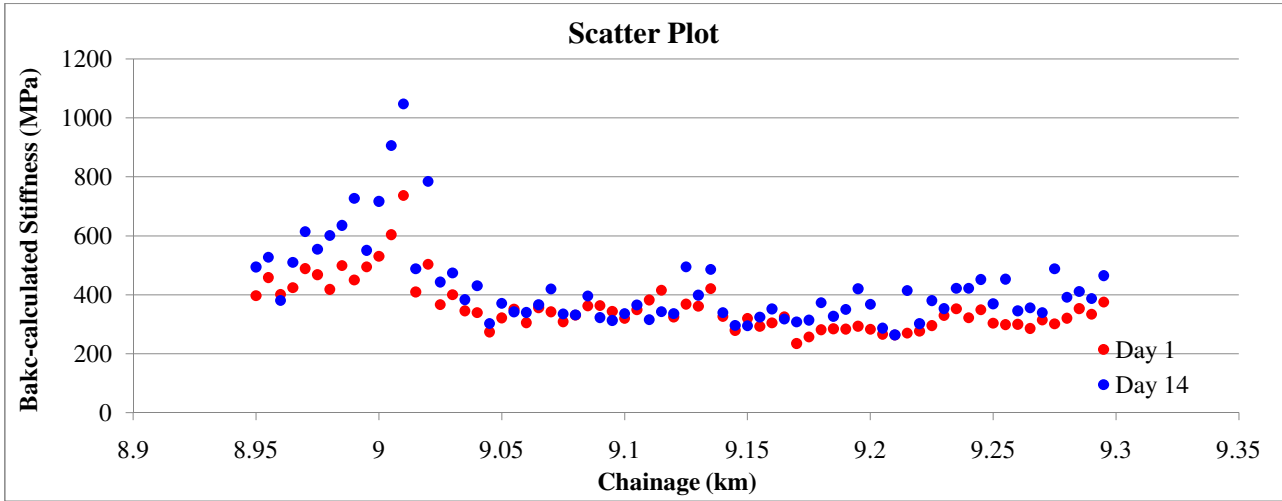
R<sup>2</sup> = 0.7855



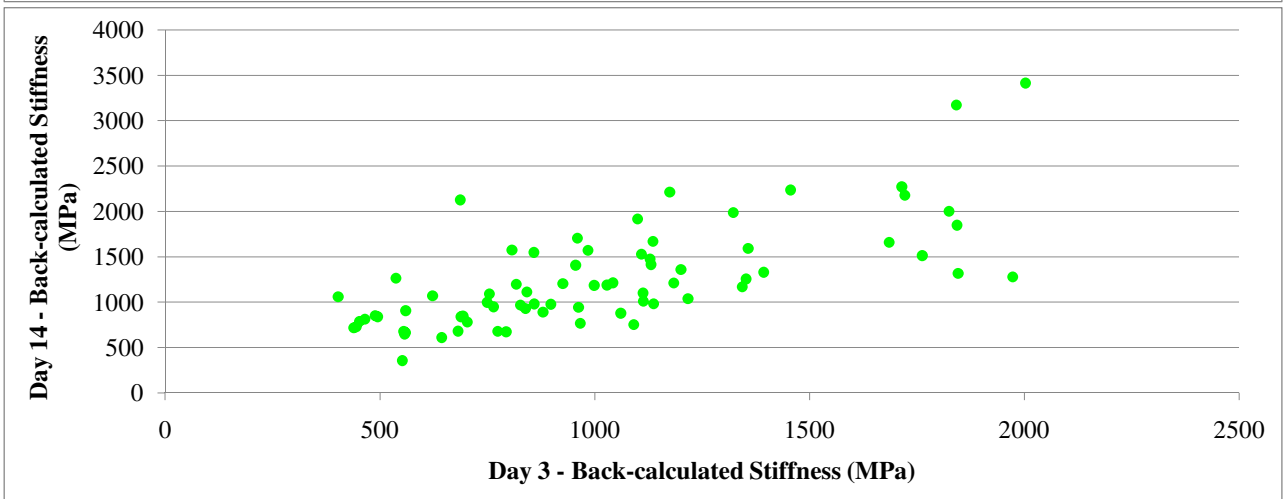
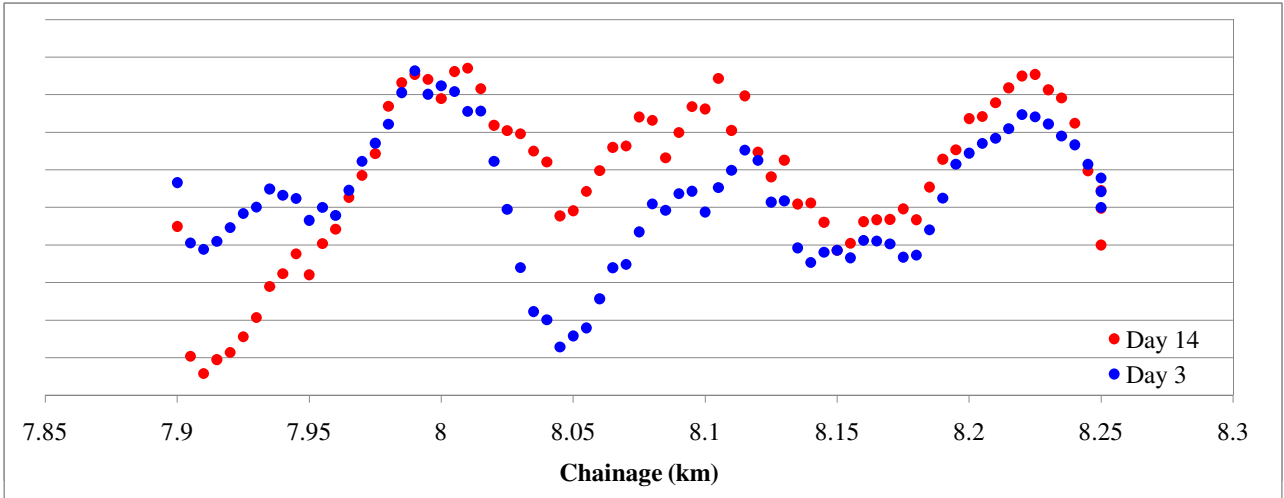
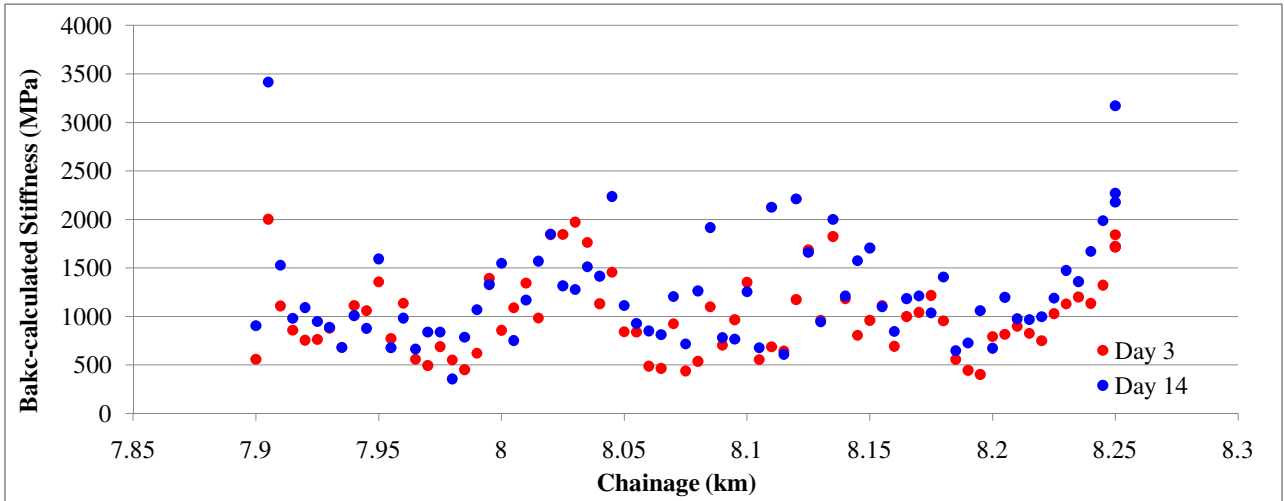
## **ADDENDUM H**

### **Correlation Co-efficient Examples**

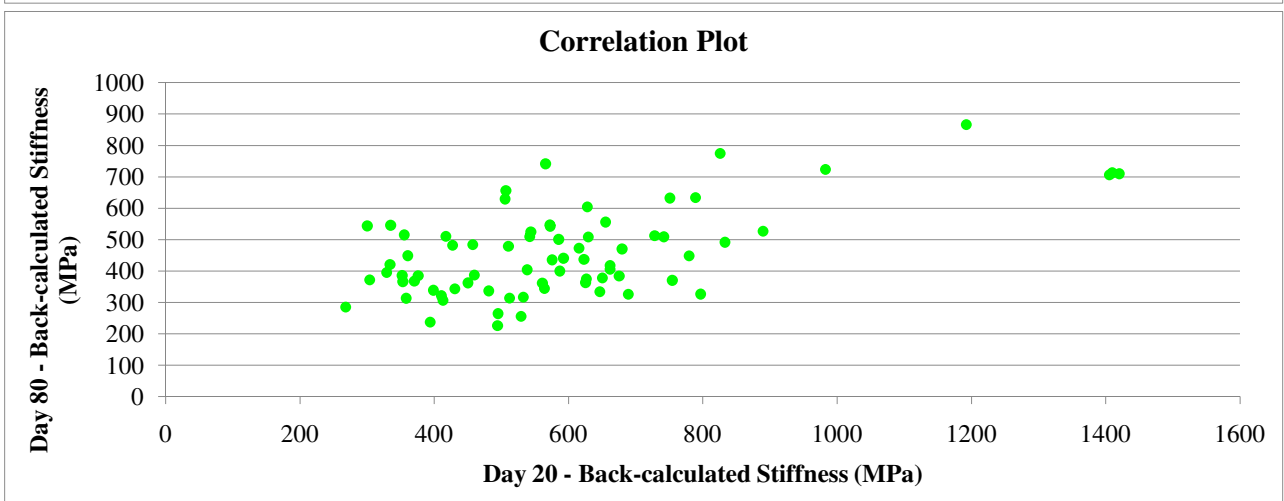
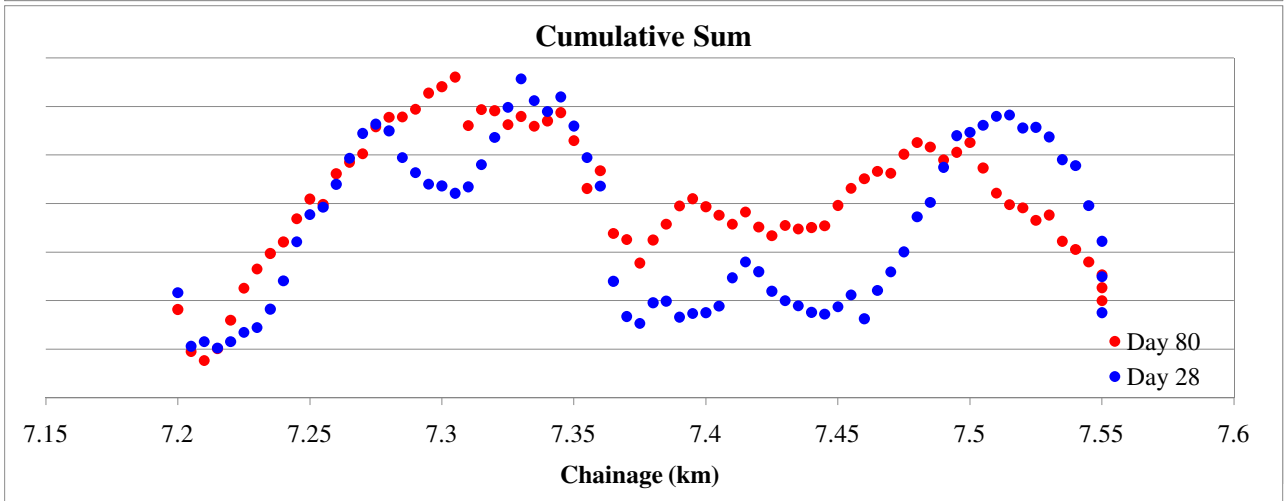
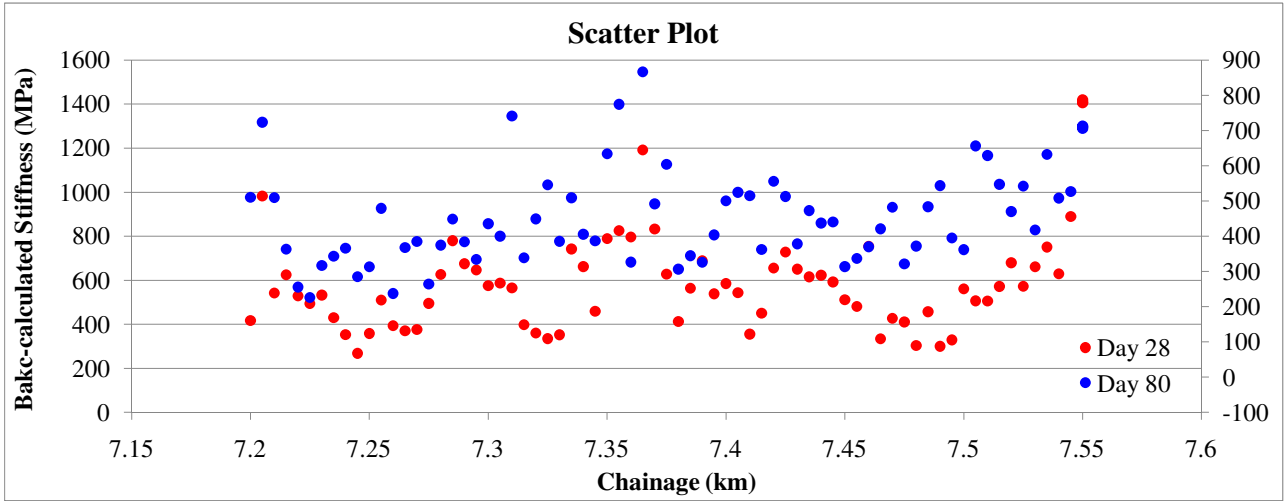
**Corellation co-efficient  $r = 0.9$  (200 FTB 1 NB)**



### Corellation co-efficient $r = 0.7$ (175 ETB 1 NB)

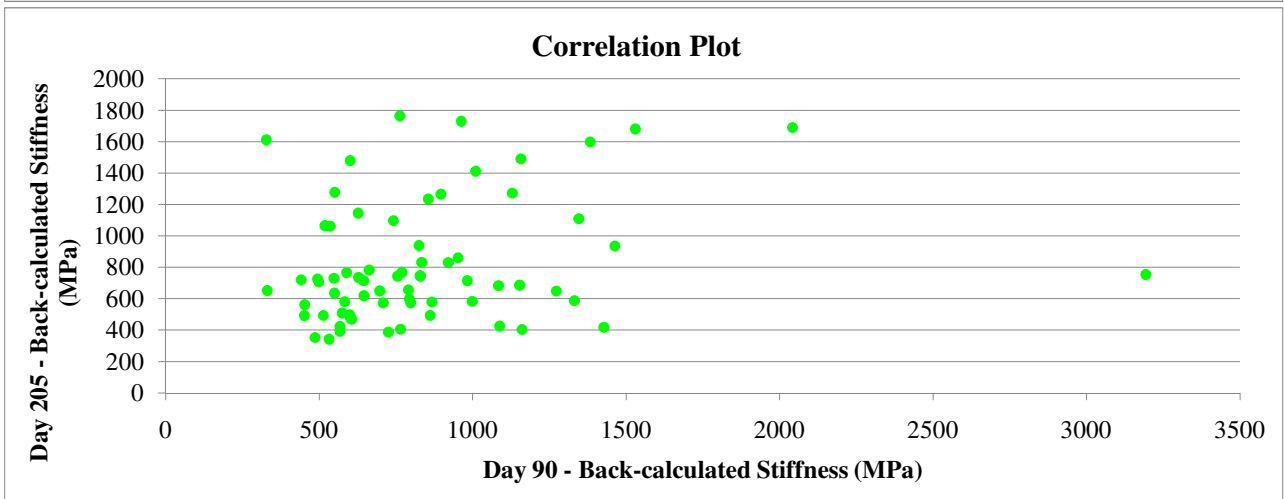
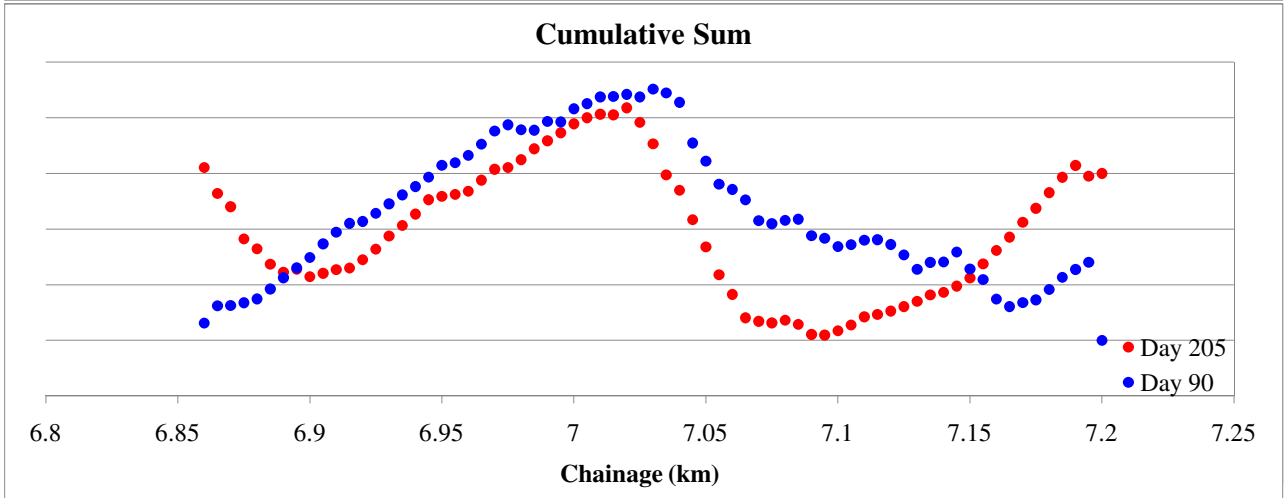
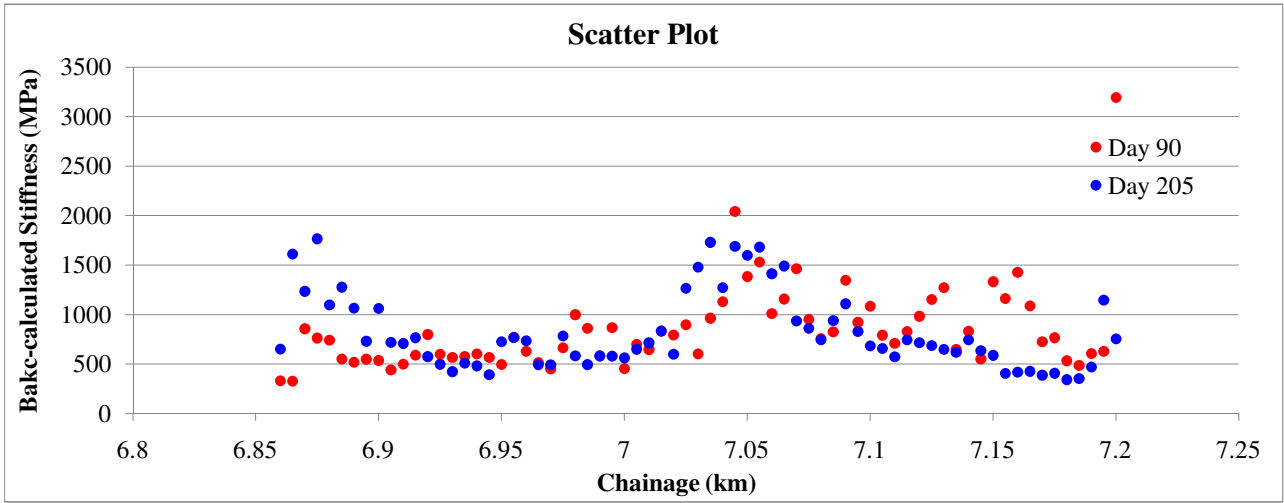


**Corellation co-efficient  $r = 0.5$  (175 ETB 1 NB)**

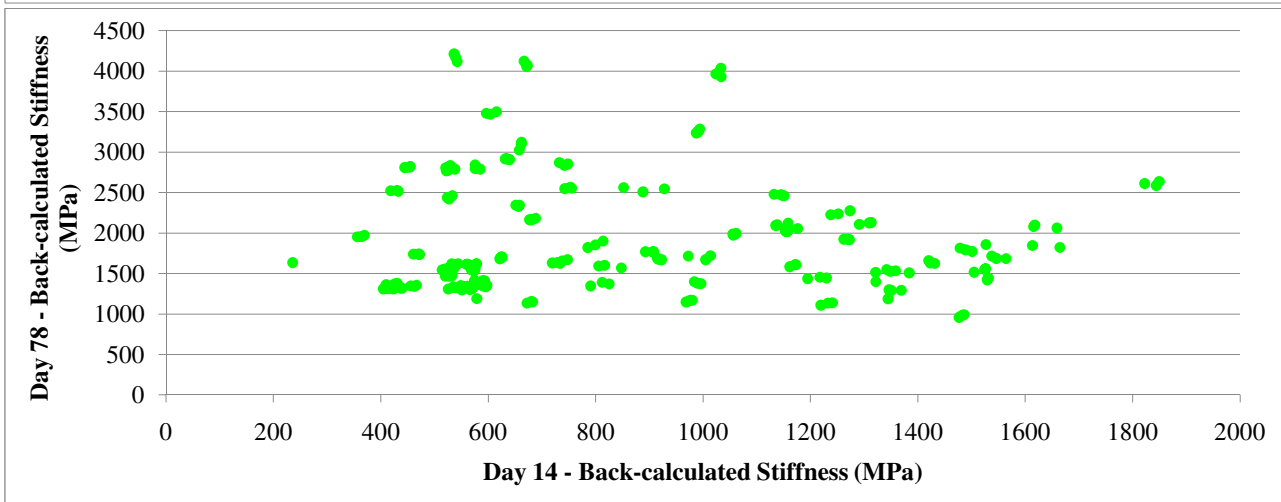
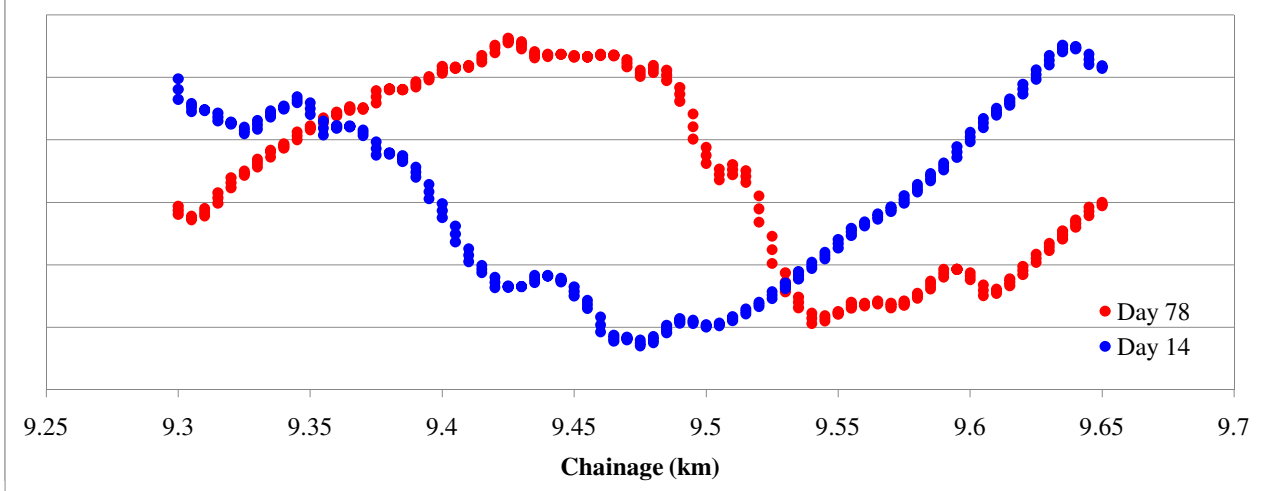
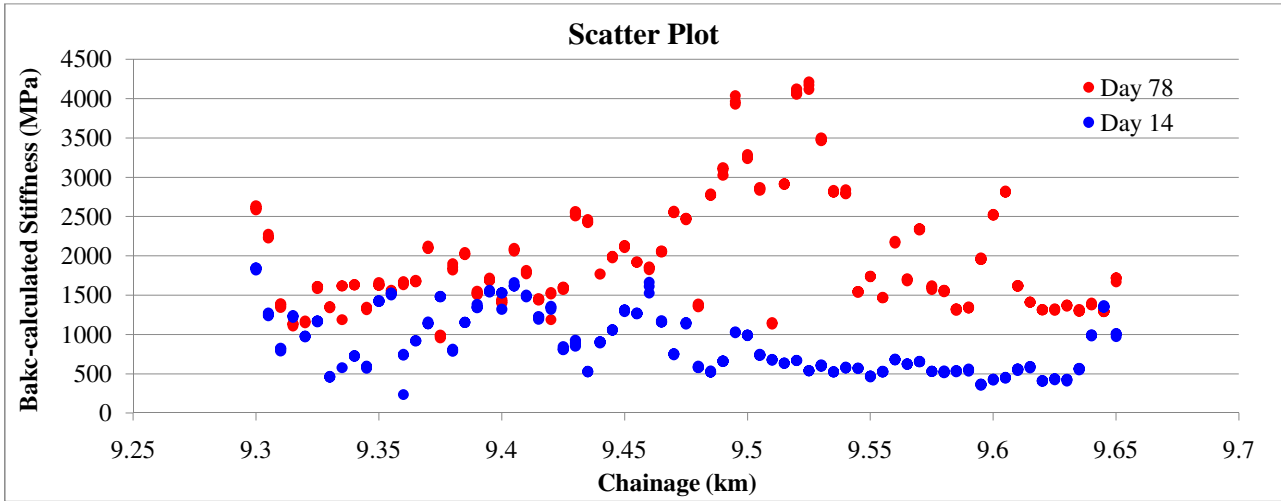




**Corellation co-efficient  $r = 0.2$  (200 C3 2 SB)**



### Corellation co-efficient $r = -0.1$ (175 FTB 2 SB)



## **ADDENDUM I**

### **2-D Base Layer Stiffness Spatial Variation Plots**

**SOUTHBOUND**

**200mm C3 – 1 (2% cement, 1% lime)**

		Chainage (km)						$\mu$ (MPa)	COV (%)	Spatial Trend	Event		
		6.50	6.55	6.60	6.65	6.70	6.75				6.80	6.85	R
Days	0							202	15%	-			
	1							349	21%	0.5			
	2							527	25%	0.6			
	3							638	31%	0.7			
	6							888	39%	0.7			
	7							884	38%	0.8			
	15							1344	40%	0.8			
	28							1647	35%	0.8			
	93							1017	36%	0.7			
	208							1239	38%	0.4			
365							1377	38%	0.5				

**200mm C3 – 2 (2% cement, 1% lime)**

		Chainage (km)						$\mu$ (MPa)	COV (%)	Spatial Trend	Event		
		6.90	6.95	7.00	7.05	7.10	7.15				7.20	R	P
Days	3							422	26%	-			
	4							425	38%	0.5			
	5							493	44%	0.8			
	6							512	40%	0.8			
	14							856	38%	0.8			
	28							1206	40%	0.6			
	90							847	51%	0.7			
	205							821	46%	0.2			
	362							667	44%	0.5			

**175mm BSM Emulsion (2.4% bitumen, 1% cement)**

		Chainage (km)						$\mu$ (MPa)	COV (%)	Spatial Trend	Event		
		7.20	7.25	7.30	7.35	7.40	7.45				7.50	7.55	R
Days	2							564	21%	-			
	7							787	27%	0.6			
	14							939	35%	0.7			
	28							1627	24%	0.8			
	92							1448	35%	0.5			
	207							929	43%	0.1			
	364							1025	27%	0.3			

**200mm BSM Emulsion (2.4% bitumen, 1% cement)**

		Chainage (km)						$\mu$ (MPa)	COV (%)	Spatial Trend	Event		
		7.55	7.60	7.65	7.70	7.75	7.80				7.85	7.90	R
Days	1							338	22%	-			
	4							546	33%	0.7			
	7							667	37%	0.6			
	14							823	36%	0.6			
	28							1337	25%	0.5			
	91							1130	26%	0.6			
	206							950	183%	0.4			
	363							1163	41%	0.0			

**175mm BSM Emulsion (2.4% bitumen, 2% cement)**

		Chainage (km)							$\mu$ (MPa)	COV (%)	Spatial Trend	Event		
		7.90	7.95	8.00	8.05	8.10	8.15	8.20				8.25	R	P
Days	1								433	24%	-			
	2								699	36%	0.7			
	8								1152	47%	0.7			
	14								1740	40%	0.7			
	90								1472	40%	0.6			
	201								958	68%	0.3			
	357								1517	43%	0.3			

**200mm BSM Emulsion (2.4% bitumen, 2% cement)**

		Chainage (km)							$\mu$ (MPa)	COV (%)	Spatial Trend	Event		
		8.25	8.30	8.35	8.40	8.45	8.50	8.55				8.60	R	P
Days	0								462	15%	-			
	1								873	24%	0.6			
	8								1775	29%	0.8			
	16								904	48%	0.5			
	23								2009	31%	0.3			
	73								2171	36%	0.4			
	188								1067	49%	0.3			
	344								1860	57%	0.4			

**175mm BSM Foam (2.4% bitumen, 1% cement)**

		Chainage (km)							$\mu$ (MPa)	COV (%)	Spatial Trend	Event		
		8.60	8.65	8.70	8.75	8.80	8.85	8.90				8.95	R	P
Days	1								397	20%	-			
	2								448	24%	0.3			
	7								752	24%	0.4			
	14								929	28%	0.8			
	28								733	52%	0.1			
	79								937	42%	0.3			
	193								548	38%	-0.2			
	349								624	34%	0.1			

**200mm BSM Foam (2.4% bitumen, 1% cement)**

		Chainage (km)							$\mu$ (MPa)	COV (%)	Spatial Trend	Event		
		8.95	9.00	9.05	9.10	9.15	9.20	9.25				9.30	R	P
Days	1								420	22%	-			
	4								686	23%	0.4			
	14								1082	25%	0.6			
	28								971	33%	0.7			
	78								2158	32%	0.5			
	192								768	72%	0.3			
	348								894	44%	0.2			

**175mm BSM Foam (2.4% bitumen, 2% cement)**

		Chainage (km)							$\mu$ (MPa)	COV (%)	Spatial Trend	Event		
		9.30	9.35	9.40	9.45	9.50	9.55	9.60				9.65	R	P
Days	0								327	17%	-			
	3								1285	35%	0.6			
	14								2447	28%	0.9			
	26								2088	30%	0.7			
	77								2906	29%	0.5			
	194								1992	37%	0.7			
	347								1931	51%	0.7			

**200mm BSM Foam (2.4% bitumen, 2% cement)**

		Chainage (km)							$\mu$ (MPa)	COV (%)	Spatial Trend	Event		
		9.65	9.70	9.75	9.80	9.85	9.90	9.95				10.0	R	P
Days	2								935	28%	-			
	10								1700	31%	0.9			
	13								1843	31%	0.9			
	25								1831	33%	0.9			
	76								2532	25%	0.8			
	190								975	77%	0.3			
	346								1236	37%	0.0			

**NORTHBOUND**

**200mm C3 – 1 (2% cement, 1% lime)**

		Chainage (km)							$\mu$ (MPa)	COV (%)	Spatial Trend	Event		
		6.50	6.55	6.60	6.65	6.70	6.75	6.80				6.85	R	P
Days since construction	0								233	23%	-			
	1								351	21%	0.5			
	2								350	24%	0.4			
	3								505	28%	0.5			
	4								676	35%	0.6			
	7								943	38%	0.8			
	14								1466	40%	0.6			
	28								1770	33%	0.7			
	88								1243	46%	0.2			
	190								1305	56%	0.8			
372								932	37%	0.6				

**200mm BSM Emulsion (0.9% residual bitumen, 1% cement)**

		Chainage (km)							$\mu$ (MPa)	COV (%)	Spatial Trend	Event		
		6.90	6.95	7.00	7.05	7.10	7.15	7.20				R	P	T
Days since construct	0								207	8%	-			
	1								236	14%	0.2			
	3								317	18%	0.2			
	7								377	21%	0.5			
	14								443	26%	0.6			
	28								311	30%	0.6			
	81								312	43%	0.5			
	183								278	32%	0.5			
	365								380	34%	0.7			

**175mm BSM Emulsion (2.4% bitumen, 1% cement)**

		Chainage (km)							$\mu$ (MPa)	COV (%)	Spatial Trend	Event		
		7.20	7.25	7.30	7.35	7.40	7.45	7.50				7.55	R	P
Days since construct	0								255	8%	-			
	1								336	17%	0.2			
	3								424	25%	0.4			
	7								598	24%	0.7			
	14								619	28%	0.7			
	28								571	35%	0.3			
	80								451	29%	0.5			
	182								683	30%	0.5			
	364								1300	29%	0.3			

**200mm BSM Emulsion (2.4% bitumen, 1% cement)**

		Chainage (km)							$\mu$ (MPa)	COV (%)	Spatial Trend	Event		
		7.55	7.60	7.65	7.70	7.75	7.80	7.85				7.90	R	P
Days since construct	0								258	19%	-			
	1								442	27%	0.7			
	4								692	35%	0.7			
	7								845	37%	0.9			
	14								1035	37%	0.9			
	28								799	42%	0.6			
	78								636	38%	0.4			
	180								858	30%	0.1			
	362								1592	22%	0.5			

**175mm BSM Emulsion (2.4% bitumen, 2% cement)**

		Chainage (km)							$\mu$ (MPa)	COV (%)	Spatial Trend	Event		
		7.90	7.95	8.00	8.05	8.10	8.15	8.20				8.25	R	P
Days since construct	0								281	11%	-			
	1								569	36%	0.2			
	2								691	37%	0.5			
	3								992	41%	0.6			
	14								1236	44%	0.7			
	28								1150	48%	0.6			
	74								1260	54%	0.3			
	175								1924	42%	0.2			
	357								3678	42%	0.4			

**200mm BSM Emulsion (2.4% bitumen, 2% cement)**

		Chainage (km)							$\mu$ (MPa)	COV (%)	Spatial Trend	Event		
		8.25	8.30	8.35	8.40	8.45	8.50	8.55				8.60	R	P
Days since construct	0								275	8%	-			
	1								559	27%	0.3			
	2								797	46%	0.6			
	7								1226	35%	0.6			
	14								1728	34%	0.6			
	28								1475	40%	0.5			
	73								2399	31%	0.3			
	174								2402	42%	0.2			
	356								3811	30%	0.3			

**175mm BSM Foam (2.4% bitumen, 1% cement)**

		Chainage (km)							$\mu$ (MPa)	COV (%)	Spatial Trend	Event		
		8.60	8.65	8.70	8.75	8.80	8.85	8.90				8.95	R	P
Days since construct	0								245	6%	-			
	1								354	19%	0.3			
	2								419	21%	0.2			
	7								540	22%	0.4			
	14								605	22%	0.5			
	28								448	23%	0.3			
	80								679	35%	0.0			
	181								565	45%	0.3			
	363								742	40%	0.5			

**200mm BSM Foam (2.4% bitumen, 1% cement)**

		Chainage (km)							$\mu$ (MPa)	COV (%)	Spatial Trend	Event		
		8.95	9.00	9.05	9.10	9.15	9.20	9.25				9.30	R	P
Days since constructio	0								251	11%	-			
	1								358	24%	0.8			
	4								427	34%	0.9			
	5								512	39%	0.8			
	7								560	28%	0.8			
	14								448	27%	0.7			
	28								399	28%	0.5			
	72								537	36%	0.1			
	173								543	48%	0.6			
	355								1070	28%	0.4			



**175mm BSM Foam (2.4% bitumen, 2% cement)**

		Chainage (km)							$\mu$ (MPa)	COV (%)	Spatial Trend	Event		
		9.30	9.35	9.40	9.45	9.50	9.55	9.60				9.65	R	P
Days since construct	0								281	10%	-			
	1								454	20%	0.5			
	3								777	25%	0.5			
	7								1077	33%	0.7			
	14								878	42%	0.7			
	28								1202	50%	0.2			
	78								1976	36%	0.2			
	168								1492	72%	-0.1			
	352								2469	41%	0.6			

**200mm BSM Foam (2.4% bitumen, 2% cement)**

		Chainage (km)							$\mu$ (MPa)	COV (%)	Spatial Trend	Event		
		9.65	9.70	9.75	9.80	9.85	9.90	9.95				10.0	R	P
Days since const	0								280	20%	-			
	3								625	36%	0.5			
	19								1492	53%	0.5			
	27								1464	65%	0.5			
	63								2072	54%	0.4			
	169								3156	41%	0.6			
	349								4229	31%	0.0			

## **ADDENDUM J**

# **Change in Base Layer Spatial Stiffness Profile Correlation Tables**

**RAINFALL**

**Southbound**

Sub-section	Days since construction			
	0 - 28	28 - 90	90 - 180	180 - 360
200mm C3-1 (2% c, 1% l)			172	274
200mm C3-2 (2% c, 1% l)			169	277
175mm Emulsion (1% c, 2.4% b)			169	277
200mm Emulsion (1% c, 2.4% b)			169	277
175mm Emulsion (2% c, 2.4% b)			169	277
200mm Emulsion (2% c, 2.4% b)			169	277
175mm Foam (1% c, 2.4% b)			169	277
200mm Foam (1% c, 2.4% b)			169	277
175mm Foam (2% c, 2.4% b)			172	274
200mm Foam (2% c, 2.4% b)			169	277

**Northbound**

Sub-section	Days since construction			
	0 - 28	28 - 90	90 - 180	180 - 360
200mm C3-1 (2% c, 1% l)		158	224	61
200mm Emulsion (0.9% b, 1% c)	101	57	235	61
175 Emulsion (1% c, 2.4% b)	101	57	235	61
200 Emulsion (1% c, 2.4% b)	101	57	235	61
175 Emulsion (2% c, 2.4% b)	101	57	235	61
200 Emulsion (2% c, 2.4% b)	101	57	235	61
175 Foam (1% c, 2.4% b)	101	57	235	61
200 Foam (1% c, 2.4% b)	101	57	235	61
175 Foam (2% c, 2.4% b)	101	71	221	61
200 Foam (2% c, 2.4% b)	101	57	235	

**PRIME APPLICATION**

**Southbound**

Sub-section	Days since construction			
	0 - 28	28 - 90	90 - 180	180 - 360
200mm C3-1 (2% c, 1% l)		Prime		
200mm C3-2 (2% c, 1% l)		Prime		
175mm Emulsion (1% c, 2.4% b)		Prime		
200mm Emulsion (1% c, 2.4% b)		Prime		
175mm Emulsion (2% c, 2.4% b)		Prime		
200mm Emulsion (2% c, 2.4% b)		Prime		
175mm Foam (1% c, 2.4% b)		Prime		
200mm Foam (1% c, 2.4% b)		Prime		
175mm Foam (2% c, 2.4% b)		Prime		
200mm Foam (2% c, 2.4% b)		Prime		

**Northbound**

Sub-section	Days since construction			
	0 - 28	28 - 90	90 - 180	180 - 360
200mm C3-1 (2% c, 1% l)		Prime		
200mm Emulsion (0.9% b, 1% c)		Prime		
175 Emulsion (1% c, 2.4% b)		Prime		
200 Emulsion (1% c, 2.4% b)		Prime		
175 Emulsion (2% c, 2.4% b)		Prime		
200 Emulsion (2% c, 2.4% b)		Prime		
175 Foam (1% c, 2.4% b)		Prime		
200 Foam (1% c, 2.4% b)		Prime		
175 Foam (2% c, 2.4% b)		Prime		
200 Foam (2% c, 2.4% b)		Prime		

**TRAFFIC**

**Southbound**

Sub-section	Days since construction			
	0 - 28	28 - 90	90 - 180	180 - 360
200mm C3-1 (2% c, 1% l)			Traffic	Traffic
200mm C3-2 (2% c, 1% l)			Traffic	Traffic
175mm Emulsion (1% c, 2.4% b)			Traffic	Traffic
200mm Emulsion (1% c, 2.4% b)			Traffic	Traffic
175mm Emulsion (2% c, 2.4% b)			Traffic	Traffic
200mm Emulsion (2% c, 2.4% b)			Traffic	Traffic
175mm Foam (1% c, 2.4% b)			Traffic	Traffic
200mm Foam (1% c, 2.4% b)			Traffic	Traffic
175mm Foam (2% c, 2.4% b)			Traffic	Traffic
200mm Foam (2% c, 2.4% b)			Traffic	Traffic

**Northbound**

Sub-section	Days since construction			
	0 - 28	28 - 90	90 - 180	180 - 360
200mm C3-1 (2% c, 1% l)			Traffic	Traffic
200mm Emulsion (0.9% b, 1% c)			Traffic	Traffic
175 Emulsion (1% c, 2.4% b)			Traffic	Traffic
200 Emulsion (1% c, 2.4% b)			Traffic	Traffic
175 Emulsion (2% c, 2.4% b)			Traffic	Traffic
200 Emulsion (2% c, 2.4% b)			Traffic	Traffic
175 Foam (1% c, 2.4% b)			Traffic	Traffic
200 Foam (1% c, 2.4% b)			Traffic	Traffic
175 Foam (2% c, 2.4% b)			Traffic	Traffic
200 Foam (2% c, 2.4% b)			Traffic	Traffic